

ÉCOLE DOCTORALE PHYSIQUE ET CHIMIE-PHYSIQUE

Institut de physique et chimie des matériaux de Strasbourg (IPCMS)

THÈSE

présentée par :

Mauricio GÓMEZ VILORIA

soutenue le : 22 octobre 2021

pour obtenir le grade de : **Docteur de l'Université de Strasbourg**

Discipline/S spécialité : Physique de la matière condensée

Effet du couplage spin-orbite sur la réponse magnétique de systèmes confinés

THÈSE dirigée par :

M. JALABERT Rodolfo A.

Professeur, Université de Strasbourg

RAPPORTEURS :

Mme. BOUCHIAT Hélène

Directrice de recherche, Laboratoire de Physique des Solides,
Orsay

M. RICHTER Klaus

Professeur, Universität Regensburg

AUTRES MEMBRES DU JURY :

M. POLONYI Janos

Professeur, Université de Strasbourg

**EFFECT OF SPIN–ORBIT COUPLING ON
THE MAGNETIC RESPONSE OF
CONFINED SYSTEMS**

UNIVERSITÉ DE STRASBOURG

Mauricio Gómez Vilorio

September 15, 2021

CONTENTS

1	INTRODUCTION	1
1.1	Magnetic response of bulk metals	3
1.2	Observed magnetic response of ensembles of gold nanoparticles	5
1.3	Theoretical hypotheses and orbital magnetism	10
1.4	Effects of the spin–orbit coupling in confined electron systems	12
1.5	Outline	14
2	MODEL AND THEORETICAL FORMALISM	15
2.1	Nanoparticle modeling	15
2.2	Electrons under spherical confinement	19
2.2.1	Eigenvalues and eigenstates	20
2.2.2	Semiclassical density of states of a spherical billiard	21
2.3	Thermodynamical formalism	23
2.3.1	Magnetic response of confined systems: Quantum approach	25
2.3.2	Quantum perturbation theory for the orbital susceptibility of spherical nanoparticles	26
2.3.3	Semiclassical thermodynamic approach	29
2.4	Weakly relativistic effects	34
2.4.1	Foldy-Wouthuysen transformation and free Dirac electrons	35
2.4.2	Weakly relativistic limit in the presence of magnetic fields and confinement	36
2.4.3	Conservation laws under the influence of spin–orbit coupling	38
2.5	Summary and correspondence with the rest of this work	39
3	ORBITAL MAGNETIC RESPONSE OF ENSEMBLES OF METALLIC NANOPARTICLES	41
3.1	Free energy of electrons in a spherical billiard	42
3.2	Grand-canonical magnetic response	44
3.3	Magnetic response of an ensemble of noninteracting nanoparticles	48
3.4	Magnetic response of individual nanoparticles	53
3.5	Comparisons to the experimental results	56
3.6	Conclusions for chapter 3	59
4	WEAKLY RELATIVISTIC CORRECTIONS TO THE MAGNETIC SUSCEPTIBILITY OF METALLIC NANOPARTICLES	61
4.1	Weakly relativistic description	62
4.1.1	Hamiltonian for the spherical symmetric case	63
4.1.2	Nonrelativistic susceptibility with spin	64

4.2	Kinetic correction in the absence of spin–orbit coupling	66
4.3	Spin-orbit coupling in a spherical nanoparticle	71
4.3.1	Perturbative treatment of the magnetic field	72
4.3.2	Relativistic correction to the zero-field susceptibility	77
4.4	Numerical evaluation of the relativistic corrections	79
4.5	Half-spherical nanoparticles	82
4.5.1	Nonrelativistic susceptibility	83
4.5.2	Spin-orbit coupling for a HS confining potential	84
4.5.3	Perturbative treatment of the magnetic field	87
4.5.4	Spin-orbit correction for the half-sphere	88
4.6	Conclusions for chapter 4	89
5	CONCLUDING REMARKS AND OUTLOOK	91
5.1	Summary	91
5.2	Outlook	92
	APPENDICES	99
A	ZERO-FIELD SUSCEPTIBILITY OF A FREE ELECTRON GAS	99
A.1	Non-relativistic Landau levels	99
A.1.1	Non relativistic bulk susceptibility	100
A.2	Landau orbital susceptibility from the density of states	101
A.3	Relativistic Landau levels and susceptibility	103
B	SEMICLASSICAL DENSITY OF STATES OF A SPHERICAL WELL	105
B.1	EBK quantization	105
B.2	Classical spherical billiards	106
B.3	EBK quantization for the spherical billiard	108
B.4	Semiclassical density of states in the absence of magnetic field	109
B.5	Semiclassical density of states at finite magnetic fields	112
C	ORBITAL SUSCEPTIBILITY OF A METALLIC NANOPARTICLE FROM QUANTUM PERTURBATION THEORY	115
C.1	Spherical nanoparticles	115
C.2	Cylindrical confinement subject to a field along the axis	116
C.2.1	Perturbative energies under a magnetic field	118
C.2.2	Grand canonical ZFS for a cylindrical confinement	119
D	EQUIVALENCE BETWEEN QUANTUM AND SEMICLASSICAL CALCULATIONS OF THE ZERO-FIELD SUSCEPTIBILITY	121
E	FOLDY-WOUTHUYSEN TRANSFORMATION	125
E.1	The problem of zitterbewegung	125

E.2	Foldy–Wouthuysen transformation for a free particle	125
E.3	Foldy-Wouthuysen transformation in the presence of a magnetic field .	127
E.4	Dirac electron in a potential	128
F	SIMPLIFIED SEMICLASSICAL EVALUATION OF THE MAGNETIC SUSCEPTIBILITY	131
F.1	Evaluation of the grand-canonical orbital magnetic susceptibility . . .	131
F.2	Derivation of the Curie-type law for ensembles of noninteracting nanoparticles	133
G	DARWIN CORRECTION	135
G.1	Finite box spherical potential	135
G.2	Matrix elements for the Darwin correction	136
H	MATRIX ELEMENTS FOR THE ANGULAR MAGNETO-ELECTRIC COUPLING	139
I	NONRELATIVISTIC SUSCEPTIBILITY USING THE COUPLED BASIS	143
J	MATRIX ELEMENTS FOR THE CASE OF THE HALF-SPHERE	145
J.1	A theorem about the wave-function values close to a potential barrier .	145
J.2	Angular integral of the matrix element (4.71)	147
J.3	Definite integrals of two spherical Bessel functions	148
	BIBLIOGRAPHY	151
	VARIABLES AND ABBREVIATIONS INDEX	167

The laws of physics cover a broad range of scales, going from elementary particles to the cosmological distances between galaxies. At each intermediary scale the equations can be completely different. What binds physics into a single field of inquiry is our ability to be able to deduce the dynamics at each scale from the physics in the layer below it. Physicists usually have two main goals, to explain the origin of this emergent phenomena and to establish their limitations. A procedure that also allows the development of technological applications and the discovery of new phenomena.

The development of quantum mechanics at the beginning of the last century, allowed physicists to understand the properties of matter under a new perspective. Early solid-state research allowed an understanding of the electrical conduction and heat capacity of 3D bulk metals by considering nearly-free charge carriers, the underlying non-relativistic dynamics and a continuous electronic band structure. However, the quest for miniaturization has led to a new era of discoveries based on quantum size effects. Some striking examples include the emergence of the electronic shell structure of metallic nanoparticles due to quantum confinement [1], the evidence of persistent current in resistive mesoscopic rings due to electronic coherence effects [2], and the discovery of effective relativistic 2D dynamics of charge carriers in graphene [3].

A nanoparticle is an object whose typical size is of the order of a few to a hundred nanometers, much smaller than the wavelength of visible light but much larger than a single atom. Metallic nanoparticles are an exemplary testing ground for emerging properties. Usually monocrystalline, these objects can be small metal clusters containing tens of atoms to large nanoparticles with up to 10^5 atoms. The number of particles to study is below the thermodynamic limit that usually applies for the electronic properties of bulk metals. Metallic nanoparticles have already lead to fascinating technological advances which include the fabrication of plasmonic metasurfaces for sensing applications [4], the harvesting of energy from photoelectrochemical water splitting [5, 6], and enhanced light absorption for localized heating of interest for cancer therapy [7] and antimicrobial treatment [8].

The sharp contrast between bulk and nanoscopic behavior is the product of quantum size effects. The surface of a metallic nanoparticle is non-negligible when compared to its volume, and thus influences the wavefunction of every electron inside the nanoparticle. In turn, these boundary conditions create a confinement potential that renders the electronic spectrum discrete and it is this quantized behavior that gives rise to the emerging properties at this scale that are not present in macroscopic



Figure 1.1: Samples of gold nanoparticles of different sizes dispersed in water [9].

samples.

In the particular case of atomic number 79 (chemical element "Au"), gold nanoparticles are well-known for their optical, plasmonic, electronic and catalytic properties, which differ from that of macroscopic samples. In fig. 1.1, it can be observed that samples of gold nanoparticles absorb different wavelengths of light and thus shine in different colors depending on the nanoparticles size, in contrast with the familiar shining yellow color of macroscopic gold. In the same way, while bulk gold is chemically inert and resistant to corrosion, it can become an interesting catalytic agent at the nanoscale [10]. As gold nanoparticles are non-toxic and easy to fabricate, they have become an outstanding material to study quantum size effects and their potential applications.

Most of the time, metallic nanoparticles are chemically synthesized, capped with long molecules or ligands that are used to functionalize the surface of the nanoparticle. The temperature of the reaction, together with the quantity and types of ligands, determines the shape and size of the nanoparticles. A common method is known as Brust-Schiffin synthesis¹, which is used to create thiol-stabilized gold nanoparticles through a protocol that results in round gold nanoparticles between 1.5 to 5 nm in diameter [12]. The nanoparticles can then be deposited on films or in a liquid solution. The ligands can be washed out or kept to physically separate the nanoparticles to avoid the formation of aggregates.

In order to probe these ensembles of nanoparticles, electric and magnetic fields can be used. The research area of nanoplasmonics is centered on the study of the coherent motion of electrons in small metallic systems and their coupling to electromagnetic fields. In metals, valence electrons are usually delocalized from their atomic nuclei, moving as nearly-free particles. Metallic nanoparticles are usually smaller than the coherence length of the material which means that electrons can propagate inside them without losing their quantum phase. This lossless dynamics gives rise to a coherent motion of the valence electrons that can be stimulated by electric fields using

¹Other procedures can produce larger nanoparticles. For example Turkevich method can produce nanoparticles with diameters from 9 to 120 nm [11].

optical light.

Nanomagnetism is the field of study of magnetic properties of nano-sized objects, that can be obtained from different nanofabrication techniques or that emerge in large samples, like for instance from the texture induced by magnetic domain walls [13]. While micrometer-sized magnetic devices are widely used for information storage, nano-sized objects are usually very sensitive to temperature. Some inorganic nanoparticles are of interest because of their permanent magnetization, and iron-based nanoparticles have demonstrated their usefulness for applications in magnetic resonance imaging [14] and paleo-magnetism [15].

In contrast, bulk gold is not considered as a magnetic material since it cannot preserve a permanent magnetization in the absence of a magnetic field. Macroscopic gold has a weak diamagnetic response, with the induced magnetization aligned in the direction opposite to an external magnetic field, which comes from the magnetic moments of core electrons. However, in the form of nanoparticles, an unexpected magnetic behavior can be observed. Gold nanoparticles have been shown to display a diverse range of magnetic responses, whose origin is still a source of debate [16, 17] as we discuss in the sequel.

In order to develop new applications based on the manipulation of gold nanoparticles, understanding their opto-chemical properties is not enough, and explaining their magnetic response could be the key for controlled manipulation of these nano-objects. As the models that fully explain the magnetic response of ensembles of metallic nanoparticles are still scarce, the goal of this thesis is to provide a rigorous theoretical understanding of the electronic effects that play a dominant role in such a system.

1.1 MAGNETIC RESPONSE OF BULK METALS

Electromagnetism is one of the four fundamental interactions in nature.² Magnetic and electric effects are tied together under Maxwell's equations. Moving charges produce magnetic fields, and fluctuating magnetic dipoles induce electric currents. In the presence of electric and magnetic fields, the orbits of charge carriers and their magnetic dipoles is perturbed, modifying in turn the electromagnetic field.

The magnetic response describes how a material reacts to a magnetic field. When providing such a description, generally two vector fields are considered, the magnetic induction or **B**-field and the applied magnetizing field or **H**-field. The relation between **B** and **H** is given in cgs-gauss units by³

$$\mathbf{B} = \mathbf{H} + 4\pi\mathbf{M}, \quad (1.1)$$

where the field **M** is the magnetization induced in the material.⁴ If the number of

²The other three interactions being gravity, weak interactions and strong interactions. The last two only concern the atomic nuclei, and gravity has little to negligible effects in solid-state physics.

³Throughout this document, every formula is expressed in centimetre-gram-second-gauss (cgs-gauss) units.

⁴In cgs-gauss units, the magnetic fields and the magnetization have the same physical dimensions

electrons is fixed (canonical ensemble) the magnetic moment \mathcal{M} (where $\mathbf{M} = \mathcal{M}/\mathcal{V}$, with \mathcal{V} the nanoparticle volume) can be derived by differentiating the free energy F with respect to the \mathbf{H} -field at fixed number of electrons N and temperature T [18], i.e.

$$\mathcal{M} = - \left(\frac{\partial F}{\partial H} \right)_{N,T}, \quad (1.2)$$

where $H = |\mathbf{H}|$ and $\mathcal{M} = |\mathcal{M}|$.

The different magnetic responses of metals are classified by the sign of the magnetic susceptibility at zero field, corresponding to the slope of the curve $M(H)$. From eq. (1.2), we can obtain the zero-field susceptibility (ZFS) in the canonical ensemble as⁵

$$\chi = \frac{1}{\mathcal{V}} \frac{\partial \mathcal{M}}{\partial H} \Big|_{H=0} = - \frac{1}{\mathcal{V}} \left(\frac{\partial^2 F}{\partial H^2} \right)_{N,T} \Big|_{H=0}. \quad (1.3)$$

Usually, for ordinary bulk metals, $|\chi| \ll 1$. Metals with a paramagnetic response are defined by a $\chi > 0$, while $\chi < 0$ indicates diamagnetism. Ferromagnetism is the special case where $\mathcal{M} \neq 0$ at $H = 0$, and the ZFS is not well defined in this case.

The magnetic response of matter at thermal equilibrium is a purely quantum mechanical effect, arising from the electron orbital and spin angular momentum. The former arises from the orbital motion of electrons subjected to a magnetic field, and in this case the Bohr-Van Leeuwen theorem [19, 20] states that the magnetic response should vanish at the classical limit. The latter is a purely quantum property and follows from the electron intrinsic magnetic moment, with magnitude equal to the Bohr magneton μ_B and a sign that depends on the two possible spin projections about a given axis.

Core electrons, bounded strongly to the atomic nucleus, contribute significantly to the magnetic response of metals. On the one hand the orbital motion of the core electrons produces a magnetic moment that opposes the magnetic field known as the Larmor diamagnetism. On the other hand, the total angular momentum (spin and orbital) in an atom is associated with a magnetic moment and produces a paramagnetic susceptibility. If the atoms are considered as independent magnetic moments, the ZFS is inversely proportional to the temperature, a phenomenon known as Curie's law.⁶

The different possible magnetic moments arising from core and conduction electrons give rise to a rich variety of magnetic responses summarized in fig. 1.2.

The magnetic response of finite systems has to be compared to that of the bulk. For metals, the delocalized valence electrons form an electron fluid that contributes to

but are usually written in different units, \mathbf{B} is usually expressed in gauss, \mathbf{H} in oersted and \mathbf{M} in oersted or magnetic moment per cm^3 .

⁵In the most general case, χ can be a three dimensional tensor, however in this thesis we only consider scalar susceptibilities.

⁶Paul Langevin developed the theory of Larmor's diamagnetism and theoretically derived Curie's law [21]. Larmor's diamagnetism is sometimes called Langevin's diamagnetism and the generalization of Curie's law is called the Langevin function. As the terms have opposite effects, in this thesis we do not call this contributions after Langevin to avoid confusion.

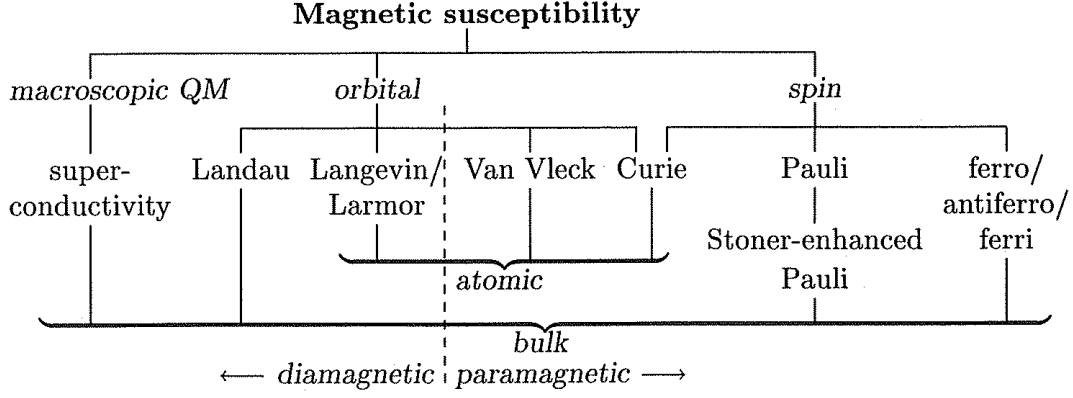


Figure 1.2: Different types of magnetic responses of bulk metals, with orbital and spin origin, ranging from weak to strong magnetism. Extracted from [22].

the magnetic response. First studied by Lev Landau [23, 24], the orbital susceptibility of a non-relativistic (nr) electron gas (see appendix A) is given by $\chi_b^{(nr)} = \chi_L + \chi_P$, resulting from the combined effect of the diamagnetic Landau susceptibility [24]

$$\chi_L = -\frac{1}{12\pi^2} \frac{e^2 k_F}{m^* c^2}, \quad (1.4)$$

arising from the orbital motion, and the paramagnetic Pauli susceptibility

$$\chi_P = 3 |\chi_L|, \quad (1.5)$$

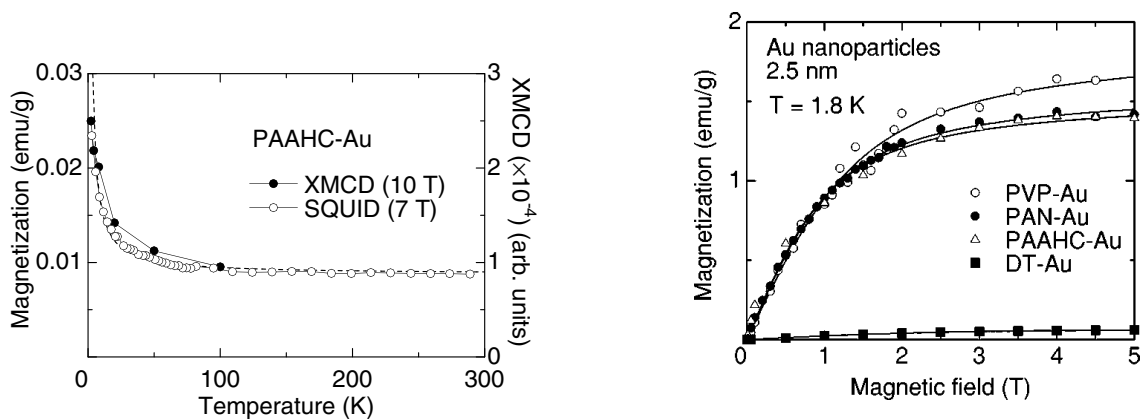
originating from the Zeeman interaction between the electron magnetic moment and the external magnetic field. We note c the speed of light, $-e < 0$ the electron charge, k_F the Fermi wave vector, and m^* the effective mass. In metals, the difference between m^* and the free electron mass m is very small (i.e., $m_{Au}^* = 1.1 m$) and therefore we will neglect this difference. The situation considerably changes when going from the case of metals to that of semiconductors, where such an identification is not valid and eq. (1.5) does not hold.

Most metals are not ferromagnetic. For bulk gold, the zero-field susceptibility is⁷ $\chi_{Au} = -9.3 |\chi_L| = -2.74 \times 10^{-6}$, with the paramagnetic contribution from the conduction electrons dominated by the Larmor diamagnetic response from the core electrons [25].

1.2 OBSERVED MAGNETIC RESPONSE OF ENSEMBLES OF GOLD NANOPARTICLES

Discrepancies in the magnetic response of metallic colloids (of the order of hundreds of micrometers) and that of the bulk were already observed at the turn of the

⁷To obtain the numerical value of the ZFS in the International System of Units (SI), multiply the cgs-gauss numerical value by 4π .



(a) Extracted from [37]. SQUID magnetization at finite field (7 teslas) of ensemble of gold nanoparticles coated with PAAHc, contrasted with the measurement of XMCD (10 teslas). Data fitted to a Curie law.

(b) Extracted from [38]. Magnetization of gold nanoparticles at 1.8 K with mean diameter 2.5 nm. The different symbols represent different protecting agents: PAN (polyacrylonitrile), PVP (polyvinyl pyrrolidone), PAAHc (polyallyl amine hydrochloride) and DT (dodecane thiol).

Figure 1.3: Magnetization of an ensemble of Au nanoparticles capped with polymers as a function of temperature (a) and of the applied magnetic field (b).

1930s [26–32].⁸ R.V. Raman had appealed to a magnetic response of orbital origin to explain the diamagnetic behavior of reduced-size samples of graphite [27] and experiments with colloidal gold already presented a weaker diamagnetic response than that of the bulk [31].

Strong paramagnetic behavior in ensembles of gold, nanoparticles was later reported in the turn of the millennium. The teams of H. Hori and Y. Yamamoto in Japan had found that an ensemble of 3–4 nm gold nanoparticles, embedded in a polymer matrix, presented a paramagnetic behavior, i.e. the magnetization as a function of the applied magnetic field of the whole sample increased with a positive slope until reaching a saturation value. The magnetization was aligned with the external field and was inversely proportional to temperature, thus described by a Curie-like law [34] as in fig. 1.3a, at odds with the bulk response of gold which is weakly diamagnetic. The different experiments [34–39] probed the samples with electron spin resonance (ESR) and X-ray magnetic circular dichroism (XMCD) and pointed to a possibly intrinsic effect of individual nanoparticles [39]. The nanoparticles had up to almost 20 electron magnetic moments μ_B each, as deduced from magnetization curves like that of fig. 1.3b. If the magnetic moments were fixed, as if some ferromagnetic nanoparticles were present, then the Curie law would be a direct consequence of an ensemble of independently magnetized particles. While being of the opposite

⁸The first scientific paper on the synthesis of colloidal gold is credited to Michael Faraday in 1857 [33].

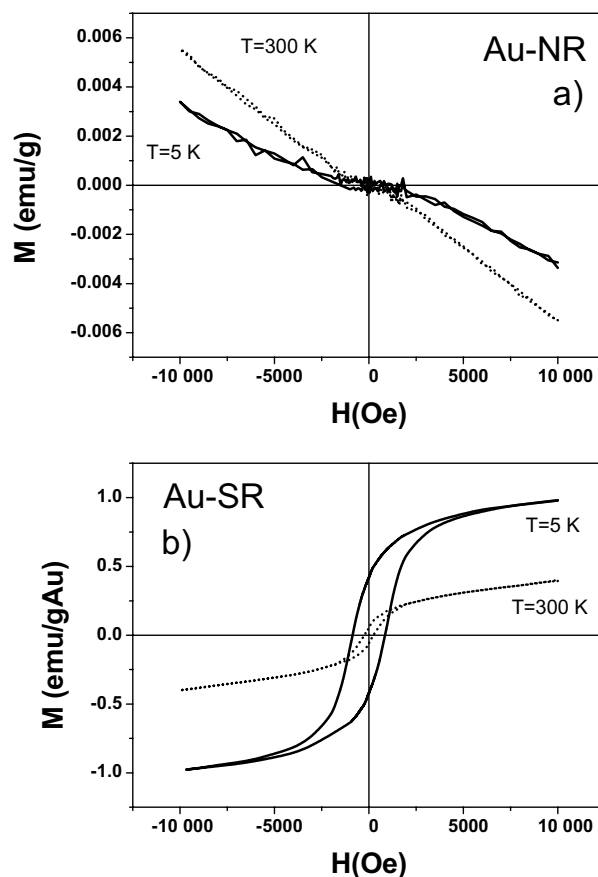
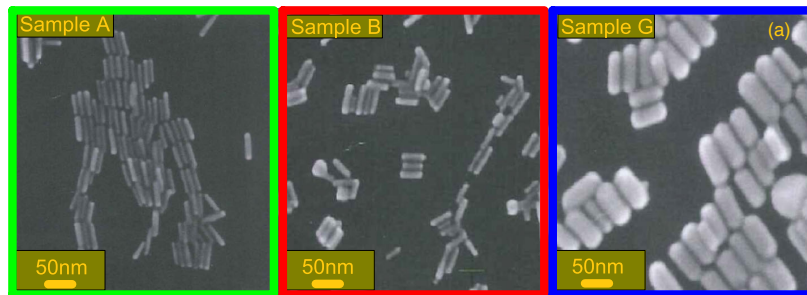


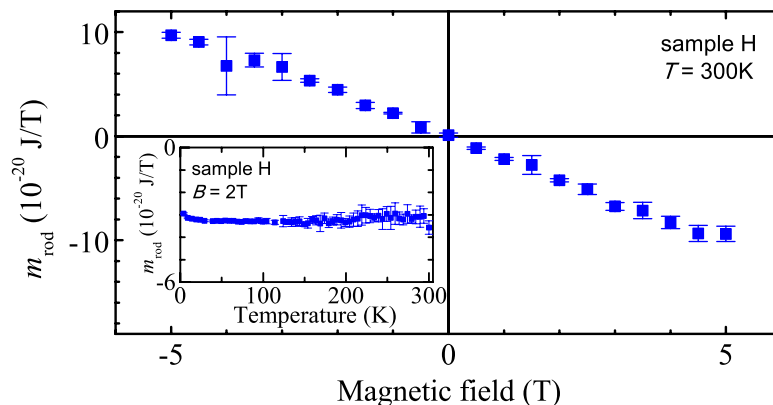
Figure 1.4: Extracted from [40]. Magnetization M of ensembles of gold nanoparticles synthesized using the Brust method, as a function of the applied magnetic field H at two different temperatures (300 K and 5 K). (a) Nanoparticles capped with dodecane alkyl chains, displaying a negative slope (diamagnetic) (b) Nanoparticles capped with tetraoctyl ammonium chains, displaying a hysteresis loop (ferromagnetic).

sign, the susceptibility at low temperature was reported to be about three orders of magnitude larger in absolute value than the susceptibility of bulk gold $|\chi_{\text{Au}}|$.

In 2004, P. Crespo et al. [40] studied ensembles of gold nanoparticles of about 1 to 2 nm in diameter capped with different thiol ligands. Two different magnetic responses were reported. One of the samples, shown in fig. 1.4a was diamagnetic with a slope of about 3 times the diamagnetic susceptibility of bulk gold. The second sample, in fig. 1.4b, showed signs of ferromagnetism, displaying a considerable hysteresis loop at 5 K. The stark contrast of the two samples was ascribed to the different ligands, while the interactions between nanoparticles were considered negligible. The possibility of magnetic impurities in the samples was also discarded, as quite surprisingly, further experiments showed that adding ferromagnetic impurities to the thiol-capped samples reduced the ferromagnetic response [41].



(a) Different TEM micrograph showing the different samples of gold nanorods.



(b) Magnetic moment per gold nanorod at room temperature as a function of the applied magnetic field displaying a negative slope (diamagnetic). Inset: Magnetic moment per gold nanorod for fixed B as a function of temperature.

Figure 1.5: Extracted from [42].

The most impressive example of diamagnetic response is found in ref. [42]. Instead of spherical nanoparticles, P.G. van Rhee et al. studied the behavior of single crystalline gold nanorods with dimensions larger than 5 nm and up to 73 nm in length, displayed in fig. 1.5a. The magnetic susceptibility of some of the ensembles reached $14\chi_{\text{Au}}$. The magnetic moment of each nanoparticle shows a negative slope (diamagnetism), as seen in fig. 1.5b and was extracted by taking into account the degree of alignment of the nanorods which was observed optically. Contrary to previous experiments that showed a paramagnetic magnetization, the magnetic moment of the nanorods was independent of the temperature. In this case the nanorods were coated with either cetyl trimethylammonium bromide (CTAB) or thiolated polyethylene glycol (mPEG-SH), claiming that these ligands do not contribute to the magnetic response.

The experimental results above-discussed represent a small fraction of more than a decade of research, dedicated to understand the diversity of response in gold nanoparticles.⁹ Paramagnetic [34–39, 44–47], diamagnetic [38, 40, 42, 44, 48] and fer-

⁹Ferromagnetic and Curie's law behavior (paramagnetism) has also been observed in ensembles of

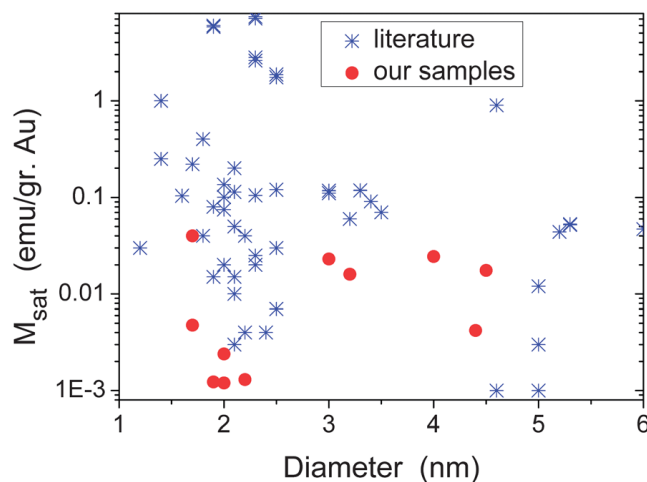


Figure 1.6: Extracted from [16]. Saturation magnetization of different samples. The set of blue dots is the compilation of values from literature. Red dots are the values obtained by the authors.

romagnetic [40, 41, 44, 45, 48–55] ensembles have been found when gold nanoparticles and their functionalizing agents have been probed with all kinds of available experimental techniques (these include ESR [34, 48], X-ray techniques [37, 40, 45], nuclear magnetic resonance [56, 57], muon spin relaxation [51], neutron scattering [53] and Mössbauer spectroscopy [52]). As ferromagnetism is present in other ensembles of non-metallic nanoparticles, some authors have even wondered if ferromagnetism is just a universal feature of inorganic nanoparticles [58], but agreed that more research on this mechanism is needed.

Since the experimentally-reported magnetic moments per nanoparticle are generally small, only the magnetization of an ensemble can be measured. Most of the measurements of the magnetization are performed using superconducting quantum interference devices (SQUID). Great attention has to be paid in order to avoid spurious sources of magnetism in the measurements from SQUID magnetometers [59, 60]. Some experiments even needed to be revised, as impurities contributing to the magnetic response were initially overlooked [61]. Ideally, one would hope to eventually measure the magnetization of a single gold nanoparticle; the use of magnetic force microscopy (MFM), spin-polarized tunnel microscopy (SP-STM) and nanoSQUIDS have been suggested for this purpose [17, 62].

An extensive review on the subject [16, 17] found no clear dependence in temperature, capping agents, or sizes and lack of reproducibility. The compilation of several measurements does not show a clear pattern as illustrated in fig. 1.6. Some experiments can even replicate the three types of magnetism by slightly modifying the chemical preparation [44]. Other publications have even found ferromagnetic behav-

silver nanoparticles [43]. Other non-magnetic metallic nanoparticles present a similar magnetic behavior but gold remains the most studied case.

ior in ensembles of bare gold nanoparticles [63].¹⁰ A dependence of the magnetic response on the spatial configuration of the nanoparticles in the ensemble has also been suggested [49].

1.3 THEORETICAL HYPOTHESES AND ORBITAL MAGNETISM

Several phenomenological mechanisms have been put forward to explain the intriguing magnetic properties of gold nanoparticles. It was proposed that the ferromagnetic response could result from modified Hund rules [38], from a Fermi-hole effect where an electron that forms a covalent bond with the functionalizing agent leaving a hole in the surface which create an spin imbalance and spin polarization [37, 38, 40, 64], or from giant electron orbits circling around single domains of ligands under spin-orbit interaction [65].

Experimental claims of superconductive metallic nanoparticles have been a source of controversy [66]. However, superconducting fluctuations that persist at temperatures which are orders of magnitude above the critical temperature were shown to result in a large diamagnetic response [67], which is still one to two orders of magnitude smaller than the one reported in the experiments of ref. [42].

These above-mentioned interpretations do not seem to explain all of the observed experimental features and are thus challenged in the literature [16, 17]. Moreover, the role of the molecules surrounding the nanoparticles in most experiments is unclear [16].

The diversity of the experimentally-observed behaviors (see refs. [16, 17]), as well as the distinct theoretical proposals, calls for a systematic study of the magnetic properties of gold nanoparticles.

An alternative interpretation of the unusual magnetic properties of ensembles of gold nanoparticles suggests that they arise from the orbital component of the electron wave function [42, 55]. The investigation of finite-size corrections, including experiments on small metal clusters and different theoretical approaches [22, 68–70], shows that the effect of confining a moderate number of electrons to a finite volume introduces a new energy scale in the problem (the mean level spacing) and leads to modifications of the Landau susceptibility.¹¹

Orbital magnetism has been experimentally and theoretically studied in previous works done in the mesoscopic regime of systems small enough and/or sufficiently cooled down to exhibit the effects of quantum coherence. In the case of multiply connected geometries, when a magnetic flux pierces a metallic [2, 71] or semiconducting [72] ring, the orbital response translates into a dissipationless persistent current [73],

¹⁰The problem with bare nanoparticles is that it is sometimes unclear whether the nanoparticles aggregate [16].

¹¹The effects on the Pauli spin susceptibility are smaller as the confinement mainly modifies the orbital wavefunction.

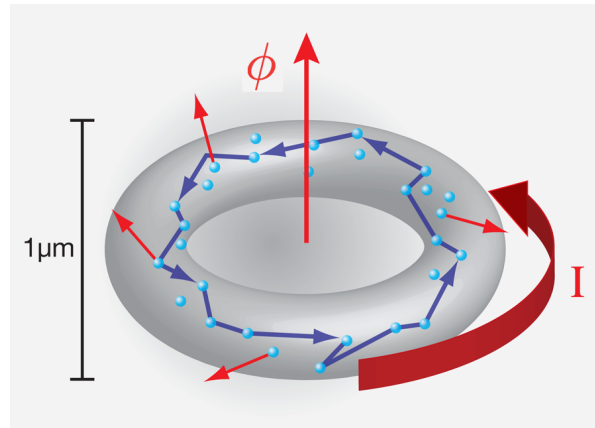


Figure 1.7: Adapted from [74]. Sketch of a resistive metallic ring, smaller than the electron coherence length. At fixed magnetic flux ϕ , a persistent current I is induced around the ring, and it does not get dissipated by the scattering from impurities in the metal.

as sketched in fig. 1.7. When the unavoidable disorder present in these systems becomes weak enough to result in an elastic mean free path of the order of the sample size, the transition from a diffusive to a ballistic regime is achieved. The sustained theoretical interest in the problem of persistent currents during the 1990's clarified the role of disorder, electron-electron interactions, and the consequences of a finite number of electrons determining the thermodynamic functions. The use of the canonical ensemble appeared as unavoidable, [75, 76] and a proper treatment of electron-electron interactions led to an orbital response of the same order of magnitude as that of noninteracting systems, in both the diffusive [77–79] and the ballistic cases [80]. Later experiments [81], using a nanomechanical detection of persistent currents in normal-metal rings, have validated the results of such mean-field approaches.

In the case of singly-connected geometries, the magnetic susceptibility of an ensemble of two-dimensional quantum dots has been experimentally [82] and theoretically [83–85] studied. In the ballistic regime, a semiclassical approach made it possible to obtain the orbital response from the magnetic field dependence of the density of states induced by the accumulated flux of the classical periodic trajectories. Interesting differences were predicted according to the chaotic or integrable nature of the two-dimensional underlying classical dynamics determined by the shape of the quantum dot boundaries. The orbital contribution to the magnetic susceptibility in an integrable dot can be diamagnetic or paramagnetic, and with typical values which are orders of magnitude larger than the two-dimensional Landau susceptibility [84]. Chaotic dynamics results in somehow smaller values of the susceptibility [86]. When moving from a single quantum dot to an ensemble of dots, the average magnetic susceptibility was shown to be paramagnetic, and smaller than the typical values of the individual case but still much larger than the bulk value [85]. Similarly to the case of persistent currents, the inclusion of weak disorder [87, 88] or electron-electron

interactions [89] did not considerably alter the clean, noninteracting results.

Toward the goal of understanding the electronic contribution to the magnetic response of metallic nanoparticles, we develop in this thesis a microscopic theory, in order to gauge the contribution of the orbital magnetism proposal to account for the experimental results of the magnetic response of ensembles of metallic nanoparticles. In particular, we try to identify the relevant parameters of experimental interest, focusing on the temperature and size dependences of the magnetization and establishing in which cases a comparison with the experimental data can be attempted. Our study of orbital magnetism in metallic nanoparticles builds on the above mentioned work done in the mesoscopic regime. These investigations are described in detail in chapter 3. One of the key results is that the magnetization of an ensemble of metallic nanoparticles could present a paramagnetic response coming from the orbital magnetic contribution. Additional ingredients are still necessary at this stage, in order to explain other kinds of magnetic responses. In particular, the spin-orbit coupling has been invoked to be responsible of the large diamagnetism measured in an ensemble of gold nanorods (as in fig. 1.5b) [42, 90]. The role of spin-orbit coupling towards an interpretation of a diamagnetic behaviour motivates the work presented in chapter 4 and the introduction of some basic concepts follows in the next section.

1.4 EFFECTS OF THE SPIN-ORBIT COUPLING IN CONFINED ELECTRON SYSTEMS

The spin-orbit coupling (SOC) is a relativistic effect having a decisive role in certain electronic properties of unconfined and confined condensed matter systems.

In its standard form, the spin-orbit (so) Hamiltonian reads

$$\mathcal{H}^{(\text{so})} = \frac{e\hbar}{4m^2c^2} \boldsymbol{\sigma} \cdot [\mathbf{E}(\mathbf{r}) \times \mathbf{p}], \quad (1.6)$$

where \hbar is Planck's reduced constant, c is the speed of light, \mathbf{r} is the position vector, and $\boldsymbol{\sigma} = \sigma_x \hat{e}_x + \sigma_y \hat{e}_y + \sigma_z \hat{e}_z$ is the vector of Pauli matrices,¹² such that the spin angular momentum operator writes $\mathbf{S} = \hbar \boldsymbol{\sigma} / 2$. The spin-orbit coupling yields a contribution

¹²The three Pauli matrices are defined as

$$\sigma_x = \begin{bmatrix} 0 & 1 \\ 1 & 0 \end{bmatrix}, \quad (1.7a)$$

$$\sigma_y = \begin{bmatrix} 0 & -i \\ i & 0 \end{bmatrix}, \quad (1.7b)$$

and

$$\sigma_z = \begin{bmatrix} 1 & 0 \\ 0 & -1 \end{bmatrix}. \quad (1.7c)$$

to the fine-structure of atomic spectra which is of the same order than those arising from other weakly-relativistic corrections, namely the kinetic energy and Darwin terms [91], that will be introduced in chapter 2.

At the fundamental level, the spin–orbit coupling is important because it alters the symmetry properties of the electronic Hamiltonian. A celebrated example of spin–orbit influence on the electronic dynamics is the departure from weak localization to anti-weak localization observed in the electronic transport through metallic films [92] or ballistic quantum dots at a semiconductor heterojunction [93, 94]. In ferromagnetic materials the spin–orbit coupling underlines the phenomena of magnetic anisotropy and the anomalous Hall effect [95]. The domain of spintronics addresses numerous cases where the spin–orbit coupling influences spin dynamics and spin relaxation [96–98].

In the domain of nanostructures, the tunneling resonances of disordered metal nanoparticles and the magnetic response of an ensemble of metallic nanoparticles are two examples of physical properties depending on the level statistics of a confined system, and thus on the spin–orbit coupling.

In the first case, the extracted g -factor of the discrete energy levels was found [99, 100] to be below the free-electron value of $g_0 = 2$. Such a reduction could be explained by the fact that the energy eigenstates in the presence of spin–orbit coupling, not being purely spin up or spin down, respond more weakly to an applied magnetic field than pure spin states [101, 102]. The statistical distribution of the g -factors has been obtained from random matrix theory, using the spin-orbit scattering rate as a phenomenological parameter in order to describe the transition between statistical ensembles [103, 104].

In the second case, the zero-field susceptibility averaged over a nanoparticle ensemble is determined [75, 76] by the magnetic field dependence of the variance in the number of energy levels below the chemical potential. Therefore, in the disordered or chaotic regimes, the ZFS depends on the transition between statistical ensembles driven by the influence of the spin–orbit coupling.

In the previously presented cases (the tunneling resonances of disordered metal nanoparticles and the magnetic response of an ensemble of metallic nanoparticles) the strength of the spin–orbit coupling is a key parameter that needs to be determined by microscopic theories. Towards this goal, the main source of spin–orbit coupling must be identified. The genesis of the spin–orbit coupling for the conduction electrons of a metallic nanoparticle lies in the existence of an inhomogeneous electrostatic potential, which may have an intrinsic origin (the host ionic lattice) or an extrinsic origin (impurities or the confining potential). Since gold is a heavy atom, spin–orbit coupling plays an important role in its band structure [105], but the effect for the conduction electrons is mainly seen by the Bloch part of the wave function, while the smooth part remains unaffected. This observation is consistent with the g -factor $g_{\text{Au}} = 2.1$ measured by electron spin resonance in macroscopic gold samples [106]. Impurities have been invoked to be responsible for the spin–orbit coupling of Ag nanoparticles intentionally doped with Au [99], but they are expected to play a lesser role in the ballistic nanoparticles where the magnetic susceptibility has been measured. In this last setup,

the electronic confinement remains as the chief source of spin–orbit coupling. The effect of this latter mechanism in the ZFS is the goal of chapter 4, where we analyze model systems of noninteracting electrons with two different kinds of confinement, making the link with experimentally relevant cases of metallic nanoparticles.

1.5 OUTLINE

We close this introduction with a brief summary of the remaining chapters.

In chapter 2, we discuss the theoretical formalism that allows us to carry out the analytical and semi-analytical calculations. In this chapter we introduce key aspects of the non-relativistic and weakly relativistic Hamiltonians, as well as the thermodynamical framework. Semiclassical treatment of the spherical confinement and quantum perturbation theory are also included there.

In chapter 3 we tackle the orbital magnetic response of single and ensembles of metallic nanoparticles employing semiclassical techniques. The grand canonical as well as the canonical contributions to the magnetic response are treated in this chapter. The magnetic response of ensembles of non-interacting nanoparticles is obtained under consideration of a smooth size distribution, and the limit of low temperatures/small sizes is discussed. We contrast and discuss the agreement of our approach with the observed magnetization of ensembles of gold nanoparticles presented in fig.1.3b and exhibiting a large paramagnetic response.

In chapter 4, we concentrate our theoretical study on the role of spin–orbit coupling (SOC) in the presence of confinement in order to derive its contribution to the magnetic response of single spherical nanoparticles. We gauge the SOC contribution against the corrections generated other weakly relativistic effects. Based on a perturbative treatment of the magnetic field we recover semi-analytical and semiclassical expressions that allows us to compare the different contributions. We also discuss in this chapter the case of half-sphere-shaped nanoparticles and the role of the reduction of spatial symmetry of the potential. In the case of the half-sphere we develop a numerical treatment.

Finally, we summarize our results and discuss the perspectives of this thesis in chapter 5. Extended calculations are presented in detail in appendices A to J.

MODEL AND THEORETICAL FORMALISM

2

With the motivation for our work presented in chapter 1, we now discuss the theoretical tools to describe the confinement of electrons in a nanoparticle and the thermodynamic formalism that will allow us to describe the magnetic response of finite systems, together with our approach to include the weakly relativistic effect. This chapter starts with a brief discussion of the basic assumptions made in this thesis and with a description of our nanoparticle modeling in sec. 2.1. Specific details of the considered spherical confinement are discussed in section 2.2, which will be the basis for our quantum and semiclassical approaches. In section 2.3 we discuss the quantum perturbation theory and the semiclassical expansion of the free energy needed to obtain the magnetic response of confined systems. We end this chapter with section 2.4 where we discuss the weakly relativistic limit of Dirac's equation yielding the corresponding corrections, including the spin-orbit coupling.

2.1 NANOPARTICLE MODELING

To model gold nanoparticles, we will mainly consider spherical nanoparticles with radius a between a few nanometers and a few tens of nanometers.¹

In order to take into account the effect of the ionic background, we use the jellium approximation [107], where electron-electron interactions are studied at a mean-field level. The resulting self-consistent confining potential is approximated by an electric static potential well with hard walls, thus neglecting the smoothness at the edges and the effects of the spill-out, describing the nonzero probability to find an electron density outside the nanoparticle.

We will describe the spin-degenerate s band and ignore the specificities of the electronic structure of noble metals. Indeed, the band structure of bulk gold indicates that the valence electrons can be treated as conduction electrons with a parabolic dispersion relation [105] with an effective mass which is close to the bare electron mass. Within such an approximation, we choose for our discussion the parameters corresponding to gold nanoparticles, as this case has covered most of the experimental effort. However, most of our results are suited for noble and alkaline metals.

It has been suggested that the ligands that are attached to the nanoparticles in most experiments may play a role in the magnetic response for specific cases [37, 40, 44, 46]. However, for certain protective agents [16, 17] it has been argued that the ligands

¹In chapter 4 we also discuss the case of half-spherical nanoparticles.

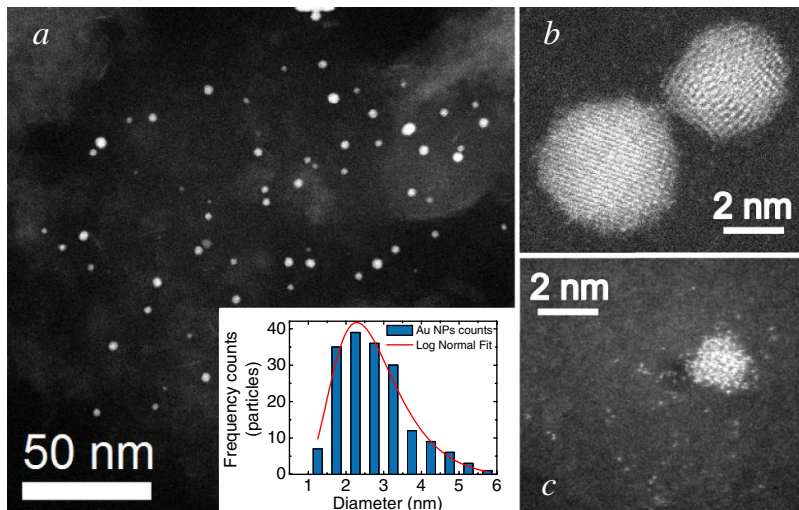


Figure 2.1: Extracted from [46]. TEM micrography of samples of gold nanoparticles (in white). Panel (a) shows nanoparticles after sonication to disperse the nanoparticles. Panel (b) shows a close up on two crystalline nanoparticles. Panel (c) is a close up on a cluster (few atoms), the smaller dots in the picture are single gold atoms. These pictures are used to determine the size distribution of the nanoparticles, indicated in the inset of panel (a).

do not play a role in the magnetic response produced by itinerant electrons and ferromagnetic responses after chemically removing the ligands from the nanoparticles has also been reported [54, 108]. In this work we will ignore the ligands and their possible influence on magnetic properties.

In the experiments, the nanoparticles in macroscopic assemblies exhibit a statistical dispersion of their radius. Transmission electron microscopy is used to perform the statistics from an extracted portion of the synthesized gold nanoparticles, see fig. 2.1. The probability density function $\mathcal{P}(a)$ is a key element in the characterization of the magnetic response of the ensemble. Often a log-normal or a Gaussian distribution are good approximations to the experimentally-observed distribution [37, 46, 48, 49, 55, 109]. However other distributions, like bimodal distributions [40] can be sometimes obtained with the same fabrication procedure. Additionally, shell effects are known to result in selective abundance spectra [1, 110] and might thus lead to sharp multiply-peaked size distributions that could be hard to discriminate. Additionally, the dispersion and the mean radius can take diverse values in experiments. We will keep the function $\mathcal{P}(a)$ non-fixed while developing our formalism, and then discuss its relevance according to different set-ups.

The Zeeman spin splitting under a magnetic field results, in the metallic case, in the Pauli susceptibility $\chi_P = -3\chi_L$. Since the mesoscopic corrections to the bulk result have been shown to be negligible [83], and since the observed effects on the zero-field susceptibility are typically much larger than $|\chi_L|$, we will postpone the inclusion of

this contribution in this section, and discuss it in the presence of spin–orbit coupling and other weakly relativistic effects in sec. 2.4.

As in experiments, we will consider a range of temperatures that span all values from cryogenic to room temperature.

Each spherical nanoparticle contains N valence electrons with charge $-e < 0$ and mass m . The mean distance between electrons is given by the Wigner-Seitz radius $r_s = (3/4\pi n_e)^{1/3}$ and relates the number of electrons to the nanoparticle radius, such that $a = r_s N^{1/3}$ [110], where n_e is the electronic density.

The nanoparticles are subjected to an external, static, and homogeneous magnetic induction $\mathbf{B} = \nabla \times \mathbf{A}$, with \mathbf{A} the associated vector potential. Within the jellium approximation [107], the orbital contribution of the Hamiltonian for the valence electrons in an individual nanoparticle (whose center is located at the coordinate origin) reads

$$\mathcal{H} = \sum_{i=1}^N \left\{ \frac{1}{2m} \left[\mathbf{p}_i + \frac{e}{c} \mathbf{A}(\mathbf{r}_i) \right]^2 + U(r_i) \right\} + \frac{1}{2} \sum_{\substack{i,j=1 \\ (i \neq j)}}^N V(\mathbf{r}_i, \mathbf{r}_j). \quad (2.1)$$

Here, c is the speed of light, while $\mathbf{r}_i = x_i \hat{e}_x + y_i \hat{e}_y + z_i \hat{e}_z$ (written in Cartesian coordinates) and \mathbf{p}_i are the position and momentum of the i th electron, respectively. In eq. (2.1), U denotes the single-particle confinement potential, which, for a spherically symmetric alkaline nanoparticle in vacuum, reads as

$$U(r) = \frac{Ne^2}{2a^3} (r^2 - 3a^2) \Theta(a - r) - \frac{Ne^2}{r} \Theta(r - a), \quad (2.2)$$

i.e., it is harmonic inside the nanoparticle and Coulombic outside. In eq. (2.2), $\Theta(z)$ denotes the Heaviside step function. Finally, V represents in eq. (2.1) the Coulomb interaction amongst electrons in the nanoparticle. In the symmetric gauge where $\mathbf{A}(\mathbf{r}) = \frac{1}{2} \mathbf{B} \times \mathbf{r}$, and choosing the z axis of the coordinate system in the direction of \mathbf{B} , the many-body (mb) Hamiltonian (2.1) can be rewritten in the form

$$\mathcal{H}^{(\text{mb})} = \sum_{i=1}^N \left[\frac{p_i^2}{2m} + U(r_i) + \frac{\omega_c}{2} L_{z,i} + \frac{m\omega_c^2}{8} (x_i^2 + y_i^2) \right] + \frac{1}{2} \sum_{\substack{i,j=1 \\ (i \neq j)}}^N V(\mathbf{r}_i, \mathbf{r}_j), \quad (2.3)$$

where $\omega_c = eB/mc$ is the cyclotron frequency, $\mathbf{B} = B \hat{e}_z$, and $L_{z,i}$ denotes the z component of the angular momentum of the i -th electron.

We will treat (2.3) within the mean-field approximation. Density functional theory calculations [111–113], indicate that in the absence of a magnetic field, the self-consistent mean-field potential can be approximated by

$$V_{\text{mf}}(r) = V_0 \Theta(r - a), \quad (2.4)$$

where $V_0 = E_F + W$, with E_F and W the Fermi energy and the work function of the considered nanoparticle, respectively. Within these approximations, we are left with

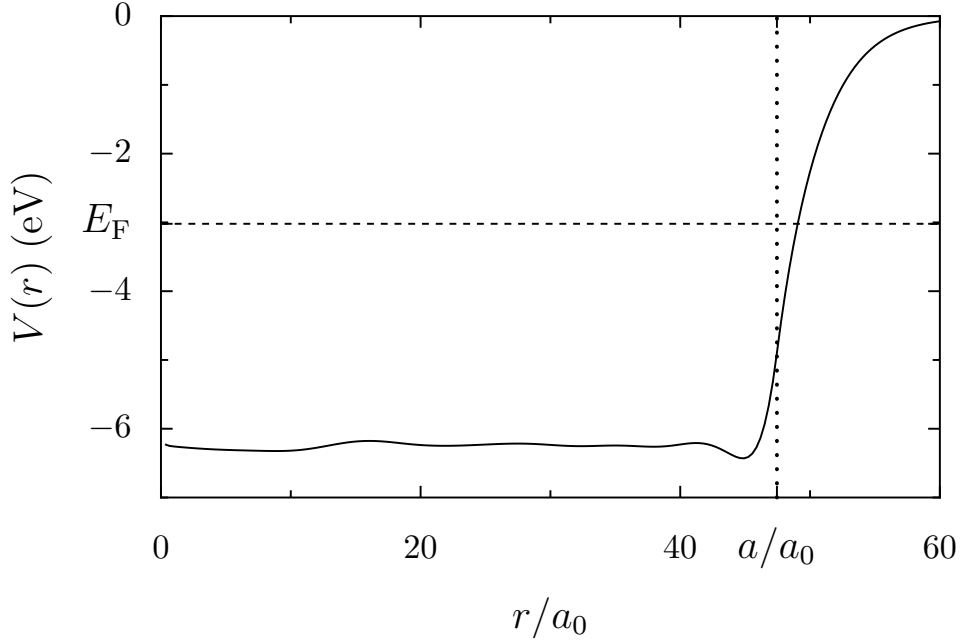


Figure 2.2: Adapted from [112]. Radial profile of the mean-field potential $V_{\text{mf}}(r)$ for a sodium nanoparticle ($N = 1760$), calculated in the framework of local density approximation (LDA). Here E_{F} (dashed line) indicates the Fermi energy and $a_0 \approx 0.5 \text{ \AA}$ is the Bohr radius.

the effective mean-field Hamiltonian

$$\mathcal{H}^{(\text{mf})} = \sum_{i=1}^N \left[\frac{p_i^2}{2m} + V_{\text{mf}}(r_i) + \frac{\omega_c}{2} L_{z,i} + \frac{m\omega_c^2}{8} (x_i^2 + y_i^2) \right] \quad (2.5)$$

corresponding to N independent electrons in a spherical billiard threaded by a static magnetic induction in the z direction. In fig. 2.2, we present an example of a mean-field confining potential obtained from density functional calculations.

For very small metallic nanoparticles (or clusters) the corrections to the ionic structure have been approached by the use of pseudopotential perturbation theory as a multipole expansion [114] and the effect of surface irregularities and the underlying crystalline lattice has been addressed with numerical methods [115, 116]. The influence of smooth disorder in low-dimensional systems has been addressed with the help of semiclassical methods [87, 88]. We will leave aside the case of very small nanoparticles while neglecting the effect of surface and/or bulk disorder, and we will then not be concerned with such corrections.

One expects that the spherical well shape of the mean-field potential remains a good approximation in the presence of a magnetic field, provided that $\hbar\omega_c$,² the energy scale set by the magnetic field, is the smallest one of the problem [117, 118].

²Using the bare mass, $\hbar\omega_c/B = 0.012 \mu\text{eV/G}$.

Since the magnetization is a property of the many-body ground state, it involves only one-body states up to the vicinity of the Fermi level.³ Thus, states that are higher in energy do not contribute to the magnetization. We can then safely assume that the height of the mean-field potential $V_0 \rightarrow \infty$.

It is important to realize that any realistic magnetic fields that are experimentally available are such that the classical trajectories of the electrons in the spherical billiard are very close to straight lines on the scale of the nanoparticle diameter. In other words, the corresponding cyclotron radius $R_c = v_F/\omega_c$ (v_F is the Fermi velocity) is much larger than the size of the nanoparticles we consider.⁴

Another effect to take into account when treating metallic nanoparticles is the Larmor diamagnetic response of the core electrons, which are not considered in the idealized model. While the effect of the core electrons on the ZFS is not altered by the confinement, its contribution must be confronted with the corrections under study in order to gauge the relevance of the latter.

The axial symmetry of the magnetic-field dependent Hamiltonian around the z -axis (2.5) greatly facilitates its quantum-mechanical resolution. Furthermore, if we are only interested in the weak-field magnetic response, a perturbative approach can be implemented. Such a scheme has been successfully used in order to explain the magnetic response of very small metal clusters [22, 68, 69]. In our case, it is important to develop simpler approaches than the full quantum calculation, towards treating larger cluster sizes, efficiently incorporating the restriction of a fixed number of electrons within the nanoparticles, and calculating the thermodynamic functions at finite temperature.

2.2 ELECTRONS UNDER SPHERICAL CONFINEMENT

Our nanoparticle modeling within the jellium approximation describes the confinement of non-interacting electrons by a spherical potential. In order to address the magnetic response of these nanoparticles, we need the magnetic-field dependence of the energy spectrum. Such a task can be pursued with a quantum perturbative approach starting with the zero-field eigenstates of the sphere, or with a semiclassical expansion of the density of states in terms of classical periodic orbits. In this section we present the two above mentioned paths (sections 2.2.1 and 2.2.2) upon which we will build the results of this thesis. A brief description of the treatment of the purely classical spherical billiard can be found in appendix B.2. The treatment of a fully relativistic spherical confinement under finite step potential has analytical solutions [119] and has been used to develop quark bag models in high energy physics [120], but it can lead to some delicate issues in the case of hard walls [121, 122].

³This statement is, strictly speaking, valid for temperatures much smaller than the Fermi temperature. As we are dealing with metals, this condition is fulfilled in all experimentally-relevant situations.

⁴ $R_c = \frac{7.6}{B} \text{G} \cdot \text{cm}$ for gold. Other relevant parameters for gold are $E_F = 5.5 \text{ eV}$, the Fermi temperature $T_F = 6.4 \times 10^4 \text{ K}$, and the Fermi wave vector $k_F = 1.2 \times 10^8 \text{ cm}^{-1}$.

2.2.1 EIGENVALUES AND EIGENSTATES

For a single valence electron, the most general non-relativistic (nr) Hamiltonian is given by

$$\mathcal{H}^{(\text{nr})} = \mathcal{H}^{(\text{orb})} + \mathcal{H}^{(Z)}, \quad (2.6)$$

with

$$\mathcal{H}^{(Z)} = g \frac{\mu_B}{\hbar} \mathbf{S} \cdot \mathbf{B}. \quad (2.7)$$

The two terms in (2.6) represent, respectively, the spin-independent Hamiltonian associated with the orbital motion (orb), and the Zeeman energy of the spin in the magnetic field (Z) where g is the g -factor. The origin of $\mathcal{H}^{(Z)}$ will be discussed in section 2.4.2.

The spin-independent term $\mathcal{H}^{(\text{orb})}$ comes from by the mean-field Hamiltonian of eq. (2.5), describing the electron orbital motion, which can be written as

$$\mathcal{H}^{(\text{orb})} = \mathcal{H}^{(0)} + \mathcal{H}^{(\text{para})} + \mathcal{H}^{(\text{dia})}, \quad (2.8)$$

with

$$\mathcal{H}^{(0)} = \frac{\mathbf{p}^2}{2m} + V_{\text{mf}}(\mathbf{r}), \quad (2.9a)$$

$$\mathcal{H}^{(\text{para})} = \frac{\omega_c}{2} L_z, \quad (2.9b)$$

$$\mathcal{H}^{(\text{dia})} = \frac{m\omega_c^2}{8} (x^2 + y^2). \quad (2.9c)$$

Here $\mathcal{H}^{(0)}$ is the zero-field Hamiltonian describing a spinless particle in the confining potential, while the terms $\mathcal{H}^{(\text{para})}$ and $\mathcal{H}^{(\text{dia})}$ are defined for calculational convenience and represent paramagnetic and diamagnetic contributions, respectively.

The quantum states of our Hamiltonian (2.6) in the absence of magnetic fields are described by a product basis with the set $\{\lambda\} = \{n, l, m_z, m_s\}$ of quantum numbers, with $n > 0$ the principal quantum number, $l \geq 0$ the azimuthal quantum number, $m_z \in [-l, l]$ the magnetic quantum number, and $m_s = \pm 1/2$ associated with the spin component along the z direction. The corresponding wave functions are given by the two-component spinors

$$\Psi_{n,l,m_z,+\frac{1}{2}}^{(0)}(\mathbf{r}) = \psi_{n,l,m_z}^{(0)}(\mathbf{r}) \begin{bmatrix} 1 \\ 0 \end{bmatrix}, \quad (2.10a)$$

$$\Psi_{n,l,m_z,-\frac{1}{2}}^{(0)}(\mathbf{r}) = \psi_{n,l,m_z}^{(0)}(\mathbf{r}) \begin{bmatrix} 0 \\ 1 \end{bmatrix}, \quad (2.10b)$$

where the orbital wave function can be written in spherical coordinates (r, θ, φ) ⁵ as

$$\psi_{n,l,m_z}^{(0)}(\mathbf{r}) = R_{n,l}(r) Y_l^{m_z}(\vartheta). \quad (2.11)$$

⁵Here $r = \sqrt{x^2 + y^2 + z^2} \geq 0$ is the radial coordinate, $0 \leq \theta \leq \pi$ is the polar angle defined from the z -axis and $0 \leq \varphi < 2\pi$ is the azimuthal angle.

We note $Y_l^{m_z}(\vartheta)$ the spherical harmonic of degree l and order m_z as a function of the solid angle $\vartheta = (\theta, \varphi)$, while $R_{n,l}(r)$ stands for the associated radial wave function and $E_{n,l} = E_0(k_{n,l}a)^2$ is the corresponding eigenenergy, with $E_0 = \hbar^2/2ma^2$.

For the confining potential (2.4), $R_{n,l}(r)$ can be expressed in terms of Bessel functions (see appendix G.1). In the limiting case of a hard-wall potential ($V_0 \rightarrow \infty$), according to eq. (G.6a), the eigenenergy of the m_z and spin-degenerate states characterized by the quantum numbers l and n is

$$E_{n,l}^{(0)} = E_0 \zeta_{n,l}^2, \quad (2.12)$$

where $\zeta_{n,l}$ is the n th root of the spherical Bessel function of the first kind $j_l(\zeta)$, while

$$R_{n,l}(r) = \sqrt{\frac{2}{a^3}} \frac{j_l(\zeta_{n,l} r/a)}{|j_{l+1}(\zeta_{n,l})|}. \quad (2.13)$$

The states $\Psi_{n,l,m_z,m_s}^{(0)}$ are no longer eigenstates once the diamagnetic term $\mathcal{H}^{(\text{dia})}$ of eq. (2.9c) is considered under a finite magnetic field. Since this term is quadratic in B , we will treat $\mathcal{H}^{(\text{dia})}$ by first-order perturbation theory in sec. 2.3.2 (see also appendix C).

2.2.2 SEMICLASSICAL DENSITY OF STATES OF A SPHERICAL BILLIARD

A detailed knowledge of the quantum spectrum, as in eq. (2.12), is more than what we need to describe the thermodynamical properties of nanoparticles. It would be useful to approximate the spectrum to some continuous function. Let us introduce the single-electron density of states, given by

$$\varrho(E, B) = \sum_{\{\lambda\}} \delta(E - E_\lambda(B)), \quad (2.14)$$

where $\delta(\zeta)$ is the Dirac delta function, and the sum runs over all eigenenergies E_λ , labeled by the quantum numbers $\{\lambda\}$ of the system.

In the semiclassical approximation, the density of states ϱ from eq (2.14) can be decomposed in what is called a trace formula [123]

$$\varrho = \bar{\varrho} + \varrho^{\text{osc}}, \quad (2.15a)$$

where $\bar{\varrho}$ represents the smooth part (or Weyl term) given by the phase-space volume enclosed by the constant- E manifold, and the oscillating part (osc) has the form

$$\varrho^{\text{osc}} = \sum_{\Lambda} A_{\Lambda} \cos(S_{\Lambda}(E)/\hbar + \lambda_{\Lambda}), \quad (2.15b)$$

as a sum over classical periodic trajectories $\{\Lambda\}$. The index Λ labels isolated periodic orbits or families of degenerate periodic orbits for the case of chaotic or integrable

systems, respectively. S_Λ is the classical action, the amplitude A_Λ admits different expressions in chaotic or integrable cases, and the Maslov index λ_Λ counts the number of conjugate points of the periodic orbit. This decomposition is always possible in the semiclassical limit $\hbar \rightarrow 0$ [88].

For example, the Gutzwiller trace formula [123], applicable in the chaotic case, can be built from Feynman's path integral formulation of quantum mechanics by applying a stationary phase condition.

In order to derive the appropriate semiclassical thermodynamic formalism, we need to construct ρ^{osc} and its \mathbf{B} dependence, for a spherical confining potential. In the absence of a magnetic field, for such an integrable and highly symmetric setup, the trajectories are degenerate and the Gutzwiller formula is not applicable. The density of states follows from the Wentzel–Kramers–Brillouin (WKB) quantization condition [124–126] applied to the three-dimensional spherical confining potential. Alternatively, ρ can also be obtained from a one-dimensional semiclassical approximation for the quantum radial problem. It is straightforward to show the equivalence between these two approaches [111, 125, 126]. In the absence of magnetic field and neglecting the modulations due to spin, the oscillating part of the density of states is given by

$$\rho^{\text{osc}}(E, 0) = \frac{4}{E_0} \sqrt{\frac{ka}{\pi}} \sum_{\nu=1}^{\infty} \sum_{\eta=2\nu+1}^{\infty} \frac{(-1)^\nu \cos \varphi_{\nu\eta} \sin^{3/2} \varphi_{\nu\eta}}{\sqrt{\eta}} \cos(\theta_{\nu\eta}(k)), \quad (2.16)$$

where $k = \sqrt{2mE}/\hbar$ is the wavevector. The topological indexes $\Lambda = (\nu, \eta)$ label the families of classical periodic orbits lying on the equatorial plane of the sphere, with ν the number of turns around the center (i.e. the winding number) and η the number of specular reflections at the boundary (i.e. the number of bounces), the quantity $\varphi_{\nu\eta} = \pi\nu/\eta$ corresponds to half the angle spanned between two consecutive bounces. The classical trajectories describe regular polygons and star polygons in the plane of motion, illustrated in fig. 2.3.

The length of the trajectory (ν, η) is given by $L_{\nu\eta} = 2\eta a \sin \varphi_{\nu\eta}$. We further defined in eq. (2.16) the k -dependent phase $\theta_{\nu\eta}(k) = kL_{\nu\eta} + \pi/4 - 3\eta\pi/2$. The contribution of the diametral orbits (1,2) as it is of higher order in \hbar (see ref. [117]) and is neglected in eq. (2.16), since it leads, small fields, to a field-independent contribution to the density of states that does not contribute to the magnetization. A calculation of eq. (2.16), using Einstein-Brillouin-Kramers (EBK) quantization, is provided in appendix B.

In the presence of weak magnetic fields such that the ratio between the radius a and the cyclotron radius R_c is small, i.e. $a/R_c \ll 1$, the oscillating density of states becomes [117]

$$\rho^{\text{osc}}(E, B) = \frac{4}{E_0} \sqrt{\frac{ka}{\pi}} \sum_{\nu=1}^{\infty} \sum_{\eta=2\nu+1}^{\infty} \frac{(-1)^\nu \cos \varphi_{\nu\eta} \sin^{3/2} \varphi_{\nu\eta}}{\sqrt{\eta}} \cos(\theta_{\nu\eta}(k)) \mathcal{M}_{\nu\eta}^{(\text{orb})}(B), \quad (2.17a)$$

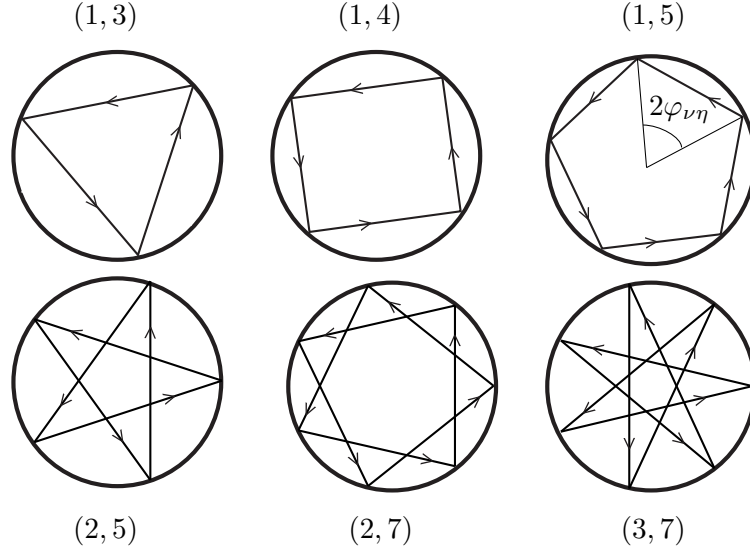


Figure 2.3: Example of families of classical periodic orbits on an equatorial plane of the sphere labeled by the topological indexes (ν, η) , with ν the winding number and η the number of bounces.

where the difference with respect to (2.16) is that each term of the sum carries a field-dependent orbital modulation factor

$$\mathcal{M}_{\nu\eta}^{(\text{orb})}(B) = j_0\left(\frac{2\pi\phi_{\nu\eta}}{\phi_0}\right). \quad (2.17b)$$

We denote the zeroth spherical Bessel function by $j_0(\zeta) = \sin(\zeta)/\zeta$, and the argument includes the flux $\phi_{\nu\eta} = B\mathcal{A}_{\nu\eta}$ enclosed by the orbit (ν, η) covering the area $\mathcal{A}_{\nu\eta} = \frac{1}{2}\eta a^2 \sin(2\varphi_{\nu\eta})$, as well as the flux quantum $\phi_0 = hc/e$. Note that for the small induced fields that we encounter, $B \approx H$ and we will thus treat indistinguishably both fields hereafter. The modulation factor $\mathcal{M}_{\nu\eta}^{(\text{orb})}(B)$ can be obtained by expanding the classical action and integrating over the angles related to the special group of rotations $\text{SO}(3)$ [117]. Appendix B also contains a simplified calculation of eq. (2.17b).

The interest of this semiclassical decomposition (2.15) will be more clear when we discuss the semiclassical thermodynamical approach in sec. 2.3.3.

2.3 THERMODYNAMICAL FORMALISM

We need to make a link between individual electrons and the macroscopic properties that are observed in experiments. As we are interested in macroscopic observable properties, we cannot describe individually the dynamics of every electron in a

nanoparticle, much less the specific dynamics of several electrons in an ensemble of nanoparticles. The emerging large-scale properties related to N (from tens to 10^5) electrons can only be described from a statistical mechanics viewpoint. Here we present the formulation that relates the quantum spectrum of a single electron to the thermodynamical quantities of the ensemble.

Electrons are particles that follow Pauli's exclusion principle (fermions). Two electrons cannot have the same set of quantum numbers. Given a set of quantum numbers $\{\lambda\}$, one has to count every possible allowed configuration by taking into account that electrons are identical and each can occupy a single state. One way to avoid the complicated combinatorics of finite systems is to work in the grand canonical (GC) ensemble suited for a system under thermal equilibrium and allowed to exchange particles with the surroundings.

A nanoparticle is instead a finite system, away from the thermodynamic limit and unable to exchange electrons with a reservoir. To study finite closed systems, it is more adequate to work in the canonical ensemble with a fixed number of electrons at thermal equilibrium. The choice of ensemble is a matter of convenience in the thermodynamic limit where $N, \mathcal{V} \rightarrow \infty$ (with N/\mathcal{V} fixed), yet the difference between the ensembles has been shown [76] to be significative at mesoscopic scales, outside the thermodynamic limit, imposing correction terms to be discussed in the following subsections.

Consider a system of independent electrons inside a volume \mathcal{V} at temperature T under a static magnetic field \mathbf{B} . We write the thermodynamic grand canonical potential Ω as

$$\Omega(T, \mu, \mathbf{B}) = -k_B T \int q(E, \mathbf{B}) \ln \left(1 + e^{-\beta(E-\mu)/k_B T} \right) dE, \quad (2.18)$$

where k_B is Boltzmann's constant, $\beta = (k_B T)^{-1}$, and μ is the chemical potential.

A Legendre transformation allows to obtain the canonical thermodynamic potential or Helmholtz' free energy, given by

$$F(T, N, \mathbf{B}) = \Omega(T, \mu, \mathbf{B}) + \mu N. \quad (2.19)$$

This relation (2.19) is not straightforward to calculate as μ depends implicitly on N . One has to calculate the number of electrons from the grand canonical potential $\Omega(T, \mu', \mathbf{B})$, ie. $N = \frac{\partial \Omega}{\partial \mu} |_{T, \mathcal{V}}$ at different chemical potentials μ' (fixed T and volume \mathcal{V}) in order to find the chemical potential that corresponds to the right number of particles N .

Two approaches to calculate the magnetic response are provided here. Sec. 2.3.1 describes how to calculate the grand canonical contribution from the quantum energy spectrum and sec. 2.3.2 provides an example exploiting quantum perturbation theory. Sec. 2.3.3 describes a semiclassical approach to obtain the magnetic response with finite-size corrections.

2.3.1 MAGNETIC RESPONSE OF CONFINED SYSTEMS: QUANTUM APPROACH

As we have an expression for the grand canonical ensemble (2.18) of an electronic system, we can use it to derive the canonical properties. Analogously to eqs. (1.2) and (1.3), we can define a grand canonical magnetization and a grand canonical ZFS, as given by

$$\mathcal{M}^{(\text{GC})} = - \left(\frac{\partial \Omega}{\partial H} \right) \Big|_{\mu, T} \quad (2.20)$$

and

$$\chi^{(\text{GC})} = \frac{1}{\mathcal{V}} \frac{\partial \mathcal{M}}{\partial H} \Big|_{H=0} = - \frac{1}{\mathcal{V}} \left(\frac{\partial^2 \Omega}{\partial H^2} \right)_{N, T} \Big|_{H=0}, \quad (2.21)$$

respectively. For systems with a fixed number of particles, $\mathcal{M}^{(\text{GC})} \rightarrow \mathcal{M}$ and $\chi^{(\text{GC})} \rightarrow \chi$ in the thermodynamic limit.

For confined systems under an homogeneous static magnetic field with magnitude $B = |\mathbf{B}|$, the energies are discrete, and we write the grand canonical potential (2.18) as the sum

$$\Omega(T, \mu, B) = -k_B T \sum_{\{\lambda\}} \ln \left(1 + e^{-\beta(E_\lambda - \mu)} \right). \quad (2.22)$$

Similarly, using (2.20) and (1.3), we can write the magnetization and the susceptibility in terms of the derivatives of the energy, which yields

$$\mathcal{M}^{(\text{GC})} = - \sum_{\{\lambda\}} f_\mu(E_\lambda) \frac{\partial E_\lambda}{\partial B}, \quad (2.23)$$

and the ZFS as [22, 68]

$$\chi^{(\text{GC})} = - \frac{1}{\mathcal{V}} \sum_{\{\lambda\}} \left[f'_\mu(E_\lambda) \frac{\partial^2 E_\lambda}{\partial^2 B} + f_\mu(E_\lambda) \left(\frac{\partial E_\lambda}{\partial^2 B} \right)^2 \right] \Big|_{B=0}. \quad (2.24)$$

The temperature dependence follows from the Fermi–Dirac, distribution

$$f_\mu(E) = \frac{1}{\exp([E - \mu]/k_B T) + 1}. \quad (2.25)$$

Equations (2.23) and (2.24) are only valid when the degeneracy of the energy levels does not depend on the magnetic field. We recall that in the regime of a small magnetic response, the magnitude of the fields H and B can be used indistinctly when taking the derivatives.

The quantum mechanical calculation of the magnetic response in the grand canonical ensemble is straightforward if the single-particle spectrum $\{E_\lambda\}$ is known. However, in order to obtain the susceptibility χ (1.3) for a fixed number of particles N , it is necessary to find the right chemical potential μ such that $N = \sum_{\{\lambda\}} f_\mu(E_\lambda)$. Finding

μ is then a numerical task that can be difficult to solve, especially if it depends on the magnetic field B . Another possible inconvenient is that the spectrum gets denser as the system gets larger, and in this case a treatment based on semiclassical density of states might be preferable.

As we are interested in the zero-field susceptibility, the exact magnetic field dependence of the spectrum is not necessary. Quantum perturbation theory allows us to calculate the energy spectrum for small magnetic fields, as we will see in the following section.

2.3.2 QUANTUM PERTURBATION THEORY FOR THE ORBITAL SUSCEPTIBILITY OF SPHERICAL NANOPARTICLES

In order to calculate the orbital contribution to the magnetic susceptibility, let us consider electrons confined in spherical nanoparticles, as described by the Hamiltonian of eqs. (2.5) and (2.8), for the case of hard walls in the absence of spin effects. Our Hamiltonian consist of three terms: the unperturbed Hamiltonian $\mathcal{H}^{(0)}$ (2.9a) that does not depend on the magnetic field, $\mathcal{H}^{(\text{para})}$ (2.9b) that is linear in the magnetic field and $\mathcal{H}^{(\text{dia})}$ that is quadratic in the magnetic field. We want to use B as our expansion parameter to perform quantum perturbation theory, keeping all contributions up to B^2 . To be consistent with the powers of B , in principle we need to calculate three B -dependent energy terms:

1. First order expansion of $\mathcal{H}^{(\text{dia})}$. As it is already proportional to B^2 we just need to calculate its trace,

$$E_{nlm_z}^{(\text{dia})} = \langle \psi_{n,l,m_z}^{(0)} | \mathcal{H}^{(\text{dia})} | \psi_{n,l,m_z}^{(0)} \rangle, \quad (2.26)$$

which is proportional to calculating the expectation value of $x^2 + y^2$ (see app. C). This calculation is analogous to the one used to derive Larmor's diamagnetism in the atomic response. The states can be degenerate but it is not necessary to apply degenerate perturbation theory for this term as the corrections are of higher order in B [22]. The off-diagonal matrix elements of $\mathcal{H}^{(\text{dia})}$ can be obtained from the identities given in appendix J.3.

2. The paramagnetic term $\mathcal{H}^{(\text{para})}$ is proportional to B . The energies associated with this term are to be calculated using degenerate perturbation theory by diagonalizing the matrix L_z in the degenerate subspaces. The leading order term in B contributes to the susceptibility with a $1/T$ dependence, analogous to the Curie contribution in atomic magnetism. Energy states that are not degenerate will not contribute to first order in B due to Kramer's theorem (described in sec. 2.4.3)[22].
3. The second order expansion of $\mathcal{H}^{(\text{para})}$, proportional to be B^2 , also contributes positively (paramagnetically) to the ZFS and it is often referred as the Van Vleck

term. J.H. Van Vleck was one of the first to consider perturbation theory to this order to describe the atomic magnetic response of rare earth salts in which the paramagnetic response has a negligible Curie contribution [127]. The Van Vleck term is related to the mixing of the off diagonal elements of L_z . The diamagnetic and the Van Vleck contributions are usually of the same order, and it can be shown that both terms are necessary to recover gauge invariance [22].

Carrying out the calculation using the unperturbed orbital basis (2.11), we find only two B -dependent terms [22, 68], as

$$E_{nlm_z}^{(\text{orb})} = E_{nl}^{(0)} + E_{m_z}^{(\text{para})} + E_{nlm_z}^{(\text{dia})}, \quad (2.27)$$

where $E_{nl}^{(0)}$ was already defined in (2.12). The first-order contribution corresponding to the paramagnetic term of the Hamiltonian (2.9b) reads

$$E_{m_z}^{(\text{para})} = \hbar\omega_c m_z / 2 \quad (2.28)$$

(in terms of the magnetic quantum number m_z), while the second-order correction (diamagnetic term of eq. (2.9c)) is

$$E_{nlm_z}^{(\text{dia})} = m\omega_c^2 a^2 \mathcal{R}_{nl} \mathcal{Y}_l^{m_z} / 8, \quad (2.29)$$

with

$$\mathcal{R}_{nl} = \frac{1}{3} \left[1 + \frac{2}{\zeta_{nl}^2} \left(l + \frac{3}{2} \right) \left(l - \frac{1}{2} \right) \right] \quad (2.30)$$

and

$$\mathcal{Y}_l^{m_z} = 1 - \frac{1}{2l+1} \left[\frac{l^2 - m_z^2}{2l-1} + \frac{(l+1)^2 - m_z^2}{2l+3} \right]. \quad (2.31)$$

The third term of the Van Vleck kind, proportional to B^2 does not appear in eq. (2.27). The reason is related to the spherical symmetry and the choice of gauge, see appendix C. In our example, $E_{m_z}^{(\text{para})}$ (2.28) does not depend on n or l , and is exact to any order in B , as L_z is already diagonal in our choice of basis (2.11). We will later show that the Van Vleck contribution will be important when we include spin-orbit coupling in chapter 4.

In fig. 2.4, we compare the perturbative spectrum (2.27) (red lines) for a given span of magnetic fields with the exact spectrum E_{ex} resulting from a numerical diagonalization of the Hamiltonian (2.5) (black lines). The magnetic fields needed to reach the regime of quantum Hall effect emerging at the right part of the plot are extremely high for the nanoparticles under consideration, but might be attainable for larger metallic nanoparticles or for semiconducting structures. The agreement between the perturbative and exact spectrum is very good up to magnetic fields corresponding to the (reduced) flux $\phi/\phi_0 \simeq 5$, with $\phi(B) = \pi a^2 B$ (compare the solid red and black lines),

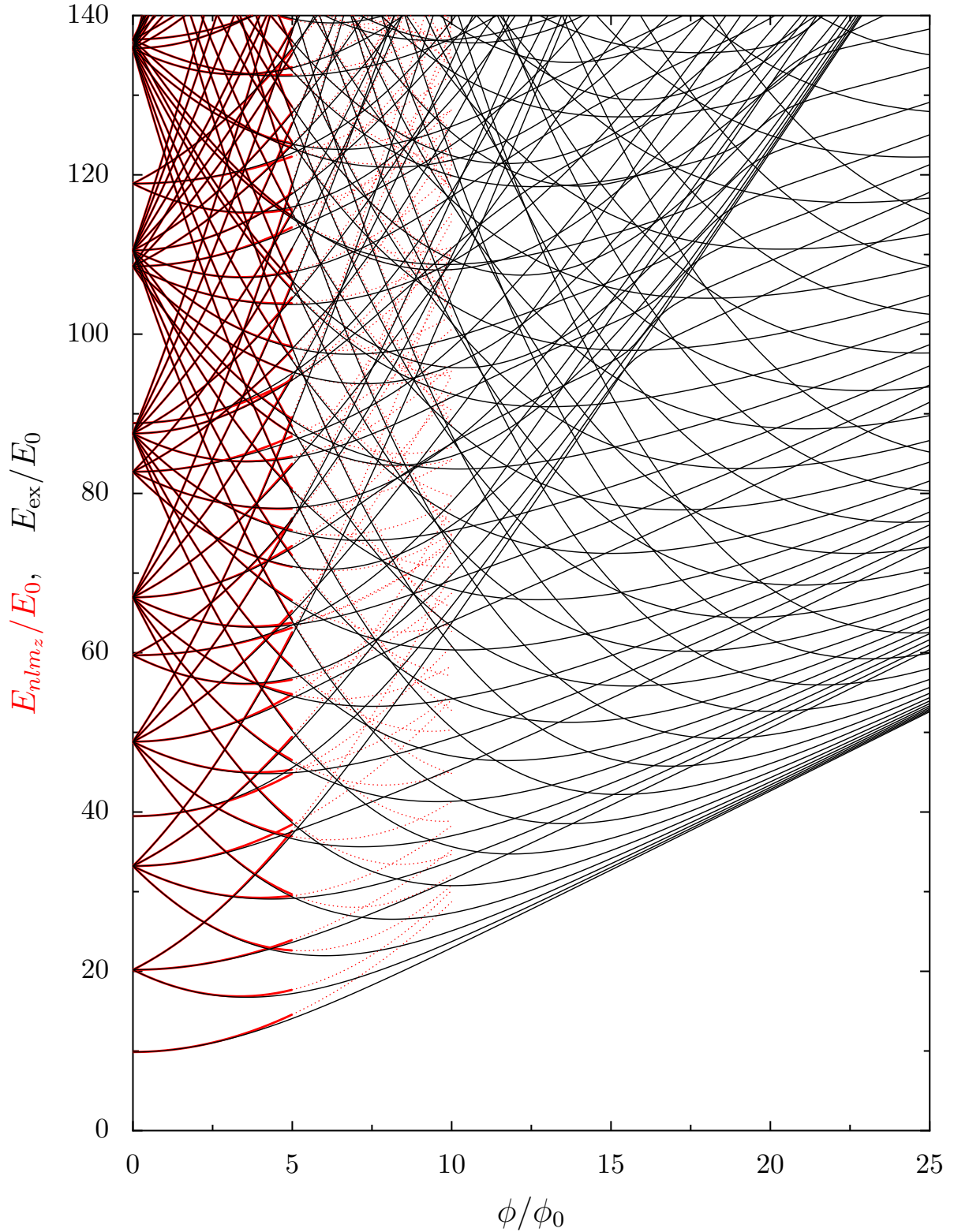


Figure 2.4: Black lines: exact spectrum E_{ex} of the mean-field Hamiltonian (2.5) (scaled by $E_0 = \hbar^2/2ma^2$) of a sphere as a function of the magnetic flux $\phi = \pi a^2 B$ in units of the flux quantum. Red lines: perturbative spectrum $E_{nlm_z}^{(orb)}$ from eq. (2.27), showing the perturbative regime ($0 < \phi/\phi_0 \lesssim 5$, solid red lines) and the region where perturbation theory starts to depart from the exact result ($5 \lesssim \phi/\phi_0 \lesssim 10$, dotted red lines).

while for larger fields, the perturbative energy levels (shown as dotted red lines) depart from the exact result. For the magnetic fields which we consider in the main text, the quantitative agreement is excellent, and the use of nondegenerate perturbation theory is appropriate since the perturbation does not break the axial symmetry of the system.

The grand canonical magnetic moment $\mathcal{M}^{(\text{GC})}$ and the corresponding zero-field susceptibility $\chi^{(\text{GC})}$ can be readily obtained from the perturbative spectrum (2.27) via the expressions (2.23) and (2.24) where we have to account for a factor of 2 due to spin degeneracy (in the absence of Zeeman interaction and spin-orbit coupling), yielding [22, 68]

$$\frac{\mathcal{M}^{(\text{orb})}}{\mu_B} = -2 \sum_{n=1}^{\infty} \sum_{l=0}^{\infty} \sum_{m_z=-l}^{+l} f_{\mu}(E_{nlm_z}^{(\text{orb})}) \left[m_z + \frac{(k_{\text{F}}a)^2 \hbar \omega_c}{4E_{\text{F}}} \mathcal{R}_{nl} \mathcal{Y}_l^{m_z} \right] \quad (2.32)$$

and $\chi^{(\text{orb})} = \chi^{(\text{para})} + \chi^{(\text{dia})}$, where

$$\frac{\chi^{(\text{para})}}{|\chi_{\text{L}}|} = -\frac{3\pi E_0}{k_{\text{F}}a} \sum_{l=0}^{\infty} l(l+1)(2l+1) \sum_{n=1}^{\infty} f'_{\mu}(E_{nl}^{(0)}), \quad (2.33a)$$

and

$$\frac{\chi^{(\text{dia})}}{|\chi_{\text{L}}|} = -\frac{3\pi}{k_{\text{F}}a} \sum_{l=0}^{\infty} (2l+1) \sum_{n=1}^{\infty} \mathcal{R}_{n,l} f_{\mu}(E_{nl}^{(0)}). \quad (2.33b)$$

$\mathcal{M}^{(\text{orb})}$ and $\chi^{(\text{orb})}$ are the grand canonical magnetic moment and susceptibility arising from the spectrum in eq. (2.27). The intermediate details of the calculation are presented in appendix C.

Each term of the sum in $\chi^{(\text{para})}$ (2.33a) has a Curie-like $1/T$ dependence, as it is multiplied by the derivative of the Fermi-Dirac distribution $f'_{\mu}(E_{n,l}^{(0)}) = -f_{\mu}(E_{n,l}^{(0)})[1 - f_{\mu}(E_{n,l}^{(0)})]/k_{\text{B}}T$.

As we will see in chapter 3, the values of $\chi^{(\text{orb})}$ can exceed the values of χ_{L} by several orders of magnitude. The expression (2.33) will later be important in order to establish a benchmark of the former and validate the use of a semiclassical approach in the cases where the quantum calculations are too difficult to be implemented, like that of the nanoparticle magnetization which necessitates to impose the condition of a constant number of electrons at finite temperature.

Quantum perturbation theory is not the only way to obtain the susceptibility of our system. As we will see next, a semiclassical thermodynamic formalism allows to expand the free energy F in terms of Ω in order to account for finite-size corrections.

2.3.3 SEMICLASSICAL THERMODYNAMIC APPROACH

In this section, we introduce a semiclassical formalism, allowing to study the magnetic properties of metallic nanoparticles in terms of classical trajectories.

The difficulty of calculating the magnetic properties of electronic systems remains to pass from the grand canonical ensemble at fixed μ to the canonical ensemble at fixed N . One way to perform such a transformation, for confined systems that are not atomically small, is to use a semiclassical thermodynamical formalism [75–77, 128]. This semiclassical approach has been used to describe the magnetic response of two-dimensional nanostructures [84, 88].

Let us define the following integrals defined from the grand-canonical ensemble (2.18) at zero temperature. First we introduce the number of particles at zero temperature as

$$N_0(E) = \int_0^E \varrho(E') dE', \quad (2.34a)$$

and the thermodynamic potential for the grand canonical ensemble at zero temperature, as

$$\Omega_0(E) = - \int_0^E N_0(E') dE'. \quad (2.34b)$$

These quantities (2.34) depend uniquely on the quantum spectrum. At finite temperature we must take a convolution with the derivative of the Fermi-Dirac distribution with respect to the energy to obtain the corresponding quantities, with the density of particles given by

$$D(\mu) = - \int_0^\infty \varrho(E) f'_\mu(E) dE, \quad (2.35a)$$

the number of particles given by

$$N(\mu) = - \int_0^\infty N_0(E) f'_\mu(E) dE, \quad (2.35b)$$

and the thermodynamical potential as

$$\Omega(\mu) = - \int_0^\infty \Omega_0(E) f'_\mu(E) dE. \quad (2.35c)$$

Integrating N (2.35b) by parts gives the usual grand canonical relation for the number of particles

$$N(\mu) = \int_0^\infty \varrho(E) f_\mu(E) dE. \quad (2.36)$$

In general we can also decompose the thermodynamical quantities as we did with the density of states in eqs. (2.15) and (2.16), so that

$$N_0^{\text{osc}}(E) = \int_0^E \varrho^{\text{osc}}(E') dE' \quad (2.37a)$$

and

$$\Omega_0^{\text{osc}}(E) = - \int_0^E N_0^{\text{osc}}(E') dE', \quad (2.37b)$$

which are the oscillatory components of eq.(2.34a) and (2.34b), respectively.

Up to leading order in \hbar the integrals can be performed doing an integration by parts, using that

$$\int_0^E A_\Lambda(E') \cos(S_\Lambda(E')/\hbar + \nu_\Lambda) dE' = \frac{\hbar}{\tau_\Lambda(\mu)} A_\Lambda(E) \sin(S_\Lambda(E)/\hbar + \eta_\Lambda),$$

where $\tau_\Lambda(E)$ is the period of the classical orbit (see app. B), given by

$$\tau_\Lambda(E) = \frac{\partial S_\Lambda}{\partial E}. \quad (2.38)$$

This implies the following relations:

$$N_0^{\text{osc}}(E) = \sum_\Lambda N_{0,\Lambda}(E) \quad ; \quad N_{0,\Lambda}(E) = -\frac{\hbar}{\tau_\Lambda(\mu)} \text{Shift}(\varrho_\Lambda) \quad (2.39)$$

and

$$\Omega_0^{\text{osc}}(E) = \sum_\Lambda \Omega_{0,\Lambda}(E) \quad ; \quad \Omega_{0,\Lambda}(E) = \left[\frac{\hbar}{\tau_\Lambda(\mu)} \right]^2 \text{Shift}(\varrho_\Lambda). \quad (2.40)$$

Here, the density of states has been decomposed as $\varrho^{\text{osc}} = \sum_\Lambda \varrho_\Lambda$ and the function $\text{Shift}(x)$ adds a phase of $\pi/2$ to a trigonometric function: $\text{Shift}[\cos(x + \varphi)] = \cos(x + \varphi + \pi/2) = \sin(x + \varphi)$. The quantities D^{osc} , N^{osc} and Ω^{osc} are obtained again by convolution of ϱ^{osc} , n^{osc} and Ω_0^{osc} , respectively, along with the derivatives of the the Fermi-Dirac distribution close to μ . To first order in \hbar and $\tau_\Lambda(\mu) \gg \hbar\beta$, the Fermi-Dirac distribution translates into a thermal factor⁶

$$R(\tau_\Lambda(\mu)/\tau_T) = \frac{\tau_\Lambda(\mu)/\tau_T}{\sinh(\tau_\Lambda(\mu)/\tau_T)}. \quad (2.41)$$

For low temperatures, $R(\zeta)$ is a quadratic polynomial similar to the Sommerfeld expansion for ballistic systems [88]. In the opposite limit R decays exponentially for high T or when the period is longer than a certain threshold i.e. $\tau_\Lambda \gg \tau_T$, given by

$$\tau_T = \frac{\hbar\beta}{\pi}. \quad (2.42)$$

In the case of metallic billiard-like systems, the ratio τ_Λ/τ_0 can be replaced with the ratio of the orbit lengths L_Λ/L_T , where $L_\Lambda = v_F\tau_\Lambda$ (v_F is the Fermi speed) is the length of the trajectory and $L_T = \tau_T v_F$ the thermal length. In this way the thermal factor $R(L_\Lambda/L_T)$ exponentially suppresses the zero-temperature contribution of each family of trajectories with length $L_\Lambda \gg L_T$ [88].

⁶The integral $R(\pi x) = \int_{-\infty}^{\infty} \frac{e^y}{(e^y+1)^2} e^{ixy} dy$ is recurrent when using integration by parts of the Fermi-Dirac distribution multiplied by an oscillating function [24].

The oscillating parts of the thermodynamic quantities in the grand canonical ensemble are given by the following expressions

$$D^{\text{osc}}(\mu) = \sum_{\lambda} D_{\Lambda}(\mu) \quad ; \quad D_{\Lambda}(\mu) = \varrho_{\Lambda}(\mu)R(L_{\Lambda}/L_T), \quad (2.43a)$$

$$N^{\text{osc}}(\mu) = \sum_{\Lambda} N_{\Lambda}(\mu) \quad ; \quad N_{\Lambda}(\mu) = -\frac{\hbar}{\tau_{\Lambda}(\mu)}\text{Shift}(\varrho_{\Lambda}(\mu))R(L_{\Lambda}/L_T), \quad (2.43b)$$

and

$$\Omega^{\text{osc}}(\mu) = \sum_{\Lambda} \Omega_{\Lambda}(\mu) \quad ; \quad \Omega_{\Lambda}(\mu) = \left(\frac{\hbar}{\tau_{\Lambda}(\mu)}\right)^2 \varrho_{\Lambda}(\mu)R(L_{\Lambda}/L_T). \quad (2.43c)$$

The main result is that the oscillatory part of all the thermodynamic quantities are given by the oscillating term of the density of states (2.15).

In order to make a systematic transition to the canonical ensemble (CE) at fixed N , we use these oscillating quantities (2.43) related the grand canonical ensemble. Let us start by remarking the semiclassical aspect: the decomposition of the density of states eq. (2.15) gives us an ϱ^{osc} that is of the same order in \hbar as $\bar{\varrho}$ due to the infinite sum. Nevertheless the temperature damping R introduces a cutoff to D^{osc} making it one order in \hbar lower compared to its smooth part \bar{D} , hence D^{osc}/\bar{D} can be used as an expansion parameter for the free energy F (2.19) [85].

Let us call $N = N(\mu) = \bar{N}(\bar{\mu})$ with $\bar{\mu}$ the number of particles and the mean chemical potential in the CE, respectively. We can use the relation $\frac{\partial N}{\partial \mu} = D$ and we can expand around D^{osc}/\bar{D} to obtain the variance in the chemical potential $\mu = \bar{\mu} + \Delta\mu$, so that

$$-\bar{D}(\bar{\mu})\Delta\mu = N^{\text{osc}}(\bar{\mu}), \quad (2.44)$$

where $\Delta\mu$ is illustrated in fig. 2.5.

Consequently, the thermodynamic relation (2.19) between the CE and GC potentials can now be expanded about $\mu + \Delta\mu$ and μ using (2.44), which yields

$$F(N) \approx \bar{\mu}N + \Delta\mu N + \bar{\Omega}(\bar{\mu}) + \Omega^{\text{osc}}(\bar{\mu}) - N(\bar{\mu})\Delta\mu - \frac{1}{2}D(\bar{\mu})(\Delta\mu)^2, \quad (2.45)$$

where we have used the usual thermodynamical properties of the GC ensemble, $\frac{\partial \Omega}{\partial \mu} = -N$. Simplifying the expansion of F (2.45) using the expression for $N^{\text{osc}}(\bar{\mu})$ (2.44), we can determine each order of correction from the powers of $\Delta\mu$.

If we gather the first order of the expansion, we find that the free energy can be written as

$$F(N) \simeq F^0 + \Delta F^{(1)} + \Delta F^{(2)}, \quad (2.46a)$$

where

$$F^0 = \Omega_0(\bar{\mu}) + \bar{\mu}N, \quad (2.46b)$$

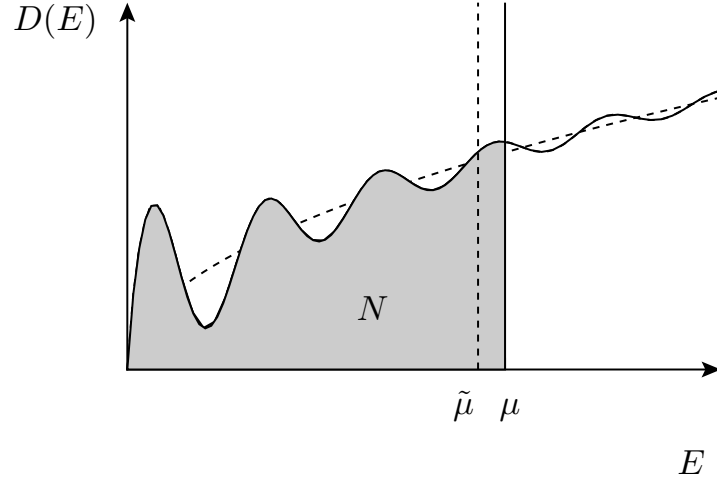


Figure 2.5: Schematic illustration of the semiclassical formalism approach in 3 dimensions. The density of particles $D(E)$ is plotted with a continuous line as a function of E . The density of states can be approximated to $\bar{D}(E) \propto E^{1/2}$ (dashed line). The number of particles N is included in the shaded area and equal to the area under the shaded line up to $\bar{\mu}$.

$$\Delta F^{(1)} = \Omega^{\text{osc}}(\bar{\mu}), \quad (2.46c)$$

and

$$\Delta F^{(2)} = -\frac{(N^{\text{osc}}(\bar{\mu}))^2}{\bar{D}(\bar{\mu})} = \frac{1}{2q^0(\bar{\mu})} \left[\int_0^\infty dE q^{\text{osc}}(E) f_{\bar{\mu}}(E) \right]^2. \quad (2.46d)$$

We have used $\bar{q} = q^0(E)$ as the density of states of the bulk in (3-dimensions) given by

$$q^0(E) = \frac{2\sqrt{E}}{3\pi E_0^{3/2}}, \quad (2.47)$$

accounting for the spin degeneracy.

In the semiclassical regime, the magnetic response calculated for $F^0 + \Delta F^{(1)}$ is equivalent to the one that can be calculated from $\Omega(\mu)$ in the GC ensemble (2.20). Taking the derivative with respect to B while keeping N constant is equivalent to leaving the chemical potential constant, at this order of the approximation. The term $\Delta F^{(2)}$ (2.46d) is the interesting factor as it corresponds to the first canonical correction to the grand canonical ensemble.

It is important to indicate that the bulk term $F^{(0)}$ (2.46b) has an intrinsic magnetic field dependence and thus still contributes to the magnetic susceptibility, yielding χ_L (see appendix A.2).

The formalism presented in this subsection is the framework that will allow us to calculate the magnetic response of ensembles of metallic nanoparticles in chapter 3. As explained in sec. 2.3.1, to calculate F from the quantum approach it is necessary to

use numerical calculations [22, 68]. The sizes of the metallic nanoparticles in consideration are large enough to consider a semiclassical development, which will allow us to keep the analytic approach and better understand the magnetic response theoretically. We will come back to the quantum approach of sec. 2.3.2 when discussing the weakly relativistic corrections.

2.4 WEAKLY RELATIVISTIC EFFECTS

We close this chapter with a discussion on the weakly relativistic effects that will be included in the treatment of the magnetic response to be developed in chapter 4.

Relativistic corrections to the magnetic response are usually discussed in astrophysics [129–131], as very energetic electrons found in white dwarfs and neutron stars are subjected to the influence of large magnetic fields. Even if the energy and magnetic field scales are completely different than in our case, it is nevertheless interesting to consider the physical analogies between the two set-ups.

The relativistic version of Landau’s susceptibility can be obtained from Dirac equation in the absence of fields (see sec 2.4.1). At the weakly relativistic limit where $v_F \ll c$, the zero-field susceptibility reads [132]

$$\chi_b^{(\text{wr})} = \left[2 - \frac{1}{3} \left(\frac{v_F}{c} \right)^2 \right] \chi_L, \quad (2.48)$$

generalizing Landau and Pauli susceptibilities to the case of a relativistic electron gas at low energies. The quantum mechanical calculation that leads to eq. (2.48) can be found in appendix A.3.

In normal metals, the relativistic effects can have some influence on the melting point and optical properties [133]. The color of gold is attributed to relativistic corrections, usually related to the spin–orbit effects of electrons in the d orbitals [133]. However, the weakly-relativistic correction to the ZFS in metals is negligible with respect to the non-relativistic bulk ZFS $\chi_b^{(\text{nr})}$. In chapter 3, we will show the dramatic increase of the ZFS with respect to χ_L induced by the electronic confinement in the nonrelativistic case. One might ask if a similar effect occurs for the weakly-relativistic susceptibility, and in particular for the contribution arising from the spin–orbit coupling. We will develop these corrections in chapter 4.

The section 2.4.1 below discusses the Foldy-Wouthuysen transformation that allows to recover the non-relativistic and weakly relativistic corrections of a free particle from the Dirac equation. The same procedure is later used in sec. (2.4.2) to provide some insight into the weakly-relativistic corrections that appear under magnetic fields and quantum confinement. Lastly, sec. 2.4.3 discusses two important theorems, Wigner–Eckart and Kramer’s theorems, related to the spin–orbit coupling.

2.4.1 FOLDY-WOUTHUYSEN TRANSFORMATION AND FREE DIRAC ELECTRONS

To derive the spin-orbit coupling properly and systematically for a general system, it is necessary to start from a fully relativistic quantum description. In order to describe electrons, we need Dirac equation, i.e.

$$\mathcal{H}^{(\text{Dirac})} \begin{pmatrix} \Psi_0 \\ \mathcal{U}_0 \end{pmatrix} = E \begin{pmatrix} \Psi_0 \\ \mathcal{U}_0 \end{pmatrix}, \quad (2.49a)$$

which describes the dynamics of relativistic fermions with spin- $\frac{1}{2}$, with

$$\mathcal{H}^{(\text{Dirac})} = \boldsymbol{\alpha} \cdot \mathbf{p}c + \gamma_0 mc^2, \quad (2.49b)$$

where Ψ_0 and \mathcal{U}_0 are 2-entry spinor wavefunctions, E is the energy, and $\boldsymbol{\alpha}$ and γ_0 are defined as⁷

$$\boldsymbol{\alpha} = \begin{pmatrix} 0 & \boldsymbol{\sigma} \\ \boldsymbol{\sigma} & 0 \end{pmatrix} \quad (2.50a)$$

and

$$\gamma_0 = \begin{pmatrix} \mathbb{1}_2 & 0 \\ 0 & -\mathbb{1}_2 \end{pmatrix}, \quad (2.50b)$$

where $\mathbb{1}_2$ is the 2×2 identity matrix.

Dirac's equation can be sometimes inconvenient at low energies, particularly as it acts on the bispinor (Ψ_0, \mathcal{U}_0) that describes a coupled system of a particle and its own antiparticle. As we are interested in the weakly relativistic limit, we can avoid this inconvenience by considering the approach developed by L.L. Foldy and S.A. Wouthuysen [134], which consist in a canonical transformation which allows to recover the single particle description. The procedure consists in finding a unitary operator \mathcal{U} such that the change of basis $(\Psi, \mathcal{U}) = \mathcal{U}(\Psi_0, \mathcal{U}_0)$ produces a new $\mathcal{H}^{(\text{FW})} = \mathcal{U}\mathcal{H}\mathcal{U}^\dagger$ that decouples into independent equations for each of the two spinors components.

The unitary operator for $\mathcal{U}^{(\text{Dirac})}$ is well known and is given by

$$\mathcal{U}^{(\text{Dirac})} = \exp\left(\gamma_0 \frac{\boldsymbol{\alpha} \cdot \mathbf{p}}{|\mathbf{p}|} \theta^{(\text{Dirac})}\right) = \cos \theta^{(\text{Dirac})} + \gamma_0 \frac{\boldsymbol{\alpha} \cdot \mathbf{p}}{|\mathbf{p}|} \sin \theta^{(\text{Dirac})}, \quad (2.51a)$$

where

$$\tan(2\theta^{(\text{Dirac})}) = \frac{|\mathbf{p}|}{2m}, \quad (2.51b)$$

which leads to

$$\mathcal{H}^{(\text{Dirac-FW})} = \mathcal{U}^{(\text{Dirac})} \mathcal{H}^{(\text{Dirac})} (\mathcal{U}^{(\text{Dirac})})^\dagger = \gamma_0 \sqrt{m^2 c^4 + \mathbf{p}^2 c^2}. \quad (2.52)$$

⁷Arrays between square brackets $[\cdot]$ represent tensors and statevectors for two-level systems (spinors). Arrays in between parentheses (\cdot) represent higher dimensional arrays (like the 4-entry bi-spinors of the Dirac Hamiltonian).

Thus, after a Foldy-Wouthuysen transformation we find a new Hamiltonian (2.52) for (Ψ, \mathcal{U}) , where Ψ is independent of \mathcal{U} and viceversa. The positive energies can be read directly from (2.52) and represent the energy of a free relativistic particle $E = \sqrt{\mathbf{p}^2 c^2 + m^2 c^4}$ which recovers the classical energies of a free particle at the classical limit of low speeds. Thus for $|\mathbf{p}| \ll mc$, we recover

$$\frac{\mathbf{p}^2}{2m} \Psi = -\frac{\hbar}{2m} \nabla^2 \Psi = E \Psi \quad (2.53)$$

which is just the time-independent Schrödinger equation (in the absence of a potential) for a spin- $\frac{1}{2}$ fermion.

The next order correction is the weakly relativistic correction of the kinetic energy for a free particle given by

$$\mathcal{H}^{(k\text{-free})} = -\frac{\mathbf{p}^4}{8m^3 c^2}. \quad (2.54)$$

This kinetic energy correction (2.54) is a key ingredient for the fine structure of hydrogen and in general is of the same order of correction as the spin-orbit coupling. In chapter 4 we show that the relativistic corrections to the kinetic energy are fundamental to recover the weakly relativistic response of the bulk, but first we need to introduce the effect of electric and magnetic fields.

2.4.2 WEAKLY RELATIVISTIC LIMIT IN THE PRESENCE OF MAGNETIC FIELDS AND CONFINEMENT

For a single electron in the presence of time-independent external electromagnetic fields,⁸ one can recover the equations that include the electromagnetic interaction by means of a minimal coupling substitution $\mathbf{p} \rightarrow \mathbf{p} + \frac{e}{c} \mathbf{A}(\mathbf{r})$ and the addition of an electric potential $\phi_e(\mathbf{r})$, which provides the Hamiltonian

$$\mathcal{H}^{(\text{EM-Dirac})} = \boldsymbol{\alpha} \cdot \left[\mathbf{p} + \frac{e}{c} \mathbf{A}(\mathbf{r}) \right] c + \gamma_0 m c^2 - e \phi_e(\mathbf{r}), \quad (2.55)$$

where $\mathbf{A}(\mathbf{r})$ is the magnetic vector potential and $\phi_e(\mathbf{r})$ is the electrostatic potential, that define the magnetic field $\mathbf{B}(\mathbf{r}) = \nabla \times \mathbf{A}(\mathbf{r})$ and the electric field $\mathbf{E}(\mathbf{r}) = -\nabla \phi_e(\mathbf{r})$. We will be interested in the effect of $\mathbf{A}(\mathbf{r})$ as it is responsible for the magnetic effects but $\phi_e(\mathbf{r})$ and is necessary as it defines our confining potential, cf. discussion of sec. 2.1.

For our model we need to consider both $\mathbf{A}(\mathbf{r})$ and $\phi_e(\mathbf{r})$ as in chapter 4. For pedagogical reasons, let us discuss first only two simpler cases: (1) presence of magnetic fields and no confinement $\phi_e(\mathbf{r}) = 0$ and (2) presence of confinement and no magnetic field.

For the case of a single electron that is subject to magnetic fields only, the Foldy-Wouthuysen transformation can be carried out exactly. The result follows similarly to

⁸For the whole study, we will consider only static fields. Many of the equations presented here are generalizable for time-dependent fields.

the free Dirac electron of the previous section 2.4.1. When $\phi_e(\mathbf{r}) = 0$, the Hamiltonian can be completely decoupled and is analogous to (2.52), with the replacement $\mathbf{p}^2 \rightarrow \{\boldsymbol{\sigma} \cdot [\mathbf{p} + e\mathbf{A}(\mathbf{r})/c]\}^2$. More details can be found in appendix E. In the classical limit the resulting equation is

$$\mathcal{H}^{(\text{nr})}\Psi = E\Psi, \quad (2.56)$$

which is known as Pauli's equation (in the absence of a potential). The Hamiltonian $\mathcal{H}^{(\text{nr})}$ is the one from eq. (2.6) which includes the Zeeman interaction of the form

$$\mathcal{H}^{(\text{Z})} = \frac{e\hbar}{2mc}\boldsymbol{\sigma} \cdot \mathbf{B}(\mathbf{r}), \quad (2.57)$$

which is equivalent to eq. (2.7) with $g = g_0 = 2$.⁹ Experimentally, the g-factor of a free electron is 2.00231304386 [136]. The correction with respect to g_0 comes from the polarization of the vacuum and can be calculated with high precision using quantum electrodynamics (QED). This polarization of the vacuum can also shift slightly the energies of atomic orbitals, an effect known as the Lamb shift, with energy corrections of an order of magnitude smaller than those from the weakly relativistic regime [137].

Electrons in metals have are described using effective g-factors, which are dependent on the specifics of the band structure, but the numeric values remain close to the bare electron g-factor. For the purposes of this document, we will neglect these corrections, and we will set $g = 2$ for the rest of this document.

For the case where $\phi_e(\mathbf{r}) \neq 0$, there is in general no exact expression for the decoupled system. However, the unitary transformation of the Hamiltonian (2.55) can be expanded in powers of $|\mathbf{p}|/mc^2$ as a series of uncoupled terms using Baker—Campbell—Hausdorff formula.¹⁰ This expansion allows to read directly the non-relativistic Hamiltonian and all the relativistic corrections to any desired order. For the weakly-relativistic limit, only the first order correction in $|\mathbf{p}|/mc$ is kept and the Hamiltonian reads

$$\mathcal{H}^{(\text{wr})} = \mathcal{H}^{(\text{nr})} + \Delta\mathcal{H}, \quad (2.59)$$

where the non-relativistic Hamiltonian $\mathcal{H}^{(\text{nr})}$ is the same from eq. (2.6).

For the case where $\phi_e(\mathbf{r}) \neq 0$ and $\mathbf{A}(\mathbf{r}) = 0$, the weakly-relativistic correction in (2.59) has four ingredients

$$\Delta\mathcal{H}|_{\mathbf{A}(\mathbf{r})=0} = \mathcal{H}^{(\text{k-free})} + \mathcal{H}^{(\text{so})} + \mathcal{H}^{(\text{D})} + \mathcal{H}^{(\text{r})}. \quad (2.60)$$

$\mathcal{H}^{(\text{k-free})}$ is the correction to the relativistic kinetic energy as seen previously in eq. (2.54), $\mathcal{H}^{(\text{so})}$ is the spin-orbit coupling (1.6) defined at the beginning of this chapter

⁹While here the factor of 2 was found using a relativistic quantum equation, the electron g-factor and its spin are not usually considered as a relativistic effect. It can be shown that linearizing the wave equation for the free particle recovers the same result in non-relativistic quantum mechanics [135].

¹⁰For two operators \mathcal{O}_1 and \mathcal{O}_2 , the Baker—Campbell—Hausdorff formula reads

$$e^{\mathcal{O}_1}\mathcal{O}_2e^{\mathcal{O}_1} = \mathcal{O}_2 + [\mathcal{O}_1, \mathcal{O}_2] + \frac{1}{2}[\mathcal{O}_1, [\mathcal{O}_1, \mathcal{O}_2]] + \dots \quad (2.58)$$

and $\mathcal{H}^{(D)}$ stands for the Darwin term, i.e.

$$\mathcal{H}^{(D)} = \frac{e\hbar^2}{8m^2c^2} \nabla \cdot \mathbf{E}(\mathbf{r}), \quad (2.61)$$

that originates from the zitterbewegung effect related to interference between particle–antiparticle components described in appendix E. The last term,

$$\mathcal{H}^{(r)} = \frac{ie\hbar}{8m^2c^2} \boldsymbol{\sigma} \cdot [\nabla \times \mathbf{E}(\mathbf{r})], \quad (2.62)$$

vanishes for conservative potentials. These expressions become more complicated in the presence of magnetic fields. The general case, with $\phi_e(\mathbf{r}) \neq 0$ and $\mathbf{A}(\mathbf{r}) \neq 0$ is treated in more detail in appendix E and will be necessary for chapter 4.

The four elements of eq. (2.60) slightly correct the spectrum of hydrogen. These corrections become important for heavier atoms, as the electrostatic potential becomes stronger. Free particles and particles under static magnetic fields do not feel these relativistic effects. Thus, the spin–orbit coupling is relevant for systems in the presence of confinement. All the terms of (2.60), except for the correction to the kinetic energy, depend on derivatives of \mathbf{E} , so there are only important in the presence of space-dependent potentials.

As stated before, in the case of metals, the valence electrons can be treated as nearly-free particles. Here the spin-orbit coupling of form (1.6), can play a role due to the electrostatic confining potential. The reason why we can disregard much of the complexity and interactions in metals finds its support on Landau’s theory of Fermi liquids [138, 139]. At low temperatures, one can start with a gas of non-interacting electrons and turn interactions adiabatically to recover a gas of weakly-interacting quasi-electrons with effective physical parameters (like an interaction-induced effective mass). The different effects of spin–orbit coupling can be more involved in the case of semiconductors, where the spin–orbit coupling can take different forms depending on the lattice structure [97, 140].

The spin–orbit coupling (1.6) is thus recovered at the weak relativistic limit, whenever a single-particle description is possible. For strong enough potentials, the spin–orbit coupling could be expected to lead to drastic effects. The narrow confinement that we have considered (2.4), may boost the contribution of the spin–orbit correction. The quantitative evaluation of this effect is one of the goals of this work.

2.4.3 CONSERVATION LAWS UNDER THE INFLUENCE OF SPIN–ORBIT COUPLING

In the presence of spin–orbit coupling, the orbital and spin angular momentums are individually not conserved. In the absence of magnetic field, the total angular momentum $\mathbf{J} = \mathbf{S} + \mathbf{L}$ is the conserved quantity and it is natural to work the eigenstates of $J^2 = |\mathbf{J}|^2$ with eigenvalue $\hbar^2 j(j+1)$ and the projection on the z-axis J_z with eigenvalues $\hbar m_j$.¹¹ For electrons, the rule of addition of angular momentum results in

¹¹This substitution is sometimes called a Russel–Saunders or L – S coupling.

$[l] \otimes [1/2] = [l - 1/2, l] \oplus [l + 1/2, l]$, where the left-hand side is the tensor product of the orbital angular momentum $l \neq 0$ subspace with that of the spin $1/2$ and the right-hand side represents the direct sum of the subspaces with total angular momenta $j = l \mp 1/2$ and orbital angular momentum l . For radially symmetric electrostatic potentials the separability between radial and angular coordinates allows to write the eigenstates of the coupled basis in terms of the spinors [119]

$$\Phi_{n,j,m_j}^{(\pm)}(\mathbf{r}) = R_{n,j\pm 1/2}(r) Y_{j,m_j}^{(\pm)}(\vartheta), \quad (2.63)$$

where we have defined the spinor spherical harmonics

$$Y_{j,m_j}^{(\pm)}(\vartheta) = \frac{1}{\sqrt{2(j \pm 1/2) + 1}} \begin{bmatrix} \mp \sqrt{j \pm 1/2 \mp m_j + 1/2} Y_{j\pm 1/2}^{m_j-1/2}(\vartheta) \\ \sqrt{j \pm 1/2 \pm m_j + 1/2} Y_{j\pm 1/2}^{m_j+1/2}(\vartheta) \end{bmatrix} \quad (2.64)$$

in terms of the usual spherical harmonics $Y_l^{m_z}$ introduced in eq. (2.11). The label (\pm) corresponds to $l = j \pm 1/2$, and sets the parity $(-1)^{j\pm 1/2}$ of the state.

As we are interested in calculating the expectation value of different angular momentum operators L_i, S_i ; $i \in \{x, y, z\}$, we introduce the Wigner-Eckart theorem for angular momentum operators, which reads [141]

$$\mathbf{J}' = \frac{1}{\hbar^2 j(j+1)} \langle \Phi_{n,j,m_j}^{(\pm)} | \mathbf{J}' \cdot \mathbf{J} | \Phi_{n,j,m_j}^{(\pm)} \rangle \mathbf{J}, \quad (2.65)$$

where we are interested in the angular momentum operators \mathbf{J}' that are linear combinations of \mathbf{L} and \mathbf{S} . This theorem (2.65) is only valid to calculate matrix elements in the same subspace defined by the same $[n, j, (\pm)]$. When $\mathbf{J}' = \mathbf{L} + 2\mathbf{S}$, eq. (2.65) allows us to recover the proportionality constant known as the Landé g-factor [141].

Another important principle is Kramer's degeneracy theorem [142, 143] related to the time inversion symmetry. Kramer's theorem states that for a system with an odd number of electrons (half-integer total spin), in the absence of external magnetic fields,¹² the spectrum remains at least doubly degenerate (exactly doubly degenerate for spin-1/2 fermions). Thus the spin-orbit coupling term alone cannot break the degeneracy of the energy spectrum.

2.5 SUMMARY AND CORRESPONDENCE WITH THE REST OF THIS WORK

With this chapter we have introduced all the preliminary ingredients necessary for the two main chapters of this thesis.

¹²One may think that it does not make any difference if the field is external or not, as under consideration of electromagnetic forces only, time inversion is a symmetry of the physical dynamics. However an external magnetic field effectively breaks the time inversion symmetry of the local dynamics, as the sources that create the field are not taken into account in the local Hamiltonian.

In chapter 3, we will derive the orbital contribution to the magnetic response of individual and ensembles of metallic nanoparticles using the semiclassical thermodynamic formalism developed in subsection 2.3.3 up to the first canonical corrections. For that purpose, we apply the nanoparticle model from sec. 2.1 to describe the electronic orbital magnetism of the nanoparticles and in subsection 2.2.2 we discussed the semiclassical density of states for electrons under spherical confinement. In section 2.3 we introduced the thermodynamical formalism, including the orbital magnetic response of spherical nanoparticles from a quantum perturbative approach in subsection 2.3.2, which will serve as benchmark for our semiclassical calculations.

In chapter 4, we will be interested in the weakly relativistic contributions, already introduced in sec. 2.4, to the magnetic response of individual metallic nanoparticles. Subsections 2.4.1 and 2.4.2 discussed the Foldy–Wouthyusen method to systematically derive the weakly relativistic corrections, including the spin–orbit coupling. Subsection 2.4.3 also discussed symmetry considerations related to the spin–orbit coupling that will be of interest when calculating matrix elements and when dealing with other geometries. Chapter 4 also build on non-relativistic discussions for the spherical confinement that were presented in section 2.2, as well as the grand canonical formalism to derive the ZFS discussed in subsection 2.3.1, which is the basis of the quantum perturbative approach.

ORBITAL MAGNETIC RESPONSE OF ENSEMBLES OF METALLIC NANOPARTICLES

3

As described in section 1.2, the observed magnetic response of macroscopic ensembles of gold nanoparticles is very diverse and many aspects remain still unexplained [16, 17]. In this chapter we develop a theoretical model to attempt to predict the magnetic response of an ensemble of metallic nanoparticles starting from the microscopic Hamiltonian presented in section 2.1. As the Zeeman contribution (2.7) is not significantly modified by the confinement, this chapter will only be concerned with the orbital contribution to the magnetic response.

Based on analytical semiclassical methods, together with numerical calculations, the mesoscopic approach presented in this chapter allows us to show that the orbital response of an individual nanoparticle can be exceedingly large as compared to the bulk one and is either diamagnetic or paramagnetic depending on its size. In contrast, the orbital susceptibility of a statistically-distributed (in size) ensemble of nanoparticles is always paramagnetic at low magnetic fields in the absence of interactions between the nanoparticles, provided that the size distribution is smooth and not too narrow. In particular, we predict that the ensemble averaged zero-field susceptibility follows a Curie-type law for small nanoparticle sizes and/or low temperature. We further calculate the field-dependent magnetization of individual as well as ensembles of nanoparticles and show that the latter results are in good agreement with existing experiments measuring a large paramagnetic response.

The chapter is organized as follows: we start by evaluating the free energy of an individual nanoparticle in sec. 3.1, in order to calculate the grand-canonical component of the magnetic response of individual nanoparticles (sec. 3.2) and of ensembles of noninteracting nanoparticles with a size distribution (sec. 3.3). Section 3.4 deals with the magnetic response of individual nanoparticles when canonical corrections are taken into account. In sec. 3.5, we discuss the relevance of our theoretical work toward the understanding of existing experiments. We conclude the chapter in sec. 3.6. The physical concepts of this chapter are adapted from the results of ref. [144].

3.1 FREE ENERGY OF ELECTRONS IN A SPHERICAL BILLIARD

The magnetic susceptibility and the magnetization follow from the free energy of the canonical ensemble at fixed number of particles N and temperature T [see eqs. (1.2) and (1.3)]. The semiclassical thermodynamical formalism introduced in sec. 2.3.3 allows us to expand the free energy $F = F^0 + \Delta F^{(1)} + \Delta F^{(2)}$ in terms of corrections that can be expressed as a function of the grand canonical potential. In turn we also define $\mathcal{M}^{(1)}$ and $\chi^{(1)}$ as the magnetic moment and susceptibility obtained from eqs. (1.2) and (1.3), respectively, by replacing F by $\Delta F^{(1)}$. Analogously, $\mathcal{M}^{(2)}$ and $\chi^{(2)}$ are obtained from the first canonical correction $\Delta F^{(2)}$.

To leading order in $k_F a \gg 1$, we can replace the density of states of a spherical billiard under a small magnetic field given in eq. (2.17a) in the expression for the free energy (2.46c), which yields

$$\Delta F^{(1)} = 4E_F \sqrt{\frac{k_F a}{\pi}} \sum_{\nu=1}^{\infty} \sum_{\eta=2\nu+1}^{\infty} \frac{(-1)^\nu \cos \varphi_{\nu\eta}}{\eta^{5/2} \sqrt{\sin \varphi_{\nu\eta}}} R(L_{\nu\eta}/L_T) \cos(\theta_{\nu\eta}(k_F)) j_0(2\pi\phi_{\nu\eta}/\phi_0), \quad (3.1)$$

where R is the thermal factor (2.41) and $\phi_{\nu\eta}, L_{\nu\eta}, \theta_{\nu\eta}$ (angle between bounces, length of the orbit, magnetic flux and action, respectively) are quantities related to the classical orbits, defined in sec. 2.2.2 and determined by the number of bounces η and winding number ν , see fig. 2.3.

In a similar fashion, the energy integral of eq. (2.46d) leads to the second-order correction

$$\Delta F^{(2)} = 12E_F \left[\sum_{\nu=1}^{\infty} \sum_{\eta=2\nu+1}^{\infty} \frac{(-1)^\nu \cos \varphi_{\nu\eta} \sqrt{\sin \varphi_{\nu\eta}}}{\eta^{3/2}} \times R(L_{\nu\eta}/L_T) \sin(\theta_{\nu\eta}(k_F)) j_0(2\pi\phi_{\nu\eta}/\phi_0) \right]^2. \quad (3.2)$$

In evaluating eqs. (2.46c) and (2.46d), we identified μ^0 with the Fermi energy E_F , neglecting the temperature correction to the chemical potential which is of order $(T/T_F)^2 \ll 1$.

The canonical correction (3.2) to the free energy is an order $\sqrt{k_F a}$ lower than the grand-canonical contribution (3.1). The condition $\Delta F^{(2)} \ll |\Delta F^{(1)}|$, on which the validity of the decomposition (2.46a) is based, then reposes on a more stringent constraint than that of the semiclassical approximation ($k_F a \gg 1$). The fulfillment of the condition $\Delta F^{(2)} \ll |\Delta F^{(1)}|$ translates into $|\chi^{(2)}| \ll |\chi^{(1)}|$ for sufficiently large $k_F a$, but the previous inequality might not hold for moderate values of $k_F a$ (in the same way as we may have $|\Delta F^{(1)}| \ll F^0$ and $|\chi^{(1)}| \gg |\chi_L|$). When $|\chi^{(2)}| \ll |\chi^{(1)}|$, the orbital response of an individual nanoparticle is dominated by the grand-canonical contribution. However, as we will see, in certain cases the latter may become negligible

once the average over an ensemble of nanoparticles is performed. Thus, eq. (3.2) is crucial to obtain nonvanishing quantities for the resulting magnetic response of an ensemble of noninteracting nanoparticles with an important size dispersion (see sec. 3.3).

Using the leading-in- \hbar , field-dependent contribution (3.1) to the free energy, the grand-canonical contribution to the magnetic moment [see eqs. (1.2) and (2.46c)] is given by the semiclassical expression

$$\frac{\mathcal{M}^{(1)}}{\mu_B} = -\frac{4}{\sqrt{\pi}}(k_F a)^{5/2} \sum_{\substack{v>0 \\ \eta>2v}} \frac{(-1)^v \cos^2 \varphi_{v\eta} \sqrt{\sin \varphi_{v\eta}}}{\eta^{3/2}} \\ \times R(L_{v\eta}/L_T) \cos(\theta_{v\eta}(k_F)) j'_0(2\pi\phi_{v\eta}/\phi_0). \quad (3.3)$$

Here, $j'_0(z)$ denotes the derivative of $j_0(z)$ with respect to z . The corresponding zero-field susceptibility is [70]

$$\frac{\chi^{(1)}}{|\chi_L|} = 6\sqrt{\pi}(k_F a)^{3/2} \sum_{\substack{v>0 \\ \eta>2v}} \frac{(-1)^v \cos^3 \varphi_{v\eta} \sin^{3/2} \varphi_{v\eta}}{\sqrt{\eta}} R(L_{v\eta}/L_T) \cos(\theta_{v\eta}(k_F)). \quad (3.4)$$

Similarly, from eq. (3.2) we obtain the semiclassical expressions for the canonical contribution to the magnetic moment

$$\frac{\mathcal{M}^{(2)}}{\mu_B} = -24(k_F a)^2 \sum_{\substack{v>0 \\ \eta>2v}} \sum_{\substack{v'>0 \\ \eta'>2v'}} \frac{\mathcal{F}_{v\eta}^{v'\eta'}}{\eta \cos \varphi_{v\eta} \sin \varphi_{v\eta}} R(L_{v\eta}/L_T) R(L_{v'\eta'}/L_T) \\ \times \sin(\theta_{v\eta}(k_F)) \sin(\theta_{v'\eta'}(k_F)) j'_0(2\pi\phi_{v\eta}/\phi_0) j_0(2\pi\phi_{v'\eta'}/\phi_0) \quad (3.5)$$

and the zero-field susceptibility

$$\frac{\chi^{(2)}}{|\chi_L|} = 36\pi k_F a \sum_{\substack{v>0 \\ \eta>2v}} \sum_{\substack{v'>0 \\ \eta'>2v'}} \mathcal{F}_{v\eta}^{v'\eta'} R(L_{v\eta}/L_T) R(L_{v'\eta'}/L_T) \sin(\theta_{v\eta}(k_F)) \sin(\theta_{v'\eta'}(k_F)). \quad (3.6)$$

In eqs. (3.5) and (3.6) we have defined

$$\mathcal{F}_{v\eta}^{v'\eta'} = (-1)^{v+v'} \eta^{1/2} \eta'^{-3/2} \cos^3 \varphi_{v\eta} \cos \varphi_{v'\eta'} \sin^{5/2} \varphi_{v\eta} \sin^{1/2} \varphi_{v'\eta'}. \quad (3.7)$$

In the following sections we will evaluate the previous semiclassical expressions in different parameter regimes.

Notice that the magnetization and susceptibility in this chapter refer exclusively to an orbital character, for that reason we do not use the label (orb) employed in other chapters.

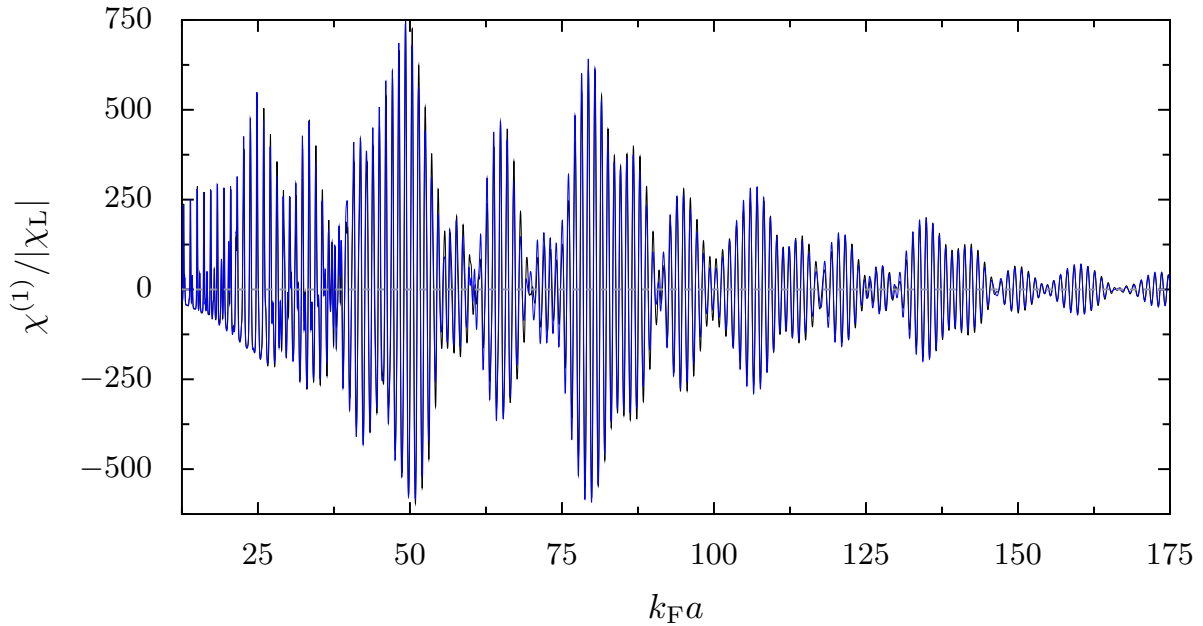


Figure 3.1: Grand-canonical zero-field susceptibility $\chi^{(1)}$, in units of the absolute value of the Landau susceptibility χ_L , as a function of the radius a (scaled with the Fermi wave vector k_F). Blue line: semiclassical result from eq. (3.4). Black line: quantum-mechanical result from eq. (2.33). In the figure, room temperature ($T/T_F = 5 \times 10^{-3}$) is chosen and $\chi = 0$ is indicated by the dashed gray line.

3.2 GRAND-CANONICAL MAGNETIC RESPONSE

The grand-canonical sums (3.3) and (3.4) over the topological indexes can be readily evaluated numerically since the thermal factor (2.41) acts as a cutoff for long trajectories, keeping us away from the typical convergence problems of semiclassical expansions. At the practical level, we perform the sums by only retaining trajectories that are shorter than $10L_T$, and since the sum over η converges relatively fast (the summand decreases as $1/\eta^2$ when $\eta \gg \nu$), we perform it up to $\eta_{\max} = 100\nu$ (for a given ν). We have checked that including trajectories with larger ν and/or η does not lead to significant changes in the final results.

The zero-field susceptibility (3.4) is shown in fig. 3.1 as a blue solid line as a function of the size a for a temperature $T/T_F = 5 \times 10^{-3}$ that approximately corresponds to room temperature. As can be seen from the figure, $\chi^{(1)}$ oscillates and changes sign as a function of $k_F a$. Moreover, the magnetic susceptibility can take values that are much larger in magnitude than the Landau value $|\chi_L|$. Depending on the nanoparticle size, large paramagnetic or diamagnetic responses can be obtained. The rapidly oscillating behavior of the zero-field susceptibility as a function of the sphere radius stems from the dependence of the density of states on the action of the dominant periodic orbits. A similar behavior has been found in two dimensions [84, 85], and also

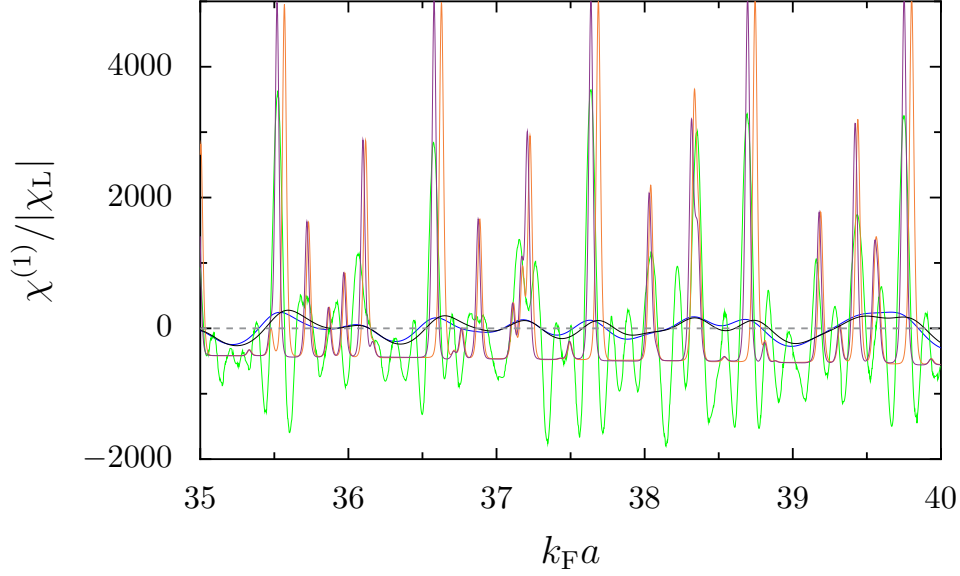


Figure 3.2: Same quantity from eq. (3.4) as in fig. 3.1, in a restricted a interval for $T/T_F = 5 \times 10^{-3}$ (blue line) and $T/T_F = 5 \times 10^{-4}$ (violet line). The quantum-mechanical result (2.33) (black line: $T/T_F = 5 \times 10^{-3}$; orange line: $T/T_F = 5 \times 10^{-4}$) and approximate semiclassical result (3.8) for $T/T_F = 5 \times 10^{-4}$ (green line) are shown for comparison purposes.

the prefactor $(k_F a)^{3/2}$ of $\chi^{(1)}$ in eq. (3.4) is in line with the two-dimensional case. The beating pattern present in the susceptibility $\chi^{(1)}$ is due to interferences between periodic trajectories of different length. The overall amplitude of these beatings decays for the largest sizes due to the thermal factor (2.41) appearing in eq. (3.4), such that $\lim_{k_F a \rightarrow \infty} \chi^{(1)} = 0$. Within this limit, one thus recovers the Landau bulk susceptibility χ_L for the total orbital susceptibility of the system.

The fact that the result of the semiclassical sum (3.4) with the above explicated approximations gives a good account of the quantum results can be checked in the parameter range accessible to both approximations (compare the blue and black lines in fig. 3.1, which are almost indistinguishable on the scale of the figure, as well as the violet and orange lines in fig. 3.2). The perturbative quantum calculation (up to second order in the magnetic field), limited to small clusters and low temperatures, results from a numerical evaluation over the eigenstates of the unperturbed problem [22, 68] presented in section 2.3.2. The equivalence between $\chi^{(1)}$ and the result that can be obtained from the quantum approach of eqs. (2.33) is demonstrated in appendix D.

While the previous agreement is not surprising, given that fig. 3.1 presents results in the semiclassical limit $k_F a \gg 1$ for high (room) temperature, fig. 3.2 shows that at low temperatures ($T/T_F = 5 \times 10^{-4}$) the semiclassical sum (3.4) also reproduces the quantum result (2.33). The paramagnetic peaks, with values that exceed the Landau susceptibility by orders of magnitude, are observed at the eigenenergies of the unperturbed system ($k_F a = \zeta_{n,l}$), while the negative (diamagnetic) background is given

by the small quadratic (in magnetic field) contribution represented by the last term on the right-hand side of eq. (2.33). Although not visible on the scale of fig. 3.2, the diamagnetic background increases with k_{Fa} due to the incorporation of more states in the sums as the Fermi energy increases. The dependence of the energy levels on the applied magnetic field, discussed in section 2.3.2 and shown in fig. 2.4, allows for an understanding of the peak structure in the susceptibility that is found at low temperatures (see fig. 3.2). The positive curvature of the individual levels yields the diamagnetic background that becomes stronger when more levels are occupied. The crossings of levels with different magnetic quantum number at zero applied field translate in a diverging negative curvature of the total energy and a corresponding paramagnetic peak when the chemical potential coincides with such a level crossing. Temperature smears out the peaks and limits their height due to admixtures of contributions from neighboring levels. The oscillations of the susceptibility found at room temperature as a function of the sphere radius are the remainders of that peak structure. It is remarkable that a semiclassical expansion like that of eq. (3.4) is able to reproduce signatures characteristic of individual eigenenergies. We notice, however, that each energy represents $2(2l + 1)$ degenerate unperturbed states, with l the angular momentum quantum number, and that very long trajectories have to be included in the semiclassical calculation to approach the quantum result of fig. 3.2.

The semiclassical sum (3.4) may be challenging to implement at low temperature, due to the non-negligible contribution from very long trajectories to $\chi^{(1)}$. It is then useful to further develop the semiclassical expansion (3.4) by an approximate analytical calculation. Such a calculation, presented in appendix F.1, relies on trading the thermal factor (2.41) by a Heaviside function that limits the contributing trajectories to the maximal length $L_{\max} = \alpha L_T$ and performs the ν sum by Poisson summation rule, followed by a stationary-phase approximation. The cutoff length L_{\max} is chosen as that in which the thermal factor (2.41) presents the maximum derivative, yielding $\alpha \simeq 1.6$. When the thermal factor is replaced by $\Theta(L_{\max} - L_{\nu\eta})$, such a value of α yields at low temperature results for $\chi^{(1)}$ in excellent agreement with the original expression (3.4). The resulting magnetic susceptibility is then given in the limit $k_{Fa} \frac{T}{T_F} \ll 1$ (keeping $k_{Fa} \gg 1$) by

$$\frac{\chi^{(1)}}{|\chi_L|} \simeq \frac{3}{4(k_{Fa})^2} \sum_{\eta=3}^{\infty} \sum_{\substack{\ell=\ell_{\min} \\ (\ell \text{ odd})}}^{\ell_{\max}} \ell^3 \sqrt{1 - \left(\frac{\ell}{2k_{Fa}}\right)^2} \cos(\eta S_{\ell}), \quad (3.8)$$

where the phase factor S_{ℓ} , which corresponds to the (dimensionless) radial action, is defined as

$$S_{\ell} = \sqrt{(2k_{Fa})^2 - \ell^2} - \ell \arccos\left(\frac{\ell}{2k_{Fa}}\right) - \frac{3\pi}{2}. \quad (3.9)$$

In eq. (3.8), the summation over ℓ (which must be an odd integer) depends on the value of η . For $3 \leq \eta \leq \eta_c$, with $\eta_c = \alpha L_T / 2a = (\alpha/\pi)(k_{Fa} \frac{T}{T_F})^{-1}$, we have $\ell_{\min} = 1$ and $\ell_{\max} = \lfloor 2k_{Fa} \cos \vartheta_{\eta} \rfloor$ with $\vartheta_{\eta} = \pi/2\eta$ if η is odd and $\ell_{\min} = \lfloor 2k_{Fa} \sin \vartheta_{\eta} \rfloor$ and $\ell_{\max} = \lfloor 2k_{Fa} \cos \vartheta_{\eta} \rfloor$ if η is even. For $\eta > \eta_c$, we have $\ell_{\min} =$

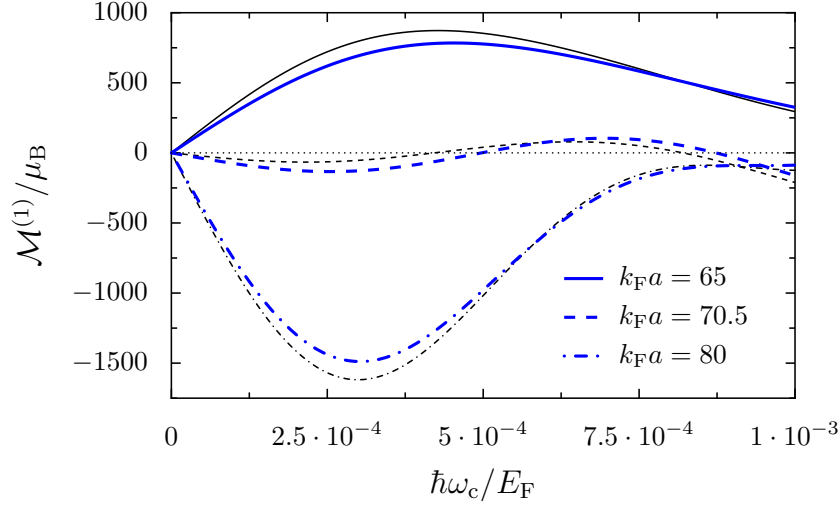


Figure 3.3: Grand-canonical magnetic moment $\mathcal{M}^{(1)}$ in units of the Bohr magneton μ_B for three different nanoparticle sizes as a function of the cyclotron frequency $\omega_c \propto H$ (in units of E_F/\hbar). Blue lines: semiclassical result from eq. (3.3). Black lines: perturbative quantum result from eq. (2.32). In the figure, $T/T_F = 5 \times 10^{-3}$.

$\lceil 2k_F a \cos(\arcsin(\eta_c/\eta) + \vartheta_\eta) \rceil$ and $\ell_{\max} = \lfloor 2k_F a \cos \vartheta_\eta \rfloor$. Here, $\lfloor x \rfloor$ and $\lceil x \rceil$ denote the floor and ceiling functions, respectively.

The sum (3.8) is considerably simpler to implement, as compared with that of eq. (3.4), and gives rather accurate results for low temperatures and/or small nanoparticle sizes (see the green line in fig. 3.2). For high temperatures, the sharp cutoff imposed when $L_{\nu\eta} > L_{\max}$ is a too restrictive approximation that ignores the exponential fall off of the thermal factor (2.41), and the previous agreement deteriorates. Nevertheless, in this regime the evaluation of eq. (3.4) is again simple, since we only need to include the contribution of the shortest trajectories with a winding number of $\nu = 1$ and the appropriate exponential fall off resulting from $R(L_{1\eta}/L_T)$ (results not shown).

The grand-canonical finite-field magnetization according to the semiclassical expression (3.3) is presented in fig. 3.3 as a function of the cyclotron frequency $\omega_c \propto H$ (blue lines). The range of $\hbar\omega_c/E_F$ corresponds to realistic values of the magnetic field that are at present experimentally available (for Au, $\hbar\omega_c/E_F = 10^{-3}$ corresponds to a field of the order of $H = 45 \times 10^4$ Oe). The different slopes at the origin obtained for the selected values of a are in line with the rapid oscillations of $\chi^{(1)}$ as a function of size (see fig. 3.1). The diamagnetic or paramagnetic character of the zero-field susceptibility might change at finite fields due to the possible nonmonotonic behavior of $\mathcal{M}^{(1)}(H)$ and its possible sign inversion for particular values of $k_F a$ (see dashed lines in fig. 3.3). Large values of the magnetic moment (of several hundreds of μ_B) can be attained. We further show in fig. 3.3 by black lines the perturbative quantum result from eq. (2.32). As it is the case for the zero-field susceptibility shown in figs. 3.1 and

3.2, the semiclassical result gives a very good qualitative account of the quantum one.

3.3 MAGNETIC RESPONSE OF AN ENSEMBLE OF NONINTERACTING NANOPARTICLES

The experiments yielding unusual magnetism in gold nanoparticles are typically performed on ensembles of nanoparticles [16, 17]. We thus consider in this section the orbital response of such ensembles, neglecting any possible interparticle interaction. This approximation should be valid in relatively dilute samples.

For an ensemble of \mathcal{N} nanoparticles, the expected value of the zero-field susceptibility is

$$\chi_{\text{ens}}(\bar{a}, \delta a) = \overline{\chi^{(1)}} + \overline{\chi^{(2)}}, \quad (3.10)$$

while the root-mean-square deviation with respect to the previous value is

$$\chi_{\text{rmsd}} \simeq \frac{1}{\sqrt{\mathcal{N}}} \left[\overline{(\chi^{(1)})^2} \right]^{1/2}. \quad (3.11)$$

The averages indicated by a bar are taken with respect to a probability distribution of sizes $\mathcal{P}(a)$. In writing eq. (3.11), we have used the fact that the typical values of $\chi^{(1)}$ are much larger than those of $\chi^{(2)}$, which is valid for sufficiently large values of $k_{\text{F}}a$ and T/T_{F} .

The magnetic response of an ensemble of nanoparticles crucially depends on its size distribution. The large diversity that can be encountered for the latter is at the origin of the rich range of observed physical behaviors. In order to provide quantitative predictions, we will focus on setups well described by a Gaussian probability distribution

$$\mathcal{P}(a) = \frac{1}{\sqrt{2\pi}\delta a} \exp\left(-\frac{(a - \bar{a})^2}{2\delta a^2}\right), \quad (3.12)$$

characterized by the average radius \bar{a} of the ensemble and its size dispersion δa .

The rapidly oscillating cosine in eq. (3.4) (see figs. 3.1 and 3.2) results in a $\overline{\chi^{(1)}}$ which decreases exponentially with $k_{\text{F}}\delta a$ and is thus much smaller than $|\chi_{\text{L}}|$ when the size dispersion $\delta a \gtrsim k_{\text{F}}^{-1} \sim 1 \text{ \AA}$. In situations where the dispersion δa is larger than 1 \AA , as is usually the case in experiments [16, 109], $\overline{\chi^{(1)}}$ is therefore negligible. It is thus $\overline{\chi^{(2)}}$ which yields the dominant contribution to the averaged magnetic susceptibility of the ensemble. Similar considerations and definitions hold for the magnetic moment per particle. The identification of χ_{ens} with the measure on an ensemble of \mathcal{N} nanoparticles is statistically sound only for a sufficiently large \mathcal{N} such that $\chi_{\text{rmsd}} \ll \chi_{\text{ens}}$. There are then two parameters that might result in large variations of the zero-field susceptibility: the size dispersion δa and the number of nanoparticles \mathcal{N} .

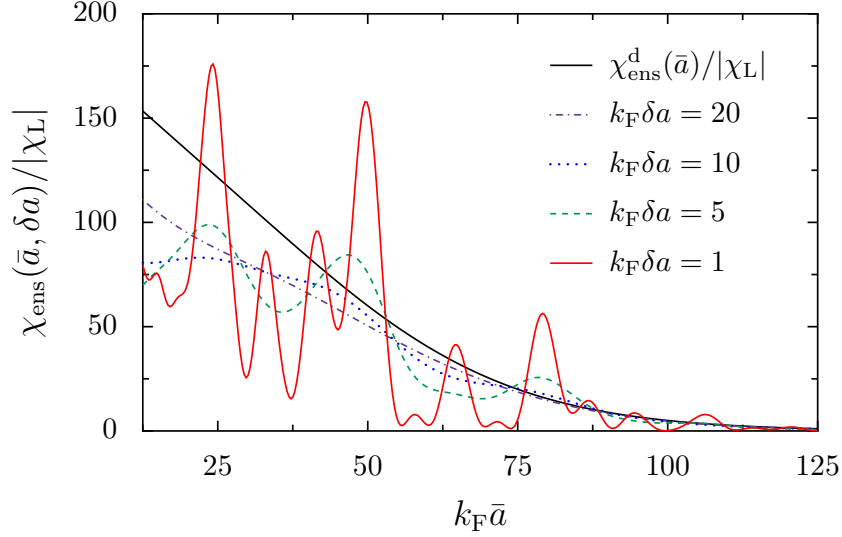


Figure 3.4: Zero-field susceptibility of a nanoparticle ensemble with average radius \bar{a} for various size dispersions δa at $T/T_F = 5 \times 10^{-3}$, from eq. (3.14). The diagonal contribution to the averaged susceptibility $\chi_{\text{ens}}^d(\bar{a})$ [eq. (3.15)] is shown for comparison as a black solid line.

Averaging $\mathcal{M}^{(2)}$ and $\chi^{(2)}$ [cf. eqs. (3.5) and (3.6)] over the Gaussian distribution (3.12) (for $k_F \delta a \gtrsim 1$), we obtain

$$\begin{aligned} \frac{\mathcal{M}_{\text{ens}}(\bar{a}, \delta a)}{\mu_B} &= -12(k_F \bar{a})^2 \sum_{\substack{v>0 \\ \eta>2v}} \sum_{\substack{v'>0 \\ \eta'>2v'}} \frac{\mathcal{F}_{v\eta}^{v'\eta'}}{\eta \cos \varphi_{v\eta} \sin \varphi_{v\eta}} \cos(\theta_{v\eta}(k_F) - \theta_{v'\eta'}(k_F)) \\ &\quad \times R(L_{v\eta}/L_T) R(L_{v'\eta'}/L_T) e^{-2[k_F \delta a (\eta \sin \varphi_{v\eta} - \eta' \sin \varphi_{v'\eta'})]^2} \\ &\quad \times j'_0(2\pi\phi_{v\eta}/\phi_0) j_0(2\pi\phi_{v'\eta'}/\phi_0) \end{aligned} \quad (3.13)$$

and

$$\begin{aligned} \frac{\chi_{\text{ens}}(\bar{a}, \delta a)}{|\chi_L|} &= 18\pi k_F \bar{a} \sum_{\substack{v>0 \\ \eta>2v}} \sum_{\substack{v'>0 \\ \eta'>2v'}} \mathcal{F}_{v\eta}^{v'\eta'} \cos(\theta_{v\eta}(k_F) - \theta_{v'\eta'}(k_F)) \\ &\quad \times R(L_{v\eta}/L_T) R(L_{v'\eta'}/L_T) e^{-2[k_F \delta a (\eta \sin \varphi_{v\eta} - \eta' \sin \varphi_{v'\eta'})]^2}, \end{aligned} \quad (3.14)$$

respectively. In eqs. (3.13) and (3.14), the quantities $L_{v\eta}$ and $\theta_{v\eta}$ (defined in sec. 2.3.3) are evaluated for $a = \bar{a}$, and $\mathcal{F}_{v\eta}^{v'\eta'}$ is given in eq. (3.7).

Sums like (3.13) and (3.14), running over four topological indexes (corresponding to two different families of periodic orbits), are even more challenging to evaluate than those running over two indexes, as eqs. (3.3) and (3.4), especially at low temperatures, where a large number of classical trajectories has to be considered. The ensemble-averaged zero-field susceptibility resulting from eq. (3.14) at high (room)

temperature $T/T_F = 5 \times 10^{-3}$ is presented in fig. 3.4 as a function of the average nanoparticle radius \bar{a} , for increasing size dispersions δa . The orbital response of the nanoparticle ensemble at zero magnetic field is *paramagnetic* ($\chi_{\text{ens}} > 0$) in all tested cases. As discussed in the introduction, such is also the case in ensembles of quasi-two-dimensional semiconductor quantum dots [82–85, 87, 88]. The orbital susceptibility of the ensemble χ_{ens} can reach large values (in units of $|\chi_L|$) for not too large mean radii, but it goes to zero when $k_F \bar{a} \gg 1$. The monotonic decrease of χ_{ens} with $k_F \bar{a}$ obtained for large size dispersions ($k_F \delta a \gtrsim 20$ in fig. 3.4) evolves into an oscillating behavior for smaller size dispersions.

The dependence on magnetic field of the ensemble-averaged magnetic moment per particle according to eq. (3.13) is presented for various average radii and size dispersions in fig. 3.5. The ensemble-averaged magnetic moment per nanoparticle can reach several tens of μ_B for room temperature ($T/T_F = 5 \times 10^{-3}$). Moreover, the behavior of \mathcal{M}_{ens} as a function of the applied magnetic field in a given interval depends significantly on the average size of the ensemble. For the smallest size considered in fig. 3.5 ($k_F \bar{a} = 20$, black lines), the magnetic moment increases monotonically with the magnetic field for the whole range of the parameter $\hbar\omega_c/E_F \propto H$ considered. For $k_F \bar{a} = 60$ (red lines), \mathcal{M}_{ens} becomes a decreasing function of the magnetic field after a critical value that depends on the size dispersion δa . For larger sizes ($k_F \bar{a} = 100$, blue lines), the previous nonmonotonic behavior appears at a smaller critical field, and eventually there occurs a sign inversion of \mathcal{M}_{ens} for even larger fields. In sec. 3.5 we link these findings with the existing experimental results found in the literature.

In the case $k_F \delta a \gg 1$, the exponential factor in eqs. (3.13) and (3.14) selects only the “diagonal” subensemble of topological indexes for which $\nu = \nu'$ and $\eta = \eta'$. When applicable, such an approximation considerably simplifies the evaluation of the semi-classical expressions and allows for simple estimations of the zero-field susceptibility and the magnetic moment. The diagonal part of the magnetic susceptibility (3.14) can be written as

$$\frac{\chi_{\text{ens}}^{\text{d}}(\bar{a})}{|\chi_L|} = 18\pi k_F \bar{a} \sum_{\substack{\nu > 0 \\ \eta > 2\nu}} \mathcal{F}_{\nu\eta}^{\nu\eta} R^2(L_{\nu\eta}/L_T), \quad (3.15)$$

which is positive since $\mathcal{F}_{\nu\eta}^{\nu\eta} > 0$ [cf. eq. (3.7)]. As can be seen in fig. 3.4, this diagonal contribution (black solid line) provides a good account of the behavior of χ_{ens} for large $k_F \delta a$.

Interestingly, eq. (3.15) is a function of the single parameter $k_F \bar{a} \frac{T}{T_F} = 2\bar{a}/\pi L_T$ when scaled with $k_F \bar{a}$. This can be seen from the argument of the thermal function (2.41), $L_{\nu\eta}/L_T = \pi\eta \sin \varphi_{\nu\eta} k_F \bar{a} \frac{T}{T_F}$, and is exemplified in fig. 3.6, where the circles correspond to a numerical evaluation of the sum over the topological indexes in eq. (3.15). Remarkably, for $k_F \bar{a} \frac{T}{T_F} \ll 1$ (with $k_F \bar{a} \gg 1$), eq. (3.15) follows the Curie-type law

$$\frac{\chi_{\text{ens}}^{\text{d}}}{|\chi_L|} = \frac{C}{T/T_F}, \quad (3.16)$$

independent of the average size \bar{a} of the nanoparticles.

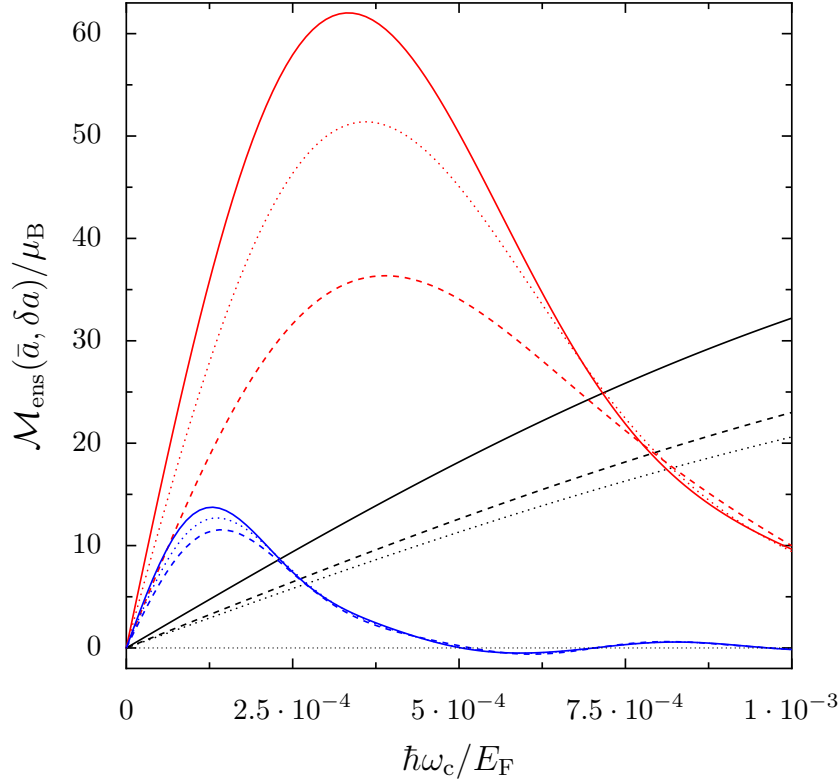


Figure 3.5: Ensemble-averaged magnetic moment per particle from eq. (3.13) as a function of magnetic field with mean radius $k_F \bar{a} = 20$ (black lines), 60 (red lines), 100 (blue lines), and for size dispersions $k_F \delta a = 5$ (dashed lines) and 10 (dotted lines). The diagonal contribution $\mathcal{M}_{\text{ens}}^d(\bar{a})$ [cf. eq. (3.19)] is shown as solid lines. In the figure, $T/T_F = 5 \times 10^{-3}$.

The prefactor C of the above Curie law can be analytically evaluated along the lines leading to the semiclassical result (3.8) and presented in appendix F.2. First, the thermal factor (squared) in eq. (3.15) is replaced by a Heaviside step function which cuts trajectories longer than $L_{\text{max}} = \alpha L_T$ ($\alpha \simeq 1.6$, see sec. 3.2). Second, the sums over the topological indexes are approximately evaluated by replacing them by integrals. To leading order in $k_F \bar{a} \frac{T}{T_F} \ll 1$, we then obtain

$$C = \frac{9\alpha}{16}. \quad (3.17)$$

The result (3.16), together with eq. (3.17), is shown by the solid line in fig. 3.6. As can be seen from the main figure, there is excellent quantitative agreement between the numerical evaluation of eq. (3.15) (circles) and the approximate result (3.16) (solid line) for small nanoparticle sizes and/or low temperatures.

For larger values of the parameter $k_F \bar{a} \frac{T}{T_F}$, the susceptibility resulting from eq. (3.15) deviates from the Curie-type law and is exponentially suppressed with temperature.

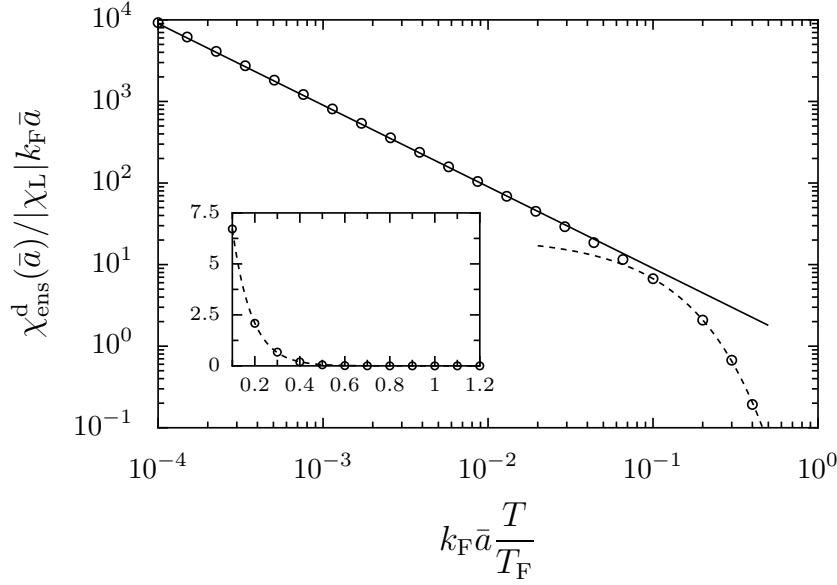


Figure 3.6: Log-log plot of the diagonal contribution $\chi_{\text{ens}}^{\text{d}}(\bar{a})$ to the ensemble-averaged zero-field susceptibility (in units of $|\chi_{\text{L}}|$) scaled with $k_{\text{F}}\bar{a}$ as a function of $k_{\text{F}}\bar{a}\frac{T}{T_{\text{F}}}$. Circles: numerical evaluation of eq. (3.15). Solid line: Curie-type law (3.16), with C as given in eq. (3.17). Dashed line: exponential fit (3.18), with $c_1 \simeq 22$ and $c_2 \simeq 12$. Inset: Linear-scale plot of the same data, but for a different range of $k_{\text{F}}\bar{a}\frac{T}{T_{\text{F}}}$.

It can be fitted by

$$\frac{\chi_{\text{ens}}^{\text{d}}(\bar{a})}{|\chi_{\text{L}}|} = c_1 k_{\text{F}}\bar{a} \exp\left(-c_2 k_{\text{F}}\bar{a} \frac{T}{T_{\text{F}}}\right), \quad (3.18)$$

with $c_1 \simeq 22$ and $c_2 \simeq 12$. Such a behavior can be traced back to the exponential suppression induced by the thermal factor (2.41) even for the shortest trajectories, in line with our discussion of the high-temperature regime for $\chi^{(1)}$ in sec. 3.2.

Similarly to the case of the zero-field susceptibility, we consider the diagonal contribution [terms with $\nu = \nu'$ and $\eta = \eta'$ in eq. (3.13)]

$$\begin{aligned} \frac{\mathcal{M}_{\text{ens}}^{\text{d}}(\bar{a})}{\mu_{\text{B}}} &= -12(k_{\text{F}}\bar{a})^2 \sum_{\substack{\nu > 0 \\ \eta > 2\nu}} \frac{\mathcal{F}_{\nu\eta}^{\nu\eta}}{\eta \cos \varphi_{\nu\eta} \sin \varphi_{\nu\eta}} \\ &\times R^2(L_{\nu\eta}/L_T) j_0'(2\pi\phi_{\nu\eta}/\phi_0) j_0(2\pi\phi_{\nu\eta}/\phi_0) \end{aligned} \quad (3.19)$$

to the magnetic moment per nanoparticle, which becomes dominant in the case $k_{\text{F}}\delta a \gg 1$ (solid lines in fig. 3.5). Once scaled with $(k_{\text{F}}\bar{a})^2$, eq. (3.19) only depends on the two following parameters: (i) the normalized flux $\bar{\phi}/\phi_0$ appearing in the argument of the spherical Bessel function and its derivative in eq. (3.19) ($\bar{\phi} = \pi\bar{a}^2 H$ is the magnetic flux through an average-size nanoparticle); (ii) the ratio between average radius and thermal length $2\bar{a}/\pi L_T = k_{\text{F}}\bar{a}\frac{T}{T_{\text{F}}}$ through the argument of the ther-

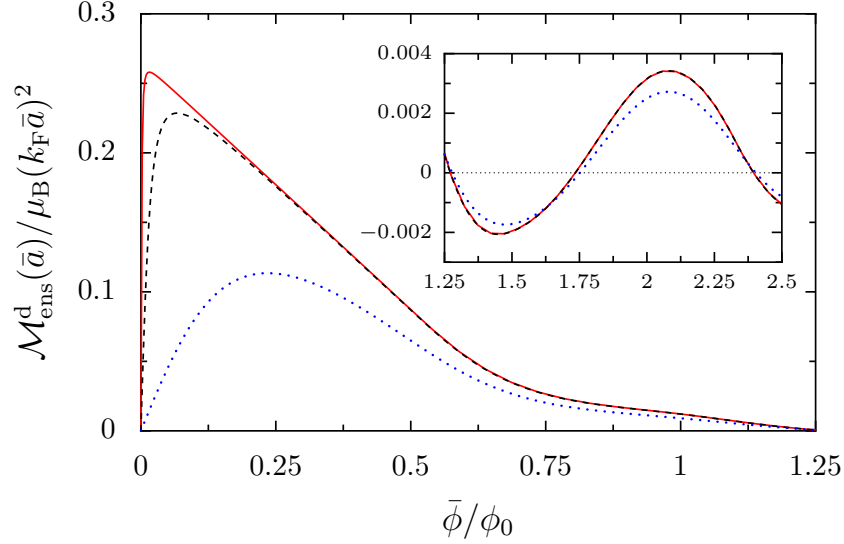


Figure 3.7: Diagonal contribution to the ensemble-averaged magnetic moment from eq. (3.19) scaled with $(k_F\bar{a})^2$ as a function of the reduced magnetic flux $\bar{\phi}/\phi_0$ for $k_F\bar{a}T/F = 10^{-3}$ (red solid line), 10^{-2} (black dashed line), and 10^{-1} (blue dotted line). Inset: Same as the main figure for a different range of $\bar{\phi}/\phi_0$.

mal reduction factor (2.41). Figure 3.7 presents the flux dependence of the diagonal contribution (3.19) scaled with $(k_F\bar{a})^2$. For weak flux, $\bar{\phi} \ll \phi_0$, the magnetic moment increases linearly with magnetic field and its temperature dependence follows a Curie-type law as shown for the susceptibility [see eq. (3.16)]. For larger flux, a maximal value is attained and $\mathcal{M}_{\text{ens}}^d$ decreases until it reaches negative values and oscillates as a function of flux, resembling the de Haas-van Alphen oscillations [24] that would occur for much larger magnetic flux. As the temperature decreases, the magnetic moment increases significantly at weak magnetic field, reaching very high values.

3.4 MAGNETIC RESPONSE OF INDIVIDUAL NANOPARTICLES

In the previous section we discussed the situation of a nanoparticle ensemble, which is the case where the magnetic response has been extensively measured. The orbital magnetic response of an individual nanoparticle, given by

$$\mathcal{M} = \chi_L H + \mathcal{M}^{(1)} + \mathcal{M}^{(2)} \quad (3.20)$$

and

$$\chi = \chi_L + \chi^{(1)} + \chi^{(2)}, \quad (3.21)$$

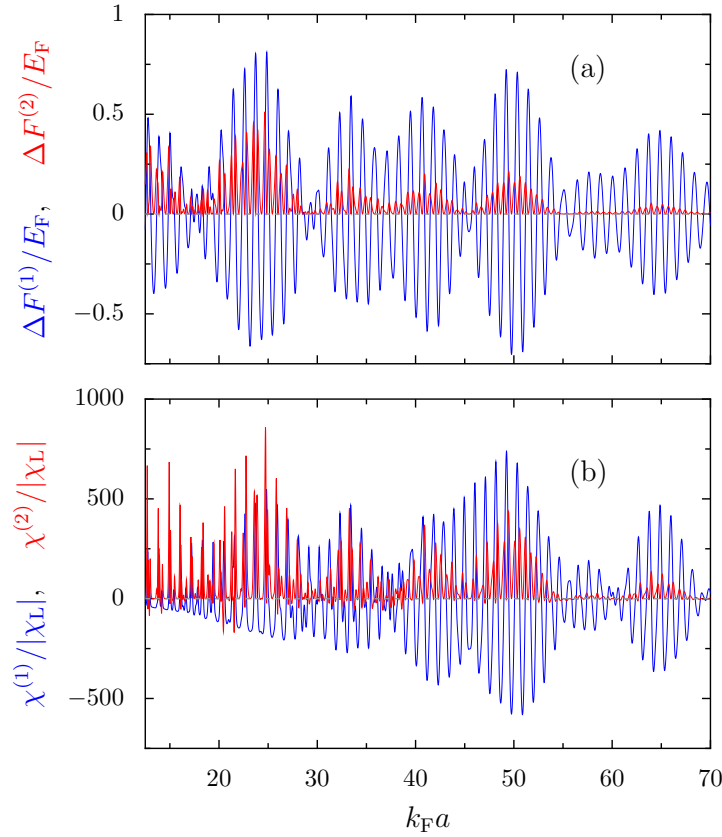


Figure 3.8: Blue lines: grand-canonical (a) free energy $\Delta F^{(1)}$ at $H = 0$ (scaled with the Fermi energy E_F) from eq. (3.1) at a temperature $T/T_F = 5 \times 10^{-3}$ and (b) corresponding zero-field susceptibility $\chi^{(1)}$ from eq. (3.4) (cf. blue line in fig. 3.1) as a function of $k_F a$. Red lines: canonical contribution $\Delta F^{(2)}$ from eq. (3.2) [panel (a)] and zero-field susceptibility $\chi^{(2)}$ from eq. (3.6) [panel (b)].

has considerable interest for two reasons. Firstly, \mathcal{M} and χ become relevant when analyzing the experimental conditions aiming at measurements on relatively small numbers of particles or in the case of single nanoparticles. These conditions could be achieved, e.g., using magnetic force microscopy [17, 145] of nanoparticles deposited on a nonmagnetic substrate. Secondly, if interactions among the nanoparticles of the ensemble are included in the description, the single-particle magnetic moment \mathcal{M} becomes a crucial ingredient of the model describing the magnetic response of coupled nanoparticles [146].

As discussed in sec. 2.3.3, the fulfillment of the condition $\Delta F^{(2)} \ll |\Delta F^{(1)}|$, at the basis of our semiclassical thermodynamic formalism, depends on the values of $k_F a$ and T/T_F . In order to quantify these constraints, we present in fig. 3.8(a) [fig. 3.8(b)] the values of $\Delta F^{(1)}$ [$\chi^{(1)}$] in blue, and $\Delta F^{(2)}$ [$\chi^{(2)}$] in red, for room temperature ($T/T_F = 5 \times 10^{-3}$) and a reduced $k_F a$ span as compared to the one shown in

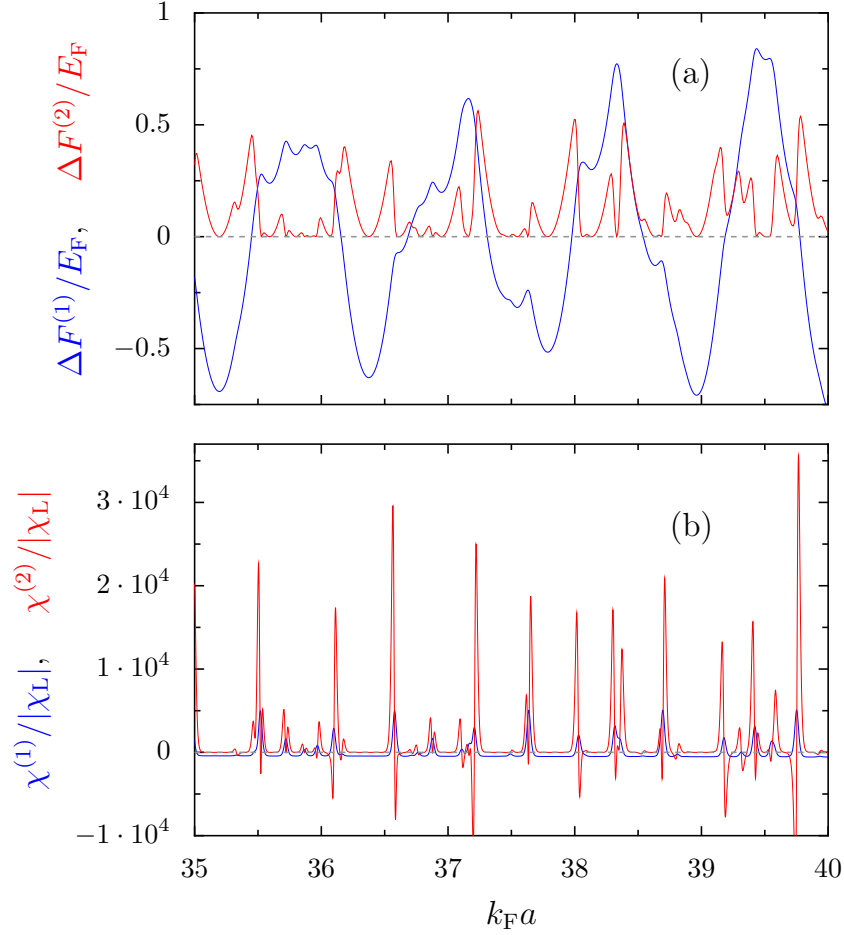


Figure 3.9: Low-temperature $T/T_F = 5 \times 10^{-4}$ results for the contributions to (a) the free energy and (b) the susceptibility. As in fig. 3.8, blue lines represent the grand-canonical contributions from eqs. (3.1) and (3.4), and red lines depict the canonical contributions of eqs. (3.2) and (3.6).

fig. 3.1. At the lowest values considered for k_{Fa} , $\Delta F^{(2)}$ is comparable to $|\Delta F^{(1)}|$, but it rapidly becomes comparatively smaller for $k_{Fa} \gtrsim 30$ and then completely negligible for $k_{Fa} \gtrsim 50$. The semiclassical thermodynamic formalism is then applicable at room temperature over almost all the k_{Fa} range, even if $|\chi^{(2)}|$ typically dominates $|\chi^{(1)}|$ up to $k_{Fa} \simeq 30$. Consistent with these results, the magnetic moment \mathcal{M} of an individual nanoparticle at room temperature is essentially given by $\mathcal{M}^{(1)}$ for the sizes shown in fig. 3.3, where \mathcal{M} as a function of k_{Fa} is indistinguishable from $\mathcal{M}^{(1)}$ on the scale of the figure (data not shown).

The situation at low temperature $T/T_F = 5 \times 10^{-4}$ is presented in fig. 3.9 for a smaller range of k_{Fa} . Again, we can observe that the canonical contribution $\Delta F^{(1)}$ (blue line) is typically larger than the grand-canonical one $\Delta F^{(2)}$ (red line). Even though the grand-canonical contribution to the susceptibility is larger than the canonical one, we expect the semiclassical formalism to yield at least qualitatively correct

results for these and larger values of $k_F a$.

Our treatment of the magnetic response of individual nanoparticles demonstrates that very large paramagnetic zero-field susceptibilities, can be achieved at sufficiently low temperatures, which might translate in emerging magnetic instabilities once a dipolar coupling between the nanoparticles magnetic moments is considered [146].

3.5 COMPARISONS TO THE EXPERIMENTAL RESULTS

The variety of possible magnetic responses (diamagnetic, paramagnetic, or ferromagnetic) experimentally observed calls for a systematic evaluation of the results yielded by different theoretical descriptions. Within our model presented in sec. 2.1, we obtained in sec. 3.3 a paramagnetic response at weak fields for the case of an ensemble with a large number of noninteracting nanoparticles and a rather large size dispersion, as it is often the case in experiments. For increasing fields the magnetization of the nanoparticle ensemble could switch from its low-field paramagnetic behavior to a diamagnetic response (decreasing of the magnetization with the field and even a magnetization antialigned with the applied field, see figs. 3.5 and 3.7). While these changes are often observed in experiments [16], such behavior is usually interpreted as coming from spurious diamagnetic elements of the sample [59].

In order to test the relevance of our approach, we will disregard the cases where the parameters of the sample are not completely known and exclude observations of ferromagnetism where, presumably, the interparticle interactions are important. We will thus concentrate on the experiments where the paramagnetic behavior has been clearly established.

The pioneering experiments of refs. [34, 35], which also included palladium nanoparticles, have been extremely important in fostering the interest on the subject, by yielding large values of the saturation magnetic moment per nanoparticle (about $20\mu_B$) in a regime where the magnetic interaction between the nanoparticles could be neglected. In fig. 3.10, we reproduce the magnetization per gram of gold in the sample M_{ens} of refs. [34, 35] for gold nanoparticles surrounded by polyvinylpyrrolidone (PVP) ligands (red dots) having a mean diameter $2\bar{a} \simeq 2.5$ nm and a relatively narrow size dispersion ($2\delta a \simeq 0.4$ nm) at $T = 1.8$ K. These experimental data, well represented by the Langevin function and exhibiting quasiparamagnetic field and temperature dependences, have been reproduced in different samples with various ligands (see triangles in fig. 3.10), except in the case where strong covalent bonds get established with the nanoparticles [38].

The solid line in fig. 3.10 represents $\mathcal{M}_{\text{ens}}/\rho\mathcal{V}$, where \mathcal{M}_{ens} is given in eq. (3.13) and $\rho_{\text{Au}} = 19.3$ g/cm³ is the mass density of gold, for the temperature, mean diameter, and width of the size distribution of the experimental data.¹ As no fitting parameters

¹Given the high numerical cost of performing the four summations of eq. (3.13) at the low temperature of the experiment, we limited ourselves to the case $\nu' = \nu$ (verifying that for the corresponding value of $k_F \delta a$ the exponential factor strongly suppresses the terms having $\nu' \neq \nu$), and we replaced the thermal factor R_T by a Heaviside step function, similarly to what we have done in secs. 3.2

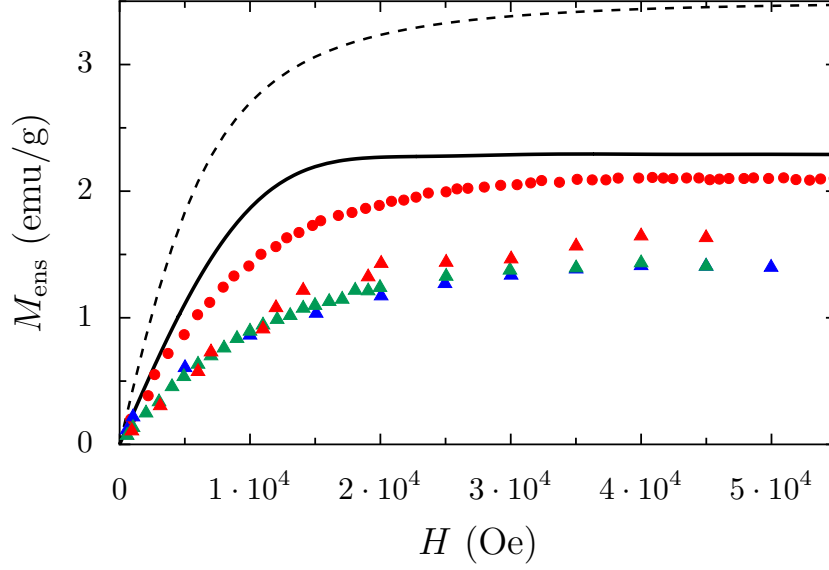


Figure 3.10: Dots and triangles: measured magnetization M_{ens} of an ensemble of Au nanoparticles functionalized with various ligands (in electromagnetic units per gram of gold nanoparticles in the sample) as a function of applied field H (in oersted), with mean diameter $2\bar{a} = 2.5$ nm, size dispersion $2\delta a = 0.4$ nm, and at a temperature $T = 1.8$ K. The data are taken from the experiments of refs. [34, 35, 38], c.f. fig. 1.3b. The corresponding ligands are: polyvinyl pyrrolidone (PVP) [red dots (refs. [34, 35]) and red triangles (ref. [38])], polyacrylonitrile (PAN) [green triangles (ref. [38])], and polyallyl amine hydrochloride (PAAHC) [blue triangles (ref. [38])]. Solid line: nondiagonal magnetization from eq. (3.13) with $2\delta a = 0.4$ nm. Dashed line: diagonal approximation (3.19), corresponding to $2\delta a \rightarrow \infty$.

are invoked, the qualitative agreement between our theory and these sets of data makes us conclude that the orbital response is indeed a crucial ingredient in the cases where the nanoparticle interaction is negligible.

It should be remarked that for the small values of a and T used in fig. 3.10, the semi-classical thermodynamic formalism becomes questionable. Notwithstanding, while in the formalism in chapter 2 the temperature is the only parameter to smooth out the oscillations of the density of states of an individual nanoparticle, in an ensemble of nanoparticles there are other additional factors that contribute to smooth the density of states and then reduce the values of $\overline{\Delta F^{(2)}}$. Among them, the size dispersion characterized by $\mathcal{P}(a)$, the possibility of having deviations with respect to the perfectly spherical shape, and effects of structural or impurity-induced disorder. It is based on the latter effect that the canonical correction has been obtained for the problem of persistent currents in metallic nanostructures [76, 77].

and 3.3 when deriving eqs. (3.8) and (3.17), respectively (verifying also the applicability of such an approximation).

For comparison purposes, we also present in fig. 3.10 (dashed line) M_{ens} according to the diagonal approximation (3.19). On the one hand, we see that the simple diagonal approximation is enough to provide a qualitative agreement with respect to the experimental data. On the other hand, we verify that the effect of the size dispersion δa , which is responsible for the difference between the two expressions, appears as a key element in achieving a more quantitative agreement.

The existing data yielding a paramagnetic zero-field susceptibility are more difficult to relate with the theoretical prediction of figs. 3.4 and 3.6, and eqs. (3.14) and (3.16), than those concerning the magnetization. While the value of χ that can be extracted from the magnetization curve of refs. [34, 35] is in qualitative agreement with eq. (3.16) and the reported zero-field susceptibility follows a clear Curie law, the numerical values associated to the experiment are two orders of magnitude larger than the theoretical prediction. The inconsistency between the experimentally reported values of the magnetization and susceptibility of refs. [34, 35] might be due to an incorrect handling of the units [147].

The magnetization measurements of Y. Yamamoto *et al.* [37] yielded a paramagnetic susceptibility for an ensemble of gold nanoparticles with $2\bar{a} = 1.9$ nm and a log-normal size distribution. The reported susceptibility follows a Curie-type law, but with values which are several orders of magnitude smaller than the previously-discussed data or the theoretical curve of fig. 3.6, and it has been explained from the orbital moment of the Au 5*d* electrons.

The susceptibility results of Bartolomé *et al.* [46] on gold nanoparticles with naturally thiol-containing protective agents, between $T = 2.7$ K and 10 K, exhibit a paramagnetic response with a clear Curie law, but an order of magnitude smaller than the data of refs. [34, 35]. The findings of ref. [46] have been interpreted by invoking the holes of the Au 5*d* band induced by the thiols, and thus the comparison with our ligand-independent theoretical approach is problematic.

Some of the reported ferromagnetic samples present an extremely narrow hysteresis loop [44, 45], such that a quasiparamagnetic zero-field susceptibility can be inferred. The values thus obtained from the low-temperature data of refs. [44, 45] result in a paramagnetic susceptibility which is one to two orders of magnitude smaller than our theoretical prediction, depending on the nature of the protective ligands.

We thus conclude that the orbital magnetism contribution is always important for analyzing the cases yielding a paramagnetic response of an ensemble of nanoparticles. In the cases where the ligands do not considerably alter the electronic states of the isolated nanoparticles, a qualitative agreement between theory and experiment is obtained for the magnetization curves and in the fulfillment of a Curie-type law of the zero-field susceptibility for a large range of temperatures (up to about room temperature, for sufficiently small nanoparticles).

The diamagnetic response obtained in some experiments [40, 42, 44, 48] could also be accounted for from the orbital magnetism, provided a narrow size dispersion or a peaked size distribution of the nanoparticles in the ensemble allow for the fluctuations of $\chi^{(1)}$ (see figs. 3.1 and 3.2) to dominate over the paramagnetic contribution

of $\chi^{(2)}$. Another proposal to account for the diamagnetic behavior is to invoke the effect of the spin-orbit coupling [42, 90], that unlike the case of persistent currents in disordered rings [148], would reverse the sign of the magnetic response.

3.6 CONCLUSIONS FOR CHAPTER 3

In this chapter, we have investigated orbital magnetism in gold nanoparticles. Specifically, we have considered spherical metallic particles in the jellium approximation and treated the electron-electron interactions within a mean-field approach. The orbital response of individual as well as ensembles of nanoparticles with a smooth size distribution have been calculated within a semiclassical formalism. While the magnetic response at weak fields of an individual nanoparticle can be anything from strongly diamagnetic to strongly paramagnetic depending on its size, the ensemble-averaged response is always paramagnetic when neglecting the interparticle interactions. In particular, we have predicted that the ensemble-averaged zero-field susceptibility should present a Curie-type law at low temperature, independent of the average size of the nanoparticles. We have obtained a qualitative agreement with the existing experimental data on the magnetization of ensembles of diluted nanoparticles in the case where interparticle interactions are negligible and where the local modifications induced by the surrounding ligands are irrelevant. Our results do not depend on details of the electronic structure and are thus not limited to gold but can be applied to any spherically-symmetric metallic nanoparticles. Moreover, the proposed mechanism does not rely on organic ligands surrounding the particles.

An important conclusion of this chapter is to counter the claim [37, 38] that the strong paramagnetic response of the nanoparticle ensemble constitutes a proof that the individual nanoparticles are ferromagnetic. Indeed, we have shown that the orbital response of a large nanoparticle ensemble with a relatively broad size distribution can attain a large paramagnetic value through the flux accumulation of the underlying classical trajectories.

In order to obtain analytically-tractable results, we assumed that the nanoparticles are perfectly spherical. Other symmetric geometries can be approached with the tools presented in this chapter, like the cases of half-spherical and cylindrical nanoparticles (analyzed in sec. 4.5 and appendix C.2, respectively). Importantly, crystallographic faceting at the surfaces of the particles, as well as static impurities inside the clusters, would reduce the geometric symmetries and tend to render chaotic the underlying classical dynamics of the electrons. As is well known [83–85, 87, 88], the orbital magnetism of classically-chaotic and/or disordered systems is less pronounced than that of purely integrable ones. The high values of magnetic susceptibilities we obtain should thus be taken with care when comparing our results with existing experiments using larger nanoparticles and/or when disorder becomes important. However, the qualitative trends we are predicting should not be affected by fine details of the electron dynamics.

The work presented in this chapter is an important step toward understanding

the effect of orbital magnetism in assemblies of nanoparticles. While the results presented here may explain a tendency toward the low-field paramagnetic behavior of certain samples, two potentially important ingredients for fully understanding some experiments reporting an anomalous magnetic behavior of gold nanoparticles have been put aside in this work, namely the interparticle magnetic dipolar interactions and a nonsmooth, peaked size distribution. The former may be necessary to obtain ferromagnetic behavior, as is observed in certain samples, and can in principle be addressed with the same thermodynamical formalism developed until this point [146]. The latter might occur depending on the fabrication process due to shell effects [1, 110]. The size dispersion was shown to be a crucial factor in determining the magnetic response, and in the limit where it becomes so small as to represent a peaked size distribution, we no longer expect the vanishing of the contribution of $\chi^{(1)}$ upon the ensemble average. The resulting strong oscillation as a function of nanoparticle size could explain the variation in the observed behavior from strong paramagnetism to strong diamagnetism in macroscopically similar samples having very narrow size distributions.

The suggestion that a paramagnetic response of the ensemble could turn into a diamagnetic one under the influence of spin-orbit coupling [42, 90], in analogy with the sign inversion of the magnetoconductance [92–94, 149], is the main subject of chapter 4, where we study the weakly-relativistic effects in the magnetic response of gold nanoparticles.

WEAKLY RELATIVISTIC CORRECTIONS TO THE MAGNETIC SUSCEPTIBILITY OF METALLIC NANOPARTICLES

4

In the previous chapter we only considered the orbital electronic dynamics in spherical nanoparticles and found that the magnetic response of the non-interacting (Gaussian-averaged) ensemble behaved paramagnetically. The large diversity of magnetic behaviors of metallic nanoparticles, that includes also ferromagnetic and strongly diamagnetic responses [16, 17], is hard to account for based solely on orbital magnetism. In sec. 1.4, we introduced the effects of spin-orbit coupling (SOC) in confined systems. It has been suggested that SOC could be the main ingredient to invert the magnetic response from paramagnetic to diamagnetic [42, 90] in ensembles of gold nanorods, analogous to systems that show similar inversions such as the one observed going from weak localization to weak antilocalization in various nanostructures [92–94, 149].

Kramer’s theorem (sec. 2.4.3) states that the degeneracy of the single-particle spectrum cannot be removed in the absence of magnetic fields, but the SOC can significantly modify the statistical properties of the spectrum. The statistics of energy levels in time-reversal symmetric (chaotic or disordered) confined systems changes from orthogonal to symplectic (Gaussian or circular) distributions when going from vanishing to strong spin-orbit coupling [150, 151]. The previous transition is controlled by the strength of the SOC, and therefore it is important to evaluate such a critical parameter, a task that will be undertaken in this chapter. Knowing the strength of the SOC is not only relevant to assess the possible switch between paramagnetic and diamagnetic behavior, but also relevant toward accounting for the reduced g -factor measured in the tunneling resonances of disordered metallic nanoparticles [99, 100, 103, 104]. Moreover, as bulk gold already presents noticeable relativistic features [133], the SOC has also been invoked in phenomenological theoretical models attempting to explain the anomalous ferromagnetic response of gold nanoparticles [65].

The SOC in gold nanoparticles may have different origins and in this chapter we focus on the effects of SOC due to the spatial confinement. As we are considering the electronic response in pure nanoparticles, the effects of SOC coming from the atomic nuclei or from impurities are not considered here. In chapter 3, we saw that the orbital zero-field susceptibility was amplified by orders of magnitude as compared to the Landau susceptibility χ_L . It is thus important to estimate if confinement can also lead to an important increase of the weakly relativistic corrections to the bulk case, i.e. $\chi_b^{(wr)}$ (2.48).

The spin, which was neglected in the previous chapter is reintroduced here in the non-relativistic spectrum, as the Zeeman interaction (2.7) will now couple different orbital subspaces when we include both, SOC and confinement. In this chapter we work in the weakly relativistic limit obtained from the Dirac Hamiltonian in the presence of electric and magnetic fields (see sec. 2.4.2). The spherical geometry is considered in detail, leading to semi-analytical formulas for the zero-field susceptibility in the presence of additional weakly relativistic effects such as the Darwin term and relativistic corrections to the kinetic energy in the presence of magnetic fields. The corrections to the non-relativistic ZFS, coming from SOC depend on the symmetry of the problem and are dominated by the weakly-relativistic kinetic energy correction, which is reduced by a relativistic factor proportional to $(v_F/c)^2$. In order to investigate the influence of symmetry, we also treat in detail the case of half-spherical nanoparticles. For this geometry with reduced symmetry, the calculations require a numerical treatment.

This chapter is organized as follows: In sec. 4.1 we present the remaining ingredients for the weakly relativistic Hamiltonian, which we employ in order to assess the relevance of weakly-relativistic effects for the ZFS of spherical nanoparticles. In sec. 4.2 we treat in detail the relativistic kinetic energy correction in the absence of spin-orbit coupling which will be important for comparison purposes. The perturbative calculation of the ZFS in the presence of spin-orbit coupling is given in section 4.3 and the numerical calculations for the case of the sphere are presented in section 4.4. The case of half-spherical nanoparticles is treated in sec. 4.5. We conclude this chapter in sec. 4.6. The findings presented in this chapter are based on the results of ref. [152].

4.1 WEAKLY RELATIVISTIC DESCRIPTION

The weakly-relativistic Hamiltonian for an electron subject to a static electric field was given in eq. (2.60). For our discussion we need to include also the static magnetic induction field [91, 134].

The nonrelativistic Hamiltonian $\mathcal{H}^{(\text{nr})} = \mathcal{H}^{(\text{orb})} + \mathcal{H}^{(\text{Z})}$ was already described in section 2.6. As we now include spin it is convenient to group the paramagnetic (2.9b) and Zeeman (2.57) components in a term representing the coupling of the total magnetic moment

$$\boldsymbol{\mu} = -\frac{\mu_B}{\hbar} (\mathbf{L} + g_0 \mathbf{S}) \quad (4.1)$$

to the magnetic induction \mathbf{B} , leading to

$$\begin{aligned} \mathcal{H}^{(\mu)} &= \mathcal{H}^{(\text{para})} + \mathcal{H}^{(\text{Z})} \\ &= -\boldsymbol{\mu} \cdot \mathbf{B}. \end{aligned} \quad (4.2)$$

The weakly relativistic correction $\Delta\mathcal{H}$ from eq. (2.59), can be obtained from the Dirac equation using a Foldy–Wouthuysen transformation as detailed in appendix E. The full term reads

$$\Delta\mathcal{H} = \mathcal{H}^{(\text{k})} + \mathcal{H}^{(\text{so-ame})} + \mathcal{H}^{(\text{D})} + \mathcal{H}^{(\text{r})}, \quad (4.3)$$

where $\mathcal{H}^{(D)}$ is the Darwin term from eq. (2.61) and $\mathcal{H}^{(r)}$ from eq. (2.62) vanishes for conservative potentials as previously discussed. The other two terms are different from the case $\mathbf{A}(\mathbf{r}) = 0$ seen in eq. (2.60), and given by

$$\mathcal{H}^{(k)} = -\frac{1}{8m^3c^2} \left\{ \boldsymbol{\sigma} \cdot \left[\mathbf{p} + \frac{e}{c} \mathbf{A}(\mathbf{r}) \right] \right\}^4, \quad (4.4a)$$

$$\mathcal{H}^{(\text{so-ame})} = \frac{e\hbar}{4m^2c^2} \boldsymbol{\sigma} \cdot \left\{ \mathbf{E}(\mathbf{r}) \times \left[\mathbf{p} + \frac{e}{c} \mathbf{A}(\mathbf{r}) \right] \right\}. \quad (4.4b)$$

The term $\mathcal{H}^{(\text{so-ame})}$ combines the spin-orbit coupling from (1.6) and the angular magneto-electric (ame) [153] couplings. $\mathcal{H}^{(k)}$ is the first weakly-relativistic correction to the kinetic energy and contains $\mathcal{H}^{(k-\text{free})}$ from eq. (2.54) with the addition of magnetic and spin dependent terms.

The correction (4.4b) takes the form

$$\mathcal{H}^{(\text{so-ame})} = \mathcal{H}^{(\text{so})} + \mathcal{H}^{(\text{ame})}, \quad (4.5)$$

with

$$\mathcal{H}^{(\text{so})} = \frac{1}{2m^2c^2} \mathbf{S} \cdot [\nabla V_{\text{mf}}(\mathbf{r}) \times \mathbf{p}], \quad (4.6a)$$

$$\mathcal{H}^{(\text{ame})} = \frac{e}{4m^2c^3} \mathbf{S} \cdot [\nabla V_{\text{mf}}(\mathbf{r}) \times (\mathbf{B} \times \mathbf{r})], \quad (4.6b)$$

while the Darwin term (2.61) can be written as

$$\mathcal{H}^{(D)} = \frac{\hbar^2}{8m^2c^2} \nabla^2 V_{\text{mf}}(\mathbf{r}). \quad (4.7)$$

Our main interest is the effect of the SOC (1.6) correction on the magnetic response of different kinds of nanoparticles. In order to assess its relevance, we need to also examine the role of the other weakly-relativistic corrections.

4.1.1 HAMILTONIAN FOR THE SPHERICAL SYMMETRIC CASE

We here consider a spherically-symmetric confinement defined by a step potential (2.4). The spherical symmetry of the problem allows one to further simplify the expressions of eqs. (4.6a) and (4.6b) for the spin-orbit and angular magneto-electric couplings, respectively, as

$$\mathcal{H}^{(\text{so})} = \frac{1}{2m^2c^2} \frac{1}{r} \left(\frac{dV_{\text{mf}}}{dr} \right) \mathbf{S} \cdot \mathbf{L}, \quad (4.8a)$$

$$\mathcal{H}^{(\text{ame})} = -\frac{\mu_B B}{2mc^2\hbar} r \left(\frac{dV_{\text{mf}}}{dr} \right) \sin(\theta) \mathbf{S} \cdot \hat{\mathbf{e}}_\theta, \quad (4.8b)$$

while the Darwin term (2.61) can be written as

$$\mathcal{H}^{(D)} = \frac{\hbar^2}{8m^2c^2} \frac{1}{r^2} \frac{d}{dr} \left(r^2 \frac{dV_{\text{mf}}}{dr} \right). \quad (4.9)$$

The finite height V_0 of the confining wall is responsible for the spill-out effect [113]. A proper description of this effect, as well as the lifetime of the surface plasmon resonance necessitates to go beyond the discontinuous form (2.4) of the confining potential, including the abruptness of the potential jump at the nanoparticle surface. In the case of the ZFS, the abruptness of the potential jump is not a crucial parameter, and moreover, the careful analysis of the wave-function behavior close to a potential discontinuity, that we perform next, shows that the precise value of V_0 is not determinant for the nonrelativistic ZFS, nor for the weakly-relativistic corrections (with the exception of the Darwin contribution discussed in appendix G), justifying the limit of $V_0 \rightarrow \infty$ commonly adopted in the nonrelativistic case [22, 68, 69].

When going from the description of the ideal model system to that of a gold nanoparticle, we should in principle use g_{Au} instead of g_0 in the expression (4.1) for the total magnetic moment. However, the small difference between g_{Au} and g_0 , like the one between m^* and m , only induces very small corrections.

4.1.2 NONRELATIVISTIC SUSCEPTIBILITY WITH SPIN

As seen before in chapter 3, the magnetization and the ZFS in the nonrelativistic case can be calculated in the case of a spherical geometry by quantum perturbation theory [22, 68], or by the semiclassical expansions for the DOS developed in appendix B. We showed in appendix D the connection between the two approaches. The quantum procedure was derived in chapter 2 (secs. 2.2 and 2.3.2).

The action of a magnetic field over the spin through the term $\mathcal{H}^{(\mu)}$ of eq. (4.2) is, on the one hand, to break the degeneracy of the $B = 0$ eigenenergies without giving rise to a new basis of eigenstates. On the other hand, the states $\Psi_{n,l,m_z,m_s}^{(0)}$ [cf. eq. (2.10)] are no longer eigenstates once the diamagnetic term $\mathcal{H}^{(\text{dia})}$ of eq. (2.9c) is considered under a finite magnetic field. Thus, up to terms of order B^2 , the perturbed energies are

$$E_{n,l,m_z,m_s}^{(\text{nr})} = E_{n,l}^{(0)} + \delta E_{n,l,m_z,m_s}^{(\text{nr})}, \quad (4.10)$$

where $\delta E_{n,l,m_z,m_s}^{(\text{nr})}$ is the magnetic-field correction, which reads

$$\delta E_{n,l,m_z,m_s}^{(\text{nr})} = E_{m_z,m_s}^{(\mu)} + E_{n,l,m_z}^{(\text{dia})}. \quad (4.11)$$

Consistently with eq. (4.2), we denote

$$E_{m_z,m_s}^{(\mu)} = E_{m_z}^{(\text{para})} + E_{m_s}^{(\text{Z})}, \quad (4.12)$$

with

$$E_{m_s}^{(\text{Z})} = g_0 \mu_B m_s B, \quad (4.13)$$

$E_{m_z}^{(\text{para})}$ was defined in eq. (2.28) and $E_{n,l,m_z}^{(\text{dia})}$ in eq. (2.29).

According to eq. (2.24), the nonrelativistic ZFS is determined from the following parameters directly obtained from eqs. (2.28), (2.29), and (4.13),

$$E_{n,l,m_z,m_s}^{(\text{nr})} \Big|_{B=0} = E_{n,l}^{(0)}, \quad (4.14a)$$

$$\frac{\partial E_{n,l,m_z,m_s}^{(\text{nr})}}{\partial B} \Big|_{B=0} = \mu_B (m_z + 2m_s), \quad (4.14b)$$

$$\frac{\partial^2 E_{n,l,m_z,m_s}^{(\text{nr})}}{\partial B^2} \Big|_{B=0} = \frac{\mu_B^2}{2E_0} \mathcal{R}_{n,l} \mathcal{Y}_l^{m_z}. \quad (4.14c)$$

Treating separately each of the field-dependent energy contributions (2.28), (4.13), the nonrelativistic ZFS following from eqs. (2.24) and (4.14) can be written as

$$\chi^{(\text{nr})} = \chi^{(\text{Z})} + \chi^{(\text{orb})}, \quad (4.15)$$

in terms of a spin-dependent susceptibility $\chi^{(\text{Z})}$ and the orbital component $\chi^{(\text{orb})}$. The latter admits the decomposition

$$\chi^{(\text{orb})} = \chi^{(\text{para})} + \chi^{(\text{dia})}. \quad (4.16)$$

Performing the m_z sum in eq. (2.24), we have

$$\chi^{(\text{Z})} = -\frac{2\mu_B^2}{\mathcal{V}} \sum_{l=0}^{\infty} (2l+1) \sum_{n=1}^{\infty} f'_{\bar{\mu}_0}(E_{nl}^{(0)}), \quad (4.17)$$

as well as the expressions from eqs. (2.33) [22, 68] with the replacement $\mu = \bar{\mu}_0$.

The mean chemical potential $\bar{\mu}_0$ is associated with the spectrum of the Hamiltonian $\mathcal{H}^{(0)}$ presented in eq. (2.9a). Trading the sum over the principal quantum number n by an integral over energy allows to recast eq. (4.17) as

$$\frac{\chi^{(\text{Z})}}{|\chi_L|} = -\frac{9\pi E_0}{k_F a} \sum_{l=0}^{\infty} (2l+1) \int_0^{\infty} dE \, q_l(E) f'_{\bar{\mu}_0}(E), \quad (4.18)$$

where we have introduced the l -fixed density of states $q_l(E)$ corresponding to the radial problem, itself related to the zero-field DOS from eq. (2.15) and (2.16). The prefactor of 2 in the equation above takes into account the spin degeneracy, as we follow the standard convention of using a spinless $q_l(E)$ and a spinful $q(E, B)$.

For a degenerate electron gas, where $E_F \gg k_B T$, we use $f'_{\mu}(E) = -\delta(E - \mu)$, and thus eq. (4.18) leads to the standard result of the spin-dependent susceptibility [138]

$$\chi^{(\text{Z})} = \frac{\mu_B^2}{\mathcal{V}} q(E_F, 0). \quad (4.19)$$

In the unconstrained case of $a \rightarrow \infty$, the use of the DOS per unit volume for the zero-field, three-dimensional, free electron gas $g^{(3D)}(E) = (m/\pi^2 \hbar^2) \sqrt{2mE/\hbar^2}$

in eq. (4.19), results in the form (1.5) of the Pauli susceptibility. In the constrained case of a finite a , the trace formula separation (2.15a) and the fact that $\bar{\rho}(E, 0) = \rho^0 = g^{(3D)}(E)\mathcal{V}$ result in a mean spin-dependent susceptibility $\bar{\chi}^{(Z)} = \chi_P$. Thus, the confinement only adds a small contribution to the bulk susceptibility, which is associated with $\rho^{\text{osc}}(E, 0)$ [83].

In the constrained case, the numerical implementation of eqs. (4.17) and (2.33) leads to the nonrelativistic ZFS $\chi^{(\text{nr})}$ presented in fig. 4.1 (in black) as a function of $k_F a$. In the shown interval, these numerical results are almost indistinguishable from those in which $\chi_b^{(\text{nr})} = 2|\chi_L|$ is added to the semiclassical ZFS $\chi^{(1)} = \chi^{(\text{orb})-\text{osc}}$ of eq. (3.4). The suppression of the ZFS oscillations for large sizes can be understood, at the semiclassical level, by the thermal damping (2.41) acting on the contribution of each family of classical periodic orbits. For very large a (inset), the oscillations of $\chi^{(\text{nr})}$ are quite reduced, and we can see that they are around the bulk ZFS $\chi_b^{(\text{nr})}$, given by eqs. (1.4) and (1.5), as the confinement becomes irrelevant in such a limit. The typical values of $\chi^{(\text{nr})}$ are important in order to assess the relevance of the relativistic corrections to be calculated in the sequel. Also for comparison purposes, we show in fig. 4.1 (in red) the ZFS $\chi^{(2)} + \chi_b^{(\text{nr})}$ arising from finite- N corrections to the free energy (2.46d) using the semiclassical expression for the oscillating part of the density of states $\rho^{\text{osc}}(E, B)$ given by eqs. (B.24), (2.17a), and (2.17b), as detailed in chapter 3. In addition, we show in fig. 4.1 (blue line) the ZFS $\chi_{\text{ens}}^{\text{d}} + \chi_b^{(\text{nr})}$ of an ensemble of metallic nanoparticles with an important size dispersion. Here, $\chi_{\text{ens}}^{\text{d}}$ is the ensemble average of $\chi^{(2)}$ over a Gaussian probability distribution of the size parameter a , cf. eq. (3.15).

4.2 KINETIC CORRECTION IN THE ABSENCE OF SPIN-ORBIT COUPLING

The zero-field Dirac equation in a spherical potential box admits an exact solution [119, 122]. While the inclusion of an infinitesimal magnetic field allowing to address the ZFS can in principle be implemented as a perturbation [154], it is simpler to proceed from the weakly-relativistic Hamiltonian (4.3). The kinetic term (4.4a) can be written as $\mathcal{H}^{(\text{k})} = -\left\{\mathcal{H}^{(\text{nr})} + e\phi_e\right\}^2/2mc^2$. Therefore, in the case of a hard wall confinement, and up to quadratic terms in B , it leads to the energy correction

$$\begin{aligned}
 E_{n,l,m_z,m_s}^{(\text{k})} &= -\frac{1}{2mc^2} \\
 &\times \langle \Psi_{n,l,m_z,m_s}^{(0)} | \left(\frac{\mathbf{p}^2}{2m} \right)^2 + \frac{\mathbf{p}^2}{m} \mathcal{H}^{(\mu)} + \left(\mathcal{H}^{(\mu)} \right)^2 + \frac{\mathbf{p}^2}{2m} \mathcal{H}^{(\text{dia})} + \mathcal{H}^{(\text{dia})} \frac{\mathbf{p}^2}{2m} | \Psi_{n,l,m_z,m_s}^{(0)} \rangle \\
 &= -\frac{\left(E_{n,l}^{(0)} \right)^2}{2mc^2} + \delta E_{n,l,m_z,m_s}^{(\text{k})}, \tag{4.20}
 \end{aligned}$$

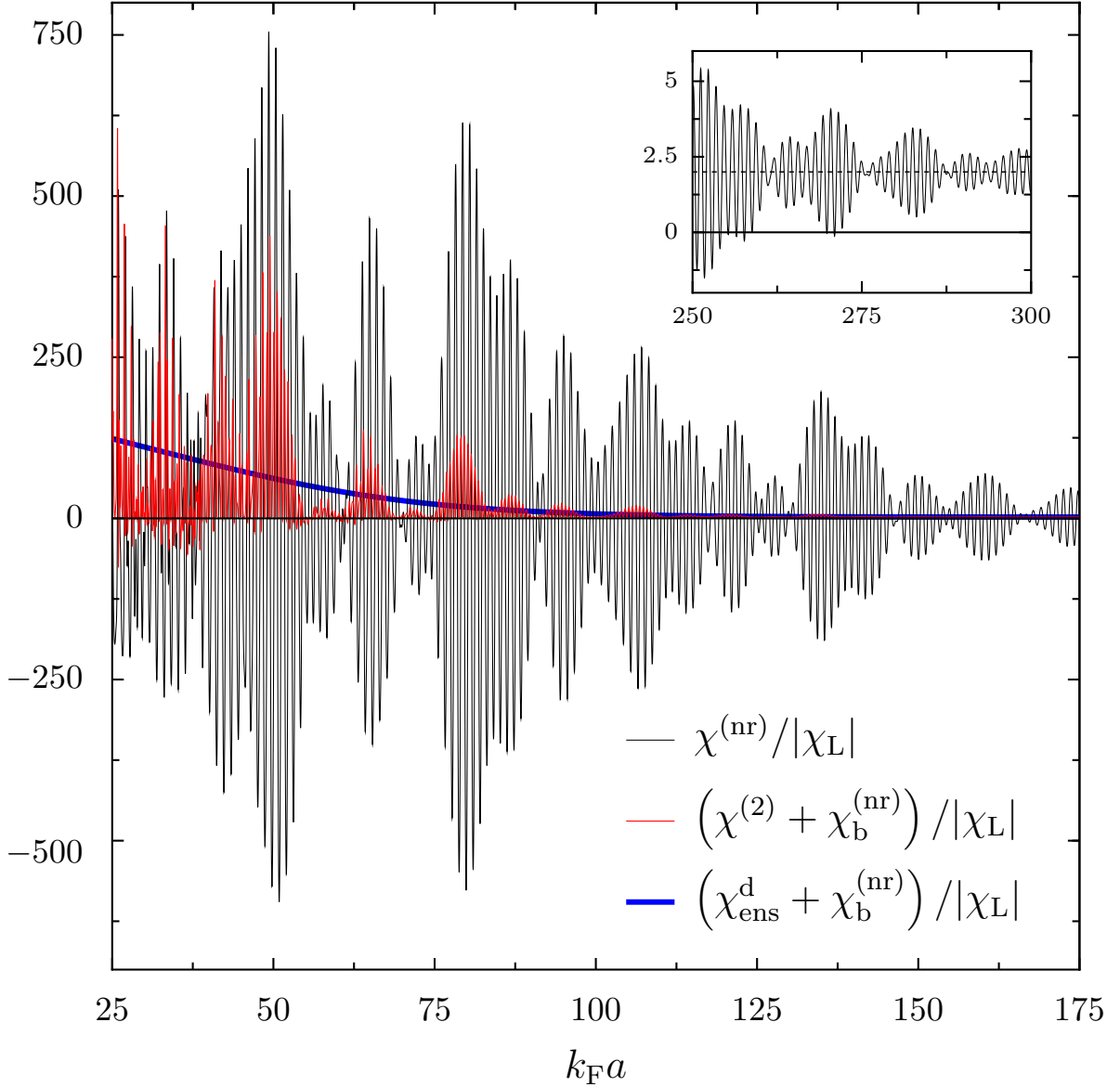


Figure 4.1: In black: nonrelativistic ZFS $\chi^{(nr)}$ for $k_B T/\bar{\mu}_0 = 5 \times 10^{-3}$ (corresponding to room temperature in the case of gold) obtained from eqs. (4.17)–(2.33) (in units of the absolute value of the Landau susceptibility χ_L), as a function of the nanoparticle radius a (scaled with the Fermi wave vector k_F). In red: $\chi^{(2)} + \chi_b^{(nr)}$, with $\chi^{(2)}$ obtained from the finite- N correction (2.46d) to the free energy and the oscillating part of the B -dependent density of states $\rho^{osc}(E, B)$. In blue: ZFS of an ensemble of nanoparticles with an important size dispersion, $\chi_{ens}^d + \chi_b^{(nr)}$, where χ_{ens}^d is obtained by taking the average of $\chi^{(2)}$ over a Gaussian probability distribution (in size). Inset: Corresponding ZFSs for larger nanoparticle radii, showing the approach to the bulk value given by eqs. (1.4) and (1.5) indicated by a dashed line.

where the B -dependent component is given by

$$\delta E_{n,l,m_z,m_s}^{(k)} = -\frac{1}{2mc^2} \left[2E_{n,l}^{(0)} E_{m_z,m_s}^{(\mu)} + \left(E_{m_z,m_s}^{(\mu)} \right)^2 + 2E_{n,l}^{(0)} E_{n,l,m_z}^{(\text{dia})} \right], \quad (4.21)$$

with $E_{n,l}^{(0)}$, $E_{m_z,m_s}^{(\mu)}$, and $E_{n,l,m_z}^{(\text{dia})}$ given, respectively, by eqs. (2.12), (4.12), and (2.29). Since the product basis is constituted of eigenvectors of \mathbf{p}^4 and $\mathcal{H}^{(\mu)}$, the off-diagonal matrix elements of $\mathcal{H}^{(k)}$ are of quadratic order in B , and thus do not need to be considered.

Even if the modification of the nonrelativistic ZFS $\chi^{(\text{nr})}$ due to the kinetic correction (4.20) does not have a physical meaning by itself, it is nevertheless interesting to calculate it in view of weighting its importance against the other weakly-relativistic modifications. Moreover, in the case of a very large radius a , where the role of the confining potential $V_{\text{mf}}(r)$ should become irrelevant, the ZFS $\chi^{(\text{nr-k})}$ taking only into account the modification of $\chi^{(\text{nr})}$ due to the correction (4.20), can be compared with the bulk weakly-relativistic ZFS $\chi_b^{(\text{wr})}$ of eq. (2.48).

An important aspect of the correction (4.20) is that it induces at $B = 0$ an energy shift of all levels. In particular, within the grand canonical ensemble, the shift of the Fermi level translates into a renormalization

$$\Delta\mu^{(k)} \simeq -\frac{\bar{\mu}_0^2}{2mc^2} \quad (4.22)$$

of the zero-field nonrelativistic mean chemical potential $\bar{\mu}_0$.

The kinetic correction (4.20) results in the eigenenergies $E_{n,l,m_z,m_s}^{(\text{nr-k})} = E_{n,l,m_z,m_s}^{(\text{nr})} + E_{n,l,m_z,m_s}^{(k)}$ from which the ZFS $\chi^{(\text{nr-k})}$ can be obtained by using the parameters

$$E_{n,l,m_z,m_s}^{(\text{nr-k})} \Big|_{B=0} = E_{n,l}^{(0)} \left[1 - \frac{E_{n,l}^{(0)}}{2mc^2} \right], \quad (4.23a)$$

$$\frac{\partial E_{n,l,m_z,m_s}^{(\text{nr-k})}}{\partial B} \Big|_{B=0} = \mu_B (m_z + 2m_s) \left[1 - \frac{E_{n,l}^{(0)}}{mc^2} \right], \quad (4.23b)$$

$$\frac{\partial^2 E_{n,l,m_z,m_s}^{(\text{nr-k})}}{\partial B^2} \Big|_{B=0} = \mu_B^2 \left(\frac{1}{2E_0} \mathcal{R}_{n,l} \mathcal{Y}_l^{m_z} \left[1 - \frac{E_{n,l}^{(0)}}{mc^2} \right] - \frac{1}{mc^2} (m_z + 2m_s)^2 \right). \quad (4.23c)$$

Performing the m_z and m_s sums in eq. (2.24), while working up to linear order in

$E_{n,l}^{(0)}/mc^2$, we have

$$\begin{aligned} \frac{\chi^{(\text{nr-k})}}{|\chi_L|} = & -\frac{6\pi E_0}{k_{\text{F}}a} \sum_{l=0}^{\infty} (l+1/2) \sum_{n=0}^{\infty} \left\{ [l(l+1)+3] f'_{\bar{\mu}} \left(E_{n,l}^{(0)} \left[1 - \frac{E_{n,l}^{(0)}}{2mc^2} \right] \right) \left[1 - 2\frac{E_{n,l}^{(0)}}{mc^2} \right] \right. \\ & + \frac{\mathcal{R}_{n,l}}{E_0} f_{\bar{\mu}} \left(E_{n,l}^{(0)} \left[1 - \frac{E_{n,l}^{(0)}}{2mc^2} \right] \right) \left[1 - \frac{E_{n,l}^{(0)}}{mc^2} \right] \\ & \left. - \frac{l(l+1)+3}{mc^2} f_{\bar{\mu}} \left(E_{n,l}^{(0)} \left[1 - \frac{E_{n,l}^{(0)}}{2mc^2} \right] \right) \right\}. \end{aligned} \quad (4.24)$$

As discussed above, we are interested in the correction

$$\Delta\chi^{(\text{k})} = \chi^{(\text{nr-k})} - \chi^{(\text{nr})}, \quad (4.25)$$

where $\chi^{(\text{nr})}$ is defined in eq. (4.15), and thus associated with the mean chemical potential $\bar{\mu}_0$ of the nonrelativistic problem, while $\chi^{(\text{nr-k})}$ is associated with the renormalized mean chemical potential $\bar{\mu} = \bar{\mu}_0 + \Delta\mu^{(\text{k})}$ [cf. eq. (4.22)]. We then write

$$\begin{aligned} \frac{\Delta\chi^{(\text{k})}}{|\chi_L|} = & -\frac{6\pi E_0}{k_{\text{F}}a mc^2} \sum_{l=0}^{\infty} (l+1/2) \\ & \times \sum_{n=1}^{\infty} \left\{ [l(l+1)+3] f''_{\bar{\mu}_0}(E_{n,l}^{(0)}) + \frac{\mathcal{R}_{n,l}}{E_0} f'_{\bar{\mu}_0}(E_{n,l}^{(0)}) \right\} \left[-\frac{(E_{n,l}^{(0)})^2}{2mc^2} - \Delta\mu^{(\text{k})} \right] \\ & + \frac{6\pi E_0}{k_{\text{F}}a mc^2} \sum_{l=0}^{\infty} (l+1/2) \\ & \times \sum_{n=1}^{\infty} \left\{ 2[l(l+1)+3] E_{n,l}^{(0)} f'_{\bar{\mu}_0}(E_{n,l}^{(0)}) + \left(\frac{\mathcal{R}_{n,l}}{E_0} E_{n,l}^{(0)} + l(l+1)+3 \right) f_{\bar{\mu}_0}(E_{n,l}^{(0)}) \right\}. \end{aligned} \quad (4.26)$$

The first sum in the above equation results from the zero-field component of the correction $E_{n,l,m_z,m_s}^{(\text{k})}$, and thus it could have alternatively been derived by simply implementing in the ZFS expressions (2.33) and (4.17), the shift of $E_{n,l}^{(0)}$ to $E_{n,l}^{(0)} [1 - E_{n,l}^{(0)}/2mc^2]$, with the corresponding renormalization $\Delta\mu^{(\text{k})}$ of the chemical potential. The second sum in (4.26) represents the nontrivial effect of the magnetic-field dependent contribution $\delta E_{n,l,m_z,m_s}^{(\text{k})}$ to the kinetic correction, given by eq. (4.21).

In fig. 4.2 we present the numerical evaluation of the kinetic correction $\Delta\chi^{(\text{k})}$ to the nonrelativistic ZFS, according to eq. (4.26), as a function of $k_{\text{F}}a$. For large a (inset), the values of $\Delta\chi^{(\text{k})}$ oscillate around $-1/3 |\chi_L| (v_{\text{F}}/c)^2$, consistently with the result

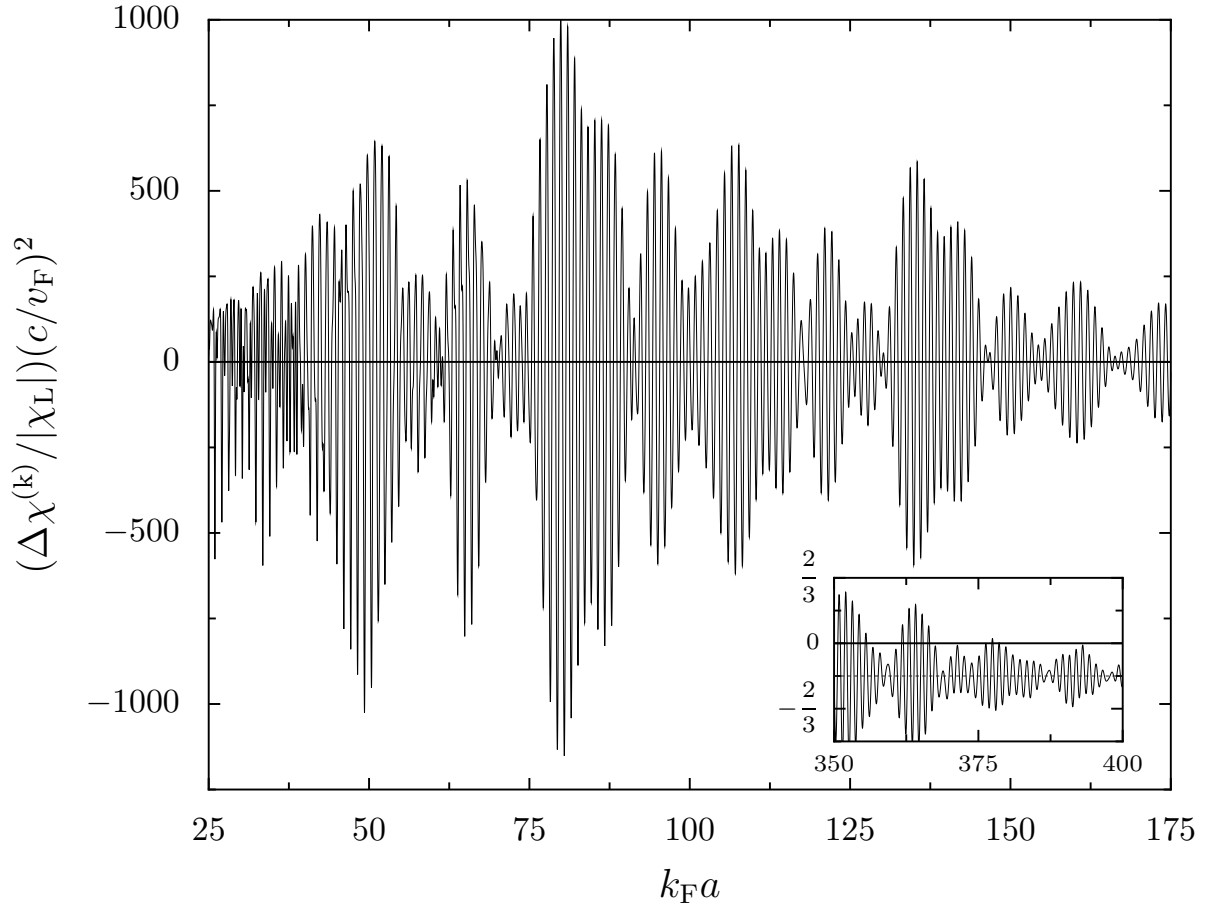


Figure 4.2: Kinetic correction $\Delta\chi^{(k)}$ to the ZFS for $k_B T/\bar{\mu}_0 = 5 \times 10^{-3}$ obtained from eq. (4.26) [in units of the absolute value of the Landau susceptibility χ_L and multiplied by the scaling factor $(c/v_F)^2$], as a function of the nanoparticle radius a (scaled with the Fermi wave vector k_F). Inset: $\Delta\chi^{(k)}$ (in the same above-mentioned units as in the main panel) corresponding to larger sizes, showing the approach to the weakly-relativistic bulk value $-1/3$ [cf. eq. (2.48)] and indicated by a dashed line.

(2.48) for the bulk ZFS $\chi_b^{(\text{wr})}$ (see also appendix sec. A.3), since in such a limit the confinement becomes irrelevant and the kinetic correction is the only weakly-relativistic effect that needs to be taken into account. The oscillations as a function of $k_F a$ are much larger than the bulk value, but remain considerably smaller than the typical values of $\chi^{(\text{nr})}$ exhibited in fig. 4.1 (and even of the finite- N correction characterizing the response of an ensemble of nanoparticles, see the blue line in fig. 4.1).

The correction $\Delta\chi^{(\text{k})}$ of eq. (4.26) admits a one-dimensional semiclassical treatment, analogous to that of the nonrelativistic ZFS treated in appendix D. In particular, the smooth part of $\Delta\chi^{(\text{k})}$ can be evaluated along the lines of eqs. (D.2)–(D.4), and we find in the leading order in $k_F a$, that the smooth part of the first sum behaves as $1/5 (k_F a)^2 (v_F/c)^2$, while the second sum cancels the previous contribution. The next-leading term of the smooth part of $\Delta\chi^{(\text{k})}$ is of order $(k_F a)^0$, but for the same reasons discussed in appendix D, the correct asymptotic value $\chi_b^{(\text{wr})}$ of the bulk yielded by the numerical calculation, is not recovered by our semiclassical approach.

4.3 SPIN-ORBIT COUPLING IN A SPHERICAL NANOPARTICLE

While the product eigenbasis of $\mathcal{H}^{(0)}$ used in sec. 4.1.2, and characterized by the set $\{\lambda\} = \{n, l, m_z, m_s\}$, remained the appropriate one once the term $\mathcal{H}^{(\mu)}$ of eq. (4.2) was taken into account, the inclusion of the SOC term $\mathcal{H}^{(\text{so})}$ of eq. (4.8a) makes it more convenient to change to the eigenbasis $\Phi_{n,j,m_j}^{(\pm)}$ (2.63) of the total angular momentum $\mathbf{J} = \mathbf{L} + \mathbf{S}$, characterized by the set $\{\tilde{\lambda}\} = \{n, j, m_j, l\}$ and written in terms of spinor spherical harmonics defined in eq. (2.64).

The associated eigenenergies of $\mathcal{H}^{(0)}$ in the case of a spherical confining potential are $\mathcal{E}_{n,j,(\pm)}^{(0)} = E_{n,j\pm 1/2}^{(0)}$, and therefore there is degeneracy between the $2j+1$ dimensional subspace $\{n, j, (+)\}$ and the $2j+3$ dimensional subspace $\{n, j+1, (-)\}$, as they are characterized by the same quantum number l .

The coupled basis remains an eigenbasis of the subspace $\{n, j, (+)\} \oplus \{n, j+1, (-)\}$ once $\mathcal{H}^{(\text{so})}$ is taken into account, while the eigenenergies change according to

$$\mathcal{E}_{n,j,(\pm)}^{(\text{so})} = \langle \Phi_{n,j,m_j}^{(\pm)} | \mathcal{H}^{(\text{so})} | \Phi_{n,j,m_j}^{(\pm)} \rangle = \frac{\hbar^2}{4m^2 c^2 a^2} \left[\mp \left(j + \frac{1}{2} \right) - 1 \right] I_{n,j\pm 1/2}^{(\text{so})}, \quad (4.27)$$

with the radial matrix element

$$I_{n,l}^{(\text{so})} = a^2 \int_0^\infty dr r [R_{n,l}(r)]^2 V'(r). \quad (4.28)$$

For the potential (2.4), we have

$$I_{n,l}^{(\text{so})} = V_0 a^3 [R_{n,l}(a)]^2. \quad (4.29)$$

In the limit where the confining potential approaches a hard wall, the product $V_0 [R_{n,l}(a)]^2$ remains finite [155]. Using the limiting expressions (G.6) and (G.7c) we obtain

$$I_{n,l}^{(\text{so})} = \frac{\hbar^2}{ma^2} \zeta_{n,l}^2, \quad (4.30)$$

and therefore

$$\mathcal{E}_{n,j,(\pm)}^{(\text{so})} = \left[\mp \left(j + \frac{1}{2} \right) - 1 \right] \zeta_{n,j\pm 1/2}^2 \frac{E_0^2}{mc^2}, \quad (4.31)$$

independently of V_0 .

Obviously, $\mathcal{E}_{n,1/2,(-)}^{(\text{so})} = 0$, since the symmetry of the s -states ($l = 0$) renders the SOC ineffective. The degeneracy between the subspaces $\{n, j, (+)\}$ and $\{n, j + 1, (-)\}$ for $B = 0$ is broken by $\mathcal{H}^{(\text{so})}$. For $B \neq 0$, the remaining degeneracy within each subspace is lifted according to the different values of m_j .

4.3.1 PERTURBATIVE TREATMENT OF THE MAGNETIC FIELD

Once the term $\mathcal{H}^{(\mu)}$ of eq. (4.2) is taken into account, m_j is still a good quantum number, but the coupled basis is no longer an eigenbasis of the subspace $\{n, j, (+)\} \oplus \{n, j + 1, (-)\}$. Therefore, in order to treat the terms $\mathcal{H}^{(\mu)}$, $\mathcal{H}^{(\text{dia})}$, $\mathcal{H}^{(\text{k})}$, $\mathcal{H}^{(\text{ame})}$ in the two lowest orders in B , the perturbative approach in magnetic field of sec. 4.1.2 yielding the nonrelativistic ZFS has to be extended using the decomposition in subspaces of fixed m_j . These are represented by

$$\{n, j, (+)\} \oplus \{n, j + 1, (-)\} = \mathcal{S}_{n,j+1/2,(\text{d})}^{\text{p}} \oplus \bigcup_{m_j=-j}^{m_j=+j} \mathcal{S}_{n,j+1/2,m_j}^{\text{e}} \oplus \mathcal{S}_{n,j+1/2,(\text{u})}^{\text{p}} \quad (4.32)$$

in terms of the down (d) and up (u) one-dimensional subspaces

$$\mathcal{S}_{n,l,(\text{d/u})}^{\text{p}} = \{n, l + 1/2, (-)\} \Big|_{m_j=\mp(l+1/2)}, \quad (4.33)$$

and the two-dimensional subspaces $\mathcal{S}_{n,l,m_j}^{\text{e}}$ subtended by the vectors $|\Phi_{n,l\mp 1/2,m_j}^{(\pm)}\rangle$ of the coupled basis, associated with the quantum numbers $\{n, l \mp 1/2, m_j, l\}$ with $l \neq 0$ and $|m_j| \leq l - 1/2$. The labels p (e) stand for “product” (“entangled”), characterizing the one (two)-dimensional subspaces where the coupled basis does (does not) coincide with the product basis. The choice of using the index l (instead of j) in order to label the subspaces is motivated in view of the book-keeping for the sum over states. We notice that the definition (4.33) is also valid for the subspaces with $l = 0$, which are not considered in the decomposition (4.32), but should be included when taking the sum over states yielding a thermodynamic quantity like the ZFS.

The Hamiltonian (2.59), restricted to the subspaces $\mathcal{S}_{n,l,m_j}^{\text{e}}$, can be expressed by the 2×2 matrix

$$\mathcal{H}_{n,l,m_j} = \begin{pmatrix} E_{n,l,m_j}^{(+)} & -\mu_{\text{B}} B \aleph_{l,m_j} \\ -\mu_{\text{B}} B \aleph_{l,m_j} & E_{m,l,m_j}^{(-)} \end{pmatrix}. \quad (4.34)$$

In the diagonal matrix elements $E_{n,l,m_j}^{(\pm)}$ we separate the field-independent and the field-dependent contributions as

$$E_{n,l,m_j}^{(\pm)} = E_{n,l,(\pm)}^{(0)} + \delta E_{n,l,m_j}^{(\pm)}, \quad (4.35)$$

with

$$E_{n,l,(\pm)}^{(0)} = E_{n,l}^{(0)} \left[1 - \frac{E_{n,l}^{(0)}}{2mc^2} \right] + E_{n,l}^{(D)} + E_{n,l,(\pm)}^{(\text{so})}. \quad (4.36)$$

The first term in the right-hand side of the above equation represents the $B = 0$ nonrelativistic eigenvalue together with its kinetic energy correction, as expressed in eq. (4.23a). The second term is the Darwin correction, given for the case of $V_0 \gg E_0$ by eq. (G.13). Recalling eq. (4.31), it is convenient to express the SOC contribution as

$$E_{n,l,(\pm)}^{(\text{so})} = \mathcal{E}_{n,l \mp 1/2,(\pm)}^{(\text{so})} = \left[\mp \left(l + \frac{1}{2} \right) - \frac{1}{2} \right] \zeta_{n,l}^2 \frac{E_0^2}{mc^2}. \quad (4.37)$$

The spin splitting in the subspace \mathcal{S}_{n,l,m_j}^e is

$$\Delta_{n,l} = E_{n,l,(-)}^{(0)} - E_{n,l,(+)}^{(0)} = E_{n,l,(-)}^{(\text{so})} - E_{n,l,(+)}^{(\text{so})} = 2 \left(l + \frac{1}{2} \right) \zeta_{n,l}^2 \frac{E_0^2}{mc^2}. \quad (4.38)$$

In reducing the Hamiltonian (2.59) to its 2×2 form (4.34), we are assuming an infinitesimal field B , and neglecting the coupling between the subspaces \mathcal{S}_{n,l,m_j}^e and \mathcal{S}_{n',l,m_j}^e . This last approximation requires $\Delta_{n,l} \ll E_{n+1,l}^{(0)} - E_{n,l}^{(0)} \simeq 2\pi\zeta_{n,l}E_0$, where we have used the asymptotic form of the zeros of $j_l(\zeta)$. The previous condition translates into $(l + 1/2)(v_F/c)^2 \ll 2\pi k_F a$, which is always verified in the weakly-relativistic limit since $l_{\text{max}} + 1/2 \simeq k_F a$ (see appendix D). Nevertheless, our perturbative treatment of $\mathcal{H}^{(\text{so})}$ can become problematic in cases of quasi-degeneracies between eigenstates $E_{n,l}^{(0)}$ and $E_{n',l}^{(0)}$ corresponding to different quantum numbers. We remark that $\mathcal{H}^{(\text{so})}$ does not induce a renormalization of the chemical potential, since the shift $-E_0 E_{n,l}^{(0)}/mc^2$ associated with each of the subspaces \mathcal{S}_{n,l,m_j}^e is compensated by the correction $lE_0 E_{n,l}^{(0)}/mc^2$ characterizing each of the two subspaces $\mathcal{S}_{n,l,(\text{d/u})}^p$.

The B -dependent components of the diagonal matrix elements (4.35) are given by

$$\delta E_{n,l,m_j}^{(\pm)} = E_{l,m_j,(\pm)}^{(\mu)} + E_{n,l,m_j,(\pm)}^{(\text{dia})} + \delta E_{n,l,m_j,(\pm)}^{(\text{k})} + E_{n,l,m_j,(\pm)}^{(\text{ame})}. \quad (4.39)$$

The first term can be obtained with the aid of the Wigner–Eckart theorem (2.65), which allows us to write

$$\mathcal{E}_{j,m_j,(\pm)}^{(\mu)} = \langle \Phi_{n,j,m_j}^{(\pm)} | \mathcal{H}^{(\mu)} | \Phi_{n,j,m_j}^{(\pm)} \rangle = \frac{j + 1/2}{j + 1/2 \pm 1/2} \mu_B B m_j, \quad (4.40)$$

independently of n , and therefore

$$E_{l,m_j,(\pm)}^{(\mu)} = \mathcal{E}_{l\mp 1/2,m_j,(\pm)}^{(\mu)} = \left(1 \mp \frac{1/2}{l+1/2}\right) \mu_B B m_j. \quad (4.41)$$

The diamagnetic contributions in eq. (4.39) follow from the matrix elements

$$\mathcal{E}_{n,j,m_j,(\pm)}^{(\text{dia})} = \langle \Phi_{n,j,m_j}^{(\pm)} | \mathcal{H}^{(\text{dia})} | \Phi_{n,j,m_j}^{(\pm)} \rangle = \left[1 + \frac{m_j^2}{j(j+1)}\right] \frac{\mu_B^2 B^2}{8E_0} \mathcal{R}_{n,j\pm 1/2}, \quad (4.42)$$

where $\mathcal{R}_{n,l}$ has been defined in eq. (2.30). Thus,

$$E_{n,l,m_j,(\pm)}^{(\text{dia})} = \mathcal{E}_{n,l\mp 1/2,m_j,(\pm)}^{(\text{dia})} = \left[1 + \frac{m_j^2}{(l\mp 1/2)(l\mp 1/2+1)}\right] \frac{\mu_B^2 B^2}{8E_0} \mathcal{R}_{n,l}. \quad (4.43)$$

The diagonal matrix elements of $\mathcal{H}^{(\text{k})}$ in the subspace \mathcal{S}_{n,l,m_j}^e can be obtained, up to quadratic order in B , by a similar expression to that of eq. (4.20), where the vectors $|\Psi_{n,l,m_z,m_s}^{(0)}\rangle$ of the product basis have to be replaced by the ones of the coupled basis, $|\Phi_{n,j,m_j}^{(\pm)}\rangle$, leading to

$$E_{n,l,m_j,(\pm)}^{(\text{k})} = -\frac{(E_{n,l}^{(0)})^2}{2mc^2} + \delta E_{n,l,m_j,(\pm)}^{(\text{k})}, \quad (4.44)$$

with

$$\delta E_{n,l,m_j,(\pm)}^{(\text{k})} = -\frac{E_{n,l}^{(0)}}{mc^2} \left(E_{l,m_j,(\pm)}^{(\mu)} + E_{n,l,m_j,(\pm)}^{(\text{dia})}\right) - \frac{(\mu_B B)^2}{2mc^2} \left[m_j^2 \left(1 \mp \frac{1}{l+1/2}\right) + \frac{1}{4}\right]. \quad (4.45)$$

The last contribution to $\delta E_{n,l,m_j}^{(\pm)}$ in eq. (4.39) results from the diagonal matrix element of $\mathcal{H}^{(\text{ame})}$ in the coupled basis, which with the help of eqs. (H.1), (4.30), and (H.7), can be written as

$$E_{n,l,m_j,(\pm)}^{(\text{ame})} = \mathcal{E}_{n,l\mp 1/2,m_j,(\pm)}^{(\text{ame})} = \mp \mu_B B \frac{E_{n,l}^{(0)}}{2mc^2} \frac{m_j(l\mp 1/2+1/2)}{(l\mp 1/2)(l\mp 1/2+1)}. \quad (4.46)$$

We remark that the expression (4.41) of $E_{l,m_j,(\pm)}^{(\mu)}$ does not simply follow from the result (4.12) for $E_{m_z,m_s}^{(\mu)}$, since the latter represents the exact energy shift associated with $\mathcal{H}^{(\mu)}$ in the product basis, while the former is just the first-order perturbative correction in the coupled basis. Similarly, the perturbative correction (4.43) for $E_{n,l,m_j,(\pm)}^{(\text{dia})}$ does not simply follow from the analogous correction (2.29) for $E_{n,l,m_z}^{(\text{dia})}$, nor does

$\delta E_{n,l,m_j,(\pm)}^{(k)}$ in eq. (4.45) from $E_{n,l,m_z,m_s}^{(k)}$ in eq. (4.20). In the same vein, the angular magneto-electric correction $E_{n,l,m_j,(\pm)}^{(\text{ame})}$ of eq. (4.46) follows from the matrix element $\mathcal{E}_{n,l\mp 1/2,m_j,(\pm)}^{(\text{ame})}$ in the coupled basis.

The off-diagonal matrix elements of the restricted Hamiltonian (4.34) need to be only obtained up to linear order in B . Thus, the nonrelativistic component does not have a term associated with $\mathcal{H}^{(\text{dia})}$, but consists only of

$$\langle \Phi_{n,l+1/2,m_j}^{(-)} | \mathcal{H}^{(\mu)} | \Phi_{n,l-1/2,m_j}^{(+)} \rangle = -\mu_B B \frac{\sqrt{(l+1/2)^2 - m_j^2}}{2(l+1/2)}, \quad (4.47)$$

independently of n . The only off-diagonal matrix element of $\mathcal{H}^{(k)}$ that we need to consider is

$$\langle \Phi_{n,l+1/2,m_j}^{(-)} | \left(-\frac{1}{mc^2} \right) \frac{\mathbf{p}^2}{2m} \mathcal{H}^{(\mu)} | \Phi_{n,l-1/2,m_j}^{(+)} \rangle = \mu_B B \frac{E_{n,l}^{(0)}}{2mc^2} \frac{\sqrt{(l+1/2)^2 - m_j^2}}{l+1/2}. \quad (4.48)$$

The remaining contribution to the off-diagonal matrix element arising from the angular magneto-electric coupling is given by eqs. (H.8) and (H.12) as

$$\langle \Phi_{n,l+1/2,m_j}^{(-)} | \mathcal{H}^{(\text{ame})} | \Phi_{n,l-1/2,m_j}^{(+)} \rangle = -\mu_B B \frac{E_{n,l}^{(0)}}{4mc^2} \frac{\sqrt{(l+1/2)^2 - m_j^2}}{l+1/2}. \quad (4.49)$$

The off-diagonal matrix element of \mathcal{H}_{n,l,m_j} with the form of eq. (4.34) is determined by the B -independent dimensionless parameter

$$\aleph_{l,m_j} = \frac{\sqrt{(l+1/2)^2 - m_j^2}}{2(l+1/2)} \left[1 - \frac{E_{n,l}^{(0)}}{2mc^2} \right]. \quad (4.50)$$

The diagonalization of \mathcal{H}_{n,l,m_j} yields the B -dependent low (l) and high (h) eigenenergies within the subspaces \mathcal{S}_{n,l,m_j}^e , respectively given by

$$E_{n,l,m_j}^{(l/h)} = \frac{E_{n,l,m_j}^{(-)} + E_{n,l,m_j}^{(+)}}{2} \mp \sqrt{\left(\frac{E_{n,l,m_j}^{(-)} - E_{n,l,m_j}^{(+)}}{2} \right)^2 + \mu_B^2 B^2 \aleph_{l,m_j}^2}. \quad (4.51)$$

In analogy with the nonrelativistic parameters of eq. (4.14), the contributions to the ZFS stemming from the (l/h) eigenstates within the subspaces \mathcal{S}_{n,l,m_j}^e are determined

by

$$E_{n,l,m_j}^{(1/h)} \Big|_{B=0} = E_{n,l,m_j}^{(\pm)} \Big|_{B=0} = E_{n,l,(\pm)}^{(0)}, \quad (4.52a)$$

$$\begin{aligned} \frac{\partial E_{n,l,m_j}^{(1/h)}}{\partial B} \Big|_{B=0} &= \frac{\partial E_{n,l,m_j}^{(\pm)}}{\partial B} \Big|_{B=0} \\ &= \mu_B m_j \left\{ \left(1 \mp \frac{1/2}{l+1/2} \right) \left[1 - \frac{E_{n,l}^{(0)}}{mc^2} \right] \mp \frac{E_{n,l}^{(0)}}{2mc^2} \frac{l \mp 1/2 + 1/2}{(l \mp 1/2)(l \mp 1/2 + 1)} \right\}, \end{aligned} \quad (4.52b)$$

$$\begin{aligned} \frac{\partial^2 E_{n,l,m_j}^{(1/h)}}{\partial B^2} \Big|_{B=0} &= \frac{\partial^2 E_{n,l,m_j}^{(\pm)}}{\partial B^2} \Big|_{B=0} \mp \frac{2\mu_B^2 \aleph_{l,m_j}^2}{\Delta_{n,l}} \\ &= \frac{\mu_B^2}{4} \left\{ \left(1 + \frac{m_j^2}{(l \mp 1/2)(l+1 \mp 1/2)} \right) \frac{\mathcal{R}_{n,l}}{E_0} \left[1 - \frac{E_{n,l}^{(0)}}{mc^2} \right] \right. \\ &\quad \left. - \frac{1}{mc^2} \left(4m_j^2 \left(1 \mp \frac{1}{l+1/2} \right) + 1 \right) \mp \frac{(l+1/2)^2 - m_j^2}{(E_0/mc^2)E_{n,l}^{(0)}(l+1/2)^3} \left[1 - \frac{E_{n,l}^{(0)}}{2mc^2} \right]^2 \right\}. \end{aligned} \quad (4.52c)$$

The eigenenergies of the down (up) state of the subspace $\mathcal{S}_{n,l,(d/u)}^P$ can be written as

$$E_{n,l}^{(d/u)} = E_{n,l,(-)}^{(0)} + \delta E_{n,l}^{(d/u)}, \quad (4.53)$$

with

$$\delta E_{n,l}^{(d/u)} = E_{l,\mp(l+1/2),(-)}^{(\mu)} + E_{n,l,\mp(l+1/2),(-)}^{(\text{dia})} + \delta E_{n,l,\mp(l+1/2),(-)}^{(k)} + E_{n,l,\mp(l+1/2),(-)}^{(\text{ame})}. \quad (4.54)$$

Therefore, in addition to the parameters (4.52), we have to consider the contributions to the ZFS associated with the (d/u) states, which follow from

$$E_{n,l}^{(d/u)} \Big|_{B=0} = E_{n,l,(-)}^{(0)}, \quad (4.55a)$$

$$\frac{\partial E_{n,l}^{(d/u)}}{\partial B} \Big|_{B=0} = \mp \mu_B (l+1) \left\{ 1 - \frac{E_{n,l}^{(0)}}{mc^2} + \frac{E_{n,l}^{(0)}}{2mc^2} \frac{1}{l+3/2} \right\}, \quad (4.55b)$$

$$\frac{\partial^2 E_{n,l}^{(d/u)}}{\partial B^2} \Big|_{B=0} = \mu_B^2 \left\{ \frac{l+1}{l+3/2} \frac{\mathcal{R}_{n,l}}{2E_0} \left[1 - \frac{E_{n,l}^{(0)}}{mc^2} \right] - \frac{1}{mc^2} (l+1)^2 \right\}. \quad (4.55c)$$

The weakly-relativistic ZFS follows from the evaluation of eq. (2.24) using the parameters of eqs. (4.52) and (4.55).

4.3.2 RELATIVISTIC CORRECTION TO THE ZERO-FIELD SUSCEPTIBILITY

The weakly-relativistic ZFS will have contributions from p and e eigenstates, and it can therefore be written as $\chi^{(\text{wr})} = \chi_{\text{p}} + \chi_{\text{e}}$. Performing the m_j summation in eq. (2.24) for each subset of eigenstates while keeping up to linear terms in $E_{n,l}^{(0)}/mc^2$, we have

$$\frac{\chi_{\text{p}}}{|\chi_{\text{L}}|} = -\frac{9\pi E_0}{k_{\text{F}a}} \sum_{l=0}^{\infty} \sum_{n=1}^{\infty} \left\{ (l+1)^2 \left[1 - \frac{2E_{n,l}^{(0)}}{mc^2} \frac{l+1}{l+3/2} \right] f'_{\bar{\mu}}(E_{n,l,(-)}^{(0)}) + \left(\frac{l+1}{l+3/2} \frac{\mathcal{R}_{n,l}}{2E_0} \left[1 - \frac{E_{n,l}^{(0)}}{mc^2} \right] - \frac{1}{mc^2} (l+1)^2 \right) f_{\bar{\mu}}(E_{n,l,(-)}^{(0)}) \right\}, \quad (4.56a)$$

$$\begin{aligned} \frac{\chi_{\text{e}}}{|\chi_{\text{L}}|} = & -\frac{3\pi E_0}{k_{\text{F}a}} \sum_{l=1}^{\infty} \sum_{n=1}^{\infty} l \left\{ \frac{l-1/2}{l+1/2} \left(l^2 \left[1 - \frac{2E_{n,l}^{(0)}}{mc^2} \frac{l}{l-1/2} \right] f'_{\bar{\mu}}(E_{n,l,(+)}^{(0)}) \right. \right. \\ & + (l+1)^2 \left[1 - \frac{2E_{n,l}^{(0)}}{mc^2} \frac{l+1}{l+3/2} \right] f'_{\bar{\mu}}(E_{n,l,(-)}^{(0)}) \\ & + \left[\left(\frac{\mathcal{R}_{n,l}}{E_0} \left[1 - \frac{E_{n,l}^{(0)}}{mc^2} \right] - \frac{l^2-l+1}{mc^2} \right) f_{\bar{\mu}}(E_{n,l,(+)}^{(0)}) \right. \\ & + \left. \left. \left(\frac{l+1}{l+3/2} \frac{\mathcal{R}_{n,l}}{E_0} \left[1 - \frac{E_{n,l}^{(0)}}{mc^2} \right] - \frac{l(l+1)}{mc^2} \right) f_{\bar{\mu}}(E_{n,l,(-)}^{(0)}) \right] \right. \\ & \left. \left. - \frac{mc^2}{2E_0 E_{n,l}^{(0)}} \left[1 - \frac{E_{n,l}^{(0)}}{mc^2} \right] \frac{l+1}{(l+1/2)^2} [f_{\bar{\mu}}(E_{n,l,(+)}^{(0)}) - f_{\bar{\mu}}(E_{n,l,(-)}^{(0)})] \right\}. \quad (4.56b) \end{aligned}$$

In the right-hand side of eq. (4.56) we identify the first term of the sums, containing $f'_{\bar{\mu}}(E_{n,l,(\pm)}^{(0)})$, which generalize the nonrelativistic paramagnetic contributions of eqs. (4.17) and (2.33a) including the corresponding weakly-relativistic corrections. Similarly, the second term of the sums, containing $f_{\bar{\mu}}(E_{n,l,(\pm)}^{(0)})$, generalizes the nonrelativistic diamagnetic contribution of eq. (2.33b). The third term in the sum of eq. (4.56b), containing $f_{\bar{\mu}}(E_{n,l,(+)}^{(0)}) - f_{\bar{\mu}}(E_{n,l,(-)}^{(0)})$, yields a paramagnetic contribution of the Van Vleck kind, since it follows from the second-order perturbation correction in $\mathcal{H}^{(\mu)}$ appearing in the coupled basis, together with a weakly-relativistic correction.

Equation (4.56) can be directly evaluated from the knowledge of the zero-field, weakly-relativistic eigenenergies (4.36). However, since we are interested in the relativistic corrections to the ZFS, we will consider

$$\Delta\chi = \chi^{(\text{wr})} - \chi^{(\text{nr})}, \quad (4.57)$$

where $\chi^{(\text{nr})}$ is defined in eq. (4.15), and thus associated with the mean chemical potential $\bar{\mu}_0$ of the nonrelativistic problem, while the weakly relativistic $\chi^{(\text{wr})}$ is associated with the renormalized mean chemical potential

$$\bar{\mu} = \bar{\mu}_0 + \Delta\mu^{(\text{k})} + \Delta\mu^{(\text{D})}, \quad (4.58)$$

where $\Delta\mu^{(\text{k})}$ and $\Delta\mu^{(\text{D})}$ are, respectively, given by eqs. (4.22) and (G.14).

Furthermore, for calculational purposes, it is convenient to treat separately the corrections from the p and e contributions. Thus, we write

$$\Delta\chi = \Delta\chi_{\text{p}} + \Delta\chi_{\text{e}}, \quad (4.59)$$

where $\chi_{\text{p}}^{(\text{nr})}$ and $\chi_{\text{e}}^{(\text{nr})}$ have been worked out in appendix I. In the weakly-relativistic limit, eqs. (4.56), (I.3), and (I.4), together with the form (4.36) of the zero-field, weakly-relativistic energy correction and that of the renormalized mean chemical potential (4.58), yield to first-order in E_0/mc^2

$$\begin{aligned} \frac{\Delta\chi_{\text{p}}}{|\chi_{\text{L}}|} &= -\frac{9\pi E_0}{k_{\text{F}}a} \sum_{l=0}^{\infty} (l+1) \\ &\times \sum_{n=1}^{\infty} \left\{ (l+1) f''_{\bar{\mu}_0}(E_{n,l}^{(0)}) + \frac{1}{l+3/2} \frac{\mathcal{R}_{n,l}}{2E_0} f'_{\bar{\mu}_0}(E_{n,l}^{(0)}) \right\} \left[-\frac{(E_{n,l}^{(0)})^2}{2mc^2} + E_{n,l}^{(\text{D})} - \Delta\mu + \frac{E_0 E_{n,l}^{(0)}}{mc^2} l \right] \\ &+ \frac{9\pi E_0}{k_{\text{F}}a mc^2} \sum_{l=0}^{\infty} (l+1) \sum_{n=1}^{\infty} \left\{ \frac{2(l+1)^2}{l+3/2} E_{n,l}^{(0)} f'_{\bar{\mu}_0}(E_{n,l}^{(0)}) \right. \\ &\left. + \left(\frac{1}{l+3/2} \frac{\mathcal{R}_{n,l}}{2E_0} E_{n,l}^{(0)} + l+1 \right) f_{\bar{\mu}_0}(E_{n,l}^{(0)}) \right\}, \end{aligned} \quad (4.60a)$$

$$\begin{aligned} \frac{\Delta\chi_{\text{e}}}{|\chi_{\text{L}}|} &= -\frac{3\pi E_0}{k_{\text{F}}a} \sum_{l=1}^{\infty} l \\ &\sum_{n=1}^{\infty} \left\{ \left[(2l^2+1) f''_{\bar{\mu}_0}(E_{n,l}^{(0)}) + \frac{\mathcal{R}_{n,l}}{E_0} \frac{2l+5/2}{l+3/2} f'_{\bar{\mu}_0}(E_{n,l}^{(0)}) \right] \left[-\frac{(E_{n,l}^{(0)})^2}{2mc^2} + E_{n,l}^{(\text{D})} - \Delta\mu \right] \right. \\ &\left. + \left[(l^2-1) f''_{\bar{\mu}_0}(E_{n,l}^{(0)}) - \frac{3}{2} \frac{\mathcal{R}_{n,l}}{E_0} \frac{l+1}{l+3/2} f'_{\bar{\mu}_0}(E_{n,l}^{(0)}) \right] \frac{E_0 E_{n,l}^{(0)}}{mc^2} \right\} \\ &+ \frac{3\pi E_0}{k_{\text{F}}a mc^2} \sum_{l=1}^{\infty} l \sum_{n=1}^{\infty} \left\{ E_{n,l}^{(0)} \frac{4l^3+6l^2+l+1}{l+3/2} f'_{\bar{\mu}_0}(E_{n,l}^{(0)}) \right. \\ &\left. + \left[\frac{2l+5/2}{l+3/2} \frac{\mathcal{R}_{n,l}}{E_0} E_{n,l}^{(0)} + 2l^2+1 \right] f_{\bar{\mu}_0}(E_{n,l}^{(0)}) \right\}. \end{aligned} \quad (4.60b)$$

Grouping the two components of eq. (4.59), we have

$$\begin{aligned}
\frac{\Delta\chi}{|\chi_L|} = & -\frac{6\pi E_0}{k_{\text{F}}a} \sum_{l=0}^{\infty} \left(l + \frac{1}{2} \right) \\
& \times \sum_{n=1}^{\infty} \left\{ \left(l^2 + l + 3 \right) f''_{\bar{\mu}_0}(E_{n,l}^{(0)}) + \frac{\mathcal{R}_{n,l}}{E_0} f'_{\bar{\mu}_0}(E_{n,l}^{(0)}) \right\} \left[-\frac{\left(E_{n,l}^{(0)} \right)^2}{2mc^2} + E_{n,l}^{(\text{D})} - \Delta\mu \right] \\
& - \frac{3\pi E_0}{k_{\text{F}}a mc^2} \\
& \times \sum_{l=0}^{\infty} \sum_{n=1}^{\infty} \left\{ 4l \left(l + \frac{1}{2} \right) (l+1) E_0 E_{n,l}^{(0)} f''_{\bar{\mu}_0}(E_{n,l}^{(0)}) - 2 \left(2l^3 + 3l^2 + 5l + 2 \right) E_{n,l}^{(0)} f'_{\bar{\mu}_0}(E_{n,l}^{(0)}) \right. \\
& \left. - \left[2 \left(l + \frac{1}{2} \right) \frac{\mathcal{R}_{n,l}}{E_0} E_{n,l}^{(0)} + 2l^3 + 3l^2 + 7l + 3 \right] f_{\bar{\mu}_0}(E_{n,l}^{(0)}) \right\}. \tag{4.61}
\end{aligned}$$

Similarly to the discussion presented after eq. (4.26), we remark that the first sum in eq. (4.61) corresponds to the zero-field weakly-relativistic correction of the eigenenergies arising from the kinetic and Darwin terms. It could then be directly obtained by implementing, in the nonrelativistic ZFS expressions (4.17)–(2.33), the shift from $E_{n,l}^{(0)}$ to $E_{n,l}^{(0)}[1 - E_{n,l}^{(0)}/2mc^2] + E_{n,l}^{(\text{D})}$, with the corresponding renormalization $\Delta\mu$ of the chemical potential. The first contribution in the second sum of eq. (4.61) corresponds to the effect of $\mathcal{H}^{(\text{so})}$, while the remaining contributions arise from the magnetic-field dependence of $\mathcal{H}^{(\text{k})}$ and $\mathcal{H}^{(\text{ame})}$.

4.4 NUMERICAL EVALUATION OF THE RELATIVISTIC CORRECTIONS

When we evaluate numerically the weakly-relativistic correction $\Delta\chi$, according to eq. (4.61), as a function of $k_{\text{F}}a$, we find no noticeable difference with the results for the kinetic correction $\Delta\chi^{(\text{k})}$ on the scale of fig. 4.2. We therefore conclude that $\Delta\chi$ is dominated by $\Delta\chi^{(\text{k})}$.

As discussed at the end of the last section, it is straightforward to disentangle in $\Delta\chi$ the different contributions arising from the various Hamiltonian components of eq. (4.3), and thus we write

$$\Delta\chi = \Delta\chi^{(\text{k})} + \Delta\chi^{(\text{D})} + \Delta\chi^{(\text{so})} + \Delta\chi^{(\text{ame})}, \tag{4.62}$$

where the kinetic correction $\Delta\chi^{(\text{k})}$ is given by eq. (4.26). The corrections arising from the energy shift associated with the Darwin term, the spin-orbit coupling, and the

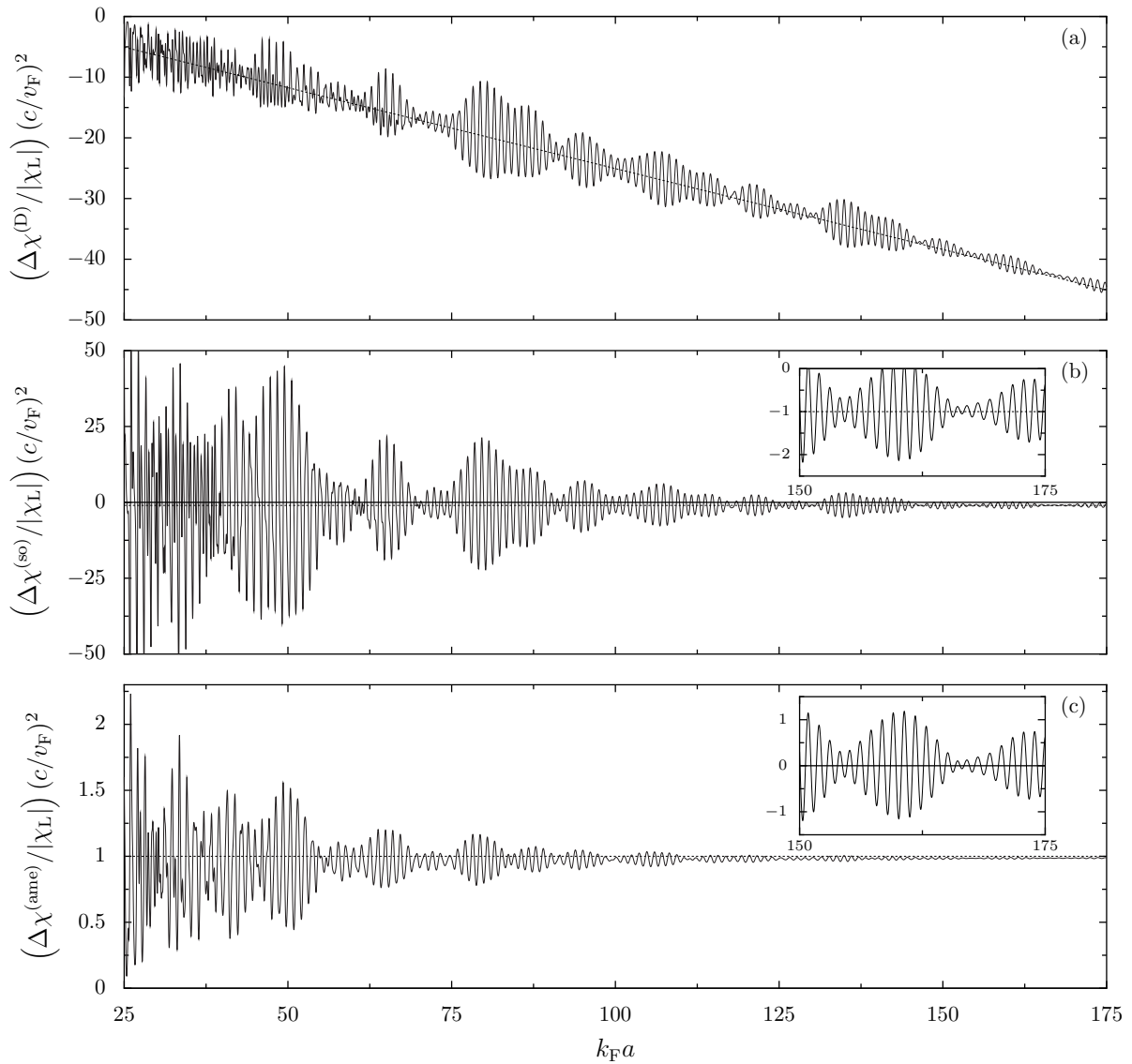


Figure 4.3: Weakly-relativistic corrections to the zero-field susceptibility arising from the (a) Darwin, (b) spin-orbit, and (c) angular magneto-electric components, for $k_B T / \bar{\mu}_0 = 5 \times 10^{-3}$, obtained from eq. (4.63), as a function of the nanoparticle radius a , using the same scaling and physical parameters in fig. 4.2. The dashed lines represent the mean (smooth), leading-order in $k_F a$, values of the different corrections according to eq. (4.64). The insets present the corrections $\Delta\chi^{(\text{so})}$ [panel (b)] and $\Delta\chi^{(\text{so-ame})} = \Delta\chi^{(\text{so})} + \Delta\chi^{(\text{ame})}$ [panel (c)] corresponding to large sizes (in the same units as in the main panels), showing the approach to the values predicted by the one-dimensional semiclassical approach given in eq. (4.64).

angular magneto-electric effect are given, respectively, by

$$\frac{\Delta\chi^{(\text{D})}}{|\chi_{\text{L}}|} = -\frac{6\pi E_0}{k_{\text{F}}a} \sum_{l=0}^{\infty} \left(l + \frac{1}{2} \right) \times \sum_{n=1}^{\infty} \left\{ \left(l^2 + l + 3 \right) f''_{\bar{\mu}_0} \left(E_{n,l}^{(0)} \right) + \frac{\mathcal{R}_{n,l}}{E_0} f'_{\bar{\mu}_0} \left(E_{n,l}^{(0)} \right) \right\} \left[E_{n,l}^{(\text{D})} - \Delta\mu^{(\text{D})} \right], \quad (4.63a)$$

$$\frac{\Delta\chi^{(\text{so})}}{|\chi_{\text{L}}|} = -\frac{12\pi E_0^2}{k_{\text{F}}a mc^2} \sum_{l=1}^{\infty} l \left(l + \frac{1}{2} \right) (l+1) \sum_{n=1}^{\infty} E_{n,l}^{(0)} f''_{\bar{\mu}_0} \left(E_{n,l}^{(0)} \right), \quad (4.63b)$$

$$\frac{\Delta\chi^{(\text{ame})}}{|\chi_{\text{L}}|} = -\frac{12\pi E_0}{k_{\text{F}}a mc^2} \sum_{l=1}^{\infty} \left(l + \frac{1}{2} \right) \sum_{n=1}^{\infty} E_{n,l}^{(0)} f'_{\bar{\mu}_0} \left(E_{n,l}^{(0)} \right). \quad (4.63c)$$

The behavior of $\Delta\chi^{(\text{k})}$, including its asymptotic dependence in $(k_{\text{F}}a)^0$, has been discussed in sec. 4.2. The numerical evaluation of the other weakly-relativistic corrections to the ZFS, given by eq. (4.63), is presented in the three panels of fig. 4.3. In all three cases, the typical values are much smaller than those of $\Delta\chi^{(\text{k})}$, and we observe oscillations as a function of $k_{\text{F}}a$ around mean values. Using a one-dimensional semiclassical treatment, analogous to that of the nonrelativistic ZFS (see appendix D) and the kinetic correction (see sec. 4.2), we can evaluate the leading-order corrections in $k_{\text{F}}a$ in the three cases. For the Darwin, spin-orbit, and angular magneto-electric contributions, in leading-order in $k_{\text{F}}a$, we have, respectively,

$$\overline{\frac{\Delta\chi^{(\text{D})}}{|\chi_{\text{L}}|}} = -\frac{1}{5} \left(u^{-1} - 2 \right) \left(\frac{v_{\text{F}}}{c} \right)^2, \quad (4.64a)$$

$$\overline{\frac{\Delta\chi^{(\text{so})}}{|\chi_{\text{L}}|}} = -\left(\frac{v_{\text{F}}}{c} \right)^2, \quad (4.64b)$$

$$\overline{\frac{\Delta\chi^{(\text{ame})}}{|\chi_{\text{L}}|}} = \left(\frac{v_{\text{F}}}{c} \right)^2, \quad (4.64c)$$

with $u = \sqrt{E_0/V_0}$.

Using the physical parameters of gold, we have $\overline{\Delta\chi^{(\text{D})}}/|\chi_{\text{L}}| = -0.27 (v_{\text{F}}/c)^2 (k_{\text{F}}a)$, which is in good agreement with the slope associated to the secular behavior of the very small oscillations present in fig. 4.3(a). The unbounded behavior obtained for large a is unphysical, since it prevents of achieving the bulk value $\chi_{(\text{b})}^{(\text{wF})}$. As discussed in appendix G, our perturbative approach is problematic for the Darwin term when treating the discontinuous electric field resulting from an abrupt electrostatic potential that confines fermions in a reduced (bag) region of space [119].

According to eqs. (4.64b) and (4.64c), we have $\overline{\Delta\chi^{(\text{so-ame})}} = 0$ to leading order in $k_{\text{F}}a$, in agreement with the numerical results [see inset in fig. 4.3(c)] and with the

expectation that in the infinite-volume limit the spin-orbit and magneto-electric couplings become irrelevant and eq. (2.48) accounts for the weakly-relativistic ZFS. The cancelation between the mean values of $\Delta\chi^{(\text{so})}$ and $\Delta\chi^{(\text{ame})}$ occurs despite the fact that the oscillations of the former are one order of magnitude larger than those of the latter. The comparison between figs. 4.2 and 4.3(b) indicates that $\Delta\chi^{(\text{so})}$ is typically more than an order of magnitude smaller than $\Delta\chi^{(\text{k})}$.

The suppression of the oscillations of $\Delta\chi^{(\text{so})}$ for large nanoparticle sizes is faster than that of $\Delta\chi^{(\text{nr})}$ since in the first case, in addition to the thermal damping (2.41) acting on the contribution of each family of classical periodic orbits, we have the fact that the SOC becomes comparatively weaker as a increases. Indeed, from eqs. (2.12) and (4.37) we have $E_{n,l,(\pm)}^{(\text{so})}/E_{n,l}^{(0)} = [\mp(l + 1/2) - 1/2]E_0/mc^2$, indicating that the relative importance of the SOC decreases with a .

4.5 HALF-SPHERICAL NANOPARTICLES

As discussed at the end of the last section, the high symmetry of the spherical potential translates into the smallness of the SOC contribution to the ZFS. Thus, a reduction of these symmetries appears as a way to boost the relative importance of the SOC. A first step in the process of progressive destruction of symmetries is to consider a half-spherical confining potential. Such a geometry has the advantage that its nonrelativistic eigenstates at zero magnetic field can be identified as a subset of those of the sphere, and many of the analytical developments performed for the case of the sphere can be readily adapted for the case in which the magnetic field is applied along the symmetry axis. Moreover, it is in metallic nanoparticles with the approximate shape of a half-sphere (HS) that the smallest g -factors (as low as 0.3) have been reported [100].

The kinetic and Darwin corrections are expected to change minimally when trading the spherical geometry by the HS, while the angular magneto-electric effect was shown, for the sphere, to be typically one order of magnitude smaller than the one arising from the SOC. Therefore, in this section we concentrate on the effect of the SOC for the ZFS for the reduced symmetry case of half-spherical nanoparticles. Since the total angular momentum is no longer a conserved quantity, the use of the coupled basis is of no aid to treat the SOC, and thus we present our calculations in the product basis, appealing to a numerical diagonalization once the SOC is included in the Hamiltonian.

Similar considerations to those discussed in sec. 2.1, concerning the passage from the ideal model of electrons confined in a sphere to the case of realistic nanoparticles, also apply for the HS geometries studied in this section.

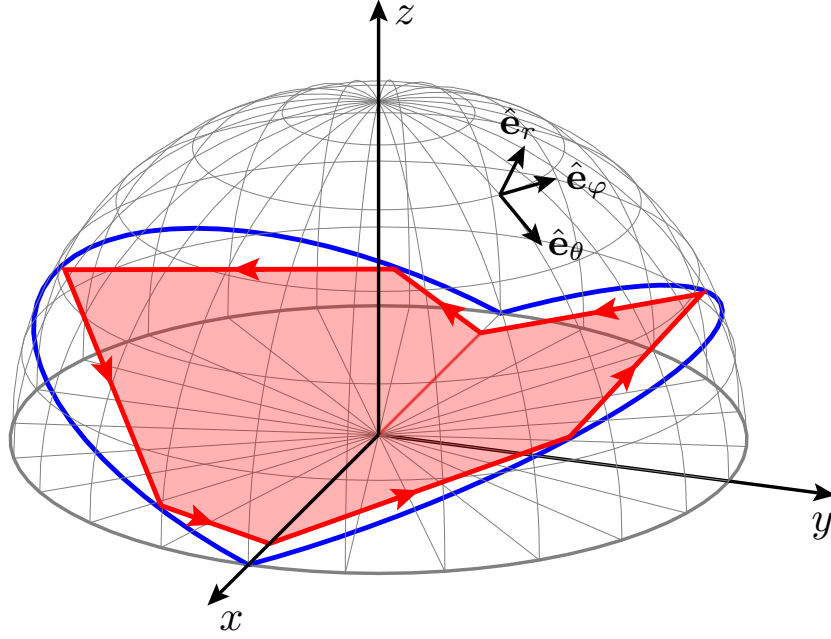


Figure 4.4: Half-spherical geometry with the coordinate axes used in the text. In red: Classical periodic orbit with the topological indices $(\nu, \eta) = (1, 5)$. In the case of the sphere (i.e. upper-right example of fig. 2.3) the associated trajectory is contained on the equatorial plane, while for the half sphere the periodic orbit is now contained in two planes (whose intersections with the HS are indicated by the two blue semi-circles).

4.5.1 NONRELATIVISTIC SUSCEPTIBILITY

We consider noninteracting electrons, described by a Hamiltonian $\mathcal{H}^{(0)}$ of the form (2.9a), confined by a potential with the shape of a HS, which, with the choice of coordinates of fig. 4.4, writes

$$V(r, \theta) = V_0 [\Theta(r - a) + \Theta(\theta - \pi/2)] . \quad (4.65)$$

For finite V_0 such a potential does not lead to a separable Schrödinger equation, and it has the unphysical feature of taking two different values (V_0 and $2V_0$) in the classically forbidden region. However, these shortcomings are no longer found in the limit $V_0 \rightarrow \infty$ of hard walls, where the corresponding eigenstates of $\mathcal{H}^{(0)}$ are characterized by the set of quantum numbers $\{\lambda\} = \{n, l, m_z, m_s\}$ with the condition $l + m_z$ odd, and the associated spinors $\Psi_{n,l,m_z,m_s}^{(\text{HS})}(\mathbf{r})$ have the form (2.10) with the orbital wave function given by

$$\psi_{n,l,m_z}^{(\text{HS})}(\mathbf{r}) = \sqrt{2} R_{n,l}(r) Y_l^{m_z}(\vartheta) . \quad (4.66)$$

The radial wave function $R_{n,l}(r)$ is given in eq. (2.13). The condition $l + m_z$ being odd arises since only the eigenstates of the sphere which are odd with respect to the

reflection off the $z = 0$ plane can be eigenstates of the HS, together with the property $Y_l^{m_z}(\pi - \theta, \varphi) = (-1)^{l+m_z} Y_l^{m_z}(\theta, \varphi)$ fulfilled by the spherical harmonics. We remark that the previous restriction excludes the isotropic $l = 0$ states. The corresponding eigenenergies $E_{n,l}^{(0)}$ are given by eq. (2.12).

The nonrelativistic case can be worked out along the lines presented in chapters 2 and 3 for the sphere, as the application of a magnetic field $\mathbf{B} = B \hat{\mathbf{e}}_z$ leads to the same energy corrections of eqs. (4.10)–(4.13). The ZFS of the half-sphere follows from eq. (2.24) by summing over m_z and m_s with the restriction of $l + m_z$ being odd. Including the spin-dependent component, we have

$$\frac{\chi^{(\text{nr})-(\text{HS})}}{|\chi_{\text{L}}|} = -\frac{6\pi}{k_{\text{F}}a} \sum_{l=0}^{\infty} \sum_{n=1}^{\infty} l \left\{ (l^2 + 2) E_0 f_{\bar{\mu}}'(E_{n,l}^{(0)}) + \frac{(l^2 - 3l/4 - 1)}{(l - 1/2)(l + 3/2)} \mathcal{R}_{n,l} f_{\bar{\mu}}(E_{n,l}^{(0)}) \right\}. \quad (4.67)$$

The numerical evaluation of the above expression for the nonrelativistic ZFS of the HS leads to a result (not shown) that is indistinguishable from that of the sphere (see the black solid line in fig. 4.1) for the presented $k_{\text{F}}a$ -interval, while very small differences appear for smaller values of $k_{\text{F}}a$.

The concordance of the ZFS of the sphere and the HS for not too small values of $k_{\text{F}}a$ is understandable from a semi-classical viewpoint. Indeed, in fig. 4.4 we see that the periodic orbits of the HS can be put in correspondence with those of the sphere [70] (see fig. 2.3) by simply symmetrizing one of the two containing planes with respect to the x – y plane and the flux of both trajectories defined by a magnetic field oriented along the z -axis is the same.

4.5.2 SPIN-ORBIT COUPLING FOR A HS CONFINING POTENTIAL

In the hard wall limit of the potential (4.65) defining a half-spherical box, the spin-orbit coupling (4.6a) is given by the Hamiltonian

$$\mathcal{H}^{(\text{so})-(\text{HS})} = \mathcal{H}^{(\text{dome})} + \mathcal{H}^{(\text{floor})}, \quad (4.68)$$

where

$$\mathcal{H}^{(\text{dome})} = \frac{1}{2m^2c^2} \frac{V_0}{r} \delta(r - a) \mathbf{S} \cdot \mathbf{L}, \quad (4.69a)$$

$$\mathcal{H}^{(\text{floor})} = \frac{1}{2m^2c^2} \frac{\hbar V_0}{ir} \delta\left(\theta - \frac{\pi}{2}\right) \mathbf{S} \cdot \left(-\hat{\mathbf{e}}_{\varphi} \partial_r + \hat{\mathbf{e}}_r \frac{1}{r \sin \theta} \partial_{\varphi} \right), \quad (4.69b)$$

represent, respectively, the effect of the dome and the floor of the confining potential.

Writing $\mathbf{S} \cdot \mathbf{L} = (S_+L_- + S_-L_+)/2 + S_zL_z$ ¹ we see that the contribution S_zL_z leads to spin-conserving matrix elements of $\mathcal{H}^{(\text{dome})}$ which are diagonal in the indices m_z and m_s . That is,

$$\langle \Psi_{n',l',m_z,m_s}^{(\text{HS})} | \mathcal{H}^{(\text{dome})} | \Psi_{n,l,m_z,m_s}^{(\text{HS})} \rangle = (-1)^{(n-n')} m_z m_s \delta_{l',l} \zeta_{n',l} \zeta_{n,l} \frac{2E_0^2}{mc^2}, \quad (4.70)$$

where we have used that $\text{sgn}[j'_l(\zeta_{n,l})] = (-1)^n$, independently of the value of l . The remaining terms of $\mathbf{S} \cdot \mathbf{L}$ result in spin-flip matrix elements of $\mathcal{H}^{(\text{dome})}$ which are nondiagonal in the indices m_z and m_s , i.e.,

$$\begin{aligned} \langle \Psi_{n',l',m'_z,m'_s}^{(\text{HS})} | \mathcal{H}^{(\text{dome})} | \Psi_{n,l,m_z,m_s=\pm 1/2}^{(\text{HS})} \rangle = \\ (-1)^{(n-n')} \delta_{m'_z,m_z\pm 1} \delta_{m'_s,-m_s} \zeta_{n',l'} \zeta_{n,l} \sqrt{(l \mp m'_z + 1)(l \pm m'_z)} \mathcal{I}_{l',l,m'_z}^{(\text{dome})} \frac{2E_0^2}{mc^2}, \end{aligned} \quad (4.71)$$

where we have defined

$$\mathcal{I}_{l',l,m'_z}^{(\text{dome})} = \int_{\text{dome}} d\vartheta \left(Y_{l'}^{m'_z}(\vartheta) \right)^* Y_l^{m'_z}(\vartheta). \quad (4.72)$$

Since $l + m_z$ and $l' + m'_z$ are both odd, the two spherical harmonics in the previous equation have different parities. Therefore, the integral over the dome does not trivially vanish in the case that interests us, where $m'_z = m_z \pm 1$, and then l and l' have a different parity. Equation (J.14), in appendix J, provides the result of the integral (4.72).

The Hamiltonian component (4.69b) writes

$$\begin{aligned} \mathcal{H}^{(\text{floor})} = \frac{1}{4m^2c^2} \frac{\hbar^2 V_0}{ir} \delta\left(\theta - \frac{\pi}{2}\right) \\ \times \left((\sigma_x \sin \varphi - \sigma_y \cos \varphi) \partial_r + \frac{1}{r} (\sigma_x \cos \varphi + \sigma_y \sin \varphi + \sigma_z \cot \theta) \partial_\varphi \right), \end{aligned} \quad (4.73)$$

and thus, the condition $\delta(\theta - \pi/2)$ results in vanishing spin-conserving matrix elements, while the nondiagonal, spin-flip matrix elements are given, in the limit of large V_0 , by

$$\begin{aligned} \langle \Psi_{n',l',m'_z,m'_s}^{(\text{HS})} | \mathcal{H}^{(\text{floor})} | \Psi_{n,l,m_z,m_s=\pm 1/2}^{(\text{HS})} \rangle \\ = \frac{\hbar^2 V_0}{4m^2c^2} \delta_{m'_s,-m_s} \int_0^a dr r \int_0^{2\pi} d\varphi \exp(\pm i\varphi) \psi_{m'_z}^{(V_0,n',l')} (r, \theta = \pi/2, \varphi) \\ \times \left\{ \mp \partial_r + \frac{1}{ir} \partial_\varphi \right\} \psi_{m_z}^{(V_0,n,l)} (r, \theta = \pi/2, \varphi). \end{aligned} \quad (4.74)$$

¹ $L_\pm = Lx \pm iLy$ are the ladder angular momentum operators.

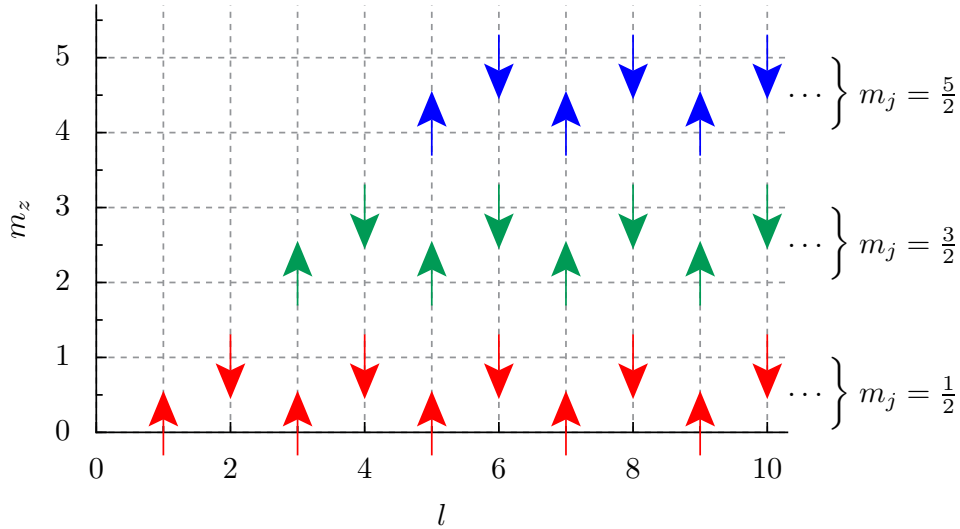


Figure 4.5: The l - m_z plane for positive $m_j = m_z + m_s$ for the half-spherical nanoparticle. Each arrow pointing up (down) represents the orientation of the spin $m_s = 1/2$ ($m_s = -1/2$) for the allowed states $l + m_z$ odd and $l > m_z$. At zero-field, the Hamiltonian of the half-spherical nanoparticle only couples states with the same m_j .

where $\psi_{m_z}^{(V_0, n, l)}(r, \theta, \varphi)$ and $\psi_{m_z'}^{(V_0, n', l')}(r, \theta, \varphi)$ converge, respectively, to the orbital wave functions $\psi_{n, l, m_z}(r, \theta, \varphi)$ and $\psi_{n', l', m_z'}(r, \theta, \varphi)$ when $V_0 \rightarrow \infty$. Thus, the limiting condition (J.8) and the form (2.13) of the radial wave function for the hard wall case allow us to write

$$\begin{aligned} & \langle \Psi_{n', l', m_z', m_s'}^{(\text{HS})} | \mathcal{H}^{(\text{floor})} | \Psi_{n, l, m_z, m_s}^{(\text{HS})} \rangle = \\ & \quad \pm \frac{(-1)^{(l+l'+m_z+m_z')/2}}{2^{l+l'}} \delta_{m_z', m_z \pm 1} \delta_{m_s', -m_s} \frac{4E_0^2}{mc^2} \mathcal{J}_{n', l', n, l, m_z} \\ & \times \frac{\sqrt{(2l+1)(2l'+1)}}{|j_{l'+1}(\zeta_{n', l'}) j_{l+1}(\zeta_{n, l})|} \frac{\sqrt{(l+m_z)!(l-m_z)!}}{(\frac{l+m_z-1}{2})! (\frac{l-m_z-1}{2})!} \frac{\sqrt{(l'+m_z')!(l'-m_z')!}}{(\frac{l'+m_z'-1}{2})! (\frac{l'-m_z'-1}{2})!}, \end{aligned} \quad (4.75)$$

where l and l' have different parities and we have expressed the integral over the radial coordinate through

$$\mathcal{J}_{n', l', n, l, m_z} = \int_0^1 \frac{d\zeta}{\zeta} j_{l'}(\zeta_{n', l'} \zeta) \left(\frac{l \mp m_z - 1}{\zeta} j_l(\zeta_{n, l} \zeta) - \zeta_{n, l} j_{l+1}(\zeta_{n, l} \zeta) \right). \quad (4.76)$$

Recalling that $j_l(\zeta) \sim \zeta^l / (2l+1)!!$ for small values of ζ , and that $l=0$ is not allowed for the HS, we verify that the integral in eq. (4.76) is divergence-free.

The axial symmetry of the HS translates in the conservation of the z -component of the total angular momentum. The subspaces with different $m_j = m_z + m_s$ are not coupled by $\mathcal{H}^{(\text{so})-(\text{HS})}$, and within each of these subspaces the coupling between

two eigenstates $\Psi_{n,l,m_z,m_s}^{(\text{HS})}$ and $\Psi_{n',l',m'_z,m'_s}^{(\text{HS})}$ of $\mathcal{H}^{(0)}$ only occurs in the following cases: (i) $\{l', m'_z, m'_s\} = \{l, m_z, m_s\}$; (ii) $m_s = 1/2$ and $\{m'_z, m'_s\} = \{m_z + 1, -1/2\}$; (iii) $m_s = -1/2$ and $\{m'_z, m'_s\} = \{m_z - 1, 1/2\}$ (with l and l' having different parity in the last two cases). These restrictions can be graphically represented in the plane l - m_z (see fig. 4.5), where only the subspaces with positive m_j are considered. The diagonalization within each of these subspaces (those with negative m_j follow from Kramer's degeneracy) leads to the eigenstates of $\mathcal{H}^{(0)} + \mathcal{H}^{(\text{so})-(\text{HS})}$

$$\Psi_{m_j,p}(\mathbf{r}) = \sum_{\substack{n,l,m_s=\pm 1/2 \\ l > |m_j - m_s| \\ l + m_j - m_s \neq 2}} C_{n,l,m_s}^{m_j,p} \Psi_{n,l,m_j - m_s, m_s}^{(\text{HS})}(\mathbf{r}), \quad (4.77)$$

labeled by the half-integer m_j and the positive integer index p , with the associated eigenenergies $E_{m_j,p}$.

4.5.3 PERTURBATIVE TREATMENT OF THE MAGNETIC FIELD

Under the application of a weak magnetic field B , the energy $E_{m_j,p}$ picks up a correction $\delta E_{m_j,p}$. According to eq. (2.24), the latter determines the ZFS of the HS through the parameters

$$\left. \frac{\partial \delta E_{m_j,p}}{\partial B} \right|_{B=0} = \mu_B \sum_{n,l,m_s} |C_{n,l,m_s}^{m_j,p}|^2 (m_j + m_s), \quad (4.78a)$$

$$\begin{aligned} \left. \frac{\partial^2 \delta E_{m_j,p}}{\partial B^2} \right|_{B=0} &= \frac{\mu_B^2}{2E_0} \sum_{n,l,m_s} \sum_{n'} \sum_{i=-1}^{+1} \left(C_{n',l+2i,m_s}^{m_j,p} \right)^* \\ &\times C_{n,l,m_s}^{m_j,p} \mathcal{R}_{n',l+2i,n,l} \mathcal{Y}_{l,i}^{m_j - m_s} \Theta(l + 2i - |m_j - m_s|), \end{aligned} \quad (4.78b)$$

where the sums over $\{n, l, m_s\}$ have the same restrictions as in eq. (4.77), and the Heaviside function prevents the consideration of unphysical terms having $l' = l - 2$. The angular matrix elements are calculated over the whole sphere, where the diagonal ones $\mathcal{Y}_{l,0}^{m_z} = \mathcal{Y}_l^{m_z}$ are given by eq. (2.31), while the nonvanishing off-diagonal ($l' = l \pm 2$) ones can be expressed, for $i = \pm 1$, as

$$\mathcal{Y}_{l,i}^{m_z} = -\frac{1}{4(l + 1/2 + i)} \sqrt{\frac{[(l + 1 + i)^2 - m_z^2][(l + i)^2 - m_z^2]}{(l + 3/2 + i)(l - 1/2 + i)}}. \quad (4.79)$$

The radial matrix elements are

$$\mathcal{R}_{n',l',n,l} = \frac{1}{a^2} \int_0^a dr r^4 R_{n',l'}(r) R_{n,l}(r). \quad (4.80)$$

The diagonal ones $\{n', l'\} = \{n, l\}$ are given by eq. (2.30), while the off-diagonal ones can be obtained by numerical integration or by recurrence formulas, as shown in appendix J.3.

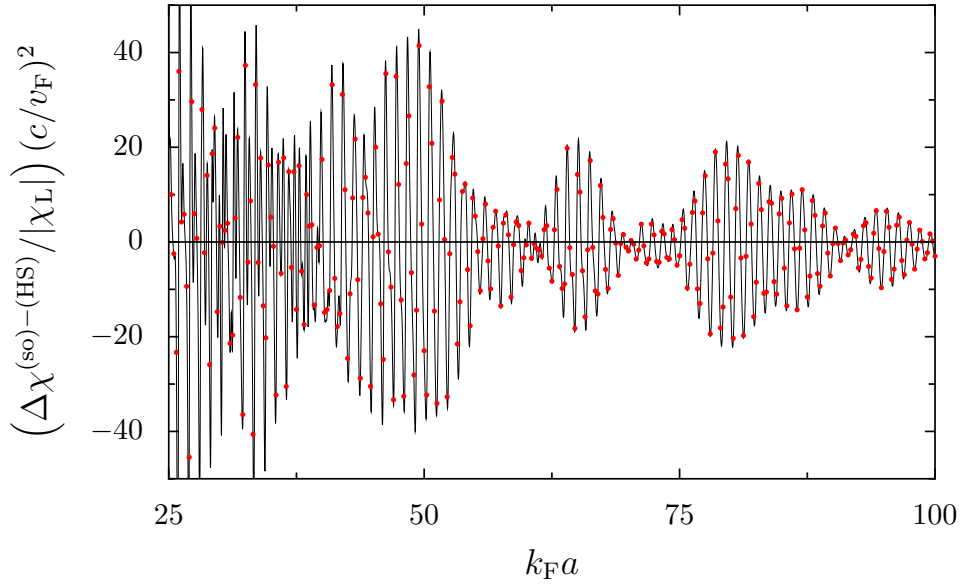


Figure 4.6: Red dots: SOC correction $\Delta\chi^{(so)-(HS)}$ to the nonrelativistic ZFS $\chi^{(nr)-(HS)}$ in a half-sphere, from eqs. (2.24) and (4.78), as a function of $k_F a$. Black line: reproduction of the result of fig. 4.3(b) obtained for the sphere using eq. (4.63b).

4.5.4 SPIN-ORBIT CORRECTION FOR THE HALF-SPHERE

In fig. 4.6 we present the numerical evaluation of the SOC correction $\Delta\chi^{(so)-(HS)}$ to the nonrelativistic ZFS $\chi^{(nr)-(HS)}$, according to eqs. (2.24) and (4.78), as a function of $k_F a$ (red dots). These results are indistinguishable from those corresponding to the SOC correction for the sphere presented in fig. 4.3(b) and reproduced by the black line of fig. 4.6. The symmetry reduction in going from the sphere to the HS is thus not enough to yield a significantly enhanced SOC correction in the last case. Upon increasing a , the SOC mixing of energy levels of the HS with different (n, l) is favored. But such a tendency is countered by the relative weakening of the SOC matrix elements, as discussed at the end of sec. 4.4.

The ZFS correction $\Delta\chi^{(so)-(HS)}$, which is very close to the corresponding correction in the sphere, can be very well approximated by only considering the energy shifts arising from only the diagonal (in m_z , m_s , and n) matrix elements (4.70), as well as the corresponding diagonal SOC matrix elements for the sphere in the product basis (not shown). These accordances indicate that for the sphere, as well as for the HS, for the considered $k_F a$ values, the SOC can be accounted for in first-order perturbation theory.

4.6 CONCLUSIONS FOR CHAPTER 4

Motivated by measurements of the magnetization in ensembles of noble-metal nanoparticles [16, 42] and the g -factor of an individual nanoparticle [99, 100], together with the theoretical proposals pointing to the key role played by the spin-orbit coupling in these experimental results [90, 103, 104], we considered in this chapter the relevance of such a relativistic effect on the magnetic response of confined electrons. In particular, we attempted to quantify the spin-orbit effect by going beyond the previous phenomenological approaches that assigned arbitrary values to its strength. We focused on the extrinsic SOC originating from the confining potential, treating model systems, and then discussing their applicability to the case of metallic nanoparticles of different shapes. The relevance of the SOC in the magnetic response was gauged against other weakly-relativistic corrections and finite-size effects inherent to the mesoscopic regime.

For spherical geometries, the inclusion of the SOC and other relativistic effects could be readily done, at the quantum level, by working in the coupled basis of the total angular momentum, within a perturbative treatment of the magnetic field.

Analogously to the nonrelativistic zero-field susceptibility characterizing electrons confined in a spherical geometry from chapter 3, the weakly-relativistic corrections present oscillations as a function of $k_F a$ between paramagnetic and diamagnetic values, which are typically much larger than the background that sets the bulk response. The oscillations corresponding to the SOC contribution are out-of-phase with respect to those of the nonrelativistic ZFS. The typical values of the SOC contribution are more than an order of magnitude larger than the ones due to the magneto-electric coupling, and more than an order of magnitude smaller than those arising from the kinetic energy correction. The latter, being the dominant weakly-relativistic correction to the ZFS, remains much smaller than the nonrelativistic ZFS. These small values of the weakly-relativistic corrections stem from their $(v_F/c)^2$ dependence, while the reduced effect of the SOC correction is associated with the high spatial symmetry of the spherical geometry.

In order to study the impact of a symmetry reduction on the magnetic response, the formalism developed to treat the SOC in the sphere was adapted to the case of a half-sphere. The nonrelativistic ZFS was shown to be the same for the sphere and the half-sphere in the semiclassical limit of large $k_F a$, as can be readily understood from semiclassical arguments. The inclusion of the SOC in the HS leads to corrections of the ZFS which are very close to those of the sphere, and therefore, much smaller than the correction arising from the kinetic energy shift and the typical values of the non-relativistic ZFS. The symmetry reduction when going from the spherical geometry to that of the HS is not enough to render relevant the SOC effects due to the electron confinement. Even if the HS confinement favors the SOC mixing of the unperturbed states in comparison with the case of the sphere, such an effect is offset by the generic suppression of the SOC matrix elements with the parameter $(v_F/c)^2$ and the size a . The SOC is thus weak enough to remain perturbative, and therefore it does not induce the transition in the statistical properties of the spectra necessary to reverse the

sign of the magnetic response of a nanoparticle ensemble.

Further symmetry reduction would lead to more quasi-degeneracies in the $B = 0$ spectrum, enhancing the effect of the SOC. However, the cases of the quarter- and eighth-sphere, which can be worked out similarly to that of the HS, do not show a significant increase of the SOC contribution to the ZFS [156]. The case of cylindrical nanoparticles is important (see app. C.2 for the non-relativistic case), as it is the geometry considered in ref. [42]. At least in the most symmetric case where the magnetic field is oriented along the cylinder axis, the SOC due to the confinement seems to have minor importance [156]. Moving forward from integrable to chaotic geometries will increase the importance of the SOC mixing, but at the same time will be accompanied by a reduction of the typical values attained by the nonrelativistic ZFS [85, 86].

CONCLUDING REMARKS AND OUTLOOK

5

5.1 SUMMARY

Several experiments have reported very unusual magnetic properties of ensembles of gold nanoparticles surrounded by organic ligands, including ferromagnetic, paramagnetic, and (large) diamagnetic responses [16, 17]. Motivated by the limited theoretical understanding of such diversity in magnetic behavior, we have investigated the electronic magnetism in confined metallic systems. Focusing on the proposal that orbital magnetism is enhanced by quantum size effects, we have constructed a theoretical model to describe the electronic magnetic response of individual and ensembles of metallic nanoparticles.

The positively-charged ion lattice was treated within a jellium model and the electron-electron interaction was approximated by adopting a mean field confinement potential. The valence electron dynamics was described by a Hamiltonian that includes the weakly relativistic and non-relativistic interactions with the magnetic field in the limit of large cyclotron radius compared to its size ($R_c \gg a$). The effect of coating agents was not included in this work, where static electric and magnetic fields are studied. The calculation of the energy spectrum and the thermodynamic quantities such as the magnetic susceptibility and magnetic moments of these nanoparticles were based on quantum perturbation theory together with semiclassical developments. The semiclassical expansion of the free energy allows to take into account the canonical corrections which are important for finite sizes.

In chapter 3, we investigated through a theoretical approach the possibility that the observed magnetization of an ensemble of gold nanoparticles could be explained by an orbital contribution enhanced by the quantum confinement. We calculated the orbital component of the zero-field susceptibility (ZFS) for an individual nanoparticle using a semiclassical expansion of the free energy, which coincides very well with the quantum perturbative approach in the grand canonical ensemble [22, 68]. The dominating grand canonical contribution to the ZFS resulted in a function of the radius of the nanoparticle with rapidly alternating sign, changing the response between paramagnetic and diamagnetic, and attaining values that are several orders of magnitude larger than the Landau susceptibility. When considering the ensemble average of a large number of non-interacting nanoparticles with Gaussian size distribution, the ZFS results to be always paramagnetic, a behaviour stemming from the canonical corrections associated with fine-size effects. Under a semiclassical treatment, we show that the ZFS of the ensemble follows a Curie-type law for small nanoparticle sizes

and/or low temperatures. Importantly, we compared our theoretical prediction of the magnetization of an ensemble of nanoparticles with the measurements of existing experiments that observed a large paramagnetic response [34, 35, 38] and we found a good agreement with our microscopic theory (without any fitting parameter).

As the calculated orbital response only exhibited a paramagnetic susceptibility, the diamagnetism and ferromagnetism observed in other experiments remained unexplained. Motivated by the theoretical suggestion that spin-orbit coupling could lead to a sign inversion of the magnetic susceptibility [90], we studied in detail such a possibility in chapter 4. As spin-orbit coupling can have various possible origins, we focused our analysis on the most relevant case, evaluating the contribution of SOC on the ZFS influenced by the self-consistent confinement potential. We quantified the contribution of the SOC to the ZFS by gauging it against the ones generated by other weakly-relativistic corrections, including the angular magneto-electric coupling, the Darwin term, and corrections to the kinetic energy under a magnetic field. Two ideal geometries were considered, the sphere and the half-sphere, focusing on the expected increased role of the spin-orbit coupling upon a symmetry reduction. The matrix elements of the different weakly-relativistic corrections were obtained and incorporated in a perturbative treatment of the magnetic field, leading to tractable semi-analytical and semiclassical expressions for the case of the sphere, while a numerical treatment becomes necessary for the half-sphere. The correction to the zero-field susceptibility arising from the spin-orbit coupling in the sphere is quite small, and it is dominated by the weakly-relativistic kinetic energy correction, which in turn remains considerably smaller than the typical values of the nonrelativistic zero-field susceptibility. We showed that the symmetry reduction going from the sphere to the half-sphere does not translate into a sign inversion of the total susceptibility.

Most of the theoretical studies considering the effect of the SOC on the symmetries of the Hamiltonian, and its physical consequences, treat the strength of such interaction as a phenomenological parameter. Our work took a completely different approach, trying to first obtain an accurate microscopic estimation of the coupling strength in particularly simple systems, and then determining its effect on measurable quantities. At the theoretical level, our work opened new avenues to explore, some of them sketched in the next section. At the same time, we expect that our results will motivate more systematic experimental studies, specially concerning the different temperatures regimes, the importance of the nanoparticles size distribution and the characteristics of the spatial organization (separation between nanoparticles).

5.2 OUTLOOK

The plethora of reported magnetic responses described in chapter 1 are diverse and cover many possible regimes. It is possible that there is no unique theory that can explain all the observed behaviors. Careful experimental investigations and theoretical analysis still need to be carried out. Many modern techniques like spin-polarized STM and magnetic force microscopy (MFM), spin-polarized tunnel microscopy (SP-

STM) and nanoSQUIDS could provide some insight to the magnetic behavior of single or pairs [146] of nanoparticles and could provide some evidence of the orbital origin of the magnetic response [17, 62].

Recent experiments have found that an instantaneous giant magnetic moment can be induced in ensembles of gold nanoparticles when interacting with pulsed light in the absence of an applied magnetic field [157]. Based on hydrodynamic and ab-initio calculations, it is claimed that this large magnetic moment originates from the coherent orbital motion of electrons [157]. Further analysis is needed to understand if the static and time-dependent cases are comparable and the calculations from this thesis would have to be adapted to treat dynamical fields.

The description presented in this thesis is limited and more ingredients can still be explored and adapted. Mainly, we ignored the effects of electron-electron interactions beyond a mean-field treatment, as well as intraparticle interactions. The experimentally observed ferromagnetic responses in lattices of gold nanoparticles [49] suggest that interactions between nanoparticles may induce a collective macroscopic behavior. Our model indicates that nanoparticles with slightly different size could have radically different orbital magnetizations. If that is the case, some nanoparticles could possess large magnetic moments, leading to important dipole-dipole interactions between nanoparticles in a sample. Such an interaction suggests a complex model of random magnetic moments reminiscent to that of spin-glasses, with the complication that each nanoparticle does not hold a magnetic moment at zero-field. Ferromagnetic responses from dipole-dipole interactions of a dimer were theoretically investigated in ref. [146], where it was found that aligned and anti-aligned magnetic-ordered phases are possible when the absolute values of the susceptibilities are of the order of 1, susceptibilities that have only been observed in ferromagnetic materials.¹ For a linear chain of identical paramagnetic particles [146], the values of the susceptibility decrease with the size of the chain until reaching a plateau. However the temperatures and dispersion in sizes needed to observe a magnetic ordering are not necessarily reached by most experiments. If the spatial ordering of nanoparticles plays a key role, other interactions may be necessary, possibly enhanced by the ligand-coating. It was also found [146] that for small susceptibilities, the diamagnetic behavior of the dimer was favored when the magnetizations are on the same axis, but a careful study has to be carried out when generalizing this result to the case of 3D ensembles of nanoparticles.

For large magnetic fields, the magnetic response of metals is described by the De Haas-Van Alphen effect [23, 24, 159], where the magnetization oscillates as a function of the applied field. In these systems, anomalies in the oscillating magnetization of gold and other noble metals had to be explained by an inversion of the \mathbf{B} and \mathbf{H} fields [160, 161], leading to non-linear phenomena sometimes known as the Shoenberg effect. In astrophysical systems like neutron stars and white dwarfs, the

¹For negative susceptibilities, $\chi \approx -1/4\pi$ is observed in superconductors, in which the magnetic field is null inside the material (perfect diamagnetism). However lower susceptibilities have been reported [158] and are of interest for the development of metamaterials.

fields are intense enough, and this effect has been invoked to explain the spontaneous magnetization of these astronomical bodies, an effect known as the Landau orbital ferromagnetism [162]. As similar oscillations appear in finite systems, even at low magnetic fields, one can wonder if the Shoenberg effect is also responsible for locking the magnetization of metallic nanoparticles and producing the observed hysteresis loops. The difficulty of this hypothesis is that it requires absolute values of the ZFS of the order $\chi \approx 1/4\pi$ [163]. This possibility has been partially explored [156], but requires very special conditions (small size dispersion, low temperatures) that could be of interest for future experiments.

Large diamagnetic susceptibilities were experimentally observed in ensembles of gold nanorods [42]. If confinement corrections to the spin-orbit coupling contribution are not the origin of this response, one may wonder if the shape of the nanorods is playing a significant effect. We have shown that cylindrical nanoparticles have a very similar magnetic response to that of the sphere when the magnetic field is parallel to its long axis, described in appendix C.2. Despite that, if the magnetic field is aligned in other directions, contributions of the Van Vleck kind become important, which amounts to include the contribution of quasiperiodic orbits (and increasing the calculation time). If the geometry is related to the diamagnetic response, the details of the faceting of the nanoparticles could also have an important effect. However, chaotic behavior and disorder is expected to reduce the magnetic response [83–85, 87, 88].

These limitations highlight the difficulty of providing a complete picture. It remains to be studied, if any of these effects is enough to produce a change in the oscillating susceptibility necessary to produce a non-paramagnetic ensemble average. However we do not discard the possibility, that some combination of these effects: dipole-dipole interactions, orbital Landau ferromagnetism and geometrical effects could work together to provide a large spectrum of magnetic response, sensitive to all kinds of experimental conditions. We propose that all three effects should be carefully theoretically studied.

In this thesis, we have also approximated the ionic lattice by a charged jellium and we have neglected contributions from the band structure. In our calculations, quantum perturbation theory was carried out by differentiating the spectrum in a perturbative regime. The introduction of lattice-like models leads to interesting fractal spectra like the Hofstadter butterfly, found in a 2D tight binding square lattice with a magnetic field [164]. Fractality is not an issue as we are considering finite systems, where the spectrum remains differentiable [165]. The effects of the band structure of gold can also provide some corrections to the spectrum and could be tackled with pseudopotentials as a multipole expansion [114].

The effect of ligands was not considered in this work. The idea of spontaneous magnetic moments produced by a "Fermi hole" in the d shell, created by an electron leaving a surface atom when forming a covalent bond with the ligand atoms, was indeed one of the first theories proposed [34]. This idea has been invoked in different ways [37, 38, 40, 64]. However the modification of the density of states by the organic ligands can be quite complex, specially in the case of strong chemical bonds [166].

If by charge transfer mechanisms, the ligands modify significantly the work function of gold [167] or behave in such a way that the d band modifies the metallic behavior of electrons in gold [64, 168], then further analysis has to be carried to extend our theory taking into account those effects as a function of the different capping agents. A certain number of first principle calculations of the different energy scales in ligand-metal interactions have been developed [166, 168] and could be adapted to the description of gold nanoparticles. Nevertheless, not every ligand that has been explored experimentally is expected to modify the metallic behavior significantly [42, 54, 63, 108].

Lastly, we indicate that calculations carried out in this thesis can be certainly adapted to semiconducting quantum dots. The band structure of semiconductors leads to a rich effective dynamics described by stronger spin-orbit couplings. In elements like silicon, a spin-orbit coupling emerges in confined systems [169, 170], which is usually negligible in the bulk. When describing quantum electronic transport in these systems, the occupation of the dots is very sensitive to the energy scales and selection rules, leading to Coulomb [171] and spin blockades [172, 173] of the current. Early calculations show that spin-orbit and angular magnetoelectric couplings can lead to novel blockade effects in coherent double quantum dots [156]. An investigation of the orbital magnetic and SOC effects in these structures can be motivated considering the implications of semiconductors for nanotechnology and quantum information processing.

APPENDICES

ZERO-FIELD SUSCEPTIBILITY OF A FREE ELECTRON GAS

A

In this appendix we derive the non-relativistic and weakly relativistic Landau susceptibilities, working in the grand-canonical ensemble. In sec. A.1.1 we obtain the bulk ZFS of metals following the quantum mechanical formalism. In sec. A.2 we recover the Landau (orbital susceptibility) from the knowledge of the density of states as a way to illustrate the semiclassical calculation. In sec. A.3 we calculate the relativistic bulk ZFS in order to retrieve the corrections to the bulk susceptibility in the weakly relativistic limit.

According to classical mechanics, Bohr-Van Leeuwen theorem [19, 20] states that at thermal equilibrium, the magnetization of a finite system must be null. Thus diamagnetism, paramagnetism, and even ferromagnetism, can only be explained by quantum mechanics.

The orbital magnetic susceptibility of a three dimensional Fermi gas is known as the Landau susceptibility. This quantization leads to a the bulk zero-field susceptibility of metals given by $\chi_b^{(\text{nr})} = 2|\chi_L|$, which is the sum of the orbital contribution given by $-|\chi_L|$ and the spin contribution coming from the Zeeman term (2.57) known as Pauli susceptibility which is $3|\chi_L|$.

Lev Landau in his paper of 1930 [23, 24], not only derived the orbital susceptibility of metals at small magnetic fields but also predicted the oscillations that appear at high magnetic fields, the so called De Haas–Van Alphen effect, which was observed a few months after in the same year [159]. The latter regime can be well described using semiclassical approximations, allowing to measure the Fermi surface of metals. Analogously, for confined systems one is allowed to expand the susceptibility in terms of semiclassical orbits as long as $k_F a T / T_F \ll 1$, where T_F is the Fermi temperature.

A.1 NON-RELATIVISTIC LANDAU LEVELS

From Landau's quantization, we know that free electrons under a uniform magnetic field $\mathbf{B} = B\hat{z}$ are quantized in terms of a principal quantum number n_L , the spin projection m_s and the wavevector k_z along the direction of the field, such that the energy of the Landau levels reads [24]

$$E_{n_L, m_s}^{(\text{L})}(k_z) = \hbar\omega_c \left(n_L + m_s + \frac{1}{2} \right) + \frac{\hbar^2 k_z^2}{2m}, \quad (\text{A.1})$$

which is the result from the Pauli Hamiltonian in the absence of a confining potential, $V(\mathbf{r}) = 0$, under symmetric gauge. Note that a third quantum number related to the angular momentum is missing from the expression of the energy, which contributes to the degeneracy of the states.

As we will be taking derivatives with respect to the magnetic field, let us rewrite the Landau levels of eq. (A.1), in terms of B and the Bohr magneton μ_B as

$$E_{n_L, m_s}^{(L)}(k_z) = \frac{\hbar^2 k_z^2}{2m} + 2\mu_B B(n_L + 1/2 + m_s). \quad (\text{A.2})$$

The third hidden quantum number m_z does not appear in the expression of the energy. The level degeneracy, for fixed k_z , due to this missing quantum number, is

$$G(B) = \mu_B B m \mathcal{A} / \pi \hbar^2, \quad (\text{A.3})$$

where \mathcal{A} is the area that is transversal to the field [24].

A.1.1 NON RELATIVISTIC BULK SUSCEPTIBILITY

In order to calculate the bulk ZFS, we use the formulas for the grand canonical potential, analogous to eq. (2.22) and (2.24). As we are calculating the bulk contribution, we can take the thermodynamic limit, where the choice of thermodynamical potential is irrelevant.

For the Landau levels (A.2), we have that

$$\Omega(\mu, B) = -\beta^{-1} \int_{-\infty}^{\infty} \frac{dk_z}{2\pi \mathcal{L}^{-1}} \sum_{n_L=0}^{\infty} \sum_{m_s=\pm\frac{1}{2}} G(B) \ln \left(1 + e^{-\beta[E_{n_L, m_s}^{(L)}(k_z) - \mu]} \right), \quad (\text{A.4})$$

where \mathcal{L} is the dimension of the box in the direction of the field, such that $\mathcal{V} = \mathcal{A}\mathcal{L}$. Yet we have to be careful as the sum over n_L in eq. (A.4) is divergent at zero field. Let us start by doing the sum over m_s as we note that the energies are just the same shifted by 1 quanta $\hbar\omega_c$, so we have

$$\begin{aligned} \Omega(\mu, B) = & -\beta^{-1} \int_{-\infty}^{\infty} \frac{dk_z}{2\pi \mathcal{L}^{-1}} G(B) \\ & \times \left\{ \ln \left(1 + e^{-\beta[E_0^{(L)}(k_z) - \mu]} \right) + 2 \sum_{n_L=1}^{\infty} \ln \left(1 + e^{-\beta[E_{n_L}^{(L)}(k_z) - \mu]} \right) \right\}, \quad (\text{A.5}) \end{aligned}$$

where $E_{n_L}^{(L)}(k_z) = 2\mu_B B n_L + \hbar^2 k_z^2 / 2m$. Next we develop the second sum using Euler-McLaurin formula (for a function \mathcal{F}_n that vanishes as $n \rightarrow \infty$)[24], it states that

$$\sum_{n=1}^{\infty} \mathcal{F}_n \approx \int_0^{\infty} \mathcal{F}(x) dx - \frac{1}{2} \mathcal{F}(0) - \frac{1}{12} \mathcal{F}'(0) \quad (\text{A.6})$$

which allows us to write

$$\begin{aligned} \Omega(\mu, B) &\approx \Omega_0 - \beta^{-1} \int_{-\infty}^{\infty} \frac{dk_z}{2\pi\mathcal{L}^{-1}} G(B) \\ &\times \left\{ \ln \left(1 + e^{-\beta[E_0(k_z) - \mu]} \right) - \ln \left(1 + e^{-\beta[E_0(k_z) - \mu]} \right) + \frac{2\mu_B B \beta}{6} f_\mu \left(\frac{\hbar^2 k_z^2}{2m} \right) \right\}, \end{aligned} \quad (\text{A.7})$$

where $f_\mu(E)$ is the Fermi-Dirac distribution and

$$\Omega_0 = -2\beta^{-1} \int_0^\infty dx \int_{-\infty}^{\infty} \frac{dk_z}{2\pi\mathcal{L}^{-1}} \frac{G(B)}{2\mu_B B} \ln \left(1 + e^{-\beta[x + \frac{\hbar^2 k_z^2}{2m} - \mu]} \right) \quad (\text{A.8})$$

does not depend on B .

Let us calculate the susceptibility, noting that we only want terms that remain at $B = 0$,

$$\chi_b^{(\text{nr})} = \frac{\beta^{-1}}{\mathcal{V}} \int_{-\infty}^{\infty} \frac{dk_z}{2\pi\mathcal{L}^{-1}} 2D'(B) \frac{\mu_B \beta}{3} f_\mu \left(\frac{\hbar^2 k_z^2}{2m} \right) \quad (\text{A.9})$$

substituting $G(B)$ yields

$$\chi_b^{(\text{nr})} = \frac{2m\mu_B^2}{3\pi^2\hbar^2} \int_0^\infty dk_z f_\mu \left(\frac{\hbar^2 k_z^2}{2m} \right) = \frac{2m\mu_B^2}{3\pi^2\hbar^2} k_F = 2|\chi_L| \quad (\text{A.10})$$

where we changed the limits of integration and assumed a degenerate electron gas. As discussed in the introduction, the result is $\chi_b^{(\text{nr})} = \chi_P + \chi_L$, where the Pauli susceptibility is $\chi_P = |\chi_L|$.

A.2 LANDAU ORBITAL SUSCEPTIBILITY FROM THE DENSITY OF STATES

Let us check the case where there is no spin interaction. When there is only the orbital contribution the energies are

$$E_{n_L}^{(\text{L-orb})}(k_z) = 2\mu_B B(n_L + 1/2) + \frac{\hbar^2 k_z^2}{2m}, \quad (\text{A.11})$$

where the degeneracy per level is $2G(B)$ due to spin degeneracy.

To provide an alternative derivation, let us calculate the Landau susceptibility from the density of states. Starting from the definition (2.14) and the spectrum of the Landau levels (A.11) we derive the density of states $\varrho_b^{(\text{orb})}$ for the bulk

$$\varrho_b^{(\text{orb})}(E) = \frac{1}{2} \varrho^0(\hbar\omega_c) \sum_{n_L=0}^{n_{\text{max}}} \sqrt{\frac{1}{E/\hbar\omega_c - (n_L + \frac{1}{2})}} \quad (\text{A.12})$$

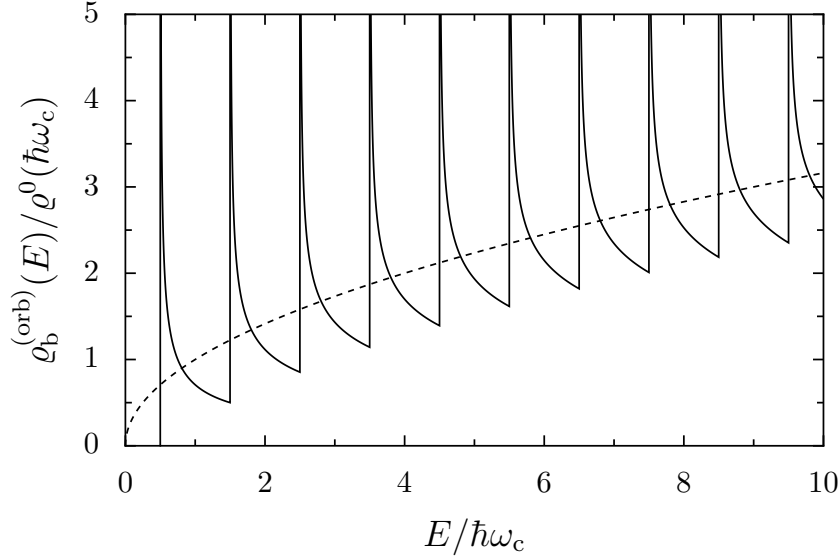


Figure A.1: Density of states of a gas of electrons in a magnetic field (solid line). The dashed line corresponds to the density of states without magnetic field.

where we have integrated over k_z and $\varrho^0(E)$ is the 3D unconfined density of states from eq. (2.47). The sum over n_L goes up to the upper bound of the relation $n_{\max} < E/\hbar\omega_c - 1/2$. For a comparison between the free solution and $\varrho_b^{(\text{orb})}$ see figure A.1. Under a static magnetic field, the singularities in the density of states appear whenever a new Landau level (A.11) is available.

The expression (A.12) is not very convenient due to the magnetic field-dependent limit of the sum. In order to calculate the susceptibility we introduce Poisson's summation formula (PSF) which allows us to approximate discrete sums. Let $\mathcal{F}(x)$ and its derivatives be bounded and continuous except maybe for a finite number of points, then

$$\sum_{n_L=n_{\min}}^{n_{\max}} \mathcal{F}(n_L) = \sum_{\eta_L=-\infty}^{\infty} \int_{n_{\min}-1/2}^{n_{\max}+1/2} \mathcal{F}(x) e^{2\pi i \eta_L x} dx, \quad (\text{A.13})$$

where n_{\min} is the lower limit of the sum.

The PSF allows us to rederive the density of states (2.14) but this time integrating first over n and performing a Gaussian integral in k_z , we obtain

$$\varrho_b^{(\text{orb})}(E) = \varrho^0(E) + \varrho^0\left(\frac{\hbar\omega_c}{2}\right) \sum_{\eta_L=1}^{\infty} (-1)^{\eta_L} \sqrt{\frac{1}{\eta_L}} \cos\left(2\pi\eta_L \frac{E}{\hbar\omega_c} - \frac{\pi}{4}\right). \quad (\text{A.14})$$

The phase shift of $\pi/4$ in the argument of the cosine in eq. (A.14) is generally called a Maslov index and it depends on the dimensionality as it does not appear for the 2D case, cf. ref. [88]. Note that we are able to write the density in the form of a trace formula as in (2.15).

For the case $\hbar\omega_c \ll k_B T \ll \mu$ we can use directly (A.12) and the Euler-MacLaurin

formula [24]. The thermodynamic potential (2.18) in this limit is

$$\Omega(T, \mu, B) = \Omega_0(\mu) + 2V \frac{m\omega_c^2}{48\pi^2} k_F, \quad (\text{A.15})$$

with Ω_0 independent of B . Now we can obtain the ZFS from eq. (1.3), which recovers χ_L .

A.3 RELATIVISTIC LANDAU LEVELS AND SUSCEPTIBILITY

The relativistic energies are easily obtained for systems where there are only magnetic fields (no electric potential) [137] from a Foldy–Wouthuysen transformation (see app. E.3). The relativistic energy spectrum reads

$$E_{n,m_s}^{(\text{rel})}(k_z) = \sqrt{(mc^2)^2 + 2mc^2 E_{n,m_s}^{(\text{L})}(k_z)} - mc^2 \quad (\text{A.16})$$

where we shifted the energies by mc^2 in order to recover the non-relativistic energy at first order in $(v_F/c)^2$. The degeneracy of each level is still $G(B)$ (A.3). The calculation of the thermodynamic potential is analog to that of the first section, after applying the Euler-MacLaurin formula, it yields

$$\Omega^{(\text{rel})}(\mu) = \Omega_0^{(\text{rel})} - \int_0^\infty \frac{dk_z}{\pi\mathcal{L}^{-1}} G(B) \frac{\mu_B B}{3} \frac{f_\mu \left(\sqrt{(mc^2)^2 + (\hbar k_z c)^2} - mc^2 \right)}{\sqrt{1 + \left(\frac{\hbar k_z}{mc} \right)^2}}, \quad (\text{A.17})$$

where

$$\begin{aligned} \Omega_0^{(\text{rel})} = & -2\beta^{-1} \int_0^\infty dx \int_{-\infty}^\infty \frac{dk_z}{2\pi\mathcal{L}^{-1}} \frac{G(B)}{2\mu_B B} \\ & \times \ln \left(1 + \exp \left\{ -\beta \left[\sqrt{(mc^2)^2 + (\hbar k_z c)^2} - mc^2 - \mu \right] \right\} \right), \end{aligned} \quad (\text{A.18})$$

independent of B .

The bulk zero-field relativistic susceptibility reads

$$\chi_b^{(\text{rel})} = \frac{2m\mu_B^2}{3\pi^2\hbar^2} \int_0^\infty dk_z \frac{f_\mu \left(\sqrt{(mc^2)^2 + (\hbar k_z c)^2} - mc^2 \right)}{\sqrt{1 + \left(\frac{\hbar k_z}{mc} \right)^2}} = 2|\chi_L| \left(\frac{\hbar k_F}{mc} \right)^{-1} \text{arcsinh} \left(\frac{\hbar k_F}{mc} \right), \quad (\text{A.19})$$

where $\text{arcsinh}(x)$ is the inverse of the hyperbolic sine.

Eq. (A.19) coincides with that of ref. [132] and recovers $\chi_b^{(\text{wr})}$ (2.48) in the weak relativistic limit.

SEMICLASSICAL DENSITY OF STATES OF A SPHERICAL WELL

B

In this appendix we calculate the semiclassical density of states of a spherical billiards. Michael V. Berry and Michael Tabor based their formalism on the EBK (Einstein–Brillouin–Keller) quantization [126, 174, 175], which is a generalization of the old Bohr–Sommerfeld quantization scheme. It allows to convert the discrete sum for the density of states (2.14) into integrals over action-angle variables or canonical coordinates, without passing explicitly by the path integral formalism [123]. We start this chapter by introducing action-angle variables and EBK quantization in sec. B.1, followed from the purely classical treatment of the spherical billiards in sec. B.2. In section B.3 we compare the EBK quantization with the quantum solution of an electron in a sphere with hard walls. The semiclassical density of states without magnetic field is recovered in sec. B.4 and with magnetic field in sec. B.5.

B.1 EBK QUANTIZATION

Suppose we have a separable classical Hamiltonian $\mathcal{H}^{(\text{cl})}$ with coordinates indexed by $i \in \{1, 2, \dots, d\}$, where each coordinate pair variable-momentum is written q_i and p_i , respectively. If every (q_i, p_i) pair is described by a closed orbit or a periodic function, then we can write the angle-action variables $\{S_i\}$ of the system as [176]:

$$S_i = \oint p_i dq_i \quad ; \quad \forall i \quad (\text{B.1})$$

where \oint refers to the integral over the smallest closed trajectory of the variable i . In phase space, the action-angle coordinates fill a d -torus [177]. Sometimes the action-angle variables (B.1) are simply called action variables as are equivalent to the calculation of the action $S = \oint p dq$ in one-dimensional systems. If the Hamiltonian is separable, the total action of the system is the sum of all the S_i [176],

$$S = \sum_{i=1}^d \Lambda_i S_i, \quad (\text{B.2})$$

where the Λ_i are dimensionless numbers that relate the proportion between the periods of motion

$$\tau_i = \frac{\partial S_i}{\partial E^{(\text{cl})}}, \quad (\text{B.3})$$

for each (p_i, q_i) pair, where $E^{(\text{cl})} = \mathcal{H}^{(\text{cl})}$ is the total energy. To assure the full motion follows a closed orbit, all the periods τ_i must be commensurable, that is for a given i, j we have

$$\Lambda_j \tau_j = \Lambda_i \tau_i, \quad (\text{B.4})$$

with Λ_i, Λ_j positive integers.

Having defined the action-angle variables, EBK quantization is given by the following rule:

$$S_i = 2\pi\hbar \left(n_i + \lambda_i^{(\text{D})}/4 + \lambda_i^{(\text{vN})}/2 \right) \quad ; \quad n_i = 0, 1, 2, \dots \quad (\text{B.5})$$

where $\lambda_i^{(\text{D})}$ is the number of classical turning points in the primitive period of the variable (Dirichlet conditions) and $\lambda_i^{(\text{vN})}$ is the number of hard walls (von Neumann conditions) [177]. The EBK method has been demonstrated to be equivalent to the connection formulas in WKB approximation to assure the continuity of the wavefunction [177]. EBK quantization is an improvement over Bohr-Sommerfeld quantization of old quantum theory, in the sense that it takes into account the conjugate points or Maslov indexes, $\lambda_i^{(\text{D})}$ and $\lambda_i^{(\text{vN})}$ of the trajectories.

B.2 CLASSICAL SPHERICAL BILLIARDS

To derive the semiclassical quantization of an electron under spherical confinement, we can start by solving the dynamics of a classical particle inside the spherical cavity. A fundamental property of metallic nanoparticles is its characteristic size, much smaller than the electronic mean free path in the bulk¹, thus we can assume a ballistic motion since no impurities are around. Under low density of impurities, a charged particle travels freely with the ions screened out by the other electrons. So the Hamiltonian can be considered to be of the form

$$\mathcal{H}^{(\text{cl})} = \frac{p_r^2}{2m} + \frac{p_\theta^2}{2mr^2} + \frac{1}{\sin^2(\theta)} \frac{p_\varphi^2}{2mr^2} + V(r) \quad (\text{B.6})$$

where p_r, p_θ and p_φ are the classical canonical momenta associated to r, θ and φ , respectively. Here we assume that $V(r)$ is a hard wall potential ($V_0 \rightarrow \infty$ in eq. (2.4)). The motion of this system was already illustrated in figure 2.3.

The Hamiltonian (B.6) has three constants of motion [176]: the total energy $E^{(\text{cl})} = \mathcal{H}^{(\text{cl})}$ as the Hamiltonian is time-indepedent, the z -component angular momentum: $L_z = p_\varphi$ as φ does not appear in $\mathcal{H}^{(\text{cl})}$, and the magnitude of the angular momentum $L^2 = p_\theta^2 + L_z^2 \csc^2 \theta$ as V depends only on r . As $V(r)$ is a central potential, the Hamiltonian can be reduced to a one-dimensional problem written as

$$\mathcal{H}^{(\text{cl})} = \frac{p_r^2}{2m} + V^{(\text{ce})}(r). \quad (\text{B.7a})$$

¹For gold the electronic mean free path is about 40 nm [178].

where we identify the centrifugal effective potential

$$V^{(\text{ce})}(r) = \frac{L^2}{2mr^2} + V(r). \quad (\text{B.7b})$$

The three angle-action integrals for the spherical billiard are

$$S_\varphi = \int_0^{2\pi} p_\varphi d\varphi = 2\pi|L_z|, \quad (\text{B.8a})$$

$$S_\theta = \oint p_\theta d\theta = 2 \int_{\theta_0}^{\pi-\theta_0} \sqrt{L^2 - L_z^2 \csc^2(\theta)} d\theta = 2\pi(L - |L_z|), \quad (\text{B.8b})$$

and

$$\begin{aligned} S_r &= \oint p_r dr = 2 \int_{a_0}^a \sqrt{2mE^{(\text{cl})} - \frac{L^2}{r^2}} dr \\ &= 2 \left[\sqrt{2mE^{(\text{cl})}a^2 - L^2} - L \arccos \left(\frac{L}{\sqrt{2mE^{(\text{cl})}a^2}} \right) \right]. \end{aligned} \quad (\text{B.8c})$$

Here θ_0 is the smallest value such that $\sin(\theta_0) = L_z^2/L^2$, determining two turning points of the θ -motion. Also, $a_0 = \sqrt{L/2mE^{(\text{cl})}a^2}$ is a smooth turning point and a is a hard wall for the r -motion. Unfortunately for this problem, I_r is a transcendental equation of E , so it cannot be solved analytically for $E(I_r, L)$.

Let us also calculate the radial period or period of libration, given by

$$\tau_r(L) = \frac{\sqrt{(ap^{(\text{cl})})^2 - L^2}}{E^{(\text{cl})}}, \quad (\text{B.9})$$

and the arcangle $\tilde{\Theta}$ swept between apogee and perigee according to [126], as the ratio between I_r and L

$$\tilde{\Theta} = -\frac{\partial I_r}{\partial L} = \frac{1}{\pi} \arccos \left(\frac{L}{ap^{(\text{cl})}} \right). \quad (\text{B.10})$$

The Hamiltonian (B.7) is independent of L_z , so each set of constants L and I_r indicates a infinite family of orbits. The commensurability condition (B.4) is imposed by noting that $\tau_\theta = \tau_\varphi$ as they are calculated implicitly from $I_r = I_r(E^{(\text{cl})}, L = I_\theta + I_\varphi)$ from eq. (B.16). By making $\nu\tau_\theta = \eta\tau_r$, with ν, η integers, we obtain the commensurability condition (B.4) for the spherical billiard:

$$L = ap^{(\text{cl})} \cos(\varphi_{\nu\eta}), \quad (\text{B.11})$$

where $p^{(\text{cl})} = \hbar k^{(\text{cl})} = \sqrt{2mE^{(\text{cl})}}$ and $\varphi_{\nu\eta} = \pi\nu/\eta$ the is half the angle spanned between to consecutive bounces with the boundaries of the sphere.

The motion is now clear, each family of orbits is described by regular polygons and star polygons labeled with two indexes (ν, η) , so that ν is the winding number and η

in the number of bounces with the walls, as in fig. 2.3. Under this condition the total action (B.2) reads $S_{v\eta} = p^{(\text{cl})}\eta L_{v\eta}$, where $L_{v\eta} = 2\eta a \sin \varphi_{v\eta}$ is the distance between two consecutive bounces with a hard wall times, η i.e. the length of the trajectory. The libration period and the arcangle are given by $\tau_{r,\eta,\nu} = mL_{v\eta}/p^{(\text{cl})}\eta$ and $\pi\tilde{\Theta}_{v\eta} = \varphi_{v\eta}$, respectively.

B.3 EBK QUANTIZATION FOR THE SPHERICAL BILLIARD

Now to obtain the semiclassical spectrum we use the EBK quantization (B.5). For the motion along φ , there are no turning points, it quantizes as

$$S_\varphi = 2\pi|L_z| = 2\pi\hbar n_\varphi. \quad (\text{B.12})$$

For the θ -motion there are two classical turning points θ_0 and $\pi - \theta_0$ from (B.8a), so $\lambda_\theta^{(\text{D})} = 2$ and

$$S_\theta = 2\pi(L - |L_z|) = 2\pi\hbar(n_\theta + 1/2). \quad (\text{B.13})$$

The motion along r has one smooth turning point a_0 and the hard wall at $r = a$ from (B.8c), so $\lambda_r^{(\text{D})} = 1$ and $\lambda_r^{(\text{vN})} = 1$:²

$$S_r = 2\pi\hbar(n - 1/4) \quad ; \quad n = 1, 2, \dots \quad (\text{B.14})$$

Comparing to the standard quantization $L^2 = \hbar^2 l(l+1)$ and $L_z = \hbar m_z$, we make the following transformation $l = n_\varphi + n_\theta$, and $m_z = \pm n_\varphi$, in order to obtain [179]:

$$\begin{cases} L_z = \hbar m_z & ; \quad m_z = 0, \pm 1, \dots, l \\ L = \hbar(l + 1/2) & ; \quad l = 0, 1, \dots, l_{\max} \end{cases} \quad (\text{B.15})$$

where l_{\max} is such that $L \simeq ap^{(\text{cl})}$. The condition for the total angular momentum L is equivalent to the Langer correction for WKB approximation, $L^2/\hbar^2 = l(l+1) \rightarrow (l + 1/2)^2$ [180].

Finally, our eigenenergies can be obtained by solving k from the following formula:

$$\pi(n - 1/4) - \sqrt{(k_{n,l}^{(\text{cl})}a)^2 - (l + 1/2)^2} + (l + 1/2) \arccos\left(\frac{l + 1/2}{k_{n,l}^{(\text{cl})}a}\right) = 0 \quad (\text{B.16})$$

derived from EBK quantization of (B.8c), where $k_{n,l}^{(\text{cl})} = \sqrt{2mE_{n,l}^{(\text{cl})}}/\hbar$. The eigenenergy equation (B.16) coincides with Keller and Rubinow solutions for spherical billiards [124].

Our semiclassical equations can be compared with the exact quantum mechanical results for the infinite spherical well, eq. (2.12).

²The minus sign is because we decided to start to count from $n = 1$.

However the semiclassical calculation (B.16) is more treatable algebraically when calculating the density of states, compared to finding the roots $\{\zeta_{n,l}\}$ of the spherical Bessel functions. The EBK result is a good approximation as it is always close to the exact result. We give a comparison between the exact and semiclassical results using EBK, shown in table B.1. The EBK method is valid for high values of energies and angular momentum, nevertheless even for low values of l and n the error of the semiclassical solutions is lower than 1%. This is no coincidence as the asymptotic forms for the zeroes of the spherical Bessel functions lead to the semiclassical eigenenergy equation [124]. The whole idea of using EBK is that it allows us to integrate the density of states by summing over the orbits (ν, η) , which have a more simpler form compared to the Bessel zeros given by l and n .

l	n	$\zeta_{n,l}$ (exact)	$k_{n,l}^{(\text{cl})} a$ (EBK)	Relative error $(1 - k_{n,l}^{(\text{cl})} a / \zeta_{n,l})$
0	1	3.14159	3.1012	0.0128581
	2	6.28319	6.26322	0.00317807
	3	9.42478	9.41149	0.00140956
	4	12.5664	12.5564	0.000792304
1	1	4.49341	4.45754	0.0079825
	2	7.72525	7.70755	0.00229079
	3	10.9041	10.8921	0.00110024
2	1	5.76346	5.72846	0.00607195
	2	9.09501	9.07832	0.00183468
	3	12.3229	12.3117	0.000915193
3	1	6.98793	6.95284	0.0050212
	2	6.98793	6.95284	0.0050212

Table B.1: Numerical roots for the energy eigenvalues $E = E_0 \zeta_{n,l}^2$ of a 3D spherical billiard, calculated from the Schrödinger equation (exact) and using the semiclassical approximations (EBK). Third column indicates the relative error between the exact and the EBK solutions.

B.4 SEMICLASSICAL DENSITY OF STATES IN THE ABSENCE OF MAGNETIC FIELD

In this subsection we derive the density of states from the EBK quantization [126, 174]. The idea is to integrate the density of states by connecting the problem to action-angle coordinates using Poisson summation formula (A.13) to sum over the different indexes. The exact quantum mechanical problem is completely determined by a set of quantum numbers n, l, m_z , so that the density of states (2.14) reads

$$\varrho(E) = 2 \sum_{n=1}^{\infty} \sum_{l=0}^{\infty} \sum_{m_z=-l}^l \delta(E - E_{n,l}^{(0)}). \quad (\text{B.17})$$

where the factor of 2 takes the spin degeneracy into account.

The eigenenergies do not depend on the quantum number m_z , so that the sum gives directly

$$\sum_{m_z=-l}^l 1 = 2l + 1. \quad (\text{B.18})$$

This sum is not that trivial when $B \neq 0$, as we will see in the next section. We can sum over each index at a time using Poisson summation formula (A.13) and replace quantum numbers $\{\lambda\} = \{n, l, m_z\}$ by semiclassical topological numbers $\{\Lambda\} = \{\nu, \eta\}$ according to EBK quantization. For the principal quantum number n we use PSF and the EBK quantization of S_r (B.14) to recover

$$Q^{\text{osc}}(E) = \frac{1}{\pi\hbar} \sum_{\substack{\eta=-\infty \\ (\eta \neq 0)}}^{\infty} e^{i\eta\pi/2} \int_{\pi\hbar/2}^{\infty} \sum_{l=0}^{\infty} (2l+1) \delta(E - \mathcal{H}_l^{(\text{cl})}(S_r)) e^{i\eta S_r/\hbar} dS_r, \quad (\text{B.19})$$

where $\mathcal{H}_l^{(\text{cl})}(S_r)$ indicates the Hamiltonian as a function of S_r and $L = \hbar(l + 1/2)$ and the properties of the Dirac delta allowed us to integrate over the energy surface³ given by equation (B.16). In eq. (B.19) η is a topological index related to the classical trajectories coming from the PSF, not to be confused with n . To perform the integral (B.19) we also need to set the lower limit $\hbar \rightarrow 0$, being a small parameter in semiclassical physics. This procedure yields

$$Q^{\text{osc}}(E) = 2 \sum_{l=0}^{l_{\text{max}}} (2l+1) Q_l^{\text{osc}}(E), \quad (\text{B.20a})$$

where

$$Q_l^{\text{osc}}(E) = 2 \sum_{\substack{\eta=-\infty \\ (\eta \neq 0)}}^{\infty} \left[\frac{1}{2\pi\hbar} \tau_r^{(l)} e^{i\eta(S_r/\hbar + \pi/2)} \right], \quad (\text{B.20b})$$

where $\tau_r^{(l)} = \tau_r(\hbar(l + 1/2))$ defined by (B.9) and

$$l_{\text{max}} = \left\lfloor \sqrt{\frac{E}{E_0}} - \frac{1}{2} \right\rfloor. \quad (\text{B.21})$$

Note that the argument inside the square bracket in (B.20b), along with the sum over η , has the form of Gutzwiller trace formula [123], because the radial motion can be reduced to a one dimensional problem with a centrifugal potential. We could have started our problem by noting that 1D systems are not degenerate, thus Gutzwiller formula is valid if we only consider the radial contribution.

³We use $\int \delta(x_0 - f(x)) dx = \int \delta(\mathcal{F}^{-1}(x_0) - x) / |\mathcal{F}'(x_0)| dx$ where $\mathcal{F}(x_0) = 0$.

The next step is to perform a PSF to remove l using its respective EBK quantization for L (B.15):

$$q^{\text{osc}}(E) = \frac{1}{\pi\hbar^3} \sum_{\substack{\eta=-\infty \\ (\eta \neq 0)}}^{\infty} \sum_{\substack{\nu=-\infty \\ (\nu \neq 0)}}^{\infty} (-1)^\nu \int_0^\infty 2L\tau_r(L) e^{i(\eta S_r + 2\pi\nu L)/\hbar + \eta\pi i/2} dL \quad (\text{B.22})$$

where we have reduced the problem to an integral that we can calculate by stationary phase approximation. The stationary phase condition, in this case $\eta\tilde{\Theta} = \nu$ is defined by the arcangle equation (B.10) and fixed the commensurability condition from eq. (B.11). To finally carry out the integral we extend the lower limit to $-\infty$, obtaining:

$$q^{\text{osc}}(E) = \frac{1}{\pi\hbar^{5/2}} \sum_{\substack{\{v,\eta\} \\ 0 < v/\eta < 1/2}} (-1)^\nu 2L\tau_r(L) \left(\left| \eta \frac{\partial \tilde{\Theta}}{\partial L} \right| \right)^{-1/2} \Bigg|_{L=ap \cos \varphi_{v\eta}} \times e^{iS_{v\eta}(E)/\hbar + \eta\pi i/2 + i \text{sign}(\eta)\pi/4}, \quad (\text{B.23})$$

where the whole action appears in the exponent.

Where the sum is now restricted to the interval $0 < v/\eta < 1/2$. Adding negative and positive terms in the sum we recover⁴

$$q^{\text{osc}}(E) = \frac{2}{\pi\hbar^{5/2}} \sum_{\nu=1}^{\infty} \sum_{\eta=2\nu+1}^{\infty} (-1)^\nu 2L\tau_r(L) \left(\eta \frac{\partial \tilde{\Theta}}{\partial L} \right)^{-1/2} \Bigg|_{L=pa \cos \varphi_{v\eta}} \times \cos \left(\frac{S_{\eta\nu}(E)}{\hbar} - 3\eta \frac{\pi}{2} + \frac{\pi}{4} \right), \quad (\text{B.24})$$

which is equivalent to Creagh-Littlejohn trace formula for rotational symmetric systems [181]. We kept the factor $2L$ coming from the sum over m_z up to this point, because it will be important in the following section when we introduce a finite magnetic field. Note that we neglected the diametrical orbits $\eta = 2\nu$ as they represent a higher order in \hbar and will not contribute to the magnetic susceptibility [117].

Finally, as already worked the classical solution of all these quantities in the previous section, we can substitute them explicitly to obtain the oscillating density of states presented in eq. (2.16). Similar equations have been derived for 2D systems using alternative semiclassical methods, e.g. ref.[182]. Keep in mind that we are summing over families of orbits, as for every η and ν there are infinite possible planes of motion in the sphere.

⁴To be able to compare with other formulas, we have replaced $\eta\pi/2 \rightarrow -3\eta\pi/2$ which is equivalent due to the periodicity of trigonometric functions.

B.5 SEMICLASSICAL DENSITY OF STATES AT FINITE MAGNETIC FIELDS

The problem of adding a magnetic field to the spherical billiard complicates the possibility to calculate the action-angle variables as $\mathcal{H}^{(\text{dia})}$ in eq. (2.9c) breaks the spherical rotational symmetry of the system. A magnetic field $\mathbf{B} = B\hat{\mathbf{e}}_z$ bends the trajectories in the $x - y$ plane. However, if we take the limit of large cyclotron radii (small B or large energies) so that $R_c \gg a$, then the bending of the orbits can be seen as a negligible next order correction [117]. In this limit, Creagh's formula for systems with broken symmetry [183] can be used to calculate a modulation factor $\mathcal{M}_{\nu\eta}$ of eq. (2.17b) to recover $\rho^{\text{osc}}(B)$ of eq. (2.17a). The oscillating density of states, as well as the density of states without magnetic field of eq. (2.16), can be obtained by integrating over the group measure of the system, in this case related to the special group of rotations $\text{SO}(3)$ [181].

We propose for this appendix, to derive eq. (2.17b) with an heuristic method that we have developed to obtain this factor using the same Berry-Tabor theory that we used to calculate the density of states without magnetic field.

We recall that the factor $2L$ in the density of states for the case $B = 0$ (B.24) comes from the sum over m_z (B.18) and the EBK quantization for L (B.15). This sum (B.18) could have waited up to the very end of the calculation.

Let us consider a perturbation that modifies very slightly the trajectories, then the density of states remains the same except for a change in the action. For our case of interest, the total action $S(B = 0) = \oint \mathbf{p} \cdot d\mathbf{r}$ gets modified by vector potential $\mathbf{p} \rightarrow \mathbf{p} + \frac{e}{c}\mathbf{A}(\mathbf{r})$. The action then reads

$$S(B) = \oint \left(\mathbf{p} + \frac{e}{c}\mathbf{A}(\mathbf{r}) \right) \cdot d\mathbf{q} = S_0 + \Delta S(B) \quad (\text{B.25a})$$

where $S_0 = S(B = 0)$ is the action without magnetic fields, and

$$\Delta S(B) = \frac{e}{c}\phi(B) \quad (\text{B.25b})$$

where $\phi(B) = H\mathcal{A}_{\nu\eta} \cos \xi$ is the magnetic flux enclosed by the orbit and ξ is the inclination angle between the normal to the plane of the orbit and the z -axis. The surface $\mathcal{A}_{\nu,\eta}$ spanned by the orbit can be calculated from polygon formulas [177] and was defined next to eq. (2.17b). The expansion of the action (B.25a) is only possible when $\Delta S(B)/S_0 \approx a/R_c \ll 1$.

The factor $2L$ of the ρ^{osc} (B.24) that came from the sum over m_z in (B.18) now reads:

$$\begin{aligned} \sum_{m_z=-l}^l e^{i\Delta S(B)/\hbar} \Big|_{L=ap \cos \varphi_{\nu\eta}} &= \sum_{m_z=-l}^l e^{2\pi i \cos \xi_l^{m_z} \phi_{\nu\eta}(B)/\phi_0} \\ &= \sin \left(2\pi \frac{\phi_{\nu\eta}(B)}{\phi_0} \right) \csc \left(\frac{\pi \phi_{\nu\eta}(B)}{ka\phi_0 \cos \varphi_{\nu\eta}} \right), \end{aligned} \quad (\text{B.26})$$

where we have used the classical relation between the components of the orbital angular momentum and its semiclassical quantization: $\cos \zeta = L_z/L \rightarrow \cos \zeta_1^{m_z} = m_z/(l + 1/2)$. The argument in the cosecant in eq. (B.26) is equivalent to $\eta a/R_c$ and can be considered small when η is not too large, as it is the same condition to expand the action. Additionally, the thermal factor $R(L_{v,\eta}/L_T)$ assures that η remains small. For this reason, we proceed to expand the cosecant to recover the factor $2L$ times the modulation factor from Berry-Tabor theory, as

$$\sum_{m_z=-l}^l e^{i\Delta S/\hbar} \approx 2ka \cos \varphi_{v\eta} j_0 \left(2\pi \frac{\phi_{v\eta}(B)}{\phi_0} \right) = \frac{2L}{\hbar} \Big|_{L=ap \cos \varphi_{v\eta}} \times \mathcal{M}_{v\eta}^{(\text{orb})}(B). \quad (\text{B.27})$$

which demonstrates eq. (2.17b). This modulation factor of eq. (2.17b) has been proved to be correct in numerical comparison with the full quantum solution [117].

ORBITAL SUSCEPTIBILITY OF A METALLIC NANOPARTICLE FROM QUANTUM PERTURBATION THEORY

C

In this appendix we illustrate in sec. C.1 the calculations to obtain the grand canonical ZFS for spherical metallic nanoparticles by following the steps of D.A. van Leeuwen [22] and in sec. C.2 we reproduce the same methodology for a cylindrical confinement with a magnetic field parallel to its axis.

C.1 SPHERICAL NANOPARTICLES

We recall that the eigenenergies of the infinite spherical potential without magnetic field are given by the zeroes of the Bessel functions ζ_{nl} as in (2.27). The eigenfunctions ψ_{n,l,m_z} can be found in eq. (2.11). This calculation could be a relatively complicated procedure as we have to use degenerate perturbation theory (same energies for different m_z) and second order perturbation theory to be consistent up to the order of B^2 . Nevertheless, for a spherical geometry under symmetric gauge, the paramagnetic term $\mathcal{H}^{(\text{para})}$ in eq. (2.9b) is trivial and leads to eq. (2.28), as our basis is composed of eigenstates of this operator with quantum numbers m_z . Moreover as L_z is diagonal in this basis, $\mathcal{H}^{(\text{para})}$ first order perturbation theory is exact (no higher orders in B). Consequently, we only have to apply first order non-degenerate perturbation to the diamagnetic term in eq. (2.9c). If the geometry was different, we would have to add a Van Vleck term that comes from second order perturbation of the terms proportional to B .¹

To calculate the expectation value of the diamagnetic term (2.9c) we write it down in spherical coordinates as $x^2 + y^2 = r^2 \sin^2(\theta)$ and we separate it into two integrals

$$\int \psi_{n,l,m_z}^*(\mathbf{r}) \frac{x^2 + y^2}{a^2} \psi_{n,l,m_z}(\mathbf{r}) d^3r = \mathcal{Y}_l^{m_z} \times \mathcal{R}_{n,l}, \quad (\text{C.1})$$

given by an angular part,

$$\mathcal{Y}_l^{m_z} = \int_0^{2\pi} \int_0^\pi |Y_l^{m_z}(\theta, \varphi)|^2 \sin^3(\theta) d\theta d\varphi, \quad (\text{C.2})$$

and a radial part,

$$\mathcal{R}_{nl} = \frac{2}{|j_{l+1}(\zeta_{nl})|} \int_0^1 j_l^2(\zeta_{nl}r) r^4 dr. \quad (\text{C.3})$$

¹Van Vleck term is important to conserve gauge invariance [22].

The integral over the angular part, given in the main text (2.31), can be obtained easily either by using the recursion of the associated Legendre polynomials $P_l^{m_z}$, given by

$$(2l + 1)\sqrt{1 - x^2}P_l^{m_z}(x) = -P_{l+1}^{m_z+1}(x) + P_{l-1}^{m_z+1}(x), \quad (\text{C.4})$$

or by using the identities of Wigner 3- j symbols.

The radial integral (C.3) needs a more specialized knowledge of the spherical Bessel functions. The integral can be derived with the help of Schafheitlin's reduction formula [184], given by

$$(n_s + 2) \int_0^{\zeta_0} \zeta^{(n_s+2)} J_\ell^2(\zeta) d\zeta = (n_s + 1) \left[\ell^2 - \frac{1}{4}(n_s + 1)^2 \right] \int_0^{\zeta_0} \zeta^{n_s} J_\ell^2(\zeta) d\zeta \\ + \frac{\zeta_0^{(n_s+1)}}{2} \left\{ \left[\zeta_0 J'_\ell(\zeta_0) - \frac{1}{2}(n_s + 1) J_\ell(\zeta_0) \right]^2 + \left[\zeta_0^2 - \ell^2 + \frac{1}{4}(n_s + 1)^2 \right] J_\ell^2(\zeta_0) \right\}, \quad (\text{C.5})$$

for any ζ_0 , ℓ and integer n_s . Eq. (C.5) returns the result of equation (2.30), with the replacements $\ell = l + \frac{1}{2}$, $\zeta_0 = \zeta_{n,l}$ and $n_s = 1$.

Having the perturbed energies we can insert our calculation in the quantum equation for the zero-field susceptibility (2.24) to recover.

$$\chi^{(\text{orb})} = -2 \frac{\mu_B^2}{\mathcal{V}} \sum_{n=1}^{\infty} \sum_{l=0}^{\infty} \sum_{m_z=-l}^l \left[f'_\mu(E_{n,l}^{(0)}) m_z^2 + f'_\mu(E_{n,l}^{(0)}) 2E_0 \mathcal{R}_{n,l} \mathcal{Y}_l^{m_z} \right], \quad (\text{C.6})$$

where the factor of 2 accounts for the spin degeneracy and the energies in the Fermi-Dirac distribution do not depend on m_z as have taken at $B = 0$. The sums over the m_z can be carried out using that

$$\sum_{m_z=-l}^l m_z^2 = \frac{2}{3} l(l+1)(l + \frac{1}{2}), \quad (\text{C.7})$$

and its corollary

$$\sum_{m_z=-l}^l \mathcal{Y}_l^{m_z} = \frac{4}{3} (l + \frac{1}{2}). \quad (\text{C.8})$$

Dividing the susceptibility in equation (C.6) by χ_L , we recover (2.33).

C.2 CYLINDRICAL CONFINEMENT SUBJECT TO A FIELD ALONG THE AXIS

A strong diamagnetic response has been observed in ensembles of gold nanorods [42]. In this section, we derive the magnetic susceptibility of a single nanorod, approximated as a cylinder. We limit this calculation to the grand canonical ZFS with the magnetic field $\mathbf{B} = B\hat{\mathbf{e}}_z$ coinciding with the rod long-axis.

We start by solving Schrödinger equation of an electron in cylindrical confinement of radius a and height a_z with hard walls. Our potential is $V(\rho, z)^{(\text{cyl})} = \lim_{V_0 \rightarrow \infty} V_0[\Theta(\rho - a) + \Theta(|z| - a_z/2)]$ where ρ, φ, z are the usual cylindrical variables (radius, azimuthal angle, height). The Hamiltonian without magnetic field is $H_0^{(\text{cyl})} = \frac{\mathbf{p}^2}{2m} + V^{(\text{cyl})}(r, z)$. Here $\rho = x^2 + y^2$ is the radial distance in cylindrical coordinates.

The equations for the orbital wavefunction are to be obtained using separation of variables:

$$\psi_{n,m_z,n_z}^{(\text{cyl})}(\mathbf{r}) = R_{n,m_z}(\rho)\Phi_{m_z}(\varphi)Z_{n_z}(z) \quad (\text{C.9})$$

The equation for $Z_{n_z}(z)$ in the interior of the cylinder

$$-\frac{d^2}{dz^2}Z_{n_z}(z) = k_{n_z}^2 Z_{n_z}(z) \quad (\text{C.10})$$

which is equivalent to the single particle in a infinite unidimensional well, whose eigenfunctions are given by

$$Z_{n_z}(z) = \sqrt{\frac{2}{a_z}} \begin{cases} \sin(k_{n_z}z) & ; (n_z - 1) \text{ odd} \\ \cos(k_{n_z}z) & ; (n_z - 1) \text{ even} \end{cases} \quad (\text{C.11})$$

and

$$k_{n_z} = \frac{\pi n_z}{a_z} \quad (\text{C.12})$$

where n_z is a positive integer.

For the transversal section, we are left with the following Schrödinger equation:

$$\left[\frac{1}{\rho} \frac{\partial}{\partial \rho} \left(\rho \frac{\partial}{\partial \rho} \right) + \frac{1}{\rho^2} \frac{\partial^2}{\partial \varphi^2} \right] R_{n,m_z}(\rho)\Phi_{m_z}(\varphi) = k_{n,m_z}^2 R_{n,m_z}(\rho)\Phi_{m_z}(\varphi) \quad (\text{C.13})$$

where $k_{n_z}^2 + k_{n,m_z}^2 = 2mE_{n,m_z,n_z}/\hbar^2$ is the respective eigenergy. As usual the angular part is set to

$$\Phi_{m_z}(\varphi) = \frac{1}{\sqrt{2\pi}} e^{im_z\varphi} \quad (\text{C.14})$$

where m_z is any integer, and the factor $(2\pi)^{-1/2}$ is just for normalization. The final equation to solve is

$$\left[\frac{1}{\rho} \frac{d}{d\rho} \left(\rho \frac{dR_{n,m_z}(\rho)}{d\rho} \right) \right] + \left[k_{n,m_z}^2 - \frac{m_z^2}{\rho^2} \right] R_{n,m_z}(\rho) = 0 \quad (\text{C.15})$$

which is just Bessel equation. We are only interested in the solutions that are bounded withing $0 < r < a$ so we set

$$R_{n,m_z}(\rho) = \frac{\sqrt{2}}{a} \frac{J_{|m_z|}(k_{n,m_z}\rho)}{|J_{|m_z|+1}(k_{n,m_z}a)|} \quad (\text{C.16})$$

at the interior of the cylinder, where $J_l(\rho)$ is the Bessel function of the first kind, and

$$k_{n,m_z} = \frac{\xi_{n,|m_z|}}{a} \quad (\text{C.17})$$

where ξ_{n,m_z} is the n -th root of Bessel function $J_l(\rho)$. Finally the eigenenergies of the system are

$$E_{n,m_z,n_z}^{(\text{nr-cyl})} = E_0 \left[\xi_{n,|m_z|}^2 + \pi^2 r_0^2 n_z^2 \right]. \quad (\text{C.18})$$

where n, n_z are positive integers and m_z is any integer. and $r_0 = a/a_z$ as the ratio radius-height of the cylinder.

C.2.1 PERTURBATIVE ENERGIES UNDER A MAGNETIC FIELD

From a minimal coupling substitution and using the symmetric gauge for the vector potential $\mathbf{A} = \mathbf{B} \times \mathbf{r}/2$, the non relativistic Hamiltonian under a magnetic field reads

$$H^{(\text{nr-cyl})} = H_0 + \frac{\mu_B}{\hbar} B L_z + \frac{\mu_B^2 B^2}{4E_0 a^2} \rho^2. \quad (\text{C.19})$$

Due to the choice of gauge and symmetry of the problem, our previous eigenfunctions are also eigenfunctions of the Hamiltonian with magnetic field up to linear terms in B , as

$$L_z \psi_{n,m_z,n_z}(\mathbf{r}) = \hbar m_z. \quad (\text{C.20})$$

For the diamagnetic term in B^2 , we consider perturbation theory up to first order, which means that we have to calculate the following integral:

$$\mathcal{R}_{n,m_z}^{(\text{cyl})} = \frac{1}{a^2} \int |R_{n,m_z}(\rho)|^2 \rho^3 d\rho = \frac{2}{\xi_{n,|m_z|}^4 [J_{|m_z|+1}(\xi_{n,|m_z|})]^2} \int_0^{\xi_{n,|m_z|}} [J_{|m_z|}(x)]^2 x^3 dx, \quad (\text{C.21})$$

which can be calculated using the Schafheitlin's reduction formula (C.5), which yields

$$\int_0^{\xi_{n,|m_z|}} [J_{|m_z|}(x)]^2 x^3 dx = \frac{1}{6} \left[1 + 2 \frac{(m_z^2 - 1)}{\xi_{n,|m_z|}^2} \right] \xi_{n,|m_z|}^4 [J_{|m_z|+1}(\xi_{n,|m_z|})]^2, \quad (\text{C.22})$$

and simplifies as

$$\mathcal{R}_{n,m_z}^{(\text{cyl})} = \frac{1}{3} \left[1 + 2 \frac{(m_z^2 - 1)}{\xi_{n,|m_z|}^2} \right]. \quad (\text{C.23})$$

Finally the energies under a magnetic field (up to second order perturbation theory) are

$$E_{n,m_z,n_z}^{(\text{nr-cyl})} = E_{n,m_z,n_z}^{(0-\text{cyl})} + \mu_B B m_z + \frac{\mu_B^2 B^2}{4E_0} \mathcal{R}_{n,m_z}^{(\text{cyl})} \quad (\text{C.24})$$

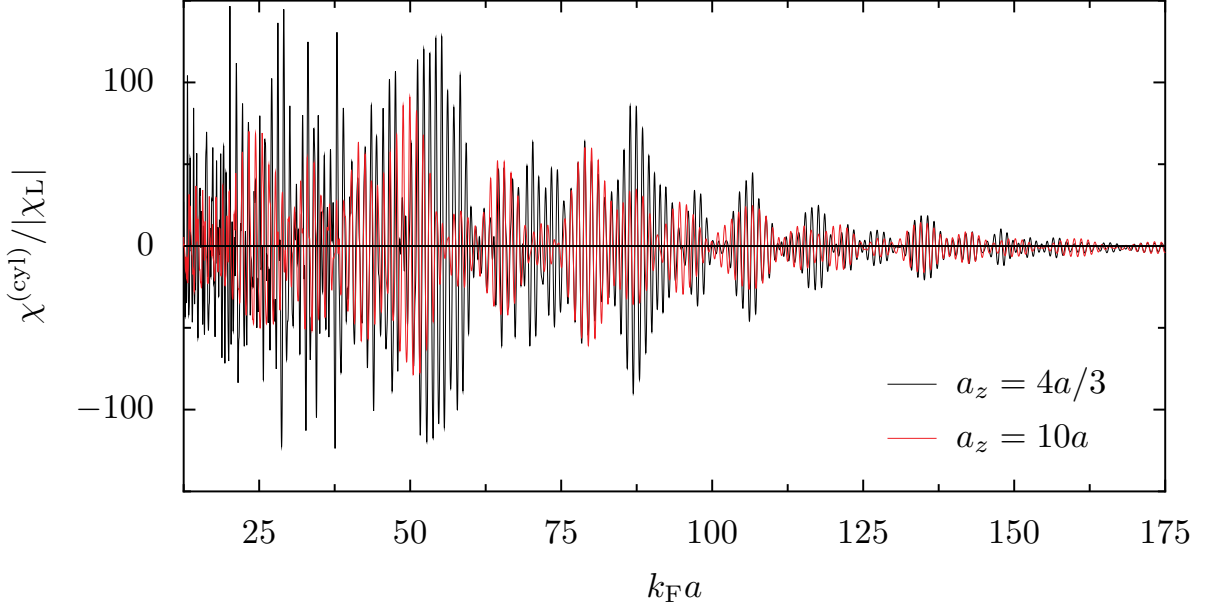


Figure C.1: Room temperature ($T/T_F = 5 \times 10^{-3}$) zero-field susceptibility of a cylinder for different ratios $r_0 = a/a_z$. The value $a_z = 4a/3$ correspond to the ratio where the volume of the cylinder is equal to the volume of the sphere.

C.2.2 GRAND CANONICAL ZFS FOR A CYLINDRICAL CONFINEMENT

As with the sphere, the magnetic zero field susceptibility is derived from eq. (2.24) taking into account the spin-degeneracy. For the cylinder, the susceptibility yields

$$\frac{\chi^{(\text{cyl})}}{|\chi_L|} = -\frac{6\pi r_0}{k_F a} \sum_{n=1}^{\infty} \sum_{n_z=1}^{\infty} \left[\mathcal{R}_{n,0}^{(\text{cyl})} f_{\mu}(E_{n,0,n_z}^{(0-\text{cyl})}) + 2 \sum_{m_z=1}^{\infty} 2E_0 m_z^2 f'_{\mu}(E_{n,m_z,n_z}^{(0-\text{cyl})}) + \mathcal{R}_{n,m_z}^{(\text{cyl})} f_{\mu}(E_{n,m_z,n_z}^{(0-\text{cyl})}) \right] \quad (\text{C.25})$$

The ZFS (C.25) for two different ratios r_0 is plotted in figure C.1. Verifying the value of the susceptibility for large $k_F a$ we confirm numerically that $\chi^{(\text{cyl})} \rightarrow -|\chi_L|$. The oscillations are of the same order of magnitude as those of the orbital susceptibility of the sphere, c.f. fig. 3.1. We observe that the amplitudes of the oscillations of the ZFS (C.25) are proportional to r_0 . This proportionality is due to flux accumulation, for larger r_0 the orbits have a flux in relation to the volume of the cylinder. This expression for $\chi^{(\text{cyl})}$ is more costly numerically than that for the ZFS of the sphere (2.33) as it comprises three sums, instead of two. Calculations of the susceptibility when the magnetic field is not in the main axis of the cylinder, include an additional Van Vleck-like term (with a duplication of the number of required summation indices), leading to an increase of the computation time.

EQUIVALENCE BETWEEN QUANTUM AND SEMICLASSICAL CALCULATIONS OF THE ZERO-FIELD SUSCEPTIBILITY

D

In this appendix, we verify the equivalence between the quantum calculation for the zero-field susceptibility χ^{orb} in eqs. (2.33) and its semiclassical version $\chi^{(1)}$ from eq. (3.4).

The semiclassical evaluation of $\chi^{(\text{orb})}$ can be addressed by trading in eqs. (2.33) the sums over the principal quantum number n by energy-integrals and the use of the Poisson summation formula for the sum over l , resulting in

$$\frac{\chi^{(\text{para})}}{|\chi_L|} = -\frac{6\pi E_0}{k_{\text{F}}a} \int_0^\infty dE f'_{\bar{\mu}_0}(E) \sum_{\nu=-\infty}^{+\infty} \int_{-1/2}^{\sqrt{E/E_0}-1/2} dl \times \exp(2\pi i \nu l) l \left(l + \frac{1}{2}\right) (l+1) q_l(E), \quad (\text{D.1a})$$

$$\frac{\chi^{(\text{dia})}}{|\chi_L|} = -\frac{6\pi}{k_{\text{F}}a} \int_0^\infty dE f_{\bar{\mu}_0}(E) \sum_{\nu=-\infty}^{+\infty} \int_{-1/2}^{\sqrt{E/E_0}-1/2} dl \times \exp(2\pi i \nu l) \left(l + \frac{1}{2}\right) \mathcal{R}_l(E) q_l(E), \quad (\text{D.1b})$$

where l is now understood as a continuous variable. Following eq. (2.30), we have defined $\mathcal{R}_l(E) = (1/3) [1 + (2E_0/E)(l + 3/2)(l - 1/2)]$.

In the leading order in $k_{\text{F}}a \gg 1$, the smooth part of $\chi^{(\text{orb})}$ is obtained by using $\bar{q}_l(E)$ in eqs. (D.1) and only keeping the $\nu = 0$ term of the sum,

$$\frac{\bar{\chi}^{(\text{para})}}{|\chi_L|} = -\frac{3}{k_{\text{F}}a} \int_0^\infty dE f'_{\bar{\mu}_0}(E) \left(\frac{E}{E_0}\right)^{1/2} \times \int_0^1 d\zeta \zeta \left(\frac{E}{E_0} \zeta^2 - \frac{1}{4}\right) \sqrt{1 - \zeta^2}, \quad (\text{D.2a})$$

$$\frac{\bar{\chi}^{(\text{dia})}}{|\chi_L|} = -\frac{1}{k_{\text{F}}a E_0} \int_0^\infty dE f_{\bar{\mu}_0}(E) \left(\frac{E}{E_0}\right)^{1/2} \times \int_0^1 d\zeta \zeta \left(1 + 2\zeta^2 - \frac{2}{E/E_0}\right) \sqrt{1 - \zeta^2}. \quad (\text{D.2b})$$

Performing the integration over the variable $\zeta = (l + 1/2)\sqrt{E_0/E}$ we have

$$\frac{\bar{\chi}^{(\text{para})}}{|\chi_L|} = -\frac{1}{k_{\text{F}}a} \int_0^\infty dE f'_{\bar{\mu}_0}(E) \left(\frac{E}{E_0}\right)^{1/2} \left(\frac{2E}{5E_0} - \frac{1}{4}\right), \quad (\text{D.3a})$$

$$\frac{\bar{\chi}^{(\text{dia})}}{|\chi_L|} = -\frac{1}{k_{\text{F}}aE_0} \int_0^\infty dE f'_{\bar{\mu}_0}(E) \left(\frac{E}{E_0}\right)^{1/2} \left(\frac{3}{5} - \frac{2E_0}{3E}\right). \quad (\text{D.3b})$$

An integration by parts in eq. (D.3b) leads to

$$\frac{\bar{\chi}^{(\text{dia})}}{|\chi_L|} = \frac{1}{k_{\text{F}}a} \int_0^\infty dE f'_{\bar{\mu}_0}(E) \left(\frac{E}{E_0}\right)^{1/2} \left(\frac{2E}{5E_0} - \frac{4}{3}\right). \quad (\text{D.4})$$

Thus, the leading-order term in $k_{\text{F}}a$ of $\bar{\chi}^{(\text{para})}$ and $\bar{\chi}^{(\text{dia})}$ cancel each other, and $\bar{\chi}^{(\text{orb})}$ is then given by next-order contributions.¹ However, such terms are not captured by the expressions of eqs. (D.3), which are only valid in the leading order in $k_{\text{F}}a$, since they result from E and l integrations in which the form (B.9) was used beyond its regime of validity of $E/E_0 \gg (l + 1/2)^2$. In ref. [85] it is shown that the magnetic field dependence of $\bar{\rho}(E, B)$, given by the so-called zero-length trajectories, results in $\bar{\chi}^{(\text{orb})} = \chi_L$, while the numerical evaluation of eqs. (4.17)–(2.33) presented in Fig. 4.1 approaches, in the limit of large radius a where the role of the confinement potential becomes irrelevant, the bulk result given by eqs. (1.4)–(1.5) (see the inset in Fig. 4.1).

The fact that $\bar{\chi}^{(\text{orb})}/|\chi_L|$ is of order $(k_{\text{F}}a)^0$, points to the importance of χ^{osc} , which is obtained by using $\rho_l^{\text{osc}}(E)$ in eq. (D.1). The rapidly oscillating (in E) phases $2\pi\nu \pm \eta S_l(E)/\hbar$ allow us to perform a stationary-phase (sp) integration over l with the condition $l_{\text{sp}} = \sqrt{E/E_0} \cos(\pi\nu/\eta) - 1/2$, yielding

$$\begin{aligned} \frac{\chi^{(\text{para})-\text{osc}}}{|\chi_L|} &= -\frac{6\sqrt{\pi}}{k_{\text{F}}a} \int_0^\infty dE f'_{\bar{\mu}_0}(E) \left(\frac{E}{E_0}\right)^{1/4} \\ &\quad \times \sum_{\substack{\nu>0 \\ \eta>2\nu}} \frac{(-1)^\nu}{\sqrt{\eta}} \sin^{3/2} \varphi_{\nu\eta} \cos \varphi_{\nu\eta} \\ &\quad \times \left[\frac{E}{E_0} \cos^2 \varphi_{\nu\eta} - \frac{1}{4} \right] \cos(\theta_{\nu\eta}(k)), \end{aligned} \quad (\text{D.5a})$$

$$\begin{aligned} \frac{\chi^{(\text{dia})-\text{osc}}}{|\chi_L|} &= -\frac{2\sqrt{\pi}}{k_{\text{F}}aE_0} \int_0^\infty dE f'_{\bar{\mu}_0}(E) \left(\frac{E}{E_0}\right)^{1/4} \\ &\quad \times \sum_{\substack{\nu>0 \\ \eta>2\nu}} \frac{(-1)^\nu}{\sqrt{\eta}} \sin^{3/2} \varphi_{\nu\eta} \cos \varphi_{\nu\eta} \\ &\quad \times \left[1 + 2 \cos^2 \varphi_{\nu\eta} - \frac{2E_0}{E} \right] \cos(\theta_{\nu\eta}(k)). \end{aligned} \quad (\text{D.5b})$$

¹For the degenerate case, in the leading order in $k_{\text{F}}a$, we have that $\bar{\chi}^{(\text{para})} = |\bar{\chi}^{(\text{dia})}| = (2/5)(k_{\text{F}}a)^2$. Notwithstanding, we stress that the separation between $\chi^{(\text{para})}$ and $\chi^{(\text{dia})}$ is only for computational purposes, and lacks physical reality.

The restriction of $\nu \neq 0$ appears since these contributions, considered in eqs. (D.2), lead to $\bar{\chi}^{(\text{orb})}$. Only positive values of ν are kept, as the sign of ν is associated with the orientation in which the periodic orbit is traveled. The condition $\eta > 2\nu$ appears as a restriction for the stationary-phase value l_{sp} to be within the integration interval. The stationary-phase procedure yielding (D.5) is analogous to that allowing to link $q_l^{\text{osc}}(E)$ and $q^{\text{osc}}(E, 0)$ [112]. Since we work in leading-order in $k_{\text{F}}a$, we can neglect the last terms in the square brackets of eqs. (D.5).

In the low-temperature limit, we use $f_{\bar{\mu}_0}(E) = \Theta(\bar{\mu}_0 - E)$ and, with the help of Fresnel integrals, to leading order in $k_{\text{F}}a$, we find

$$\begin{aligned} \frac{\chi^{(\text{dia})-\text{osc}}}{|\chi_{\text{L}}|} &= -2\sqrt{\pi}(k_{\text{F}}a)^{1/2} \sum_{\substack{\nu>0 \\ \eta>2\nu}} \frac{(-1)^\nu}{\eta^{3/2}} \sin^{1/2} \varphi_{\nu\eta} \cos \varphi_{\nu\eta} \\ &\times (1 + \cos^2 \varphi_{\nu\eta}) \sin(\theta_{\nu\eta}(k_{\text{F}})). \end{aligned} \quad (\text{D.6})$$

Thus, $\chi^{(\text{dia})-\text{osc}} \sim (k_{\text{F}}a)^{1/2}$ is of lower order in $k_{\text{F}}a$ than $\chi^{(\text{para})-\text{osc}} \sim (k_{\text{F}}a)^{3/2}$, and in the semiclassical limit we have $\chi^{(\text{orb})-\text{osc}} = \chi^{(\text{para})-\text{osc}}$.

The integration of $f'_{\bar{\mu}_0}(E)$ multiplied by a rapidly oscillating function of E results in a general expression [85], that when applied to eq. (D.5a) yields back $\chi^{(\text{orb})-\text{osc}} = \chi^{(1)}$ from eq. (3.4).

FOLDY-WOUTHUYSEN TRANSFORMATION

E

E.1 THE PROBLEM OF ZITTERBEWEGUNG

At first glance, Dirac's equation (2.49) can be non-intuitive. Gregory Breit in 1928 [185], had discovered an unusual property of the α matrices. In Heisenberg's picture, the evolution of the position operator can be written as

$$\frac{\partial \mathbf{r}_i}{\partial t} = \frac{i}{\hbar} [\mathcal{H}^{(\text{Dirac})}, r_i], \quad (\text{E.1})$$

where r_i is the i -th component of the position operator. This equation (E.1) leads to the following relation $\partial r_i / \partial t = \alpha_i c$, which identifies αc as the "velocity operator". The unusual part comes when calculating the expectation value of the velocity squared, i.e.

$$\left\langle \left(\frac{\partial \mathbf{r}}{\partial t} \right)^2 \right\rangle = c^2. \quad (\text{E.2})$$

The Ehrenfest theorem states that the expectation value of a quantum operator should recover our classical intuition, but (E.2) seems to imply that Dirac's electron is always traveling at the speed of light!

This result has been understood as an artifact now known as zitterbewegung¹ and comes from the mixed representation of particle-antiparticle components of Dirac's equation. As we will see next, this apparent paradox disappears when we perform a Foldy–Wouthuysen transformation.

E.2 FOLDY–WOUTHUYSEN TRANSFORMATION FOR A FREE PARTICLE

Let us suppose $\Psi = e^{-\mathcal{U}} \Psi'$, where \mathcal{U} is a time independent unitary operator. Then if $\mathcal{H} \Psi = E \Psi$, for an eigenstate Ψ with energy E for a Hamiltonian \mathcal{H} , we want to enforce $\mathcal{H} \Psi' = \mathcal{H} e^{-\mathcal{U}} \Psi = e^{-\mathcal{U}} E \Psi$, i.e. $\mathcal{H}' \Psi' = E \Psi'$, where $\mathcal{H}' = e^{\mathcal{U}} \mathcal{H} e^{-\mathcal{U}}$, such that \mathcal{H}' is diagonal for two spinors (separate particle-antiparticle states).

¹German for jittery motion. The name comes from the fact that integrating (E.1) leads to a mean position that oscillates back and forth with speed c , around the classical linear trajectory.

To treat Dirac's Hamiltonian (2.49), we will need the following property of the Pauli matrices

$$\sigma_i \sigma_j = \delta_{ij} + i\epsilon_{ijk} \sigma_k, \quad (\text{E.3})$$

where we used Einstein summation notation for double indexes, δ_{ij} is the Kronecker delta and ϵ_{ijk} is the Levi-Civita tensor, which implies that the Dirac α follow a similar identity

$$\alpha_i \alpha_j = \begin{pmatrix} 0 & \sigma_i \\ \sigma_i & 0 \end{pmatrix} \begin{pmatrix} 0 & \sigma_j \\ \sigma_j & 0 \end{pmatrix} = \sigma_i \sigma_j = \delta_{ij} + i\epsilon_{ijk} \sigma_k. \quad (\text{E.4})$$

Other easy to prove identities are $\alpha_i^2 = 1$, $(\gamma_0)^2 = 1$, $\{\alpha_i, \gamma_0\} = 0$, where $\{, \}$ is the anti-commutator, and $(\boldsymbol{\alpha} \cdot \mathbf{p})^2 = |\mathbf{p}|^2$.

Let us consider the following ansatz,

$$\mathcal{U} = \gamma_0 \frac{\boldsymbol{\alpha} \cdot \mathbf{p}}{|\mathbf{p}|} \theta(\mathbf{p}), \quad (\text{E.5})$$

where $\theta(\mathbf{p})$ is a function of \mathbf{p} . Then

$$e^{\pm \mathcal{U}} = \sum_{n=0}^{\infty} \frac{1}{n!} \left(\pm \gamma_0 \frac{\boldsymbol{\alpha} \cdot \mathbf{p}}{|\mathbf{p}|} \theta(\mathbf{p}) \right)^n = \sum_{n=0}^{\infty} \frac{a_n}{n!}, \quad (\text{E.6})$$

and we have

$$\begin{aligned} n=0, & \quad a_0 = 1 \\ n=1, & \quad a_1 = \pm \mathcal{U} \\ n=2, & \quad a_2 = -[\theta(\mathbf{p})]^2 \\ n=3, & \quad a_3 = \pm \mathcal{U} [\theta(\mathbf{p})]^2 \\ & \quad \vdots \quad \quad \quad \vdots \end{aligned} \quad (\text{E.7})$$

All this can be summarized as

$$e^{\pm \mathcal{U}} = \cos \theta \pm \gamma_0 \frac{\boldsymbol{\alpha} \cdot \mathbf{p}}{|\mathbf{p}|} \sin \theta, \quad (\text{E.8})$$

where we now write $\theta = \theta(\mathbf{p})$. We proceed by calculating the modified Hamiltonian:

$$\begin{aligned} \mathcal{H}^{(\text{Dirac-FW})} &= e^{\mathcal{U}} \mathcal{H}^{(\text{Dirac})} e^{-\mathcal{U}} = e^{\mathcal{U}} \left(\boldsymbol{\alpha} \cdot \mathbf{p} c + \gamma_0 m c^2 \right) \left(\cos \theta - \gamma_0 \frac{\boldsymbol{\alpha} \cdot \mathbf{p}}{|\mathbf{p}|} \sin \theta \right) \\ &= e^{\mathcal{U}} \left[\left(\boldsymbol{\alpha} \cdot \mathbf{p} c + \gamma_0 m c^2 \right) \cos \theta + \left(\gamma_0 |\mathbf{p}| c - \frac{\boldsymbol{\alpha} \cdot \mathbf{p}}{|\mathbf{p}|} m c^2 \right) \sin \theta \right] \\ &= \left(\cos \theta + \gamma_0 \frac{\boldsymbol{\alpha} \cdot \mathbf{p}}{|\mathbf{p}|} \sin \theta \right) \left[\left(\boldsymbol{\alpha} \cdot \mathbf{p} c + \gamma_0 m c^2 \right) \cos \theta + \left(\gamma_0 |\mathbf{p}| c - \frac{\boldsymbol{\alpha} \cdot \mathbf{p}}{|\mathbf{p}|} m c^2 \right) \sin \theta \right] \\ &= \left(\boldsymbol{\alpha} \cdot \mathbf{p} c + \gamma_0 m c^2 \right) (\cos^2 \theta - \sin^2 \theta) + 2 \sin \theta \cos \theta \left(\gamma_0 |\mathbf{p}| c - \frac{\boldsymbol{\alpha} \cdot \mathbf{p}}{|\mathbf{p}|} m c^2 \right) \quad (\text{E.9}) \end{aligned}$$

Thus finally we have

$$\mathcal{H}^{(\text{Dirac-FW})} = \frac{\boldsymbol{\alpha} \cdot \mathbf{p}}{|\mathbf{p}|} \left[|\mathbf{p}|c \cos(2\theta) - mc^2 \sin(2\theta) \right] + \gamma_0 \left[mc^2 \cos(2\theta) + |\mathbf{p}|c \sin(2\theta) \right]. \quad (\text{E.10})$$

We can eliminate the non-diagonal term (first term in(E.10)), by choosing $\tan(2\theta^{(\text{Dirac})}) = |\mathbf{p}|/(mc)$. With this choice and using $\tan^2 x + 1 = \sec^2 x$, we find that

$$\cos(2\theta^{(\text{Dirac})}) = \left[1 + \left(\frac{|\mathbf{p}|}{mc} \right)^2 \right]^{-1/2} \quad (\text{E.11})$$

and

$$\sin(2\theta^{(\text{Dirac})}) = \cos(2\theta^{(\text{Dirac})}) \frac{|\mathbf{p}|}{mc}. \quad (\text{E.12})$$

So finally the Hamiltonian reads

$$\mathcal{H}^{(\text{FW-Dirac})} = \gamma_0 \sqrt{(mc^2)^2 + |\mathbf{p}|^2 c^2}, \quad (\text{E.13})$$

as expected from classical relativistic mechanics. The sign given by γ_0 determines the particle-antiparticle solutions. Note that the antiparticles solutions seem to have negative energy which lead Paul Dirac to propose the concept of the Dirac sea and the prediction of the existence of antiparticles.

Note that if we calculate now the velocity operator in Heisenberg picture, we obtain a different thing

$$\left(\frac{dr_i}{dt} \right)_{(\text{FW})} = \frac{i}{\hbar} [\mathcal{H}^{(\text{Dirac-FW})}, r_i] = \gamma_0 \frac{p_i c^2}{\sqrt{p^2 c^2 + m^2 c^4}}. \quad (\text{E.14})$$

Taking the norm squared and inverting the equation we find

$$\mathbf{p}^2 = m \left(\frac{d\mathbf{r}}{dt} \right)_{(\text{FW})}^2 \left[1 - \frac{1}{c^2} \left(\frac{d\mathbf{r}}{dt} \right)_{(\text{FW})}^2 \right]^{-1}, \quad (\text{E.15})$$

which is the natural expression for the momentum in special relativity as a function of the velocity. Thus after a Foldy-Wouthuysen separation, the zitterbewegung paradox disappears as the particle-antiparticle components behave as expected by classical special relativity. This procedure is still valid under the influence of a magnetic field as long as $\phi_e(\mathbf{r}) = 0$, as we will see next.

E.3 FOLDY-WOUTHUYSEN TRANSFORMATION IN THE PRESENCE OF A MAGNETIC FIELD

Dirac Hamiltonian in an time-independent external field is obtained from Dirac's equation (2.49) after a minimal coupling substitution. Let us work out the case where

$\phi_e(\mathbf{r}) = 0$, such that $\mathcal{H}^{(\text{EM-Dirac})}|_{\phi_e=0} = \mathcal{H}^{(\text{mag})}$. By analogy with the previous part let us write everything in terms of $\mathcal{O} = \boldsymbol{\alpha} \cdot (\mathbf{p} + e\mathbf{A}/c)$, so that $\mathcal{H}^{(\text{mag})} = \mathcal{O}c + \gamma_0 mc^2$, which can be diagonalized by using

$$\mathcal{U}^{(\text{mag})} = \gamma_0 \frac{\mathcal{O}}{|\mathcal{O}|} \theta^{(\text{mag})}, \quad (\text{E.16})$$

which leads to $\tan(2\theta^{(\text{mag})}) = |\mathcal{O}|/mc^2$ and consequently

$$\mathcal{H}^{(\text{mag-FW})} = \gamma_0 \sqrt{(mc^2)^2 + \mathcal{O}^2 c^2}. \quad (\text{E.17})$$

Note that in general as long as $\phi_e(\mathbf{r}) = 0$, we have that

$$\mathcal{H}^{(\text{mag-FW})} = \gamma_0 mc^2 \sqrt{1 + 2 \frac{\mathcal{H}^{(\text{nr})}}{mc^2}}, \quad (\text{E.18})$$

where

$$\mathcal{H}^{(\text{nr})} = \frac{\mathcal{O}^2}{2m} \quad (\text{E.19})$$

is the non-relativistic Hamiltonian. To end this section let us develop \mathcal{O}^2 :

$$\begin{aligned} |\mathcal{O}|^2 &= \alpha_i \alpha_j \left(p_i - \frac{q}{c} A_i \right) \left(p_j - \frac{q}{c} A_j \right) \\ &= (\delta_{ij} + i\epsilon_{ijk} \sigma_k) \left(p_i - \frac{q}{c} A_i \right) \left(p_j - \frac{q}{c} A_j \right) = \left| \mathbf{p} - \frac{q}{c} \mathbf{A} \right|^2 - i \frac{q}{c} \epsilon_{ijk} \sigma_k (p_i A_j + A_i p_j) \\ &= \left| \mathbf{p} - \frac{q}{c} \mathbf{A} \right|^2 - \frac{\hbar q}{c} \boldsymbol{\sigma} \cdot [\nabla \times \mathbf{A}], \end{aligned} \quad (\text{E.20})$$

where we used symmetry properties of the Levi-Civita symbol (antisymmetric tensor) and the fact that $[p_i, f(\mathbf{x})] = -i\hbar \partial_i f(\mathbf{x})$. In that way we recover the Pauli Hamiltonian in the absence of potentials (2.56), whose solutions are the relativistic Landau levels of eq. (A.16).

E.4 DIRAC ELECTRON IN A POTENTIAL

Let us now solve the general case $\mathcal{H}^{(\text{Dirac-EM})}$ of (2.55) for $\phi_e \neq 0$. Let us call $\mathcal{E} = -e\phi_e$, and note that $[\mathcal{E}, \gamma_0] = 0$ and $\{\mathcal{O}, \gamma_0\} = 0$, so \mathcal{E} is even and \mathcal{O} is odd by commutation with γ_0 (hence their labels).

Inspired in the solution above, let us calculate the solution for weak fields, for small \mathcal{O}/mc , thus the right \mathcal{U} is about

$$\mathcal{U} \approx \gamma_0 \frac{\mathcal{O}}{|\mathcal{O}|} \theta^{(\text{mag})} \approx \gamma_0 \frac{\mathcal{O}}{2mc}, \quad (\text{E.21})$$

²Here $\theta^{\text{mag}} = \theta^{\text{mag}}(|\mathcal{O}|)$, depends on the absolute value of \mathcal{O} to avoid problems of commutation with γ_0 .

and we will expand \mathcal{H}_{mc} using Baker–Hausdorff–Campbell identity [119].

$$\begin{aligned} \mathcal{H}^{(\text{FW-Dirac-EM})} &= e^{\mathcal{U}} \mathcal{H}^{(\text{Dirac-EM})} e^{-\mathcal{U}} = \mathcal{H}^{(\text{Dirac-EM})} + [\mathcal{U}, \mathcal{H}^{(\text{Dirac-EM})}] \\ &\quad + \frac{1}{2!} [\mathcal{U}, [\mathcal{U}, \mathcal{H}^{(\text{Dirac-EM})}]] + \frac{1}{3!} [\mathcal{U}, [\mathcal{U}, [\mathcal{U}, \mathcal{H}^{(\text{Dirac-EM})}]]] \dots \end{aligned} \quad (\text{E.22})$$

In order to solve the nest of commutator it is useful to note that $[\mathcal{O}, \gamma_0] = -2\gamma_0 \mathcal{O}$.³ The full calculation of (E.22) will not be reproduced here (see [119]), the result yields

$$\begin{aligned} \mathcal{H}^{(\text{FW-Dirac-EM})} &= \gamma_0 mc^2 + \mathcal{E} + \gamma_0 \frac{\mathcal{O}^2}{2m} + \gamma_0 \frac{[\mathcal{O}, \mathcal{E}]}{2mc^2} - \frac{\mathcal{O}^3}{3m^2c} - \frac{[\mathcal{O}, [\mathcal{O}, \mathcal{E}]]}{8m^2c^3} \\ &\quad - \frac{\gamma_0 \mathcal{O}^4}{8m^3c^2} - \frac{\gamma_0 [\mathcal{O}, [\mathcal{O}, [\mathcal{O}, \mathcal{E}]]]}{48m^3c^4} + \frac{\gamma_0 \mathcal{O}^5}{30m^4c^3} + \frac{[\mathcal{O}, [\mathcal{O}, [\mathcal{O}, [\mathcal{O}, \mathcal{E}]]]]}{4!2^4(mc)^4} + \dots \end{aligned} \quad (\text{E.23})$$

Notice that (E.23) still has odd powers of \mathcal{O} , which we want to avoid because that couples the particle-antiparticle subspaces. In order to get rid of the undesired terms we need to do consecutive Foldy-Wouthuysen transformations. Putting all odd terms in γ_0 under a new operator \mathcal{O}' and the even terms under a new operator \mathcal{E}' . This procedure has to be repeated at least three times in order to get rid of all the odd powers of \mathcal{O} up to order $(mc^2)^{-1}$. The whole procedure is in detail in [119]. The final result is a new Hamiltonian $\mathcal{H}^{(\text{Dirac-wr})}$ given by

$$\mathcal{H}^{(\text{Dirac-wr})} = \gamma_0 mc^2 + \mathcal{E} + \gamma_0 \frac{\mathcal{O}^2}{2mc^2} - \gamma_0 \frac{\mathcal{O}^4}{8m^3c^2} - \frac{[\mathcal{O}, [\mathcal{O}, \mathcal{E}]]}{8m^2c^2} \quad (\text{E.24a})$$

which heuristically is equivalent to (E.23) without the odd powers of \mathcal{O} up to first relativistic correction.

To end this appendix we give the result for fifth term in eq. (E.24a):

$$[\mathcal{O}, [\mathcal{O}, \mathcal{E}]] = -\hbar \boldsymbol{\sigma} \cdot [\nabla \mathcal{E} \times (\mathbf{p} + \frac{e}{c} \mathbf{A})] - \hbar^2 \nabla^2 \mathcal{E} - i\hbar \boldsymbol{\sigma} \cdot \nabla \times \mathcal{E}. \quad (\text{E.25})$$

Selecting for the particle-component of the Hamiltonian, recovers the weakly relativistic corrections $\Delta \mathcal{H}$ defined that are found in eq. (4.3).

³In general for two operators \mathcal{O}_1 and \mathcal{O}_2 that anti-commute, $\{\mathcal{O}_1, \mathcal{O}_2\} = 0$, we have that $[\mathcal{O}_1, \mathcal{O}_2] = -2\mathcal{O}_2\mathcal{O}_1$.

SIMPLIFIED SEMICLASSICAL EVALUATION OF THE MAGNETIC SUSCEPTIBILITY

F

In this appendix, we provide a simplified semiclassical calculation (sec. F.1) of the grand-canonical orbital magnetic susceptibility leading to tractable expressions, as in eq. (3.8) in chapter 3. We use a similar formalism in sec. F.2, together with the so called diagonal approximation, that only considers selected pairs of trajectories in the corresponding semiclassical sum, to demonstrate the Curie-type law for the orbital magnetic susceptibility of noninteracting ensembles of metallic nanoparticles that arises at low temperature and/or for small sizes [cf. eq. (3.16) in the main text].

F.1 EVALUATION OF THE GRAND-CANONICAL ORBITAL MAGNETIC SUSCEPTIBILITY

In the limit of low temperatures and/or small sizes ($k_F a \frac{T}{T_F} \ll 1$), we replace the thermal factor appearing in the semiclassical expansion (3.4) by a Heaviside step function that limits the contributing trajectories to the maximal length $L_{\max} = \alpha L_T$, yielding the condition on the topological index $\eta \leq \eta_c$, with $\eta_c = \alpha L_T / 2a = (\alpha / \pi) (k_F a \frac{T}{T_F})^{-1} \gg 1$. Here, the parameter $\alpha \simeq 1.6$ is chosen in such a way that the thermal factor (2.41) presents the maximum derivative. Taking into account the above restriction and reordering the summations over ν and η in eq. (3.4) then lead to

$$\begin{aligned} \frac{\chi^{(1)}}{|\chi_L|} &\simeq 6\sqrt{\pi}(k_F a)^{3/2} \sum_{\eta=3}^{\infty} \sum_{\nu=1}^{\nu_{\max}(\eta)} \operatorname{Re} \left\{ e^{-i\theta_{\nu\eta}(k_F)} \right\} \\ &\times \frac{(-1)^\nu \cos^3 \varphi_{\nu\eta} \sin^{3/2} \varphi_{\nu\eta}}{\sqrt{\eta}}. \end{aligned} \quad (\text{F.1})$$

We have defined $\nu_{\max}(\eta) = \lfloor \frac{\eta-1}{2} \rfloor$ for $3 \leq \eta \leq \lfloor \eta_c \rfloor$ and $\nu_{\max}(\eta) = \lfloor \frac{\eta}{\pi} \arcsin \left(\frac{\eta_c}{\eta} \right) \rfloor$ for $\eta \geq \lceil \eta_c \rceil$. The grid of points that represent the topological indexes (ν, η) contributing to the double sums of eq. (F.1) are represented by red dots in fig. F.1.

The summation over the winding number ν in eq. (F.1) is then expressed using the

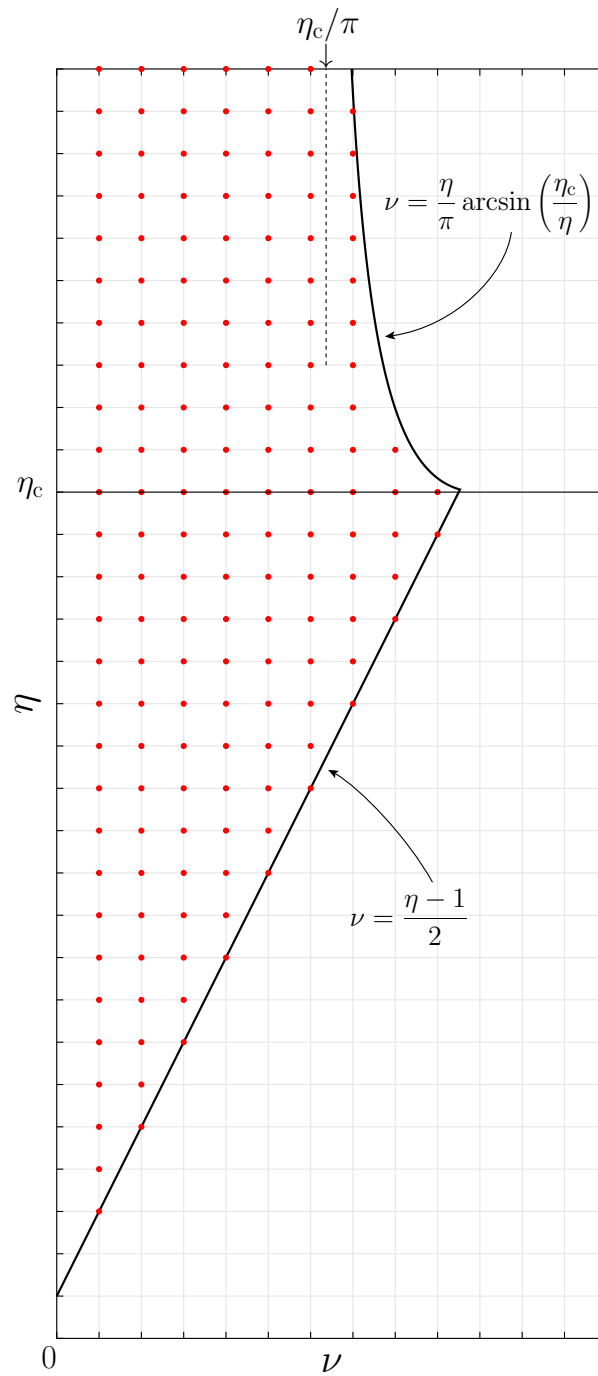


Figure F.1: Topological indexes (ν, η) contributing to the double sums in eqs. (F.1) and (F.5) (red dots). The critical value $\eta_c = \alpha L_T/2a$ separates the two summation regions with different values of $\nu_{\max}(\eta)$ given by the explicit formulas (solid lines). The dotted line depicts the limiting value of ν_{\max} when $\eta \rightarrow \infty$.

Poisson summation formula, yielding

$$\begin{aligned} & \sum_{\nu=1}^{\nu_{\max}(\eta)} (-1)^\nu \cos^3 \varphi_{\nu\eta} \sin^{3/2} \varphi_{\nu\eta} e^{-i\theta_{\nu\eta}(k_F)} = \\ & \sum_{l=-\infty}^{+\infty} \int_{1/2}^{\nu_{\max}(\eta)+1/2} d\nu \cos^3 \varphi_{\nu\eta} \sin^{3/2} \varphi_{\nu\eta} e^{i\Xi_{\nu\eta,l}}, \end{aligned} \quad (\text{F.2})$$

with the phase $\Xi_{\nu\eta,l} = (2l + 1)\pi\nu - \theta_{\nu\eta}$. The above integral over ν is then performed using a stationary phase approximation that results in the stationary points $\bar{\nu} = (\eta/\pi) \arccos([l + 1/2]/k_F a)$. Imposing that the latter belong to the ν integration interval in eq. (F.2) gives the following restriction over the index l :

$$2k_F a \cos\left(\frac{\pi}{\eta} \left[\nu_{\max}(\eta) + \frac{1}{2} \right]\right) \leq 2l + 1 \leq 2k_F a \cos\left(\frac{\pi}{2\eta}\right). \quad (\text{F.3})$$

Substituting $\ell = 2l + 1$ in eq. (F.2) thus leads to

$$\begin{aligned} & \sum_{\nu=1}^{\nu_{\max}(\eta)} (-1)^\nu \cos^3 \varphi_{\nu\eta} \sin^{3/2} \varphi_{\nu\eta} e^{-i\theta_{\nu\eta}(k_F)} = \\ & \sum_{\text{odd } \ell} \left(\frac{\ell}{2k_F a}\right)^3 \sqrt{1 - \left(\frac{\ell}{2k_F a}\right)^2} \sqrt{\frac{\eta}{\pi k_F a}} e^{-i\eta S_\ell}, \end{aligned} \quad (\text{F.4})$$

where the reduced radial action S_ℓ is defined in eq. (3.9) and where the summation over the odd integer ℓ is restricted by the condition (F.3). Incorporating the result (F.4) into eq. (F.1) then yields eq. (3.8).

F.2 DERIVATION OF THE CURIE-TYPE LAW FOR ENSEMBLES OF NONINTERACTING NANOPARTICLES

Here and in what follows, we adopt the notation of previous section with the modification of changing the individual nanoparticle radius a by the average radius \bar{a} of the ensemble.

Starting the diagonal (in trajectory pairs) provided by eq. (3.15), in the limit $k_F \bar{a} \frac{T}{T_F} \ll 1$ we replace the thermal factor squared by a Heaviside step function which cuts trajectories longer than $L_{\max} = \alpha L_T$, leading to

$$\frac{\chi_{\text{ens}}^d}{|\chi_L|} \simeq 18\pi k_F \bar{a} \sum_{\eta=3}^{\infty} \sum_{\nu=1}^{\nu_{\max}(\eta)} \mathcal{F}_{\nu\eta}^{\nu\eta}, \quad (\text{F.5})$$

with $\mathcal{F}_{\nu\eta}^{\nu\eta} = \frac{1}{\eta} \cos^4 \varphi_{\mu\eta} \sin^3 \varphi_{\mu\eta}$ [cf. eq. (3.7)]. Like in the case of appendix F.1, the grid (ν, η) of points contributing to the double sums of eq. (F.5) are represented by red dots

in fig. F.1. Since $\mathcal{F}_{\nu\eta}^{\nu\eta}$ has a smooth dependence on ν , we approximate the summation over ν in eq. (F.5) by an integral, leading to

$$\sum_{\nu=1}^{\nu_{\max}(\eta)} \mathcal{F}_{\nu\eta}^{\nu\eta} \simeq \frac{1}{\pi} \left\{ \frac{1}{5} \left[\cos^5 \left(\frac{\pi}{\eta} \right) - \cos^5 \left(\frac{\pi\nu_{\max}(\eta)}{\eta} \right) \right] - \frac{1}{7} \left[\cos^7 \left(\frac{\pi}{\eta} \right) - \cos^7 \left(\frac{\pi\nu_{\max}(\eta)}{\eta} \right) \right] \right\}. \quad (\text{F.6})$$

In eq. (F.5) the summation over η is dominated by relatively large values of η . Therefore we make the approximation $\cos^5(\pi/\eta) \approx \cos^7(\pi/\eta) \approx 1$ in the expression above. Moreover, for $\eta \leq \lfloor \eta_c \rfloor$, we have $\cos(\pi\nu_{\max}(\eta)/\eta) \simeq \sin(\pi/2\eta)$, so that $\cos^5(\pi\nu_{\max}(\eta)/\eta) \approx \cos^7(\pi\nu_{\max}(\eta)/\eta) \approx 0$, while for $\eta \geq \lceil \eta_c \rceil$, we have $\cos(\pi\nu_{\max}(\eta)/\eta) = [1 - (\eta_c/\eta)^2]^{1/2}$. Thus, eq. (F.5) yields

$$\frac{\chi_{\text{ens}}^{\text{d}}}{|\chi_{\text{L}}|} \simeq 18\pi k_{\text{F}} \bar{a} \left\{ \frac{2\eta_c}{35} + \int_{\eta_c}^{\infty} d\eta \left[\frac{1}{5} \left(1 - \left[1 - \left(\frac{\eta_c}{\eta} \right)^2 \right]^{5/2} \right) - \frac{1}{7} \left(1 - \left[1 - \left(\frac{\eta_c}{\eta} \right)^2 \right]^{7/2} \right) \right] \right\} \quad (\text{F.7})$$

in the limit $\eta_c \gg 1$. Performing the remaining η integral, we find the Curie-type law (3.16), with the prefactor C as given in eq. (3.17).

DARWIN CORRECTION

In this appendix, we consider the Darwin correction for a spherically symmetric confinement, given by the Hamiltonian contribution $\mathcal{H}^{(D)}$ of eq. (4.9). In order to address the corresponding matrix elements, we first tackle a technical issue concerning the eigenvalues and eigenvectors of a spherical box confined by a finite-height potential.

G.1 FINITE BOX SPHERICAL POTENTIAL

The spherical symmetry of the potential (2.4) allows to write the eigenstates as in eqs. (2.10)–(2.11), where the radial wave function of the bound states is given by

$$R_{n,l}(r) = \sqrt{\frac{2}{a^3}} \frac{1}{|c_{n,l}|^{1/2}} \begin{cases} j_l(k_{n,l} r), & r \leq a, \\ \frac{j_l(k_{n,l} a)}{k_l(\kappa_{n,l} a)} k_l(\kappa_{n,l} r), & r > a. \end{cases} \quad (\text{G.1})$$

We follow the standard convention of using $j_l(\zeta)$ for the spherical Bessel function of the first kind and order l . Similarly, we note $k_l(\zeta)$ the modified spherical Bessel function of the second kind and order l , obtained from the imaginary-argument spherical Hankel function $h_l^{(1)}(\zeta)$, i.e., $k_l(\zeta) = -i^l h_l^{(1)}(i\zeta)$. The condition of a bound state implies that its energy $E_{n,l}^{(0)} = E_0(k_{n,l} a)^2$ is smaller than V_0 . We have defined $E_0 = \hbar^2/2ma^2$ and $\kappa_{n,l} = \sqrt{2m(V_0 - E_{n,l}^{(0)})}/\hbar$. The normalization is settled by the constant

$$c_{n,l} = \left(\frac{j_l(k_{n,l} a)}{k_l(\kappa_{n,l} a)} \right)^2 k_{l-1}(\kappa_{n,l} a) k_{l+1}(\kappa_{n,l} a) - j_{l-1}(k_{n,l} a) j_{l+1}(k_{n,l} a). \quad (\text{G.2})$$

The allowed $E_{n,l}^{(0)}$ and $k_{n,l}$ result from the solutions of the quantization condition

$$\kappa_{n,l} a \frac{k'_l(\kappa_{n,l} a)}{k_l(\kappa_{n,l} a)} = k_{n,l} a \frac{j'_l(k_{n,l} a)}{j_l(k_{n,l} a)}, \quad (\text{G.3})$$

which can be recast as

$$\kappa_{n,l} a \frac{k_{l+1}(\kappa_{n,l} a)}{k_l(\kappa_{n,l} a)} = k_{n,l} a \frac{j_{l+1}(k_{n,l} a)}{j_l(k_{n,l} a)}, \quad (\text{G.4})$$

once we employ the useful recurrence relationship

$$q'_l(\zeta) = \frac{l}{\zeta} q_l(\zeta) - q_{l+1}(\zeta), \quad (\text{G.5})$$

valid for $q_l(\zeta) = j_l(\zeta)$, as well as for $q_l(\zeta) = \kappa_l(\zeta)$.

In the limiting case of a hard-wall potential ($V_0 \rightarrow \infty$), the support of the wave function is $r < a$, and the previous expressions result in

$$k_{n,l} a \rightarrow \zeta_{n,l}, \quad (\text{G.6a})$$

$$c_{n,l} \rightarrow [j_{l+1}(\zeta_{n,l})]^2, \quad (\text{G.6b})$$

where $\zeta_{n,l}$ stands for the n th root of $j_l(\zeta)$, and thus the radial wave function (G.1) takes the simpler form of eq. (2.13).

In the case where V_0 is large but remains finite, the second-order expansion of (G.4) around $\zeta_{n,l}$ in the small parameter $u = \sqrt{E_0/V_0}$ allows to write the corrections to eq. (G.6) and to other important parameters as

$$k_{n,l} a \simeq \zeta_{n,l} (1 - u + u^2), \quad (\text{G.7a})$$

$$c_{n,l} \simeq [j_{l+1}(\zeta_{n,l})]^2 (1 + 3u + 3u^2), \quad (\text{G.7b})$$

$$j_l(k_{n,l} a) \simeq j_{l+1}(\zeta_{n,l}) \zeta_{n,l} u, \quad (\text{G.7c})$$

$$j_l(k_{n,l} a) j'_l(k_{n,l} a) \simeq -[j_{l+1}(\zeta_{n,l})]^2 \zeta_{n,l} (u + 2u^2), \quad (\text{G.7d})$$

$$\kappa_{n,l} a \simeq u^{-1} - \frac{1}{2} \zeta_{n,l}^2 u + \zeta_{n,l}^2 u^2. \quad (\text{G.7e})$$

It is important to remark that eq. (G.7c) is valid up to quadratic order in u , and this limiting condition leads to the expression (4.30) of the SOC radial matrix element, which does not depend on V_0 .

G.2 MATRIX ELEMENTS FOR THE DARWIN CORRECTION

According to eq. (4.9), the diagonal Darwin energy correction is

$$E_{n,l}^{(D)} = \frac{E_0}{4mc^2} I_{n,l}^{(D)}, \quad (\text{G.8})$$

with the radial matrix element

$$I_{n,l}^{(D)} = a^2 \int_0^\infty dr [R_{n,l}(r)]^2 \frac{d}{dr} \left(r^2 \frac{dV_{\text{mf}}}{dr} \right). \quad (\text{G.9})$$

For the potential (2.4) we have $V'_{\text{mf}}(r) = V_0 \delta(r - a)$ and therefore the integral (G.9) can be trivially performed, yielding

$$I_{n,l}^{(D)} = -V_0 a^4 \frac{d}{dr} [R_{n,l}(r)]^2 \Big|_{r=a}, \quad (\text{G.10})$$

that, using the form (G.1) of the radial wave function, results in

$$I_{n,l}^{(D)} = -4V_0 \frac{k_{n,l} a}{|c_{n,l}|} j_l(k_{n,l} a) j_l'(k_{n,l} a). \quad (\text{G.11})$$

According to eq. (G.7c), the radial matrix element $I_{n,l}^{(D)}$ diverges as $\sqrt{V_0}$ in the large V_0 -limit. Such a divergence is unphysical since an infinite V_0 would imply an infinite electric field, for which the weakly-relativistic approach leading to eq. (4.3) would not be valid. The subtleties related with a relativistic particle hitting a steep wall are extensively discussed in the literature [119, 122]. The appearance of a divergence in our weakly-relativistic approach calls for a systematic expansion in the small parameter $u = \sqrt{E_0/V_0}$, as presented in the first part of this appendix. In addition, we need to verify that the physical constants of the problem are such that we work in the regime of validity of the perturbative approach. For the case of gold nanoparticles, the values of $E_F = 5.5$ eV and $W = 4.3$ eV [138] result in $u \simeq 0.75 (k_F a)^{-1}$. Therefore, in the semiclassical limit of $k_F a \gg 1$, to which our study is restricted, u is indeed a small parameter.

Using the second-order expressions of eq. (G.7), the radial matrix element (G.11) can be approximated by

$$I_{n,l}^{(D)} = 4V_0 \zeta_{n,l}^2 u (1 - 2u), \quad (\text{G.12})$$

and thus, the Darwin energy correction is

$$E_{n,l}^{(D)} = \frac{E_0^2 \zeta_{n,l}^2}{mc^2} (u^{-1} - 2). \quad (\text{G.13})$$

Notice that the forms (G.13) and (4.31), respectively, of the Darwin and spin-orbit energy corrections, are both valid up to terms of order $(V_0)^0$. We remark that, while $\mathcal{H}^{(D)}$ couples states with different n , the resulting second-order corrections in v_F/c can be neglected.

Similarly to the case of the kinetic correction treated in section 4.2, the Darwin energy (G.13) induces, at $B = 0$, a renormalization of the chemical potential

$$\Delta\mu^{(D)} = (u^{-1} - 2) \frac{\bar{\mu}_0 E_0}{mc^2}. \quad (\text{G.14})$$

MATRIX ELEMENTS FOR THE ANGULAR MAGNETO-ELECTRIC COUPLING

H

In this appendix we calculate the matrix elements of the angular magneto-electric Hamiltonian $\mathcal{H}^{(\text{ame})}$ restricted to the subspace \mathcal{S}_{n,l,m_j}^e , as discussed in section 4.3.1. According to eq. (4.8b) the diagonal matrix element is

$$\begin{aligned} \mathcal{E}_{n,j,m_j,(\pm)}^{(\text{ame})} &= \langle \Phi_{n,j,m_j}^{(\pm)} | \mathcal{H}^{(\text{ame})} | \Phi_{n,j,m_j}^{(\pm)} \rangle \\ &= \frac{\mu_B B}{4mc^2} I_{n,j\pm 1/2}^{(\text{so})} \mathcal{I}_{j,m_j}^{(\text{d-ame})^{(\pm)}}. \end{aligned} \quad (\text{H.1})$$

The radial matrix element coincides with that arising from the spin-orbit coupling (4.30) since, in the hard-wall limit,

$$\int_0^a dr r^3 [R_{n,l}(r)]^2 V'(r) = I_{n,l}^{(\text{so})}. \quad (\text{H.2})$$

Using the standard notation $\sigma_{\pm} = \sigma_x \pm i\sigma_y$, the angular matrix element is

$$\mathcal{I}_{j,m_j}^{(\text{d-ame})^{(\pm)}} = \langle Y_{j,m_j}^{(\pm)} | \sin^2 \theta \sigma_z - \frac{\sin \theta \cos \theta}{2} (e^{-i\varphi} \sigma_+ + e^{i\varphi} \sigma_-) | Y_{j,m_j}^{(\pm)} \rangle. \quad (\text{H.3})$$

The spin-conserving component of $\mathcal{I}_{j,m_j}^{(\text{d-ame})^{(+)}}$ is given by

$$\langle Y_{j,m_j}^{(+)} | \sin^2 \theta \sigma_z | Y_{j,m_j}^{(+)} \rangle = -\frac{m_j}{2} \left(\frac{j(j+2) + j + 1 + m_j^2}{j(j+1)(j+2)} \right). \quad (\text{H.4})$$

Since the two spin-flip components coincide, we only need

$$\begin{aligned} &\langle Y_{j,m_j}^{(+)} | \sin \theta \cos \theta e^{-i\varphi} \sigma_+ | Y_{j,m_j}^{(+)} \rangle \\ &= (-1)^{(m_j+1/2)} \sqrt{\frac{2\pi}{15}} \frac{\sqrt{(j+1)^2 - m_j^2}}{j+1} \int d\vartheta Y_{j+1/2}^{-(m_j+1/2)}(\vartheta) Y_2^1(\vartheta) Y_{j+1/2}^{m_j-1/2}(\vartheta) \\ &= (-1)^{(m_j+1/2)} \sqrt{\frac{2}{3}} \sqrt{(j+1)^2 - m_j^2} \\ &\times \begin{pmatrix} j+1/2 & j+1/2 & 2 \\ 0 & 0 & 0 \end{pmatrix} \begin{pmatrix} j+1/2 & j-1/2 & 2 \\ -(m_j+1/2) & m_j-1/2 & 1 \end{pmatrix}, \end{aligned} \quad (\text{H.5})$$

where we have used the integration formula of three spherical harmonics in terms of Wigner-3j symbols. The first of the 3j symbols can be trivially calculated, while the use of Regge and permutation symmetries for the second one leads to¹

$$\langle Y_{j,m_j}^{(+)} | \sin \theta \cos \theta e^{-i\varphi} \sigma_+ | Y_{j,m_j}^{(+)} \rangle = \frac{m_j}{2} \frac{(j+1)^2 - m_j^2}{j(j+1)(j+2)}. \quad (\text{H.6})$$

Proceeding analogously with the other basis vector $Y_{j,m_j}^{(-)}$, while combining the spin-conserving and spin-flipping components, we have

$$\mathcal{I}_{j,m_j}^{(\text{d-ame})(\pm)} = \mp \frac{m_j(j+1/2)}{j(j+1)}. \quad (\text{H.7})$$

The off-diagonal matrix element of $\mathcal{H}^{(\text{ame})}$ restricted to the subspace \mathcal{S}_{n,l,m_j}^e is

$$\langle \Phi_{n,j,m_j}^{(-)} | \mathcal{H}^{(\text{ame})} | \Phi_{n,j,m_j}^{(+)} \rangle = \frac{\mu_B B}{4mc^2} I_{n,j,\pm 1/2}^{(\text{so})} \mathcal{I}_{j,m_j}^{(\text{od-ame})(\pm)}, \quad (\text{H.8})$$

with

$$\mathcal{I}_{j,m_j}^{(\text{od-ame})} = \langle Y_{j+1,m_j}^{(-)} | \sin^2 \theta \sigma_z - \frac{\sin \theta \cos \theta}{2} (e^{-i\varphi} \sigma_+ + e^{i\varphi} \sigma_-) | Y_{j,m_j}^{(+)} \rangle. \quad (\text{H.9})$$

The spin-conserving component of $\mathcal{I}_{j,m_j}^{(\text{od-ame})(+)}$ is given by

$$\langle Y_{j+1,m_j}^{(-)} | \sin^2 \theta \sigma_z | Y_{j,m_j}^{(+)} \rangle = -\frac{1}{2} \frac{\sqrt{(j+1)^2 - m_j^2}}{(j+1)} \left(1 + \frac{m_j^2}{j(j+2)} \right). \quad (\text{H.10})$$

Since here too the two spin-flip components coincide, we only need

$$\begin{aligned} & \langle Y_{j+1,m_j}^{(-)} | \sin \theta \cos \theta e^{-i\varphi} \sigma_+ | Y_{j,m_j}^{(+)} \rangle \\ &= -(-1)^{(m_j+1/2)} \sqrt{\frac{8\pi}{15}} \frac{m_j}{j+1} \int d\vartheta Y_{j+1/2}^{-(m_j+1/2)}(\vartheta) Y_2^1(\vartheta) Y_{j+1/2}^{m_j-1/2}(\vartheta) \\ &= -\frac{m_j^2}{2} \frac{\sqrt{(j+1)^2 - m_j^2}}{j(j+1)(j+2)}, \end{aligned} \quad (\text{H.11})$$

¹We used the identity

$$\begin{aligned} & \begin{pmatrix} j_1 & j_2 & j_1 - j_2 + 1 \\ m_j & -m_j & 0 \end{pmatrix} \\ &= (-1)^{-j_1+2j_2-m_j} 2m_j \frac{\sqrt{(2j_2-1)!} \sqrt{(2j_1-2j_2+1)!} \sqrt{(j_1+m_j)!} \sqrt{(j_1-m_j)!}}{(j_1-j_2)! \sqrt{(2j_1+2)!} \sqrt{(j_2-m_j)!} \sqrt{(j_2+m_j)!}}. \end{aligned}$$

and thus

$$\mathcal{I}_{j,m_j}^{(\text{od-ame})} = -\frac{1}{2} \frac{\sqrt{(j+1)^2 - m_j^2}}{(j+1)}. \quad (\text{H.12})$$

which leads to the off-diagonal matrix element (4.49). The simple structure of the angular matrix elements (H.7) and (H.12) is a consequence of the Wigner–Eckart theorem (2.65) applied to the diagonal and off-diagonal matrix elements of $\mathcal{H}^{(\text{ame})}$, given by eqs. (H.1) and (H.8), respectively.

NONRELATIVISTIC SUSCEPTIBILITY USING THE COUPLED BASIS

I

As discussed in Secs. 4.3 and 4.3.1, the treatment of the SOC is greatly simplified by working in the coupled basis of total angular momentum within the subspace decomposition (4.32). It is therefore useful to recast the nonrelativistic ZFS as the sum of two components arising from the p (product) and e (entangled) states associated, respectively, with the subspaces $\mathcal{S}_{n,l,(d/u)}^p$ and \mathcal{S}_{n,l,m_j}^e , writing

$$\chi^{(\text{nr})} = \chi_p^{(\text{nr})} + \chi_e^{(\text{nr})}. \quad (\text{I.1})$$

The p-states (d/u) are characterized, respectively, by the quantum numbers $\{n, l, m_z = -l, m_s = -1/2\}$ and $\{n, l, m_z = l, m_s = +1/2\}$ of the product basis, that can be expressed in a compact way as $\{n, l, m_z = \mp l, m_s = (1/2)(m_z/l)\}$. According to eq. (4.10), at finite magnetic field, these states are associated with the energies

$$E_{n,l}^{(\text{nr}) (d/u)} = E_{n,l}^{(0)} \mp \mu_B B(l+1) + E_{n,l,\mp l}^{(\text{dia})}. \quad (\text{I.2})$$

Applying eq. (2.24) and summing over $m_z = \mp l$ we have

$$\frac{\chi_p^{(\text{nr})}}{|\chi_L|} = -\frac{9\pi E_0}{k_{\text{Fa}}} \sum_{l=0}^{\infty} \sum_{n=1}^{\infty} \left\{ (l+1)^2 f'_{\tilde{\mu}_0}(E_{n,l}^{(0)}) + \frac{\mathcal{R}_{n,l}}{2E_0} \frac{l+1}{l+3/2} f_{\tilde{\mu}_0}(E_{n,l}^{(0)}) \right\}. \quad (\text{I.3})$$

In the nonrelativistic case, the subspace \mathcal{S}_{n,l,m_j}^e can be characterized by the product-basis states with quantum numbers $\{n, l, m_z = \mp l, m_s = -(1/2)(m_z/l)\}$ and $\{n, l, m_z \in [-l+1, l-1], m_s = \pm 1/2\}$. For each couple (n, l) , there are two states of the first kind and $4l-2$ of the second one, whose energies at finite magnetic field follow from eq. (4.10). Once the sum over m_z is performed in eq. (2.24), they yield

$$\frac{\chi_e^{(\text{nr})}}{|\chi_L|} = -\frac{3\pi E_0}{k_{\text{Fa}}} \sum_{l=1}^{\infty} \sum_{n=1}^{\infty} l \left\{ (2l^2+1) f'_{\tilde{\mu}_0}(E_{n,l}^{(0)}) + \frac{\mathcal{R}_{n,l}}{E_0} \frac{2l+5/2}{l+3/2} f_{\tilde{\mu}_0}(E_{n,l}^{(0)}) \right\}. \quad (\text{I.4})$$

Obviously, the addition of eqs. (I.3) and (I.4) results in the expression of $\chi^{(\text{nr})}$ presented in sec. 4.1.2 [cf. eq. (4.15)].

MATRIX ELEMENTS FOR THE CASE OF THE HALF-SPHERE

J

In this appendix we prove a general result concerning the limiting values of the wave function and its derivative at a potential discontinuity, in one- and three-dimensional geometries, which is crucial in order to obtain the spin-orbit matrix elements (4.70) and (4.74). We also use nontrivial recurrence relations allowing to calculate the angular matrix element (4.71) and the radial one, eq. (4.80).

J.1 A THEOREM ABOUT THE WAVE-FUNCTION VALUES CLOSE TO A POTENTIAL BARRIER

We consider a one-dimensional Schrödinger equation with a potential barrier of height V_0 at $x = a$ (see Fig. J.1). We will prove that its solutions $\psi(x)$ verify

$$\lim_{V_0 \rightarrow \infty} \frac{\sqrt{2mV_0}}{\hbar} \psi(a) = -\psi'(a^-). \quad (\text{J.1})$$

Without loss of generality, we take $V(x) = 0$ for $x \in (a - \epsilon, a)$ and $V(x) = V_0$ for $x \in (a, a + \epsilon)$, where ϵ is a small, but finite length. Integrating the Schrödinger equation in the small interval $(a - \epsilon, a + \epsilon)$ yields

$$-\frac{\hbar^2}{2m} [\psi'(a + \epsilon) - \psi'(a - \epsilon)] + V_0 \int_a^{a+\epsilon} dx \psi(x) = E \int_{a-\epsilon}^{a+\epsilon} dx \psi(x). \quad (\text{J.2})$$

Assuming that the barrier extends to $x = +\infty$, we have $\psi(x) = \psi(a) \exp(-\kappa x)$ in the interval $(a, a + \epsilon)$, with $\kappa = \sqrt{2m(V_0 - E)}/\hbar$. Taking the limit of large V_0 while keeping a finite value of ϵ we obtain

$$\psi'(a + \epsilon) = -\kappa \psi(a) \exp(-\kappa\epsilon) \simeq 0, \quad (\text{J.3a})$$

$$V_0 \int_a^{a+\epsilon} dx \psi(x) \simeq \frac{V_0}{\kappa} \psi(a). \quad (\text{J.3b})$$

Thus, in the leading order in V_0 , eq. (J.2) can be recast as

$$\frac{\hbar^2}{2m} \psi'(a - \epsilon) + \sqrt{\frac{V_0 \hbar^2}{2m}} \psi(a) = 0. \quad (\text{J.4})$$

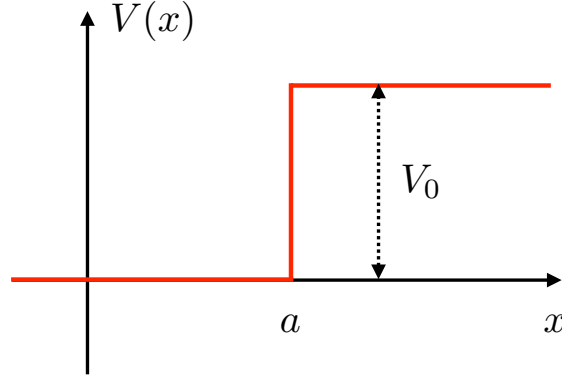


Figure J.1: Sketch of a one-dimensional sharp potential barrier of height V_0 at $x = a$.

Since $\psi'(x)$ is a continuous function in the open interval $(a - \epsilon, a)$, we promptly obtain the announced result (J.1). The particular case of the radial wave function is contained in eq. (G.7) and has been used in obtaining eq. (4.30).

The calculation of the spin-orbit matrix elements in the case of the HS necessitates the generalization of (J.1) to a two-dimensional potential barrier. Since the potential (4.65) defining the confinement in the HS with a finite height V_0 has cylindrical symmetry, m_z is a good quantum number, and the eigenfunctions have the form $\psi_{m_z}(r, \theta, \varphi) = \mathfrak{f}_{m_z}(r, \theta) \exp(im_z \varphi)$, with \mathfrak{f}_{m_z} verifying

$$-\frac{\hbar^2}{2m} \left(\frac{1}{r^2} \partial_r r^2 \partial_r + \frac{1}{r^2 \sin \theta} \partial_\theta \sin \theta \partial_\theta - \frac{m_z^2}{r^2 \sin^2 \theta} \right) \mathfrak{f}_{m_z}(r, \theta) + V(r, \theta) \mathfrak{f}_{m_z}(r, \theta) = E \mathfrak{f}_{m_z}(r, \theta). \quad (\text{J.5})$$

Marching on the footprints of the derivation for the one-dimensional case, we integrate the previous equation in the small angular interval $(\pi/2 - \epsilon, \pi/2 + \epsilon)$, obtaining

$$-\frac{\hbar^2}{2m} \left(\frac{2\epsilon}{r^2} \partial_r r^2 \partial_r \mathfrak{f}_{m_z}(r, \theta) \Big|_{\theta=\pi/2} + \frac{1}{r^2} \partial_\theta \mathfrak{f}_{m_z}(r, \theta) \Big|_{\theta=\pi/2-\epsilon}^{\theta=\pi/2+\epsilon} - \frac{2\epsilon m_z^2}{r^2} \mathfrak{f}_{m_z}(r, \theta) \Big|_{\theta=\pi/2} \right) + V_0 \int_{\pi/2}^{\pi/2+\epsilon} d\theta \mathfrak{f}_{m_z}(r, \theta) = 2\epsilon E \mathfrak{f}_{m_z}(r, \theta) \Big|_{\theta=\pi/2}. \quad (\text{J.6})$$

In the leading order in V_0 we have $\mathfrak{f}_{m_z}(r, \theta) = \mathfrak{f}_{m_z}(r, \theta = \pi/2) \exp(-\sqrt{2mV_0}r^2[\theta - \pi/2]/\hbar)$ in the interval $(\pi/2, \pi/2 + \epsilon)$. Thus, taking the limit of large V_0 and then that of $\epsilon \rightarrow 0$ we obtain

$$\frac{r\sqrt{2mV_0}}{\hbar} \mathfrak{f}_{m_z}(r, \theta = \pi/2) \simeq -\partial_\theta \mathfrak{f}_{m_z}(r, \theta) \Big|_{\theta=\pi/2^-}, \quad (\text{J.7})$$

which generalizes eq. (J.1) to the case of a two-dimensional potential barrier with cylindrical symmetry.

Taking the hard-wall limit of $V_0 \rightarrow \infty$ for the potential (4.65), the solutions $\psi_{m_z}^{(V_0, n, l)}(r, \theta, \varphi)$ converge towards the orbital wave functions (4.66), with the condition of $l + m_z$ being odd. Thus, we can write

$$\frac{\sqrt{mV_0}}{\hbar} \psi_{m_z}^{(V_0, n, l)}(r, \theta = \pi/2, \varphi) \simeq -\sqrt{l(l+1) - m_z(m_z+1)} \frac{R_{nl}(r)}{r} e^{-i\varphi} Y_l^{m_z+1}(\theta = \pi/2, \varphi), \quad (\text{J.8})$$

where we have used

$$\frac{\partial Y_l^{m_z}(\theta, \varphi)}{\partial \theta} = m_z \cot(\theta) Y_l^{m_z}(\theta, \varphi) + \sqrt{(l-m_z)(l+m_z+1)} e^{-i\varphi} Y_l^{m_z+1}(\theta, \varphi), \quad (\text{J.9})$$

taking $\theta = \pi/2$.

J.2 ANGULAR INTEGRAL OF THE MATRIX ELEMENT (4.71)

The angular integral (4.72) appearing in the nondiagonal matrix element (4.71) of $\mathcal{H}^{(\text{so})-(\text{HS})}$ can be expressed as

$$\mathcal{I}_{l', l, m'_z}^{(\text{dome})} = \frac{1}{2} \sqrt{(2l+1)(2l'+1)} \sqrt{\frac{(l-m)! (l'-m'_z)!}{(l+m'_z)! (l'+m'_z)!}} \mathcal{Y}_{l', l}^{m'_z}, \quad (\text{J.10})$$

where we have used the definition of the spherical harmonic $Y_l^{m_z}(\vartheta)$ in terms of the associated Legendre function $P_l^{m_z}(\cos \theta)$ [with the standard convention of assigning the Condon-Shortley phase $(-1)^{m_z}$ to the latter], and introduced

$$\mathcal{Y}_{l', l}^{m'_z} = \int_0^1 dx P_{l'}^{m'_z}(x) P_l^{m'_z}(x). \quad (\text{J.11})$$

In the case that interests us, with $l' + m'_z$ odd and $l + m'_z$ even, we can prove, directly from the differential equations fulfilled by the associated Legendre functions $P_l^{m'_z}$ and $P_{l'}^{m'_z}$ with $l \neq l'$, the following useful identity:

$$\mathcal{Y}_{l', l}^{m'_z} = -\frac{l'+1-m'_z}{l'(l'+1)-l(l+1)} P_l^{m'_z}(0) P_{l'+1}^{m'_z}(0), \quad (\text{J.12})$$

which, together with the relationship

$$P_l^{m'_z}(0) = \frac{(-1)^{(l+m'_z)/2}}{2^l} \frac{(l+m'_z)!}{\left(\frac{l+m'_z}{2}\right)! \left(\frac{l-m'_z}{2}\right)!}, \quad (\text{J.13})$$

valid for even $l + m'_z$, lead to

$$\mathcal{I}_{l',l,m}^{(\text{dome})} = \frac{(-1)^{m+(l+l'+1)/2}}{2^{l+l'}} \frac{\sqrt{(2l+1)(2l'+1)}}{l(l+1)-l'(l'+1)} \frac{\sqrt{(l+m)!(l-m)!}}{\left(\frac{l+m}{2}\right)!\left(\frac{l-m}{2}\right)!} \frac{\sqrt{(l'+m)!(l'-m)!}}{\left(\frac{l'+m-1}{2}\right)!\left(\frac{l'-m-1}{2}\right)!}, \quad (\text{J.14})$$

allowing to give a closed expression to the nondiagonal matrix element (4.71) of $\mathcal{H}^{(\text{dome})}$.

J.3 DEFINITE INTEGRALS OF TWO SPHERICAL BESSEL FUNCTIONS

The radial matrix elements (4.80), appearing in the perturbative treatment of the magnetic field for the HS of sec. 4.5.3, as well as in the diagonalization to obtain the finite-field spectrum of the sphere in fig. 2.4, can be expressed as

$$\mathcal{R}_{n',l',n,l} = \frac{2 L_{l',l}^{(4)}(\zeta_{n',l'}, \zeta_{n,l})}{|j_{l'+1}(\zeta_{n',l'}) j_{l+1}(\zeta_{n,l})|}, \quad (\text{J.15})$$

with

$$L_{l',l}^{(q)}(\alpha, \beta) = \int_0^1 d\zeta \zeta^q j_{l'}(\alpha\zeta) j_l(\beta\zeta), \quad (\text{J.16})$$

and where α and β are such that $j_{l-2}(\alpha) = 0$ and $j_l(\beta) = 0$, respectively.

The particular case of $\mathcal{R}_{n',l,n,l}$ appearing in the first term of eq. (4.78b) requires a simpler term

$$K_l^{(q)}(\alpha, \beta) = L_{l,l}^{(q)}(\alpha, \beta), \quad (\text{J.17})$$

invoking the definite integral of two spherical Bessel functions with the same order. Using repetitively the recursive formulas developed for the indefinite integrals of spherical Bessel functions of the same order [186], we have

$$\begin{aligned} K_l^{(4)}(\alpha, \beta) = & \left(\frac{\alpha^2 + \beta^2}{2\alpha\beta}\right)^l K_0^{(4)}(\alpha, \beta) - \sum_{d=1}^l \frac{(\alpha^2 + \beta^2)^{d-1}}{(2\alpha\beta)^d} \left\{ 2j_{l-d}(\alpha) j_{l-d}(\beta) \right. \\ & - \alpha \left(\frac{2[2(l-d)+3]}{\alpha^2 - \beta^2} - 1 \right) j_{l+1-d}(\alpha) j_{l-d}(\beta) \\ & \left. + \beta \left(\frac{2[2(l-d)+3]}{\alpha^2 - \beta^2} + 1 \right) j_{l-d}(\alpha) j_{l+1-d}(\beta) \right\} \end{aligned} \quad (\text{J.18})$$

with

$$\begin{aligned} K_0^{(4)}(\alpha, \beta) = & \frac{1}{2\alpha\beta} \left\{ \frac{1}{(\alpha - \beta)^3} \left[2(\alpha - \beta) \cos(\alpha - \beta) + ((\alpha - \beta)^2 - 2) \sin(\alpha - \beta) \right] \right. \\ & \left. - \frac{1}{(\alpha + \beta)^3} \left[2(\alpha + \beta) \cos(\alpha + \beta) + ((\alpha + \beta)^2 - 2) \sin(\alpha + \beta) \right] \right\}. \end{aligned} \quad (\text{J.19})$$

The recursive formulas developed for the indefinite integrals of spherical Bessel functions of different orders [186] allow us to write

$$L_{l-2,l}^{(4)}(\alpha, \beta) = \frac{2l-1}{2} \frac{\alpha}{\beta} K_{l-1}^{(4)}(\alpha, \beta) - \frac{2l+1}{2} K_{l-2}^{(4)}(\alpha, \beta), \quad (\text{J.20})$$

which can be directly evaluated from eq. (J.18), and also expressed as

$$\begin{aligned} L_{l-2,l}^{(4)}(\alpha, \beta) = & \frac{1}{4} \left[(2l-1) \left(\frac{\alpha}{\beta} \right)^2 - 2l - 3 \right] \left[\left(\frac{\alpha^2 + \beta^2}{2\alpha\beta} \right)^{l-2} K_0^{(4)}(\alpha, \beta) \right. \\ & - \sum_{d=1}^{l-2} \frac{(\alpha^2 + \beta^2)^{d-1}}{(2\alpha\beta)^d} \left\{ 2j_{l-2-d}(\alpha) j_{l-2-d}(\beta) \right. \\ & - \alpha \left(\frac{2[2(l-d)-1]}{\alpha^2 - \beta^2} - 1 \right) j_{l-1-d}(\alpha) j_{l-2-d}(\beta) \\ & \left. \left. + \beta \left(\frac{2[2(l-d)-1]}{\alpha^2 - \beta^2} + 1 \right) j_{l-2-d}(\alpha) j_{l-1-d}(\beta) \right\} \right] \\ & + \frac{2l-1}{4} \frac{\alpha}{\beta^2} \left(\frac{2[2l-1]}{\alpha^2 - \beta^2} - 1 \right) j_{l-1}(\alpha) j_{l-2}(\beta). \end{aligned} \quad (\text{J.21})$$

The integral $L_{l+2,l}^{(4)}(\alpha, \beta)$ can be obtained from the expression of $L_{l-2,l}^{(4)}(\alpha, \beta)$ above by implementing the shift of l to $l+2$ while exchanging the role of α and β . The closed form of the definite integrals of two spherical Bessel functions, developed in this appendix, constitutes a general result that may find its applications beyond the use of evaluating the matrix elements for the problem at hand.

BIBLIOGRAPHY

- [1] W. D. Knight et al. 'Electronic Shell Structure and Abundances of Sodium Clusters'. *Phys. Rev. Lett.* 52.24 (1984), pp. 2141–2143. DOI: [10 . 1103 / PhysRevLett . 52 . 2141](https://doi.org/10.1103/PhysRevLett.52.2141) (cited on pp. 1, 16, 60).
- [2] L. P. Lévy, G. Dolan, J. Dunsmuir, and H. Bouchiat. 'Magnetization of mesoscopic copper rings: Evidence for persistent currents'. *Phys. Rev. Lett.* 64.17 (Apr. 1990), pp. 2074–2077. DOI: [10 . 1103 / PhysRevLett . 64 . 2074](https://doi.org/10.1103/PhysRevLett.64.2074) (cited on pp. 1, 10).
- [3] K. S. Novoselov. 'Electric Field Effect in Atomically Thin Carbon Films'. *Science* 306.5696 (Oct. 2004), pp. 666–669. DOI: [10 . 1126 / science . 1102896](https://doi.org/10.1126/science.1102896) (cited on p. 1).
- [4] W. Xu et al. 'Gold nanoparticle-based terahertz metamaterial sensors: mechanisms and applications'. *ACS Photonics* 3.12 (2016), pp. 2308–2314. DOI: [10 . 1021 / acsp Photonics . 6b00463](https://doi.org/10.1021/acsp Photonics . 6b00463) (cited on p. 1).
- [5] V. Avasare, Z. Zhang, D. Avasare, I. Khan, and A. Qurashi. 'Room-temperature synthesis of TiO₂ nanospheres and their solar driven photoelectrochemical hydrogen production'. *Int. J. Ener. Res.* 39.12 (2015), pp. 1714–1719. DOI: [10 . 1002 / er . 3372](https://doi.org/10.1002/er.3372) (cited on p. 1).
- [6] F. Ning et al. 'TiO₂/graphene/NiFe-layered double hydroxide nanorod array photoanodes for efficient photoelectrochemical water splitting'. *Ener. Envi. Sci.* 9.8 (2016), pp. 2633–2643. DOI: [10 . 1039 / C6EE01092J](https://doi.org/10.1039/C6EE01092J) (cited on p. 1).
- [7] P. K. Jain, I. H. El-Sayed, and M. A. El-Sayed. 'Au nanoparticles target cancer'. *nano today* 2.1 (2007), pp. 18–29. DOI: [10 . 1016 / S1748 - 0132 \(07 \) 70016 - 6](https://doi.org/10.1016/S1748-0132(07)70016-6) (cited on p. 1).
- [8] P. AshaRani, G. Low Kah Mun, M. P. Hande, and S. Valiyaveetil. 'Cytotoxicity and genotoxicity of silver nanoparticles in human cells'. *ACS nano* 3.2 (2009), pp. 279–290. DOI: [10 . 1021 / nm800596w](https://doi.org/10.1021/nm800596w) (cited on p. 1).
- [9] Nikonianman. *Au nanoparticles*. Wikimedia Commons, distributed under a CC-BY-SA-4.0 license. 2012. URL: https://commons.wikimedia.org/wiki/File:Au_nanoparticles.jpg (visited on 08/01/2021) (cited on p. 2).
- [10] M.-C. Daniel and D. Astruc. 'Gold nanoparticles: assembly, supramolecular chemistry, quantum-size-related properties, and applications toward biology, catalysis, and nanotechnology'. *Chem. Reviews* 104.1 (2004), pp. 293–346. DOI: [10 . 1021 / cr030698 % 2B](https://doi.org/10.1021/cr030698%2B) (cited on p. 2).

- [11] J. Kimling et al. 'Turkevich method for gold nanoparticle synthesis revisited'. *J. Phys. Chem. B* 110.32 (2006), pp. 15700–15707. DOI: [10.1021/jp061667w](https://doi.org/10.1021/jp061667w) (cited on p. 2).
- [12] M. Brust, M. Walker, D. Bethell, D. J. Schiffrin, and R. Whyman. 'Synthesis of thiol-derivatised gold nanoparticles in a two-phase Liquid–Liquid system'. *J. Chem. Soc., Chem. Comm.* 0.7 (1994), pp. 801–802. DOI: [10.1039/C39940000801](https://doi.org/10.1039/C39940000801) (cited on p. 2).
- [13] N. Usov and M. Nesmeyanov. 'Multi-domain structures in spheroidal Co nanoparticles'. *Scientific Reports* 10.1 (2020), pp. 1–9. DOI: [10.1038/s41598-020-67173-5](https://doi.org/10.1038/s41598-020-67173-5) (cited on p. 3).
- [14] C. Rügenapp, B. Gleich, and A. Haase. 'Magnetic nanoparticles in magnetic resonance imaging and diagnostics'. *Pharmaceutical research* 29.5 (2012), pp. 1165–1179. DOI: [10.1007/s11095-012-0711-y](https://doi.org/10.1007/s11095-012-0711-y) (cited on p. 3).
- [15] R. J. Harrison, R. E. Dunin-Borkowski, and A. Putnis. 'Direct imaging of nanoscale magnetic interactions in minerals'. *Proc. of the National Academy of Sci.* 99.26 (2002), pp. 16556–16561. DOI: [10.1073/pnas.262514499](https://doi.org/10.1073/pnas.262514499) (cited on p. 3).
- [16] G. L. Nealon et al. 'Magnetism in gold nanoparticles'. *Nanoscale* 4 (2012), p. 5244. DOI: [10.1039/C2NR30640A](https://doi.org/10.1039/C2NR30640A) (cited on pp. 3, 9, 10, 15, 41, 48, 56, 61, 89, 91).
- [17] B. Donnio, J.-L. Gallani, and M. V. Rastei. 'Characterization of Magnetism in Gold Nanoparticles'. In: *Magnetic Characterization Techniques for Nanomaterials*. Ed. by C. S. S. R. Kumar. Springer-Verlag, Berlin, 2017. DOI: [10.1007/978-3-662-52780-1](https://doi.org/10.1007/978-3-662-52780-1) (cited on pp. 3, 9, 10, 15, 41, 48, 54, 61, 91, 93).
- [18] B. Diu, C. Guthman, D. Lederer, and B. Roulet. *Éléments de la physique statistique*. Hermann, 1996 (cited on p. 4).
- [19] N. Bohr. 'Studier over metallernes Elektrontheori'. PhD thesis, University of Copenhagen, 1911 (cited on pp. 4, 99).
- [20] H.-J. van Leeuwen. 'Problèmes de la théorie électronique du magnétisme'. *J. Phys. Radium* 2 (1921), p. 361. DOI: [10.1051/jphysrad:01921002012036100](https://doi.org/10.1051/jphysrad:01921002012036100) (cited on pp. 4, 99).
- [21] P. Langevin. 'Sur la théorie du magnétisme'. *J. Phys. Theor. Appl.* 4.1 (1905), pp. 678–693. DOI: [10.1051/jphystap:019050040067800](https://doi.org/10.1051/jphystap:019050040067800) (cited on p. 4).
- [22] D. A. van Leeuwen. *Magnetic Moments in Metacluster Molecules*. PhD thesis, University of Leiden, unpublished, 1993 (cited on pp. 5, 10, 19, 25–27, 29, 34, 45, 64, 65, 91, 115).
- [23] L. Landau. 'Diamagnetismus der metalle'. *Zeitschrift für Physik* 64.9 (1930), pp. 629–637. DOI: [10.1007/BF01397213](https://doi.org/10.1007/BF01397213) (cited on pp. 5, 93, 99).
- [24] L. D. Landau and E. M. Lifshitz. *Statistical Physics*. Pergamon, Oxford, 1985 (cited on pp. 5, 31, 53, 93, 99, 100, 103).

- [25] M. Suzuki et al. 'Measurement of a Pauli and Orbital Paramagnetic State in Bulk Gold Using X-Ray Magnetic Circular Dichroism Spectroscopy'. *Phys. Rev. Lett.* 108 (4 Jan. 2012), p. 047201. DOI: [10.1103/PhysRevLett.108.047201](https://doi.org/10.1103/PhysRevLett.108.047201) (cited on p. 5).
- [26] P. Ehrenfest. 'Opmerkingen over het Diamagnetisme van vast Bismuth'. *Physica* 5 (1925), p. 388 (cited on p. 6).
- [27] C. V. Raman. 'Diamagnetism and Crystal Structure'. *Nature* 123.3112 (June 1929), pp. 945–945. DOI: [10.1038/123945a0](https://doi.org/10.1038/123945a0) (cited on p. 6).
- [28] V. I. Vaidyanathan. 'Influence of Particle Size on Diamagnetism'. *Nature* 124.3133 (Nov. 1929), pp. 762–762. DOI: [10.1038/124762d0](https://doi.org/10.1038/124762d0) (cited on p. 6).
- [29] V. I. Vaidyanathan. 'Influence of Chemical Colloidisation on the Anomalous Diamagnetism of Bismuth and Antimony'. en. *Nature* 125.3157 (May 1930), pp. 672–672. DOI: [10.1038/125672c0](https://doi.org/10.1038/125672c0) (cited on p. 6).
- [30] S. Ramachandra Rao. 'Diamagnetism and the Colloidal State'. *Nature* 128.3221 (July 1931), pp. 153–153. DOI: [10.1038/128153b0](https://doi.org/10.1038/128153b0) (cited on p. 6).
- [31] V. I. Vaidhianathan and B. Singh. 'Magnetism of Colloidal Gold'. *Nature* 128.3225 (Aug. 1931), pp. 302–303. DOI: [10.1038/128302b0](https://doi.org/10.1038/128302b0) (cited on p. 6).
- [32] V. I. Vaidhianathan and B. S. Puri. 'Magnetism of Precipitates of Colloidal Silver'. *Nature* 129.3248 (Jan. 1932), pp. 170–170. DOI: [10.1038/129170a0](https://doi.org/10.1038/129170a0) (cited on p. 6).
- [33] M. Faraday. 'X. The Bakerian Lecture. —Experimental relations of gold (and other metals) to light'. *Philosophical Transactions of the Royal Soc. of London* 147 (Jan. 1857), pp. 145–181. DOI: [10.1098/rstl.1857.0011](https://doi.org/10.1098/rstl.1857.0011) (cited on p. 6).
- [34] H. Hori et al. 'Anomalous magnetic polarization effect of Pd and Au nanoparticles'. *Phys. Lett. A* 263 (1999), p. 406. DOI: [10.1016/S0375-9601\(99\)00742-2](https://doi.org/10.1016/S0375-9601(99)00742-2) (cited on pp. 6, 8, 9, 56–58, 92, 94).
- [35] Y. Nakae et al. 'Anomalous spin polarization in Pd and Au nano-particles'. *Physica B* 284-288 (2000), p. 1758. DOI: [10.1016/S0921-4526\(99\)02928-2](https://doi.org/10.1016/S0921-4526(99)02928-2) (cited on pp. 6, 8, 56–58, 92).
- [36] H. Hori, T. Teranishi, and Y. Yamamoto. 'Spontaneous Spin Polarization and Electronic States in Platinum Nano-Particle'. In: *New Trends in Superconductivity*. Ed. by J. F. Annett and S. Kruchinin. Springer Netherlands, 2002, pp. 267–276. DOI: [10.1007/978-94-010-0544-9_24](https://doi.org/10.1007/978-94-010-0544-9_24) (cited on pp. 6, 8).
- [37] Y. Yamamoto et al. 'Direct Observation of Ferromagnetic Spin Polarization in Gold Nanoparticles'. *Phys. Rev. Lett.* 93 (2004), p. 116801. DOI: [10.1103/PhysRevLett.93.116801](https://doi.org/10.1103/PhysRevLett.93.116801) (cited on pp. 6, 8–10, 15, 16, 58, 59, 94).
- [38] H. Hori et al. 'Diameter dependence of ferromagnetic spin moment in Au nanocrystals'. *Phys. Rev. B* 69 (2004), p. 174411. DOI: [10.1103/PhysRevB.69.174411](https://doi.org/10.1103/PhysRevB.69.174411) (cited on pp. 6, 8, 10, 56, 57, 59, 92, 94).

- [39] Y. Yamamoto and H. Hori. 'Direct observation of the ferromagnetic spin polarization in gold nanoparticles: A review'. *Rev. Adv. Mater. Sci.* 12 (2006), pp. 23–32 (cited on pp. 6, 8).
- [40] P. Crespo et al. 'Permanent Magnetism, Magnetic Anisotropy, and Hysteresis of Thiol-Capped Gold Nanoparticles'. *Phys. Rev. Lett.* 93 (2004), p. 087204. DOI: [10.1103/PhysRevLett.93.087204](https://doi.org/10.1103/PhysRevLett.93.087204) (cited on pp. 7–10, 15, 16, 58, 94).
- [41] P. Crespo et al. 'Fe Impurities Weaken the Ferromagnetic Behavior in Au Nanoparticles'. *Phys. Rev. Lett.* 97 (2006), p. 177203. DOI: [10.1103/PhysRevLett.97.177203](https://doi.org/10.1103/PhysRevLett.97.177203) (cited on pp. 7, 9).
- [42] P. G. van Rhee et al. 'Giant Magnetic Susceptibility of Gold Nanorods Detected by Magnetic Alignment'. *Phys. Rev. Lett.* 111 (2013), p. 127202. DOI: [10.1103/PhysRevLett.111.127202](https://doi.org/10.1103/PhysRevLett.111.127202) (cited on pp. 8, 10, 12, 58–61, 89, 90, 94, 95, 116).
- [43] L. Suber, D. Fiorani, G. Scavia, P. Imperatori, and W. R. Plunkett. 'Permanent Magnetism in Dithiol-Capped Silver Nanoparticles'. *Chem. of Mat.* 19.6 (Mar. 2007), pp. 1509–1517. DOI: [10.1021/cm062093a](https://doi.org/10.1021/cm062093a) (cited on p. 9).
- [44] E. Guerrero et al. 'Surface plasmon resonance and magnetism of thiol-capped gold nanoparticles'. *Nanotechnology* 19.17 (Mar. 2008), p. 175701. DOI: [10.1088/0957-4484/19/17/175701](https://doi.org/10.1088/0957-4484/19/17/175701) (cited on pp. 8, 9, 15, 58).
- [45] E. Guerrero et al. 'Electronic structure, magnetic properties, and microstructural analysis of thiol-functionalized Au nanoparticles: role of chemical and structural parameters in the ferromagnetic behaviour'. *J. Nanoparticle Research* 10.1 (Dec. 2008), pp. 179–192. DOI: [10.1007/s11051-008-9445-5](https://doi.org/10.1007/s11051-008-9445-5) (cited on pp. 8, 9, 58).
- [46] J. Bartolomé et al. 'Strong Paramagnetism of Gold Nanoparticles Deposited on a *Sulfolobus acidocaldarius* S Layer'. *Phys. Rev. Lett.* 109.24 (Dec. 2012), p. 247203. DOI: [10.1103/PhysRevLett.109.247203](https://doi.org/10.1103/PhysRevLett.109.247203) (cited on pp. 8, 15, 16, 58).
- [47] M. Agrachev et al. 'Magnetic Ordering in Gold Nanoclusters'. *ACS Omega* 2.6 (June 2017), pp. 2607–2617. DOI: [10.1021/acsomega.7b00472](https://doi.org/10.1021/acsomega.7b00472) (cited on p. 8).
- [48] P. Dutta, S. Pal, M. S. Seehra, M. Anand, and C. B. Roberts. 'Magnetism in dodecanethiol-capped gold nanoparticles: Role of size and capping agent'. *App. phys. Lett.* 90.21 (May 2007), p. 213102. DOI: [10.1063/1.2740577](https://doi.org/10.1063/1.2740577) (cited on pp. 8, 9, 16, 58).
- [49] B. Donnio, P. García-Vázquez, J.-L. Gallani, D. Guillon, and E. Terazzi. 'Dendronized Ferromagnetic Gold Nanoparticles Self-Organized in a Thermotropic Cubic Phase'. *Adv. Mater.* 19 (2007), p. 3534. DOI: [10.1002/adma.200701252](https://doi.org/10.1002/adma.200701252) (cited on pp. 9, 10, 16, 93).
- [50] B. Donnio et al. 'Very slow high-temperature relaxation of the remnant magnetic moment in 2 nm mesomorphic gold nanoparticles'. *Soft Matter* 6 (2010), p. 965. DOI: [10.1039/b918602f](https://doi.org/10.1039/b918602f) (cited on p. 9).

- [51] E. Goikolea et al. 'Evidence of intrinsic ferromagnetic behavior of thiol capped Au nanoparticles based on μ SR results'. *J. Non-Crys. Solids* 354.47-51 (Dec. 2008), pp. 5210–5212. DOI: [10.1016/j.jnoncrysol.2008.07.042](https://doi.org/10.1016/j.jnoncrysol.2008.07.042) (cited on p. 9).
- [52] J. S. Garitaonandia et al. 'Chemically Induced Permanent Magnetism in Au, Ag, and Cu Nanoparticles: Localization of the Magnetism by Element Selective Techniques'. *Nano Lett.* 8 (2008), p. 661. DOI: [10.1021/nl1073129g](https://doi.org/10.1021/nl1073129g) (cited on p. 9).
- [53] J. de la Venta et al. 'X-ray Magnetic Circular Dichroism and Small Angle Neutron Scattering Studies of Thiol Capped Gold Nanoparticles'. *J. Nanosci. Nanotechnol.* 9 (2009), p. 6434. DOI: [10.1166/jnn.2009.1877](https://doi.org/10.1166/jnn.2009.1877) (cited on p. 9).
- [54] U. Maitra, B. Das, N. Kumar, A. Sundaresan, and C. N. R. Rao. 'Ferromagnetism Exhibited by Nanoparticles of Noble Metals'. *ChemPhysChem* 12 (2011), p. 2322. DOI: [10.1002/cphc.201100121](https://doi.org/10.1002/cphc.201100121) (cited on pp. 9, 16, 95).
- [55] R. Gréget et al. 'Magnetic Properties of Gold Nanoparticles: A Room-Temperature Quantum Effect'. *ChemPhysChem* 13 (2012), p. 3092. DOI: [10.1002/cphc.201200394](https://doi.org/10.1002/cphc.201200394) (cited on pp. 9, 10, 16).
- [56] M. Tokita and E. Haga. 'Nuclear magnetic resonance of ^{197}Au in gold metal'. en. *J. Molecular Structure* 83 (Jan. 1982), pp. 143–153. DOI: [10.1016/0022-2860\(82\)85174-0](https://doi.org/10.1016/0022-2860(82)85174-0) (cited on p. 9).
- [57] M. Kawakami, H. Enokiya, and T. Okamoto. ' ^{197}Au NMR study of Au impurities in Fe and FCC Co'. *J. Physics F: Metal Physics* 15.7 (July 1985), pp. 1613–1621. DOI: [10.1088/0305-4608/15/7/018](https://doi.org/10.1088/0305-4608/15/7/018) (cited on p. 9).
- [58] A. Sundaresan and C. Rao. 'Ferromagnetism as a universal feature of inorganic nanoparticles'. *Nano Today* 4.1 (Feb. 2009), pp. 96–106. DOI: [10.1016/j.nantod.2008.10.002](https://doi.org/10.1016/j.nantod.2008.10.002) (cited on p. 9).
- [59] M. A. Garcia et al. 'Sources of experimental errors in the observation of nanoscale magnetism'. *J. App. phys.* 105.1 (Jan. 2009), p. 013925. DOI: [10.1063/1.3060808](https://doi.org/10.1063/1.3060808) (cited on pp. 9, 56).
- [60] P. Stamenov and J. M. D. Coey. 'Sample size, position, and structure effects on magnetization measurements using second-order gradiometer pickup coils'. en. *Review of Scientific Instruments* 77.1 (Jan. 2006), p. 015106. DOI: [10.1063/1.2149190](https://doi.org/10.1063/1.2149190) (cited on p. 9).
- [61] S. Ramachandran et al. 'Correction to "Synthesis of Magnetic Noble Metal (Nano)Particles"'. *Langmuir* 31.1 (Jan. 2015), pp. 651–653. DOI: [10.1021/la502782h](https://doi.org/10.1021/la502782h) (cited on p. 9).
- [62] M. Roda-Llordes et al. 'Quantum Size Effects in the Magnetic Susceptibility of a Metallic Nanoparticle'. *arXiv:2010.14370 [cond-mat, physics:quant-ph]* (Oct. 2020). arXiv: 2010.14370 (cited on pp. 9, 93).

- [63] C.-Y. Li et al. 'Intrinsic magnetic moments of gold nanoparticles'. *Phys. Rev. B* 83.17 (May 2011), p. 174446. DOI: [10.1103/PhysRevB.83.174446](https://doi.org/10.1103/PhysRevB.83.174446) (cited on pp. 10, 95).
- [64] A. Hernando et al. 'Revisiting magnetism of capped Au and ZnO nanoparticles: Surface band structure and atomic orbital with giant magnetic moment'. *physica status solidi (b)* 248.10 (2011), pp. 2352–2360. DOI: [10.1002/pssb.201147227](https://doi.org/10.1002/pssb.201147227) (cited on pp. 10, 94, 95).
- [65] A. Hernando, P. Crespo, and M. A. García. 'Origin of Orbital Ferromagnetism and Giant Magnetic Anisotropy at the Nanoscale'. *Phys. Rev. Lett.* 96.5 (Feb. 2006), p. 057206. DOI: [10.1103/PhysRevLett.96.057206](https://doi.org/10.1103/PhysRevLett.96.057206) (cited on pp. 10, 61).
- [66] B. Skinner. 'Repeated noise pattern in the data of arXiv:1807.08572, "Evidence for Superconductivity at Ambient Temperature and Pressure in Nanostructures"'. *arXiv:1808.02929 [cond-mat]* (Aug. 2018) (cited on p. 10).
- [67] Y. Imry. 'Superconducting fluctuations and large diamagnetism of low- T_c nanoparticles'. *Phys. Rev. B* 91.10 (Mar. 2015), p. 104503. DOI: [10.1103/PhysRevB.91.104503](https://doi.org/10.1103/PhysRevB.91.104503) (cited on p. 10).
- [68] J. M. van Ruitenbeek and D. A. van Leeuwen. 'Model calculation of size effects in orbital magnetism'. *Phys. Rev. Lett.* 67 (1991), p. 640. DOI: [10.1103/PhysRevLett.67.640](https://doi.org/10.1103/PhysRevLett.67.640) (cited on pp. 10, 19, 25, 27, 29, 34, 45, 64, 65, 91).
- [69] J. M. van Ruitenbeek and D. A. van Leeuwen. 'SIZE EFFECTS IN ORBITAL MAGNETISM'. *Mod. Phys. Lett. B* 07 (1993), p. 1053. DOI: [10.1142/S0217984993001053](https://doi.org/10.1142/S0217984993001053) (cited on pp. 10, 19, 64).
- [70] S. Frauendorf, V. M. Kolomietz, A. G. Magner, and A. I. Sanzhur. 'Supershell structure of magnetic susceptibility'. *Phys. Rev. B* 58.9 (Sept. 1998), pp. 5622–5627. DOI: [10.1103/PhysRevB.58.5622](https://doi.org/10.1103/PhysRevB.58.5622) (cited on pp. 10, 43, 84).
- [71] V. Chandrasekhar et al. 'Magnetic response of a single, isolated gold loop'. *Phys. Rev. Lett.* 67.25 (Dec. 1991), pp. 3578–3581. DOI: [10.1103/PhysRevLett.67.3578](https://doi.org/10.1103/PhysRevLett.67.3578) (cited on p. 10).
- [72] D. Mailly, C. Chapelier, and A. Benoit. 'Experimental observation of persistent currents in GaAs-AlGaAs single loop'. *Phys. Rev. Lett.* 70.13 (Mar. 1993), pp. 2020–2023. DOI: [10.1103/PhysRevLett.70.2020](https://doi.org/10.1103/PhysRevLett.70.2020) (cited on p. 10).
- [73] M. Büttiker, Y. Imry, and R. Landauer. 'Josephson behavior in small normal one-dimensional rings'. *Phys. Lett. A* 96.7 (July 1983), pp. 365–367. DOI: [10.1016/0375-9601\(83\)90011-7](https://doi.org/10.1016/0375-9601(83)90011-7) (cited on p. 10).
- [74] H. Bouchiat. 'New clues in the mystery of persistent currents'. *Physics* 1 (2008). Illustration by A. Stonebraker, p. 7 (cited on p. 11).
- [75] H. Bouchiat and G. Montambaux. 'Persistent currents in mesoscopic rings : ensemble averages and half-flux-quantum periodicity'. *J. Phys. (France)* 50 (1989), p. 2695. DOI: [10.1051/jphys:0198900500180269500](https://doi.org/10.1051/jphys:0198900500180269500) (cited on pp. 11, 13, 30).

- [76] Y. Imry. in *Coherence effects in Condensed Matter Systems*, ed. by B. Kramer. Plenum, New York, 1991 (cited on pp. [11](#), [13](#), [24](#), [30](#), [57](#)).
- [77] A. Schmid. 'Persistent currents in mesoscopic rings by suppression of charge fluctuations'. *Phys. Rev. Lett.* 66 (1 Jan. 1991), pp. 80–83. DOI: [10.1103/PhysRevLett.66.80](#) (cited on pp. [11](#), [30](#), [57](#)).
- [78] F. von Oppen and E. K. Riedel. 'Average persistent current in a mesoscopic ring'. *Phys. Rev. Lett.* 66.1 (Jan. 1991), pp. 84–87. DOI: [10.1103/PhysRevLett.66.84](#) (cited on p. [11](#)).
- [79] B. L. Altshuler, Y. Gefen, and Y. Imry. 'Persistent differences between canonical and grand canonical averages in mesoscopic ensembles: Large paramagnetic orbital susceptibilities'. *Phys. Rev. Lett.* 66.1 (Jan. 1991), pp. 88–91. DOI: [10.1103/PhysRevLett.66.88](#) (cited on p. [11](#)).
- [80] A. Müller-Groeling, H. A. Weidenmüller, and C. H. Lewenkopf. 'Interacting Electrons in Mesoscopic Rings'. *Europhysics Lett. (EPL)* 22.3 (Apr. 1993), pp. 193–198. DOI: [10.1209/0295-5075/22/3/006](#) (cited on p. [11](#)).
- [81] A. C. Bleszynski-Jayich et al. 'Persistent Currents in Normal Metal Rings'. *Science* 326.5950 (Oct. 2009), pp. 272–275. DOI: [10.1126/science.1178139](#) (cited on p. [11](#)).
- [82] L. P. Lévy, D. H. Reich, L. Pfeiffer, and K. West. 'Aharonov-Bohm ballistic billiards'. *Physica B: Condensed Matter* 189.1 (June 1993), pp. 204–209. DOI: [10.1016/0921-4526\(93\)90161-X](#) (cited on pp. [11](#), [50](#)).
- [83] F. von Oppen. 'Magnetic susceptibility of ballistic microstructures'. *Phys. Rev. B* 50 (23 Dec. 1994), pp. 17151–17161. DOI: [10.1103/PhysRevB.50.17151](#) (cited on pp. [11](#), [16](#), [50](#), [59](#), [66](#), [94](#)).
- [84] D. Ullmo, K. Richter, and R. A. Jalabert. 'Orbital Magnetism in Ensembles of Ballistic Billiards'. *Phys. Rev. Lett.* 74 (3 Jan. 1995), pp. 383–386. DOI: [10.1103/PhysRevLett.74.383](#) (cited on pp. [11](#), [30](#), [44](#), [50](#), [59](#), [94](#)).
- [85] K. Richter, D. Ullmo, and R. A. Jalabert. 'Orbital magnetism in the ballistic regime: geometrical effects'. *Phys. Rep.* 276 (1996), p. 1. DOI: [10.1016/0370-1573\(96\)00010-5](#) (cited on pp. [11](#), [32](#), [44](#), [50](#), [59](#), [90](#), [94](#), [122](#), [123](#)).
- [86] K. Richter and B. Mehlig. 'Orbital magnetism of classically chaotic quantum systems'. *Europhys. Lett.* 41 (1998), p. 587. DOI: [10.1209/epl/i1998-00197-2](#) (cited on pp. [11](#), [90](#)).
- [87] K. Richter, D. Ullmo, and R. A. Jalabert. 'Smooth-disorder effects in ballistic microstructures'. *Phys. Rev. B* 54 (8 Aug. 1996), R5219–R5222. DOI: [10.1103/PhysRevB.54.R5219](#) (cited on pp. [11](#), [18](#), [50](#), [59](#), [94](#)).
- [88] K. Richter, D. Ullmo, and R. A. Jalabert. 'Integrability and disorder in mesoscopic systems: Application to orbital magnetism'. *J. Math. Phys.* 37.10 (1996), pp. 5087–5110. DOI: [10.1063/1.531677](#) (cited on pp. [11](#), [18](#), [22](#), [30](#), [31](#), [50](#), [59](#), [94](#), [102](#)).

- [89] D. Ullmo, H. U. Baranger, K. Richter, F. von Oppen, and R. A. Jalabert. ‘Chaos and Interacting Electrons in Ballistic Quantum Dots’. *Phys. Rev. Lett.* 80.5 (Feb. 1998), pp. 895–899. DOI: [10.1103/PhysRevLett.80.895](https://doi.org/10.1103/PhysRevLett.80.895) (cited on p. 12).
- [90] B. Murzaliev, M. Titov, and M. I. Katsnelson. ‘Diamagnetism of metallic nanoparticles as a result of strong spin-orbit interaction’. *Phys. Rev. B* 100 (2019), p. 075426. DOI: [10.1103/PhysRevB.100.075426](https://doi.org/10.1103/PhysRevB.100.075426) (cited on pp. 12, 59–61, 89, 92).
- [91] F. Schwabl. *Advanced Quantum Mechanics*. Springer-Verlag, Berlin, 1997 (cited on pp. 13, 62).
- [92] G. Bergmann. ‘Weak localization in thin films: a time-of-flight experiment with conduction electrons’. *Phys. Rep.* 107 (1984), p. 1. DOI: [https://doi.org/10.1016/0370-1573\(84\)90103-0](https://doi.org/10.1016/0370-1573(84)90103-0) (cited on pp. 13, 60, 61).
- [93] J. B. Miller et al. ‘Gate-Controlled Spin-Orbit Quantum Interference Effects in Lateral Transport’. *Phys. Rev. Lett.* 90 (2003), p. 076807. DOI: [10.1103/PhysRevLett.90.076807](https://doi.org/10.1103/PhysRevLett.90.076807) (cited on pp. 13, 60, 61).
- [94] O. Zaitsev, D. Frustaglia, and K. Richter. ‘Semiclassical theory of weak antilocalization and spin relaxation in ballistic quantum dots’. *Phys. Rev. B* 72 (15 2005), p. 155325. DOI: [10.1103/PhysRevB.72.155325](https://doi.org/10.1103/PhysRevB.72.155325) (cited on pp. 13, 60, 61).
- [95] N. Nagaosa, J. Sinova, S. Onoda, A. H. MacDonald, and N. P. Ong. ‘Anomalous Hall effect’. *Rev. Mod. Phys.* 82 (2010), p. 1539. DOI: [10.1103/RevModPhys.82.1539](https://doi.org/10.1103/RevModPhys.82.1539) (cited on p. 13).
- [96] I. Žutić, J. Fabian, and S. Das Sarma. ‘Spintronics: Fundamentals and applications’. *Rev. Mod. Phys.* 76 (2004), p. 323. DOI: [10.1103/RevModPhys.76.323](https://doi.org/10.1103/RevModPhys.76.323) (cited on p. 13).
- [97] H. Engel, E. Rashba, and B. Halperin. in *Handbook of Magnetism and Advanced Magnetic Materials*. Vol. 5, H. Kronmüller and S. Parkin (eds.) John Wiley & Sons Ltd, Chichester, 2007 (cited on pp. 13, 38).
- [98] G. A. Intronati, P. I. Tamborenea, D. Weinmann, and R. A. Jalabert. ‘Spin Relaxation near the Metal-Insulator Transition: Dominance of the Dresselhaus Spin-Orbit Coupling’. *Phys. Rev. Lett.* 108 (1 Jan. 2012), p. 016601. DOI: [10.1103/PhysRevLett.108.016601](https://doi.org/10.1103/PhysRevLett.108.016601) (cited on p. 13).
- [99] D. G. Salinas, S. Guéron, D. C. Ralph, C. T. Black, and M. Tinkham. ‘Effects of spin-orbit interactions on tunneling via discrete energy levels in metal nanoparticles’. *Phys. Rev. B* 60 (1999), p. 6137. DOI: [10.1103/PhysRevB.60.6137](https://doi.org/10.1103/PhysRevB.60.6137) (cited on pp. 13, 61, 89).
- [100] D. Davidovi and M. Tinkham. ‘Spectroscopy, Interactions, and Level Splittings in Au Nanoparticles’. *Phys. Rev. Lett.* 83 (1999), p. 1644. DOI: [10.1103/PhysRevLett.83.1644](https://doi.org/10.1103/PhysRevLett.83.1644) (cited on pp. 13, 61, 82, 89).

- [101] A. Kawabata. 'Electronic Properties of Fine Metallic Particles. III. E.S.R Absorption Line Shape'. *J. Phys. Soc. Jpn.* 29.4 (1970), pp. 902–911. DOI: [10.1143/JPSJ.29.902](https://doi.org/10.1143/JPSJ.29.902) (cited on p. 13).
- [102] W. P. Halperin. 'Quantum size effects in metal particles'. *Rev. Mod. Phys.* 58 (3 July 1986), pp. 533–606. DOI: [10.1103/RevModPhys.58.533](https://doi.org/10.1103/RevModPhys.58.533) (cited on p. 13).
- [103] P. W. Brouwer, X. Waintal, and B. I. Halperin. 'Fluctuating Spin g-Tensor in Small Metal Grains'. *Phys. Rev. Lett.* 85 (2000), p. 369. DOI: [10.1103/PhysRevLett.85.369](https://doi.org/10.1103/PhysRevLett.85.369) (cited on pp. 13, 61, 89).
- [104] K. A. Matveev, L. I. Glazman, and A. I. Larkin. 'g-Factors of Discrete Levels in Nanoparticles'. *Phys. Rev. Lett.* 85 (2000), p. 2789. DOI: [10.1103/PhysRevLett.85.2789](https://doi.org/10.1103/PhysRevLett.85.2789) (cited on pp. 13, 61, 89).
- [105] T. Rangel et al. 'Band structure of gold from many-body perturbation theory'. *Phys. Rev. B* 86 (12 Sept. 2012), p. 125125. DOI: [10.1103/PhysRevB.86.125125](https://doi.org/10.1103/PhysRevB.86.125125) (cited on pp. 13, 15).
- [106] P. Monod and A. Janossy. 'Conduction electron spin resonance in gold'. *J. Low Temp. Phys.* 26 (Sept. 1977), p. 311. DOI: [10.1007/BF00654575](https://doi.org/10.1007/BF00654575) (cited on p. 13).
- [107] M. Brack. 'The physics of simple metal clusters: self-consistent jellium model and semiclassical approaches'. *Rev. Mod. Phys.* 65 (3 July 1993), pp. 677–732. DOI: [10.1103/RevModPhys.65.677](https://doi.org/10.1103/RevModPhys.65.677) (cited on pp. 15, 17).
- [108] C.-M. Wu et al. 'Quantum spins in Mackay icosahedral gold nanoparticles'. *J. Nanoparticle Research* 12.1 (Jan. 2010), pp. 177–185. DOI: [10.1007/s11051-009-9592-3](https://doi.org/10.1007/s11051-009-9592-3) (cited on pp. 16, 95).
- [109] R. Gréget. 'Propriétés magnétiques de nanoparticules d'or fonctionnalisées'. Phd thesis, Université de Strasbourg, 2012 (cited on pp. 16, 48).
- [110] W. A. de Heer. 'The physics of simple metal clusters: experimental aspects and simple models'. *Rev. Mod. Phys.* 65.3 (1993), pp. 611–676. DOI: [10.1103/RevModPhys.65.611](https://doi.org/10.1103/RevModPhys.65.611) (cited on pp. 16, 17, 60).
- [111] G. Weick, R. A. Molina, D. Weinmann, and R. A. Jalabert. 'Lifetime of the first and second collective excitations in metallic nanoparticles'. *Phys. Rev. B* 72 (11 Sept. 2005), p. 115410. DOI: [10.1103/PhysRevB.72.115410](https://doi.org/10.1103/PhysRevB.72.115410) (cited on pp. 17, 22).
- [112] G. Weick. *Quantum dissipation and decoherence of collective excitations in metallic nanoparticles*. PhD thesis, Université of Strasbourg, 2006 (cited on pp. 17, 18, 123).
- [113] G. Weick, G.-L. Ingold, R. A. Jalabert, and D. Weinmann. 'Surface plasmon in metallic nanoparticles: Renormalization effects due to electron-hole excitations'. *Phys. Rev. B* 74 (16 Oct. 2006), p. 165421. DOI: [10.1103/PhysRevB.74.165421](https://doi.org/10.1103/PhysRevB.74.165421) (cited on pp. 17, 64).

- [114] W.-D. Schöne, W. Ekardt, and J. M. Pacheco. ‘Reintroduction of ionic structure in the self-consistent jellium model for metal clusters: Pseudopotential perturbation theory’. *Phys. Rev. B* 50 (15 Oct. 1994), pp. 11079–11087. DOI: [10.1103/PhysRevB.50.11079](https://doi.org/10.1103/PhysRevB.50.11079) (cited on pp. 18, 94).
- [115] J. P. Bucher, P. Xia, and L. A. Bloomfield. ‘Statistical description of the electronic-level structure of small metallic particles’. *Phys. Rev. B* 42 (17 Dec. 1990), pp. 10858–10864. DOI: [10.1103/PhysRevB.42.10858](https://doi.org/10.1103/PhysRevB.42.10858) (cited on p. 18).
- [116] N. Pavloff and M. Hansen. ‘Effects of surface roughness on the electronic structure of metallic clusters’. *Z. Phys. D* 24 (1992), p. 57. DOI: [10.1007/BF01436604](https://doi.org/10.1007/BF01436604) (cited on p. 18).
- [117] K. Tanaka, S. C. Creagh, and M. Brack. ‘Simple metal clusters in magnetic fields’. *Phys. Rev. B* 53 (23 June 1996), pp. 16050–16058. DOI: [10.1103/PhysRevB.53.16050](https://doi.org/10.1103/PhysRevB.53.16050) (cited on pp. 18, 22, 23, 111–113).
- [118] G. Weick and D. Weinmann. ‘Lifetime of the surface magnetoplasmons in metallic nanoparticles’. *Phys. Rev. B* 83.12 (2011), p. 125405. DOI: [10.1103/PhysRevB.83.125405](https://doi.org/10.1103/PhysRevB.83.125405) (cited on p. 18).
- [119] W. Greiner. *Relativistic Quantum Mechanics*. Vol. 3. Springer, 1990 (cited on pp. 19, 39, 66, 81, 129, 137).
- [120] A. W. Thomas. ‘Chiral symmetry and the bag model: A new starting point for nuclear physics’. *Advances in nuclear physics* (1984), pp. 1–137. DOI: [10.1007/978-1-4613-9892-9_1](https://doi.org/10.1007/978-1-4613-9892-9_1) (cited on p. 19).
- [121] P. N. Bogolioubov. ‘Sur un modèle à quarks quasi-indépendants’. *Annales de l’I.H.P. Physique théorique* 8.2 (1968), pp. 163–189 (cited on p. 19).
- [122] P. Alberto, M. Fiolhais, and M. Oliveira. ‘On the relativistic L-S coupling’. *Eur. J. Phys.* 19.6 (Nov. 1998), pp. 553–562. DOI: [10.1088/0143-0807/19/6/008](https://doi.org/10.1088/0143-0807/19/6/008) (cited on pp. 19, 66, 137).
- [123] M. C. Gutzwiller. *Chaos in Classical and Quantum Mechanics*. Springer-Verlag, Berlin, 1990 (cited on pp. 21, 22, 105, 110).
- [124] J. B. Keller and S. Rubirow. ‘Asymptotic solution of eigenvalue problems’. *Ann. Phys. (N.Y.)* 9.1 (1960), pp. 24–75. DOI: [10.1016/0003-4916\(60\)90061-0](https://doi.org/10.1016/0003-4916(60)90061-0) (cited on pp. 22, 108, 109).
- [125] R. Balian and C. Bloch. ‘Distribution of eigenfrequencies for the wave equation in a finite domain: III. Eigenfrequency density oscillations’. *Ann. Phys. (N.Y.)* 69.1 (1972), pp. 76–160. DOI: [https://doi.org/10.1016/0003-4916\(72\)90006-1](https://doi.org/10.1016/0003-4916(72)90006-1) (cited on p. 22).
- [126] M. Berry and M. Tabor. ‘Closed orbits and the regular bound spectrums’. *Proc. R. Soc. Lond. A* 349.1656 (1976), pp. 101–123. DOI: [10.1098/rspa.1976.0062](https://doi.org/10.1098/rspa.1976.0062) (cited on pp. 22, 105, 107, 109).
- [127] J. H. Van Vleck. *The theory of electric and magnetic susceptibilities*. Oxford University Press, 1965 (cited on p. 27).

- [128] H. Mathur, M. Gökçedağ, and A. D. Stone. ‘Mesoscopic Spin Magnetism’. *Phys. Rev. Lett.* 74 (1995), pp. 1855–1858. DOI: [10.1103/PhysRevLett.74.1855](https://doi.org/10.1103/PhysRevLett.74.1855) (cited on p. 30).
- [129] V. Ruban. ‘Magnetic properties of a relativistic plasma’. *Soviet Physics J.* 10.3 (1967), pp. 40–44. DOI: [10.1007/BF01649474](https://doi.org/10.1007/BF01649474) (cited on p. 34).
- [130] E. M. Chudnovsky. ‘Magnetic susceptibility of relativistic Fermi gas’. *J. Phys. A: Math. Gen.* 14 (1981), pp. 2091–2094. DOI: [10.1088/0305-4470/14/8/030](https://doi.org/10.1088/0305-4470/14/8/030) (cited on p. 34).
- [131] L. Homorodean. ‘Magnetic susceptibility of the relativistic electron gas’. *International J. Modern Physics B* 13.26 (1999), pp. 3133–3148. DOI: [10.1142/S0217979299002903](https://doi.org/10.1142/S0217979299002903) (cited on p. 34).
- [132] A. Rukhadze and V. Silin. ‘On the Magnetic Susceptibility of a Relativistic Electron Gas’. *J. Exp. Theor. Phys.* 11 (1960), p. 463 (cited on pp. 34, 103).
- [133] M. Reiher and A. Wolf. *Relativistic Quantum Chemistry: The Fundamental Theory of Molecular Science*. Wiley, 2015 (cited on pp. 34, 61).
- [134] L. Foldy and S. Wouthuysen. ‘On the Dirac Theory of Spin 1/2 Particles and Its Non-Relativistic Limit’. *Phys. Rev.* 78 (1 Apr. 1950), pp. 29–36. DOI: [10.1103/PhysRev.78.29](https://doi.org/10.1103/PhysRev.78.29) (cited on pp. 35, 62).
- [135] W. Greiner. *Quantum mechanics: an introduction*. Springer, 2011. Chap. 13 (cited on p. 37).
- [136] P. J. Mohr, D. B. Newell, and B. N. Taylor. ‘CODATA recommended values of the fundamental physical constants: 2014’. *J. Phys. and Chem. Reference Data* 45.4 (2016), p. 043102. DOI: [10.1063/1.4954402](https://doi.org/10.1063/1.4954402) (cited on p. 37).
- [137] V. Berestetskii, L. Pitaevskii, and E. Lifshitz. *Quantum Electrodynamics: Volume 4*. Elsevier Sci., 2012 (cited on pp. 37, 103).
- [138] N. Ashcroft and N. Mermin. *Solid State Physics*. Saunders College, Philadelphia, 1976 (cited on pp. 38, 65, 137).
- [139] L. Landau. ‘On the theory of the Fermi liquid’. *Sov. Phys. JETP* 8.1 (1959), p. 70 (cited on p. 38).
- [140] R. Winkler. *Spin-Orbit Coupling in Two-Dimensional Electron and Hole Systems*. Vol. 41. Springer, 2003 (cited on p. 38).
- [141] C. Cohen-Tannoudji, B. Diu, F. Laloe, and B. Dui. *Quantum Mechanics*. Vol. 2. Wiley-Interscience, 1976 (cited on p. 39).
- [142] H. Kramers. ‘Théorie générale de la rotation paramagnétique dans les cristaux’. *Proc. Acad. Amst* 33.6 (1930), p. 14 (cited on p. 39).
- [143] E. Wigner. ‘Über die Operation der Zeitumkehr in der Quantenmechanik’. *Nachrichten von der Gesellschaft der Wissenschaften zu Göttingen, Mathematisch-Physikalische Klasse* 1932 (1932), pp. 546–559. DOI: [10.1007/978-3-662-02781-3_15](https://doi.org/10.1007/978-3-662-02781-3_15) (cited on p. 39).

- [144] M. Gómez Vioria, G. Weick, D. Weinmann, and R. A. Jalabert. ‘Orbital magnetism in ensembles of gold nanoparticles’. *Phys. Rev. B* 98.19 (2018), p. 195417. DOI: [10.1103/PhysRevB.98.195417](https://doi.org/10.1103/PhysRevB.98.195417) (cited on p. 41).
- [145] J. Saenz et al. ‘Observation of magnetic forces by the atomic force microscope’. *J. App. Phys.* 62.10 (1987), pp. 4293–4295. DOI: [10.1063/1.339105](https://doi.org/10.1063/1.339105) (cited on p. 54).
- [146] G. J. Percebois, D. Weinmann, R. A. Jalabert, and G. Weick. ‘Spontaneous orbital magnetization of mesoscopic dipole dimers’. *arXiv:2107.04508 [cond-mat]* (July 2021). arXiv: 2107.04508 (cited on pp. 54, 56, 60, 93).
- [147] Y. Yamamoto. Private communication. 2018 (cited on p. 58).
- [148] H. Mathur and A. D. Stone. ‘Persistent-current paramagnetism and spin-orbit interaction in mesoscopic rings’. *Phys. Rev. B* 44.19 (1991), p. 10957. DOI: [10.1103/PhysRevB.44.10957](https://doi.org/10.1103/PhysRevB.44.10957) (cited on p. 59).
- [149] S. Hikami, A. I. Larkin, and Y. Nagaoka. ‘Spin-Orbit Interaction and Magnetoresistance in the Two Dimensional Random System’. *Progress of Theoretical Physics* 63.2 (Feb. 1980), pp. 707–710. DOI: [10.1143/PTP.63.707](https://doi.org/10.1143/PTP.63.707) (cited on pp. 60, 61).
- [150] N. Taniguchi, A. Hashimoto, B. D. Simons, and B. L. Altshuler. ‘Crossover Driven by Time-Reversal Symmetry Breaking in Quantum Chaos’. *Europhys. Lett.* 27 (1994), p. 335. DOI: [10.1209/0295-5075/27/5/001](https://doi.org/10.1209/0295-5075/27/5/001) (cited on p. 61).
- [151] Y. Alhassid. ‘The statistical theory of quantum dots’. *Rev. Mod. Phys.* 72 (2000), p. 895. DOI: [10.1103/RevModPhys.72.895](https://doi.org/10.1103/RevModPhys.72.895) (cited on p. 61).
- [152] M. G. Vioria, G. Weick, D. Weinmann, and R. A. Jalabert. ‘Magnetic response of metallic nanoparticles: geometrical and weakly-relativistic effects’. *arXiv preprint arXiv:2106.10113* (2021) (cited on p. 62).
- [153] R. Mondal et al. ‘Relativistic interaction Hamiltonian coupling the angular momentum of light and the electron spin’. *Phys. Rev. B* 92 (10 Sept. 2015), p. 100402. DOI: [10.1103/PhysRevB.92.100402](https://doi.org/10.1103/PhysRevB.92.100402) (cited on p. 63).
- [154] A. Mikhailov and V. Polikanov. ‘PERTURBATION THEORY FOR THE DIRAC EQUATION’. *J. Exp. Theor. Phys.* 25 (1968), p. 95 (cited on p. 66).
- [155] C. Yannouleas and R. A. Broglia. ‘Landau damping and wall dissipation in large metal clusters’. *Ann. Phys. (N.Y.)* 217 (1992), p. 105. DOI: [10.1016/0003-4916\(92\)90340-R](https://doi.org/10.1016/0003-4916(92)90340-R) (cited on p. 72).
- [156] M. Gómez Vioria. Unpublished. 2021 (cited on pp. 90, 94, 95).
- [157] O. H.-C. Cheng, D. H. Son, and M. Sheldon. ‘Light-induced magnetism in plasmonic gold nanoparticles’. en. *Nature Photonics* 14.6 (June 2020), pp. 365–368. DOI: [10.1038/s41566-020-0603-3](https://doi.org/10.1038/s41566-020-0603-3) (cited on p. 93).

- [158] J. B. Pendry, A. J. Holden, D. J. Robbins, and W. Stewart. ‘Magnetism from conductors and enhanced nonlinear phenomena’. *IEEE transactions on microwave theory and techniques* 47.11 (1999), pp. 2075–2084. DOI: [10.1109/22.798002](https://doi.org/10.1109/22.798002) (cited on p. 93).
- [159] W. de Haas and P. Van Alphen. ‘The dependence of the susceptibility of diamagnetic metals upon the field’. 33.1106 (1930), p. 170 (cited on pp. 93, 99).
- [160] D. Shoenberg. ‘The Fermi surfaces of copper, silver and gold. I. The de Haas–Van alphen effect’. *Philosophical Transactions of the Royal Soc. of London. Series A, Math. & Phys. Sci.* 255.1052 (Nov. 1962), pp. 85–133. DOI: [10.1098/rsta.1962.0011](https://doi.org/10.1098/rsta.1962.0011) (cited on p. 93).
- [161] A. Pippard. ‘Commentary on a conjecture of Shoenberg’s concerning the de Haas—van Alphen effect’. *Proc. Royal Soc. of London. Series A. Math. & Phys. Sci.* 272.1349 (Mar. 1963), pp. 192–206. DOI: [10.1098/rspa.1963.0049](https://doi.org/10.1098/rspa.1963.0049) (cited on p. 93).
- [162] V. Canuto, H. Y. Chiu, C. Chiuderi, and H. J. Lee. ‘Physical Sciences: New Source of Intense Magnetic Fields in Neutron Stars’. *Nature* 225.5227 (Jan. 1970). DOI: [10.1038/225047a0](https://doi.org/10.1038/225047a0) (cited on p. 94).
- [163] H. J. Lee. ‘Theory of Landau Orbital Ferromagnetic States for Electrons in a Metal’. *Phys. Rev. B* 2.11 (Dec. 1970), pp. 4618–4625. DOI: [10.1103/PhysRevB.2.4618](https://doi.org/10.1103/PhysRevB.2.4618) (cited on p. 94).
- [164] D. R. Hofstadter. ‘Energy levels and wave functions of Bloch electrons in rational and irrational magnetic fields’. *Phys. Rev. B* 14.6 (1976), pp. 2239–2249. DOI: [10.1103/PhysRevB.14.2239](https://doi.org/10.1103/PhysRevB.14.2239) (cited on p. 94).
- [165] J. G. Analytis, S. J. Blundell, and A. Ardavan. ‘Landau levels, molecular orbitals, and the Hofstadter butterfly in finite systems’. *American J. Physics* 72.5 (May 2004), pp. 613–618. DOI: [10.1119/1.1615568](https://doi.org/10.1119/1.1615568) (cited on p. 94).
- [166] N. Koch. *Electronic structure of interfaces with conjugated organic materials*. 2012. DOI: [10.1002/pssr.201206208](https://doi.org/10.1002/pssr.201206208) (cited on pp. 94, 95).
- [167] B. Bröker et al. ‘Gold work function reduction by 2.2 eV with an air-stable molecular donor layer’. *App. phys. Lett.* 93.24 (2008), p. 446. DOI: [10.1063/1.3049616](https://doi.org/10.1063/1.3049616) (cited on p. 95).
- [168] G. Heimel. ‘Introduction to the theory of metal/organic interfaces’. In: *THE WSPC REFERENCE ON ORGANIC ELECTRONICS: ORGANIC SEMICONDUCTORS: Basic Concepts*. World Scientific, 2016, pp. 131–158. DOI: [10.1142/9789813148598_0005](https://doi.org/10.1142/9789813148598_0005) (cited on p. 95).
- [169] F. Zwanenburg et al. ‘Silicon quantum electronics’. *Rev Mod. Phys.* 85.3 (2013), p. 961. DOI: [10.1103/RevModPhys.85.961](https://doi.org/10.1103/RevModPhys.85.961) (cited on p. 95).
- [170] A. Corna et al. ‘Electrically driven electron spin resonance mediated by spin–valley–orbit coupling in a silicon quantum dot’. *npj quantum information* 4.1 (2018), pp. 1–7. DOI: [10.1038/s41534-018-0059-1](https://doi.org/10.1038/s41534-018-0059-1) (cited on p. 95).

- [171] H. Grabert and M. H. Devoret. *Single charge tunneling: Coulomb blockade phenomena in nanostructures*. Vol. 294. Springer Science & Business Media, 2013 (cited on p. 95).
- [172] K. Ono, D. Austing, Y. Tokura, and S. Tarucha. ‘Current rectification by Pauli exclusion in a weakly coupled double quantum dot system’. *Science* 297.5585 (2002), pp. 1313–1317. DOI: [10.1126/science.1070958](https://doi.org/10.1126/science.1070958) (cited on p. 95).
- [173] D. Weinmann. ‘Spin blockades in the transport through quantum dots’. In: *Anderson Localization and Its Ramifications*. Springer, 2003, pp. 289–301. DOI: [10.1007/978-3-540-45202-7_20](https://doi.org/10.1007/978-3-540-45202-7_20) (cited on p. 95).
- [174] M. Berry and M. Tabor. ‘Calculating the Bound Spectrum by Path Summation in Action-angle Variables’. *J. Phys. A: Math. Gen* 10.3 (1977). DOI: [10.1088/0305-4470/10/3/009](https://doi.org/10.1088/0305-4470/10/3/009) (cited on pp. 105, 109).
- [175] M. Berry and M. Tabor. ‘Level Clustering in the Regular Spectrum’. *Proc. R. Soc. Lond. A* 356 (1977), pp. 375–394. DOI: [10.1098/rspa.1977.0140](https://doi.org/10.1098/rspa.1977.0140) (cited on p. 105).
- [176] H. Goldstein, J. Safko, and C. P. Poole Jr. *Classical Mechanics*. 3rd ed. England: Pearson, 2002 (cited on pp. 105, 106).
- [177] M. Brack and R. Bhaduri. *Semiclassical Physics*. 1st ed. Addison-Wesley Publishing Company Inc., 1997 (cited on pp. 105, 106, 112).
- [178] D. Gall. ‘Electron mean free path in elemental metals’. *J. App. Phys.* 119.8 (2016), p. 085101. DOI: [10.1063/1.4942216](https://doi.org/10.1063/1.4942216) (cited on p. 106).
- [179] L. Curtis and D. Ellis. ‘Use of the Einstein–Brillouin–Keller action quantization’. *Am. J. Phys.* 72 (2004). DOI: [10.1119/1.1768554](https://doi.org/10.1119/1.1768554) (cited on p. 108).
- [180] M. Berry and K. Mount. ‘Semiclassical approximations in wave mechanics’. *Rep. Prog. Phys.* 35.1 (1972), p. 315. DOI: [10.1088/0034-4885/35/1/306](https://doi.org/10.1088/0034-4885/35/1/306) (cited on p. 108).
- [181] S. Creagh and R. Littlejohn. ‘Semiclassical trace formulas in the presence of continuous symmetries’. *Phys. Rev. A* 44 (2 July 1991), pp. 836–850. DOI: [10.1103/PhysRevA.44.836](https://doi.org/10.1103/PhysRevA.44.836) (cited on pp. 111, 112).
- [182] J. Blaschke and M. Brack. ‘Periodic orbit theory of a circular billiard in homogeneous magnetic fields’. *Phys. Rev. A* 56 (1 July 1997), pp. 182–194. DOI: [10.1103/PhysRevA.56.182](https://doi.org/10.1103/PhysRevA.56.182) (cited on p. 111).
- [183] S. Creagh. ‘Trace Formula for Broken Symmetry’. *Ann. Phys.* 248 (1 1996). DOI: [10.1006/aphy.1996.0051](https://doi.org/10.1006/aphy.1996.0051) (cited on p. 112).
- [184] G. Watson. *A Treatise on the Theory of Bessel Functions*. Cambridge University, 1995, p. 138 (cited on p. 116).
- [185] G. Breit. ‘An Interpretation of Dirac’s Theory of the Electron’. *Proc. Nat. Acad. of Sci.* 14.7 (1928), pp. 553–559. DOI: [10.1073/pnas.14.7.553](https://doi.org/10.1073/pnas.14.7.553) (cited on p. 125).

- [186] J. Bloomfield, S. Face, and Z. Moss. 'Indefinite Integrals of Spherical Bessel Functions'. *arXiv:1703.06428v1* (2017) (cited on pp. [148](#), [149](#)).

VARIABLES AND ABBREVIATIONS

INDEX

Here is a (non-exhaustive) list of variables and abbreviations:

- $\mathbb{1}_2$ identity matrix, 35
- A** magnetic vector potential, 17, 36
a radius, 15
*a*₀ Bohr radius, 18
*A*_λ semiclassical amplitude, 22
 (AME) angular magneto electric, 63
- B**, *B* magnetic induction, 17
- c* speed of light, 5, 12, 17
 (CE) canonical ensemble, 32
 cgs centimetre-gram second (units), 3
- D* density of particles, 30
- E* energy, 35
e Euler's number, 37
e elementary charge, 5, 17
 (EBK) Einstein–Brillouin–Kramers, 22
*E*_F Fermi energy, 18
*E*_F Fermi energy, 17
 (ESR) Electron spin resonance, 6
- F* free energy, 4
F example function, 100
- G** Landau levels degeneracy, 100
g g-factor, 20
 *g*₀ free electron, 13
 *g*_{Au} effective (bulk gold), 13
 (GC) grand canonical, 24
- H**, *H* applied magnetizing field, 3
H Hamiltonian
- H*⁽⁰⁾ unperturbed, 20
H^(ame) angular magneto-electric, 63
H^(D) Darwin term, 38
H^(D) diamagnetic, 20
H^(Dirac) Dirac, 35
H^(k) weakly relativistic kinetic energy correction, 63
H^(orb) orbital, 20
H^(para) paramagnetic, 20
H^(so) spin-orbit, 12
H^(so-ame) spin-orbit and AME, 63
H^(wr) weakly relativistic, 37
H^(Z) Zeeman, 20
H^(μ) magnetic moment, 62
- h*_l⁽¹⁾ spherical Hankel function, 135
ħ Planck's reduced constant, 12
- I** current, 11
- J** total angular momentum operator, 38
j total azimuthal quantum number, 38
*J*_l Bessel function of the first kind, 118
*j*_l spherical Bessel function of the first kind, 21
- k*_B Boltzmann's constant, 24
*k*_F Fermi wavevector, 5
*k*_l modified spherical Bessel functions of the second kind, 135
- L** length, 100
l orbital azimuthal quantum number, 20

- L_T thermal length, 31
 m electron's mass, 17
 \mathbf{M}, M magnetization, 3
 \mathcal{M}, \mathcal{M} magnetic moment, 4
 m^* effective mass, 5
 $\mathcal{M}^{(\text{GC})}$ grand canonical magnetic moment, 25
 m_j total magnetic quantum number, 38
 m_s spin magnetic quantum number, 20
 m_z orbital magnetic quantum number, 20

 N number of electrons, 4, 17
 n principal quantum number, 20
 n_e electronic density, 17

 $P_l^{m_z}$ associated Legendre polynomial, 116
 $\mathcal{P}(a)$ size probability density, 16
(PSF) Poisson summation rule, 102

(QED) quantum electrodynamics, 37

 R thermal factor, 31
 \mathbf{r} position, 17
 r radial coordinate, 20
 R_c cyclotron radius, 19, 22
 $R_{n,l}$ unperturbed radial wavefunction, 21
 $\mathcal{R}_{n,l}$ radial diagonal matrix element, 27
 r_s Wigner-Seitz radius, 17

SI International System of Units, 5
 S_Λ action of the orbit, 22
(SOC) spin-orbit coupling, 12, 14
(SQUID) Superconducting quantum interference device, 9

 T temperature, 4, 24
 T_F Fermi temperature, 19

 U single particle confinement, 17
 \mathcal{U} unitary operator, 35

 \mathcal{V} nanoparticle volume, 4
 V_0 potential step, 17

 v_F Fermi velocity, 19
 V_{mf} mean field potential, 17
 \mathcal{V} volume, 24

 W work function, 17
(WKB) Wentzel–Kramers–Brillouin, 22

 x Cartesian coordinate, 17
(XMCD) X-ray magnetic circular dichroism, 6

 $Y_l^{m_z}$ spherical harmonic, 21
 y Cartesian coordinate, 17
 $\mathcal{Y}_l^{m_z}$ angular diagonal matrix element, 27

 z Cartesian coordinate, 17
(ZFS) zero field susceptibility, 4
 α, γ_0 , Dirac matrices, 35
 $\beta = (k_B T)^{-1}$, 24
 $\delta(x)$ Dirac delta function, 21
 $\delta_{i,j}$ Kronecker's delta, 126
 ϵ_{ijk} Levi-Civita symbol, 126
 $\zeta_{n,l}$ n -th root of j_l , 21
 η number of specular reflections, 22
 Θ Heaviside step function, 17
 θ polar angle, 20
 $\tilde{\Theta}$ arcangle between apogee/perigee, 107
 ϑ solid angle, 21
 λ quantum number, 21
 $\lambda_i^{(\text{D})}$ Maslov index (classical turning points), 106
 λ_Λ Maslov index, 22
 $\lambda_i^{(\text{vN})}$ Maslov index (hard walls), 106
 μ chemical potential, 24
 μ_B Bohr's magneton, 4, 6
 ν winding number, 22
 ζ inclination of the orbit, 112
 ρ radial distance (cylindrical), 117
 ϱ density of states, 21
 $\sigma_x, \sigma_y, \sigma_z$ Pauli matrices, 12
 $\boldsymbol{\sigma}$ vector of Pauli matrices, 12
 τ_Λ orbital period, 31
 $Y_{j,m_j}^{(\pm)}$ spinor spherical harmonics, 39

- $\Phi_{n,j,m_j}^{(\pm)}$ unperturbed spinor eigenstates
 for a spherical confinement
 with hard walls (j basis), 39
- ϕ magnetic flux, 27
- φ azimuthal angle, 20
- ϕ_0 flux quantum, 23
- ϕ_e electrostatic potential, 36
- χ susceptibility, 4
 - $\chi^{(1)}$ grand canonical orbital, 43
 - $\chi^{(2)}$ canonical correction, 43
 - χ_{Au} bulk gold, 5
 - $\Delta\chi$ weakly relativistic correction, 79
 - $\Delta\chi^{(\text{ame})}$ angular magneto-electric, 79
 - $\Delta\chi^{(\text{D})}$ Darwin correction, 79
 - $\Delta\chi^{(\text{k})}$ kinetic energy correction, 69
 - $\Delta\chi^{(\text{so})}$ spin-orbit correction, 79
 - $\chi^{(\text{dia})}$ diamagnetic, 29
 - χ_e entangled basis, 77
 - $\chi^{(\text{GC})}$ grand canonical, 25
 - $\chi^{(\text{GC})}$ grand canonical, 25
 - χ_{L} Landau, 5
 - $\chi_{\text{b}}^{(\text{nr})}$ non-relativistic (bulk), 5
 - $\chi^{(\text{orb})}$ orbital, 29
 - χ_{P} product basis, 77
 - $\chi^{(\text{para})}$ paramagnetic, 29
 - χ_{P} Pauli, 5
 - $\chi^{(\text{rel})}$ relativistic (bulk), 103
 - $\chi_{\text{b}}^{(\text{wr})}$ weakly relativistic (bulk), 34
 - $\chi^{(\text{Z})}$ Zeeman, 65
- Ψ total wavefunction, 36
- $\Psi_{n,l,m_z,m_s}^{(0)}$ spinor eigenstate for a
 spherical confinement with
 hard walls, 20
- $\psi_{n,l,m_z}^{(0)}$ orbital eigenfunction for a
 spherical confinement with
 hard walls, 20
- Ω grand canonical potential, 24
- \mathcal{U} anti-particle total wavefunction, 36
- ω_c cyclotron frequency, 17
- \aleph_{l,m_j} off-diagonal matrix element, 75

Mauricio GÓMEZ VILORIA
Effet du couplage spin-orbite
sur la réponse magnétique
de systèmes confinés

Résumé

Insérer votre résumé en français suivi des mots-clés

1000 caractères maximum

Mots clés :

Summary

Insérer votre résumé en anglais suivi des mots-clés

Keywords :